NSF/ENG-85003

PB85-194363

STRUCTURAL RESEARCH STUDIES
Department of Civil Engineering

# STATIC AND CYCLIC BEHAVIOR OF SEMI-RIGID STEEL BEAM-COLUMN CONNECTIONS

by
A. Azizinamini
J.H. Bradburn
and
J.B. Radziminski

A REPORT OF AN INVESTIGATION CONDUCTED
by
THE DEPARTMENT OF CIVIL ENGINEERING
UNIVERSITY OF SOUTH CAROLINA

Supported by
EARTHQUAKE HAZARD MITIGATION PROGRAM
DIVISION OF CIVIL AND ENVIRONMENTAL ENGINEERING
NATIONAL SCIENCE FOUNDATION
Grant No. CEE - 8115014

UNIVERSITY OF SOUTH CAROLINA
COLUMBIA, SOUTH CAROLINA
MARCH, 1985

50272-101

| REPORT DOCUMENTATION PAGE | 1. REPORT NO. NSF/ENG-85003 | 2. | 3. Recipient's Accession No. PB85 194363/AS |
|---|---|---|---|

4. Title and Subtitle
Static and Cyclic Behavior of Semi-Rigid Steel Beam-Column Connections

5. Report Date
March 1985

6.

7. Author(s)
A. Azizinamini, J.H. Bradburn, J.B. Radziminski

8. Performing Organization Rept. No.

9. Performing Organization Name and Address
University of South Carolina
Department of Civil Engineering
Columbia, SC 29208

10. Project/Task/Work Unit No.

11. Contract(C) or Grant(G) No.
(C)
(G) CEE8115014

12. Sponsoring Organization Name and Address
Directorate for Engineering (ENG)
National Science Foundation
1800 G Street, N.W.
Washington, DC 20550

13. Type of Report & Period Covered

14.

15. Supplementary Notes

16. Abstract (Limit: 200 words)

Results are presented of a study undertaken to investigate the behavior of semi-rigid beam-to-column connections subjected to static and cyclic loadings. Tests were conducted on bolted connections comprised of top and seat beam flange angles and double web angles to evaluate cyclic performance under constant amplitude and variable amplitude displacements and to determine moment-rotation behavior under static loading. In the cyclic tests, the beam-column connections exhibited ductile behavior, with generally stable moment-rotation hysteresis loops being established at each controlled displacement amplitude. From the constant amplitude cyclic tests, linear log-log equations were established. Empirical relationships established by the tests were applied to a linear cumulative damage model and the results of several variable amplitude block cyclic tests are compared with damage summations predicted by the model. Geometric parameters which affect connection performance were quantified by the static tests, and are compared with analytical models to predict initial stiffness and complete non-linear moment-rotation behavior of the connections.

17. Document Analysis a. Descriptors

| | | |
|---|---|---|
| Loads (forces) | Mathematical models | Steel structures |
| Cyclic loads | Earthquake resistant structures | Columns (supports) |
| Static loads | Dynamic structural analysis | Beams (supports) |
| Equations | | |

b. Identifiers/Open-Ended Terms

c. COSATI Field/Group

| 18. Availability Statement | 19. Security Class (This Report) | 21. No. of Pages |
|---|---|---|
| NTIS | 20. Security Class (This Page) | 22. Price |

(See ANSI-Z39.18) | See Instructions on Reverse | OPTIONAL FORM 272 (4-77) (Formerly NTIS-35) Department of Commerce

Final Report

# STATIC AND CYCLIC BEHAVIOR

# OF

# SEMI-RIGID STEEL BEAM-COLUMN CONNECTIONS

by

A. Azizinamini
J.H. Bradburn
and
J.B. Radziminski

A Report of an Investigation Conducted
by

The Civil Engineering Department
University of South Carolina

Supported by
Earthquake Hazard Mitigation Program
Division of Civil and Environmental Engineering
National Science Foundation
Grant No. CEE-8115014

UNIVERSITY OF SOUTH CAROLINA
COLUMBIA, SOUTH CAROLINA
March, 1985



/a

ABSTRACT

The purpose of the study has been to investigate the behavior of semi-rigid beam to column connections subjected to static and cyclic loadings. Tests were conducted on bolted connections comprised of top and seat beam flange angles, and double web angles, to determine moment-rotation behavior under monotonic (static) loading, and to evaluate cyclic performance under constant amplitude and variable amplitude displacements. From the static tests, geometric parameters which affect connection performance have been quantified, and compared with analytical models formulated to predict the initial stiffness and complete non-linear moment-rotation behavior of the connections.

In the cyclic tests, the beam-column connections exhibited ductile behavior, with generally stable moment-rotation hysteresis loops being established at each controlled displacement amplitude. The tests culminated in the formation and subsequent propagation of fatigue cracks at the toe of the fillet in one or more of the beam flange angles. From the constant amplitude cyclic tests, linear log-log equations have been established relating fatigue life to connection cyclic hysteretic energy absorption, and to a generalized flange angle rotation parameter. The empirical relationships established by the constant amplitude fatigue tests have been applied to a linear cumulative damage model; the results of several variable amplitude block cyclic tests are compared with damage summations predicted by the model.

TABLE OF CONTENTS

Page

LIST OF TABLES

LIST OF FIGURES

# I. INTRODUCTION

## 1.1 Background, Research Objectives

The satisfactory performance of ductile moment-resisting steel frame building structures in an earthquake environment is dependent upon the ability of the beam-column connections to provide the rigid frame behavior and energy absorption capacity necessary to withstand the seismically induced lateral forces. Considerable experimental data have been generated on the moment-rotation behavior of beam-column connections (1-45), the results of which have demonstrated that the connections can contribute adequate strength and ductility to ensure the required performance of the structural system. Recently, studies have been reported (46-58) which consider the effect of connection flexibility on the performance of building frames. The analytical predictions of frame behavior are typically based on assumed non-linear mathematical models of the beam-column connections. However, there is a continuing need for additional experimental data to substantiate the appropriateness of the mathematical models used to describe the behavior of semi-rigid connections, including those utilizing both welded and bolted connection elements. Such information is needed for modeling the load-deformation behavior of complete building systems, and for possible application to the retrofitting of existing structures as a means of improving their resistance to lateral forces.

From cyclic tests of connections and subassemblages, it has been found that the performance of steel frame building structures, under seismically induced load histories, may be limited by low cycle fatigue of the connection elements. Consequently, recent attention has been directed to the applicability of cumulative damage models for predicting the cyclic response and eventual failure of structural connections and frames subjected to earthquake type loadings (5, 59-62). Additional information, both experimental and analytical, is required to determine the efficacy of such models in assessing the total time-history performance of a complete building system.

The objective of the research program herein has been to experimentally determine the moment-rotation performance of semi-rigid beam-column connections under static (monotonic) and cyclic loadings. Specifically, the effect varying the stiffness of the various connection elements on the static response of the connections, and on their hysteretic response under cyclic controlled displacement loading, has been studied. From these tests, the significant material and geometric parameters affecting the connection behavior are identified, and used to formulate models of the non-linear connection moment-rotation response. The constant amplitude and variable amplitude cyclic tests have served to identify the mechanisms of distress under severe excursions of connection rotation, to quantify hyseretic energy absorption capacity under cyclic loading, and to establish bench-mark fatigue life relationships. A linear damage accumulation model has been examined for for prediction of connection fatigue response under variable amplitude loading.

## 1.2 Scope of Investigation

In an initial investigation, NSF Grant No. 79-23520 (63), tests were conducted of bolted beam to column connections comprised of top and seat beam flange angles, and double web angles, to determine moment-rotation behavior under monotonic (static) loading, and to measure energy absorption capability under cyclic loading. ASTM A36 steel was used for the members and connection elements; the fasteners were 3/4-inch diameter, ASTM A325 high-strength bolts. A pair of duplicate specimens was tested simultaneously by framing simply supported beam sections into a centrally-loaded stub column.

Two beam sizes, W14X38 and W8X21, were used in the test program. For the top and seat (flange) angles, the thickness, length, and gage (in the legs attached to the column flange) were varied, together with beam depth, to effect connections of varying stiffness. Variations in the thickness and length of the web angles were investigated also. The results of the static tests were used to quantify the effect of the test variables on the non-linear moment- rotation behavior of the connections, and to establish semi-empirical models of connection response. The data were compared, also, to predictions of moment-rotation behavior using a two dimensional finite element model of the connection.

The cyclic tests in the initial investigation consisted of subjecting the connections to several stages of full reversal, controlled amplitude displacements of progressively increasing magnitude. The connections exhibited ductile behavior, with generally stable moment-rotation hystersis loops being established at each displacement amplitude to the time that testing was discontinued. The tests culminated in the formation and subsequent propagation of fatigue cracks at the toe of the fillet in one or more of the beam flange angles. The cyclic tests demonstrated that the effectiveness, under seismically induced loading, of connections of the type studied may be limited by low-cycle fatigue of the connection elements.

The scope of the current investigation (Grant No. CEE-8115014) extended the initial study by including the static testing of additional bolted connections utilizing a wider range of connection element stiffnesses. Because major slip occurred in two of the earlier tests in which 3/4-inch diameter bolts were used, 7/8-inch diameter, A325 bolts were used in all of the test specimens in the present study. Slip was observed in one of the tests in which the 7/8-inch bolts were used.

The empirical equation developed in the initial study was found to offer reasonable predictions of the static moment-rotation response of the connections in the present series of tests; i.e., those using the 7/8-inch diameter bolts. In addition, a three-dimensional finite element model has been generated to represent one flange angle of the test connections; the load-displacement relationship predicted by the model has been compared to the results of a double angle pull test conducted as an extension of the test program.

As a consequence of the fatigue failures exhibited by the connection elements in the initial test program, a series of constant amplitude cyclic tests was conducted in the present study to establish bench-mark strain based fatigue life curves for bolted connections of varying stiffness. Fatigue lives on the order of $10^1$ to $10^3$ cycles to failure were considered in this phase of the study. Besides the constant amplitude tests, two specimens were subjected to several blocks of full reversal, controlled displacements of progressively decreasing magnitude for comparison with the low-to-high amplitude block loadings examined in the initial study.

From the constant amplitude cyclic tests,a linear log-log relationship between fatigue life and a generalized flange angle rotation parameter has been established for the low cycle, strain based fatigue tests considered in the investigation. A similar relationship, between fatigue life and hysteretic energy absorbed per test cycle, has also been developed. The empirical relationships established by the constant amplitude fatigue tests have been applied to a linear fatigue damage accumulation model to predict the behavior of the specimens subjected to the variable amplitude cyclic loadings. In addition, the total hysteretic energy accumulated at the connections under both constant amplitude and variable amplitude cyclic loading has been examined.

As a final phase of the present investigation, a pilot study was conducted using connections comprised of top and seat angles welded to the beam flanges and bolted to the supporting column, together with web angles also welded to the beam and bolted to the column. The results of two static tests, using connections framed to W14X38 beam sections, are reported.

### 1.3 Acknowledgements

The tests reported in this study are from an investigation conducted in the Department of Civil Engineering at the University of South Carolina, Columbia, South Carolina. The experimental data and analytical studies represent a compilation of the results obtained during both an initial investigation (Grant No. 79-23520) and the present study (Grant No. CEE-8115014) under support by the National Science Foundation. Any opinions, findings, and conclusions or recommendations expressed in this document are those of the authors and do not necessarily reflect the views of the National Science Foundation.

The investigations were conducted under the supervision of Dr. J.B. Radziminski, Professor, and Dr. J.H. Bradburn, Associate Professor, of the Department of Civil Engineering. The latest test program and associated research studies were conducted by A. Azizinamini, with assistance from F. Farley, J. Rabley, and W. Harper, Research Assistants in Civil Engineering. Guidance concerning the scope of the investigation, provided by Dr. J.B. Scalzi of the National Science Foundation, is gratefully acknowledged.

The authors wish to express their appreciation to H. Mullinax, G. Dowdy, and B. Ward, laboratory technicians in the College of Engineering, for the fabrication of the beam supports used in the testing program, for help in the machining of the test numbers, and for the fabrication of instrumentation support devices used in data acquisition. Special thanks are extended to Ms. K. Runyon for the careful typing of this final report.

# II. DESCRIPTION OF TEST PROGRAM

## 2.1 Materials

The material for all of the test specimens, including beam sections, stub columns, and framing angles, was specified to be ASTM A36 steel, supplied by two local fabricators. The mechanical properties obtained from selected coupon specimens for material supplied by each of the fabricators is given in Table 2.1. For the all-bolted specimens, the beam-column connections were made using either 3/4-inch diameter or 7/8-inch diameter ASTM A325 heavy hex high-strength bolts, and A325 hardened washers. For the combined bolted-welded test specimens, welding of the top and seat angles, and of the web angles, to the beam sections was accomplished using AWS E70 electrodes. No tests of the mechanical properties of the bolts or the filler metal were conducted.

## 2.2 Description of Test Specimens

The specimens consisted of a pair of beam sections attached to a centrally positioned stub column using the particular flange and web angles to be investigated in a given test. The connections contained top and seat angles bolted to the flanges of the supporting stub column, together with double web angles bolted to the column flanges. For the all-bolted specimens, the flange and web angles were connected to the beam sections using the same diameter bolts as those used in the connection to the column flange. In the combined bolted-welded specimens, the top and seat angles were attached to the beam flanges by continuous longitudinal and transverse fillet welds (with returns on the end of the beam); the double web angles were similarly welded to the web of the beam.

Two beam sizes, W8X21 and W14X38, have been used throughout the testing program. Each of these sections has a flange width to thickness ratio of 6.6, typical of that encountered in building applications. For the W14X38 sections, the overall test beam length was 20 feet, and for the W8X21 sections, 12 feet, so that the span-to-depth ratios were slightly less than 20 in each case. The stub column for the W8X21 beams was a W12X58 section, and a W12X96 column section was used with the W14X38 beams. Heavy column sections were selected to eliminate column panel zone distress as a contributing behavior factor, thereby confining the moment-rotation interaction to the connection elements. It is noted here that the same stub column sections were used repeatedly throughout the testing program without exhibiting any evidence of inelastic behavior. The general configurations of typical test members using the 14-inch and 8-inch deep beams are shown in Figures 2.1a, and 2.1b, respectively.

The web angles were centered on the beam web and proportioned initially for shears equal to 1-1/2 times the end reactions the member would experience at its A.I.S.C. allowable uniform load as a simply supported beam with a span equal to the length of the test beam (64). The lightest web angles used would thus be adequate, also, for shear forces corresponding to the increased loads that would be permitted if end connections had been used that were capable of developing one-half the beam allowable moment at working load.

The top and bottom flange angles were of the same size in a particular test specimen. Because the connections were to experience moment reversals, it was felt that a symmetric arrangement would reduce the parameters influencing the moment-rotation behavior, yet still represent a realistic design configuration. For each of the two beam sizes, three different thicknesses of the top and bottom angles were tested. Initial angle thicknesses were selected approximmately equal to the flange thickness of the beam being supported. It was reasoned that these sizes, together with the use of standard gages in the legs of the angles attached to the column flange, would provide the bending flexibility required of semi-rigid connection response. At the same time, the connections would be expected to exhibit sufficient moment capacity (and energy absorption capability) to contribute significantly to the resistance of a structural frame subject to earthquake induced loads.

The details of the connection angles used to frame the W14X38 and W8X21 beams to the stub columns are shown in Figures 2.2a and 2.2b, respectively (all-bolted specimens), and in Figure 2.3 (combined bolted-welded specimens). For the W14X38 beam tests, 3/8-inch, 1/2-inch, and 5/8-inch thick top and seat angles were used; these angles were of 5/16-inch, 3/8-inch, and 1/2-inch thickness for the W8X21 beam tests. For the 14-inch deep beams, the bolt diameter (3/4-inch and 7/8-inch), and the length and thickness of the web angles were varied for the static moment-rotation parameter studies. In addition, the length of the flange angle, and the gage and bolt spacing on the leg attached to the column flange were varied in one static test series of W8X21 beam specimens. Dimensions of the various connection elements are presented in the test specimen schedules, Tables 2.2 and 2.3 (all-bolted specimens using 3/4-inch and 7/8-inch diameter bolts, respectively), and Table 2.4 (combined bolted-welded test specimens).

Bolting of the connection elements was accomplished with an air wrench using the standard turn-of-the-nut method.(64) A325 flat hardened washers were used under the turned elements in all of the connections. The holes were all of standard size, 13/16-inch diameter for the 3/4-inch diameter bolts, and 15/16-inch diameter for the 7/8-inch diameter bolts.

Welding was accomplished using the shielded metal-arc process by a local steel fabricator in accordance with standard welding practice. All of the connection angles were welded to the beam sections in the fabricator's shop; the combined beam-connection assemblies were then delivered to the testing laboratory for bolting to the stub column by project personnel.

### 2.3 Testing Equipment and Test Procedures

A pair of duplicate specimens was tested simultaneously by framing the beams into a centrally loaded stub column using the arrangement shown schematically in Figure 2.4. The beam sections are supported at the ends by roller-type seats located at the beam mid-depth, and designed to allow longitudinal movement so that no direct axial forces would be introduced as the specimen deflects. The height of the beam supports is adjustable to accomodate the mounting of beams of different depth in the structural loading frame; photographs of the supports are shown in Figure 2.5.

Adjustable roller-type guides were used to ensure vertical movement of the stub column and, consequently, to prevent torsional displacements at the beam-column interface. The guides are comprised of rollers mounted on channels attached to the top and bottom of the stub column; the rollers ride against the flanges of the actuator supporting columns of the main structural loading frame. Photographs of the roller guides are shown in Figure 2.6. The rollers were oiled and checked periodically to permit freedom of movement in the vertical direction along the loading frame support columns. Photographs of the complete test set-up, including loading frame, beam supports, and roller guides are shown in Figures 2.7 and 2.8.

A 55 kip, servo-controlled, hydraulically actuated ram was used to apply load to the test members through the stub column, Figure 2.4. Local monitoring of the actuator displacement was accomplished through an X-Y plotter. In addition, the output data from the various measuring devices, described later, were transferred directly to the College of Engineering VAX 11/780 computer system for subsequent retrieval and graphic display; the basic elements of the recording system are illustrated schematically in Figure 2.9.

Using the test arrangement and loading system illustrated in Figure 2.4, the connections were subjected to combined shear and bending moment. For both the static and cyclic tests the controlled input variable was the rate and magnitude of actuator movement and, correspondingly, the displacement of the stub column. Displacement control was imposed to avoid the possibility of instantaneous collapse of the test member should complete separation occur in any of the connection elements during testing.

### 2.3.1 Static Tests

For each of the all-bolted static test specimens, the beam sections were first mounted in the end supports and then bolted to the stub column, which had been blocked in the loading frame to effect a centered, level member. The erection sequence proceeded as follows. For each beam size the actuator load cell was initialized to a load equal in magnitude and opposite in sense to the total weight of the specimen (beams plus stub column) less one-half the weight of the beams. Having thus established the initial load cell reading, the actuator was next attached to the top of the stub column. The bolts were then loosely inserted in all of the connection elements. Power was supplied to the actuator to maintain the specimen in a level position as the supporting blocks were removed from beneath the stub column. The bolts in the legs of the angles attached to the column flanges were then tightened, followed by tightening of the remaining bolts in the angle-to-beam connections. At this point the load on the specimen caused by fit-up (recorded by the load cell) was removed by adjusting the position of the stub column. Thus, the average static moment at the beam-column interface, resulting from the erection operations, was essentially null. This established the point of origin for the subsequent load-displacement (and moment-rotation) plots; the static moments thereafter calculated from the load-cell output thus excluded the weight of the specimen from the measured moment-rotation response of the connection. (The same installation and load initialization procedure was used for the bolted-welded test specimens except, of course, that erection consisted only of bolting the connection angles to the stub column, the angles having been previously shop welded to the beam sections).

It should be noted that, as a result of member configuration tolerances, slight misalignment of the connection elements, and welding distortions, local residual stresses were introduced during the erection operations. All specimens were prepared by area fabricators using standard shop practice, so that the fit-up stresses would be of the order encountered during normal field erection.

For a select number of test specimens, strain gages were mounted on both faces of the leg of the top flange angle attached to the column to determine local strains introduced during the bolting operation, and to monitor the surface conditions as testing progressed. In addition, for all tests, LVDTs were mounted to each flange of the beam sections on either side of the stub column, and seated against the flanges of the column. The device used to seat the LVDT probe and to accomodate the rotations developed during a test is illustrated in Figure 2.10. The data from a pair of LVDTs mounted on one beam section were used to determine the angle of rotation of the connection as testing progressed. The LVDT data were compared, also, to rotations calculated from the actuator displacement readings.

Besides the direct strain measurements and LVDT displacements, light gage aluminum channel-shaped devices with attached strain gages were used to detect slip between the top and bottom flange angles and the elements to which they were connected. These devices (slip monitors) were intended only to record the presence of major slip, not the magnitude thereof.

After a specimen had been mounted in the loading frame and the displacement-measuring devices attached, the test was undertaken using an actuator displacement rate of 1.0 in./min. for the 14-inch deep beams, and 0.75 in./min. for the 8-inch beams (except for specimen 8S7, for which a rate of 1.0 in./min. was used). The upward (downward for specimen 8S4) movement of the actuator (and stub column) was continuous, with load, displacement, LVDT, strain gage, and slip indicator output each being sampled two times per second. In addition, the actuator load and displacement were recorded locally on an X-Y plotter to allow continuous visual monitoring of the system behavior. A test was concluded when the actuator displacement reached 4 inches for the 20-foot long W14X38 beam specimens, and 3 inches for the 12-foot long W8X21 beams.

### 2.3.2 Cyclic Tests

The preparation and installation of the specimens in the cyclic tests was the same as that used for the static loading, described above. During mounting of a test member in the loading frame, the initial load setting was established to exclude the contribution of the weight of the specimen to the static moment at the connection in the manner described above for the static tests. In addition, the same arrangement of LVDTs and slip monitors as in the static tests was employed for measuring joint rotations and determining slip in the flange angles, respectively.

2.3.2.1 Low-to-High Amplitude Block Tests

For the low-to-high amplitude cyclic tests, Figure 2.11a, an initial range of actuator displacement of 0.4 inches (0.2-inch amplitude) was selected, approximately 10 percent of the total displacement used in the static tests of the 14-inch beams. The initial displacement amplitude was intended to produce a hysteresis loop representing minimal non-linear response (estimated from the corresponding static moment-rotation curves). In all tests, the full range of controlled displacement was set to provide equal displacement amplitudes about the initial horizontal beam position. Full reversal of displacement was chosen to provide the symmetry required for comparison of test data from beams of different depths, and to approximate the reversals that might be exhibited under extreme conditions during seismic loading.

For the specimens tested in the initial study (using 3/4-inch diameter bolts), the first displacement cycle in each test was applied sinusoidally using a frequency of 0.10 Hz. This relatively slow rate of actuator movement was selected to allow visual monitoring of the load- displacement relationship, to ensure that the strain and displacement measuring devices were recording properly, and to check the alignment of the lateral support devices. Additional individual cycles were then applied using a frequency of 0.10 Hz or 0.25 Hz until a stable hysteresis loop was established; usually this occurred within a few cycles after the initial cycle had been run. To complete the sequence, ten additional cycles were applied continuously at a frequency of 0.25 Hz, so that a total of 12 to 15 complete cycles were normally imposed at one displacement amplitude. The displacement range was then increased to 0.8 inches and the above procedure repeated; i.e., several individual cycles followed by a continuous run of 10 cycles at 0.25 Hz. Each sequence was followed by an increase of 0.4 inches in the displacement range and the process repeated, resulting in displacement-time histories typified by the block arrangement illustrated in Figure 2.11a.

For the specimens tested in the current investigation (using 7/8-inch diameter bolts), a constant test frequency of 0.25 Hz was used at each displacement amplitude. Otherwise, testing followed the same procedure as that described in the previous paragraph for specimens tested in the initial study.

2.3.2.2 High-to-Low Amplitude Block Tests

The high-to-low amplitude cyclic tests, Figure 2.11c, were intended to follow basically the reverse time-displacement histories as those imposed in the low-to-high amplitude tests, for specimens of duplicate geometry. However, for one of the specimens tested under these conditions, 8B1, fatigue cracking was not as extensive, at the conclusion of the intended block history, as that exhibited by the corresponding low-to-high test specimen, 8C3. Thus, to complete the testing of specimen 8B1, the displacement amplitude was again increased to the same magnitude, 1.2 inches, as that of the first block of cycles in the sequence. The fatigue crack then grew considerably larger during the first cycle of the higher amplitude, and the test was stopped.

The other specimen tested under the high-to-low amplitude history, 14B1, exhibited appreciable fatigue cracking during the first block of imposed cycles; the cracks continued to grow, albeit at a reduced rate, during the remainder of the test. Testing of specimen 14B1 was concluded after five blocks of loading at decreasing displacement amplitudes (compared to nine plus blocks sustained by its companion specimen, 14C3), due to the presence of extensive cracking in two of the beam flange angles.

2.3.2.3 Constant Amplitude (Fatigue) Tests

The constant displacement amplitude cyclic (fatigue) tests, Figure 2.11b, were conducted at a frequency of 0.25 Hz (with some exceptions, as noted in the tables in which the fatigue test data are reported). For several of the specimens, a number of "half" cycles (displacement excursions from the null position to the maximium displacement amplitude and return) were applied before proceeding with the full reversal test cycles. This was done to apply several initial cycles of tensile strain to the top flange angles in an effort to promote the initiation of fatigue cracking first in those angles, so that the subsequent crack propagation could be easily monitored with the specimens mounted in the testing machine. It should be noted that fatigue cracking did initiate first in the top flange angles to which the half cycles had been applied before continuing with the full reversal cycles.

All of the cyclic tests were terminated when observed fatigue cracking had progressed partially across the face(s) of one or more of the flange angles at the toe of the fillet (see following discussions of test results). No test was extended to the point of complete fracture of a connection element.

# III. EXPERIMENTAL INVESTIGATION

## 3.1 Static Tests

### 3.1.1 Scope of Investigation

Eighteen all-bolted specimens were tested in the static test investigations, eleven in the initial study (63), and seven in the current program. In addition, two combined bolted-welded members were tested in the latter investigation. The purpose of this phase of the study was twofold: (1) to quantify the static moment-rotation behavior of the semi-rigid beam-column connections; and (2) to identify and measure the effect of various geometric parameters on the connection behavior. The static tests were intended, also, to serve as a frame of reference against which the cyclic hysteresis behavior of the connections could be compared.

The geometric variables that were altered in the parametric study included: the depth of the beam sections (W8X21 and W14X38 sections), the thickness and length of the top and bottom beam flange angles, the gage and spacing of bolts in the leg of the flange angles connected to the column flange, the bolt diameter (3/4-inch and 7/8-inch), and the thickness and length of the web angles.

### 3.1.2 Test Results

Summaries of the test results for the static test investigations are presented in Table 3.1 (bolted specimens, 3/4-inch diameter bolts), Table 3.2 (bolted specimens, 7/8-inch diameter bolts), and Table 3.3 (bolted-welded specimens). Details of the corresponding specimen geometries are reported in Tables 2.2, 2.3, and 2.4, respectively.

Tables 3.1-3.3 include the initial stiffness of the connections (initial slope of the moment-rotation curve). The slope was measured tangent to the moment-rotation ($M-\phi$) curve at the origin as the derivative of a second degree polynomial fit through the first several data points. The tables also list: (1) the slope and intercept moment of a secant line from the origin and intersecting the $M-\phi$ curve at a rotation of $4.0X10^{-3}$ radians; and (2) the moment, and the slope tangent to the $M-\phi$ curve at $24X10^{-3}$ radians, a rotation achieved in all of the static tests. Although the latter slope offers a measure of the degradation of connection stiffness as the applied moment increases, it should not be interpreted as a constant or final slope for a specific connection. In some tests, the connections continue to "soften" as the moment increased, never actually reaching a constant $M-\phi$ slope at the conclusion of loading. The tangent slope at the rotation of $24X10^{-3}$ radians does, however, allow comparisons to be made among the various connections at a common point, as well as quantifying the degree of connection softening in a particular test. Similarly, the secant slope offers an additional indication of the early stiffness of the connection. In some respects the secant slope may be more representative than the initial tangent slope, because the latter is highly sensitive to any irregularities in the first few data points from which it was calculated.

The moments reported in Tables 3.1-3.3 (and the figures to follow) were calculated directly from the actuator load cell readings. To obtain the corresponding $\phi$ values, initially the displacements measured by the LVDTs mounted to each flange of the beam were converted to relative rotations between the flange of the stub column and the end of the beam. The rotations were also independently calculated using the actuator displacement and the beam span by considering rigid body movement of each beam segment and correcting for elastic curvature from bending of the beam. Because of the high stiffness of the stub column, and the transfer of load in friction between the connecting elements (except for the slip encountered in three tests) the beam did rotate essentially as a rigid body with respect to the column flange, which was maintained in a vertical position by the lateral support system.

A typical comparison of the M-$\phi$ relationship obtained from LVDT data with the results obtained from the displacement measurements is shown in Figure 3.1. The curves labeled East and West represent the data from individual pairs of LVDTs mounted to the flanges of each of the two beam segments framing into the central stub column. It can be seen from Figure 3.1 that the LVDT data obtained from each of the two connections in the test member were very close, and consistent with the M-$\phi$ curve calculated using the actuator displacements. Consequently, the data reported in Tables 3.1-3.3, and plotted in the figures to follow, use rotations calculated from actuator displacements; the results may thus be considered to represent an "average" of the behavior exhibited by the connections attached to each face of the stub column.

For each of the static tests, the beams were observed to rotate, with respect to the stub column, by pivoting about a point near the surface of the beam compression flange, as illustrated in Figures 3.2a (bolted specimens) and 3.2b (bolted-welded specimens). The heel of the tension flange angle was observed to "curl around" the end of the beam flange in the all-bolted specimens (Figure 3.2a); however, this deformation pattern was less pronounced in the bolted-welded specimens (Figure 3.2b), as the weld return served to restrain the movement of the heel of the angle. It should be noted that the beam set-back was 1/2-inch for all of the test specimens (Figures 2.2, 2.3).

Photographs of typical deformation patterns observed in the connection flange and web angles are shown in Figures 3.3 and 3.4, respectively. With the exception of specimens 14S2, 8S2, and 8S10, post-test inspection revealed no apparent inelastic deformation in either the flanges or the web of the beams. Similarly, no distress was evident in the stub columns, because, as discussed previously, intentionally heavy sections were selected to confine the study to the response of the beams and their connection elements.

In the testing of specimen 14S2, major slip first occurred when approximately one-half the final actuator displacement had been reached. After the specimen had been dismantled, the holes in both legs of the tension flange angle and in the beam flange were elongated, as were the holes in the beam web. The plastically deformed steel formed a protruding lip on the bearing surface of each of the elements exhibiting the elongated holes. Post-test inspection of specimens 8S2 and 8S10 indicated patterns of distress in the connection elements similar to those observed in specimen 14S2.

At the conclusion of each of the static tests, there was no rupture nor were there any cracks observed by visual inspection in any of the fasteners or connection elements.

### 3.1.3 Discussion of Static Test Results

#### 3.1.3.1 Bolted Test Specimens

The moment-rotation curves for the tests reported in Tables 3.1 and 3.2 are plotted in Figures 3.5 through 3.15. The figures provide comparisons of the initial stiffness and non-linear connection behavior for test members in which individual geometric parameters were altered. General observations with respect to these test results are discussed in the following paragraphs.

From practical design considerations, one of the most apparent means of increasing the initial stiffness and total moment transfer capability in a connection of the type studied is to increase the thickness of the angles attached to the top and bottom flanges of the supported beam. This flange dimension was, therefore, the principal variable investigated in both the static and cyclic test series.

Figure 3.5 presents the moment-rotation curves for two W14X38 beam specimens fastened with 3/4-inch diameter bolts, one (14S1) with flange angles of 3/8-inch thickness, and the other (14S2) with 1/2-inch thick flange angles. Both the initial stiffness and the moment developed at comparable rotations are greater for specimen 14S2. For example, at a rotation of $24X10^{-3}$ radians, specimen 14S2 developed a connection moment of about 950 k-in., or almost 1-1/2 times the 668 k-in. moment of specimen 14S1. The rotation of $24X10^{-3}$ radians has been used for purposes of comparison among the test members in Tables 3.1-3.3 and in this discussion because it was a number easily reached in all of the static tests. The rotation corresponds to a deflection of approximately 2-3/4 inches for the 14-inch beam tests, or approximately four times the mid-span deflection a W14X38 beam, 20 feet long, would exhibit as a simply supported member at its A.I.S.C. allowable uniform load (assuming full lateral support). For the 8-inch beam tests, a rotation of $24X10^{-3}$ radians corresponds to a deflection of about 1.6 inches, four times the deflection, at allowable load, of a 12-foot long simply supported beam using the W8X21 sections. These deflections were considered to be reasonably representative of a severe ductility demand, even under seismic loading conditions.

Specimen 14S2 exhibited major slip in the leg of the tension flange angle bolted to the beam (and in the legs of the web angles attached to the beam web) at a rotation of approximately $12X10^{-3}$ radians, followed by slip in the leg of the flange angle bolted to the column face at approximately $20X10^{-3}$ radians. For the static tests, in which the rate of actuator movement was the controlled input variable, slip as indicated in Figure 3.5 corresponds to a gradual drop in moment until bearing is achieved in the connected elements. With bearing established, the stiffness of the connection prior to slip is regained, with no anticipated permanent degradation in the capacity of the connection (barring premature bolt shear failure or tear-out in the connected parts).

The effect of flange angle thickness on the moment-rotation behavior of W14X38 beam connections using 7/8-inch diameter bolts is shown in Figure 3.6. As with the members fastened with 3/4-inch diameter bolts, the initial stiffness and the moment developed at comparable rotations increased with increasing flange angle thickness. The initial slope of the moment-rotation curve was $247X10^3$ k-in./radian for specimen 14S5 (3/8-inch thick angles), $286X10^3$ and $258X10^3$ k-in./radian for specimens 14S6 and 14S9, respectively (1/2-inch thick angles), and $579X10^3$ k-in./radian for specimen 14S8 (5/8-inch thick angles). Similarly, at a rotation of $24X10^{-3}$ radians, the connection moment increased from 736 k-in. for specimen 14S5 (3/8-inch thick angles) to an average of 1038 k-in. for the two specimens with 1/2-inch thick flange angles, and 1561 k-in. for specimen 14S8, with 5/8-inch thick angles. It should be noted also that in contrast to specimen 14S2, which was fabricated using 3/4-inch diameter bolts, no slip was exhibited by the 14-inch beam specimens fastened with the 7/8-inch diameter bolts.

The effect of bolt diameter on the static moment-rotation behavior of the 14-inch beam specimens is illustrated in Figures 3.7a (specimens with 3/8-in. thick flange angles) and 3.7b (specimens with 1/2-inch thick flange angles). Comparison of Figures 3.7a and 3.7b (and Tables 3.1, 3.2) shows that the initial stiffnesses of the connections (initial slope of the M-$\phi$ curve) are approximately the same for specimens with flange angles having the same thickness. Beyond the initial portions of the M-$\phi$ curves, however, the connections fastened with 7/8-inch diameter bolts developed moderately larger moments, at comparable rotations, than those fabricated using the 3/4-inch diameter bolts. For example, specimens 14S6 and 14S9 developed an average moment of approximately 1040 k-in. at $24X10^{-3}$ radians, compared to a moment of 947 k-in. for specimen 14S2. (Although specimen 14S2 exhibited major slip, a projection of the M-$\phi$ curve that might be expected had slip not occurred would still fall below those of 14S6 and 14S9). Similarly, specimen 14S5 developed a moment of 763 k-in. at a rotation of $24X10^{-3}$ radians, about 14 percent higher than the moment for specimen 14S1 at that rotation, 668 k-in.

The closeness of the initial slopes for the 14-inch beam specimens fastened with the 7/8-inch and 3/4-inch diameter bolts was not anticipated, as it was expected that the connections with the 7/8-inch diameter bolts would initially be stiffer, by developing an increased clamping force between the connected elements, by having a smaller clear distance between the bolt head (and washer) and the toe of the fillet in the angle, and by having a smaller clear distance between the two bolts on the column gage line. No explanation is offered at this time for the difference between the anticipated and observed effect of bolt diameter on initial connection stiffness for the 14-inch beam specimens (and for the 8-inch beam specimens, as discussed subsequently).

In contrast to the influence of flange angle thickness on the moment-rotation behavior of the 14-inch beam specimens, moderate changes in the size of the web angles did not as significantly affect the connection performance. Figures 3.8 and 3.9 show the effect of web angle thickness and length, respectively, on the M-$\phi$ relationships for W14X38 sections with 3/8-inch thick flange angles. For example, increasing the thickness of the web angle by 50 percent, from 1/4-inch to 3/8-inch (specimens 14S1 and 14S4), produced a corresponding increase in moment, at a rotation of $24X10^{-3}$ radians, of approximately 25 percent, from 668 k-in. to 822 k-in. An apparently lesser influence on post-elastic moment capacity was exhibited by a change in the length of the web angles, as comparison of specimens 14S1 and 14S3, Figure 3.9, indicates. At a rotation of $24X10^{-3}$ radians, specimen 14S3, with web angles having a length of 5-1/2 inches, developed a moment of 652 k-in., some 17 k-in. less than the 668 k-in. moment of specimen 14S1, which had the standard 8-1/2 inch long web angles. It should be noted that specimen 14S3 had the only non-symmetrical connection in the test series, with the legs of the web angles attached to the beam column stub each using two bolts placed in the upper two holes of the standard detail, Figûre 2.2a. In this location, with the web angles closer to the beam tension flange, they would be expected to contribute differently to the moment transfer capability of the connection than if they had been positioned at mid-depth, closer to the pivot point of the connection. The arrangement used is of practical importance, however, in that it represents a normal positioning of web angles designed for shear transfer in beams using simple (flexible) framing.

The influence of flange angle thickness on moment-rotation behavior was examined also for the W8X21 beam specimens, the results of which are shown in Figures 3.10a, 3.10b, and 3.11. Figure 3.10a presents a comparison of the M-$\phi$ curves for specimen 8S1, with a flange angle thickness of 5/16-inch, and specimen 8S2, with 3/8-inch thick flange angles. The gage in the legs of the flange angles attached to the stub column was 2 inches, and the angle length was

6 inches in both of these specimens. The bolt diameter was 3/4 inches. Although comparison of the initial portion of the moment-rotation relationships indicated a considerably stiffer connection for specimen 8S2 relative to that of 8S1 ($123.4X10^3$ k-in./radian vs. $66.7X10^3$ k-in./radian), and a correspondingly greater moment transfer capability, specimen 8S2 exhibited major slip in the connection elements at a rotation of approximately $16X10^{-3}$ radians. Unlike specimen 14S2, in which slip also occurred, specimen 8S2 did not regain nor approach the stiffness it had maintained prior to slip. The stiffness continued to degrade with continued loading, the slope of the M-$\phi$ curve reducing to only $1.5X10^3$ k-in./radian at a rotation of $24X10^{-3}$ radians. As there were no cracks nor other geometric irregularities observed in the connection elements of specimen 8S2, either during testing or upon post-test visual inspection, no explanation is offered for the singular behavior of this specimen.

In Figure 3.10b, the moment-rotation curves for specimens 8S6 (5/16-inch flange angle thickness) and 8S7 (3/8-inch angle thickness) are compared. In these specimens, the bolt diameter was 3/4 inches, the gage in the legs of the flange angles attached to the column was 2-1/2 inches, and the angle length was 6 inches. As with the 14-inch deep beam tests, both the intitial stiffness and the moments developed at common rotations were greater for the W8X21 beam connection having the heavier flange angles. For example, the 1/16-inch increase in flange angle thickness of specimen 8S7 over that of specimen 8S6 effected a greater than 50 percent increase in moment (381 k-in. vs. 244 k-in.) at a connection rotation of $24X10^{-3}$ radians. As no slip occurred in either of these two tests, the comparative behavior of the two specimens, shown in Figure 3.10b, may be considered representative of similar connections framing the 8-inch deep beams.

Figure 3.11 presents a comparison of the M-$\phi$ curves for specimens 8S8 (5/16-inch thick flange angles), 8S9 (3/8-inch thick angles), and 8S10 (1/2-inch thick angles). For each of these specimens the bolt diameter was 7/8 inches, the gage in the legs of the flange angles attached to the column was 2 inches, and the angle length was 6 inches. Again, the initial connection stiffness and the moments at comparable rotations increased with increasing flange angle thickness. At $24X10^{-3}$ radians, the connection moment developed in specimen 8S8 was 380 k-in., increasing to 423 k-in. in specimen 8S9, and 634 k-in. for specimen 8S10. It may be noted, also, that specimen 8S10 exhibited major slip at $5.3X10^{-3}$ radians; this specimen had the thickest flange angles, 1/2 inch, of all the W8X21 beam members. (It was also the only specimen fastened with 7/8-inch diameter bolts that exhibited slip in either the static or cyclic test series.) Specimen 8S10 was similar to 14S2 in that it was able to regain, after slip, the stiffness it held just prior to the occurrence of the slip (c.f., Figures 3.5 and 3.11).

The effect of bolt diameter on the moment-rotation behavior of the 8 inch beam specimens is illustrated in Figures 3.12a (specimens with 5/16-inch thick flange angles) and 3.13b (specimens with 3/8-inch thick flange angles). As with the 14-inch beam specimens discussed previously, there were no consistent, significant differences in the initial stiffnesses of the specimens fabricated using the two bolt sizes. In fact, the initial slope of the M-$\phi$ curve for specimen 8S2, with 3/4-inch diameter bolts ($123.4X10^3$ k-in./radian), is greater than that of specimen 8S9, $104X10^3$ k-in./radian, which had 7/8-inch bolts as the fasteners. It should be noted, again, that the behavior of specimen 8S2 is somewhat of an anomaly, in that it was the only specimen, of all of those tested under either static or cyclic loading, that did not regain a positive slope to the moment-rotation curve after slip occurred. Thus, comparison of the moments developed at either $4X10^{-3}$ or $24X10^{-3}$ radians cannot be significant for these two specimens. Additional data, including tests of specimens with a greater range of flange angle thicknesses, are needed before the relative effect of bolt diameter on connection behavior can be better quantified.

The effect of varying the gage in the leg of the flange angle attached to the column flange was examined in the W8X21 beam test series. With an angle thickness of 3/8 inch, gages of 2, 2-1/2, and 4-1/2 inches were used in specimens 8S2, 8S7, and 8S4, respectively. The bolt diameter was 3/4 inches for each of these specimens. To accommodate the 4-1/2 inch gage in specimen 8S4, a 6X6X3/8 angle was used in place of the smaller 6X3-1/2X3/8 and 6X4X3/8 angles used in the other two specimens. Specimens 8S1 and 8S6, with flange angles of 5/16-inch thickness, had gages of 2 inches and 2-1/2 inches, respectively. Complete details of the dimensions for these specimens are presented in Table 2.2.

The static test results for these five specimens are summarized in Table 3.1. For the two members having 5/16-inch thick flange angles, the moment-rotation curves are plotted in Figure 3.13a; the curves for the three specimens with flange angles of 3/8-inch thickness are compared in Figure 3.13b. As expected, changes in flange angle gage had a pronounced effect on both the initial slope of the M-$\phi$ curve, and on the moment capacity of the connection at large displacements. For example, with the 3/8-inch thick flange angles, the initial connection stiffness decreased from $123.4X10^3$ k-in./radian to $15.3X10^3$ k-in./radian as the angle gage was changed from 2 inches to 4-1/2 inches (specimens 8S2 and 8S4). Specimen 8S7, with a gage of 2-1/2 inches, exhibited an initial M-$\phi$ slope of $48.0X10^3$ k-in./radian, intermediate in stiffness between those of the other two members. At a rotation of $24X10^{-3}$

radians, specimen 8S7 achieved a moment of approximately 380 k-in., more than twice the 165 k-in. moment of specimen 8S4 at that rotation. It should be noted again, that specimen 8S2 sustained slip at about $16X10^{-3}$ radians, after which its moment-rotation curve reduced to a slope of only $1.5X10^{3}$ k-in./radian at a rotation of $24X10^{-3}$ radians. This behavior is not considered indicative of the performance expected of the connection had slip not occurred; consequently, comparison of specimen 8S2 with the other two members at large displacements is not appropriate.

The two connections with 5/16-inch flange angles exhibited the same relative response as those with 3/8-inch angles; i.e., decreasing the gage results in an increase in initial connection stiffness and subsequent moment capacity at large displacements. For specimen 8S1 (2-inch gage), the initial slope of the M-$\phi$ curve was $66.7X10^{3}$ k-in./radian, almost double the $39.5X10^{3}$ k-in./radian slope for specimen 8S6 with a 2-1/2 inch gage. Similarly, at a connection rotation of $24X10^{-3}$ radians, specimen 8S1 developed a moment of 329 k-in., significantly higher than the 244 k-in. moment in specimen 8S6.

For the W8X21 beam sections, the effect of changing the length of the flange angle was examined. As indicated in Table 2.2, with all other connection dimensions remaining the same, a flange angle length of 6 inches was used for specimen 8S1, and a length of 8 inches used for specimen 8S3. The one-third increase in flange angle length resulted in a corresponding increase of about one-third in the initial connection stiffness ($104.7X10^{3}$ k-in./radian vs. $66.7X10^{3}$ k-in./radian), and the development of higher moments at large displacements (422 k-in. vs. 329 k-in. at a rotation of $24X10^{-3}$ radians). The complete moment rotation curves for specimens 8S1 and 8S3 are plotted in Figure 3.14.

Finally, in Figure 3.15, a comparison is made between a W14X38 section specimen (14S1) and a W8X21 specimen (8S5) in which the dimensions of all of the connection elements were the same except for the length of the web angle (8-1/2 inches for 14S1, and 5-1/2 inches for 8S5). As seen from the M-$\phi$ curves of Figure 3.15 and the data recorded in Table 3.1, the initial slope of the moment-rotation curve is increased significantly, from $76.7X10^3$ k-in./radian to $195.0X10^3$ k-in./radian, for the W14X38 specimen in comparison to the W8X21 member. Similarly, the moment developed at $24X10^{-3}$ radians was 668 k-in. for specimen 14S1, about double the 337 k-in. moment of specimen 8S5. The increase in initial connection stiffness and moment development capability are to be expected, as the deeper beam section provides, at comparable rotations, a larger displacement of the tension flange angle (and larger force in the angle) together with a larger moment arm from the position of the tension flange angle to the pivot point of the connection in the vicinity of the compression flange.

#### 3.1.3.2 Bolted-Welded Test Specimens

The moment-rotation curves for the two bolted-welded test specimens are shown in Figure 3.16. Numerical values for the initial slope, secant slope at $4.0X10^{-3}$, and slope at $24X10^{-3}$ radians are presented in Table 3.3, together with the moment developed at both $4.0X10^{-3}$ and $24X10^{-3}$ radians. As expected, specimen 14WS2, fabricated using 1/2-inch thick flange angles, exhibited the larger initial stiffness, and developed larger moments at comparable rotations than did specimen 14WS1, which had 3/8-inch thick flange angles.

Comparison of the data in Table 3.3 for the bolted-welded specimens with the test results for comparable all-bolted specimens 14S5 (3/8-inch flange angle thickness; 7/8-inch bolt diameter), and specimens 14S6 and 14S9 (1/2-inch thick angles, 7/8-inch bolt diameter) indicates that the initial stiffnesses of the bolted-welded specimens are somewhat higher than those of the all-bolted specimens (Table 3.2). This may be attributed to the greater restraint against movement of the heel of the angle at the end of the beam flange in the welded elements, as illustrated in Figure 3.2. The weld return, together with the continuous longitudinal fillet welds connecting the top and seat angles to the beam flange, did not permit the angles the freedom to curl around the beam end (as in the all-bolted specimens) in accommodating the rotations between the end of the beam and the flange of the column. The greater restraint thus imposed by the welded connection resulted in a larger initial stiffness for those specimens in comparison to the all-bolted members, where greater relative movement was more easily achieved.

In addition to the higher initial stiffnesses, the bolted-welded specimens developed moderately larger moments than those in the bolted specimens at comparable rotations. For example, specimen 14SW2 developed a moment at 1235 k.-in. at $24X10^{-3}$ radians, almost 20 percent larger than the approximately 1040 k.-in. average moment for specimens 14S6 and 14S9. Similarly, specimen 14SW1 developed 923 k.-in. at $24X10^{-3}$ radians, compared to 763 k.-in. for specimen 14S5 at that rotation. However, because only two specimens fabricated in the bolted-welded configuration were tested in this study, the above observations should be considered preliminary, and not necessarily indicative of the relative performance of the welded specimens with respect to the all-bolted specimens when a more complete range of section depths, and flange and web angle sizes are considered. Such tests have been proposed as part of the continuation of the current investigation.

The summary of the static tests in the following section, 3.1.4, refers to the behavioı of all-bolted test specimens; generalizations regarding the performance of the combined bolted-welded specimens were not considered appropriate from the limited data available at this time.

### 3.1.4 Summary of Static Test Results

For all of the specimens tested in the static test series, the connections exhibited a moment-rotation response which becomes non-linear relatively early in the loading sequence. This non-linearity is contributed to, in part, by local yielding and eventual plastic hinge formation at each toe of the fillet in the flange angle attached to the tension flange of the beam. Another hinge develops in the vicinity of the bolt line in the leg of the flange angle attached to the column, together with progressive plastic hinging in the outstanding legs of the web angles. It is of interest to note, however, that each of the connections developed a moment greater than two times the capacity that would be predicted by simple plastic hinging mechanisms in the leg of the tension flange angle attached to the column flange and in the legs of the web angles; further analysis of this post-elastic connection response is presented below.

Inspection of Figures 3.5 through 3.15 shows that each of the test specimens (with the exception of specimen 8S2) was able to develop increasing moments through the full range of rotations imposed during the test. In fact, a nearly constant or slightly decreasing positive M-$\phi$ slope was observed during the latter stages of loading for these static test specimens. It is believed that this nearly constant stiffness at large deformations can be attributed to, in part, to material strain hardening, and to the consequences of significant changes in the geometries of the connecting angles. The increasing deflection of the tension flange angle at large connection rotations produces a continuous change in the internal force distribution in the legs of the angle, with axial tension becoming an increasingly larger factor (relative to bending) as the angle progressively "flattens out." A gradual transition from a predominantly flexural to a combined flexural-axial response in the tension flange angle, with the accompanying strain hardening, can thus be expected to contribute to the ability of the connection to achieve a considerably greater moment capacity than that predicted by a simple plastic hinge mechanism, as noted above.

From the static tests, was been found that the geometric parameters that most significantly affect the static moment-rotation performance of the semi-rigid connections investigated were: the depth of the beam section to which the connection elements were framed; the thickness of the flange angles; and the gage in the leg of the flange angles attached to the column flange. Although the data are inconclusive, it appears that bolt diameter has a minimal effect on the initial stiffness of the connections; however, increasing the bolt diameter effects a corresponding increase in moment capacity at large rotations (beyond about $4X10^{-3}$ radians). Variations in the length of the flange angles, and in the length and thickness of the web angles, had a less pronounced effect on connection response than the other parameters listed above.

Analytical models proposed in the initial investigation (63) to predict the initial stiffness of the semi-rigid connections have been applied to the specimens tested in the current study. Comparisons of the predicted stiffnesses with the experimental data from the static test investigations are presented in Section 4.1. Further, using the results of the parametric study, a semi-empirical analytical model has been developed to generate complete non-linear moment-rotation curves for the connections; the results of this phase of the study are reported also in Section 4.1.

## 3.2 Cyclic Tests

### 3.2.1 Scope of Investigation

The purpose of this phase of the investigation was twofold: (1) from the variable amplitude cyclic tests, to quantify the cyclic moment-rotation behavior of the semi-rigid beam-column connections; and (2) from the constant amplitude cyclic tests, to obtain base-line fatigue data for connections of varying stiffness. The objectives of the variable amplitude tests have been to determine energy absorption capabilities under complete reversal of moment, and to qualitatively describe the characteristics of the attendant hysteresis loops. From the constant amplitude tests, fatigue life relationships have been developed for application to appropriate cumulative damage models for predicting total fatigue lives of connections subjected to variable amplitude displacement histories. The fatigue tests have served, also, to provide additional data from which the total energy absorption capacities of connections of varying stiffness could be evaluated.

The intent of the cyclic tests was to examine the connection response to moment reversals, not the behavior of a complete subassemblage under seismic loading. Consequently, the rate of loading in the cyclic tests was "quasi-static," and was not intended to suggest that the loading would be the direct result of actual earthquake induced ground motions.

### 3.2.2 Variable Amplitude Block Tests

Seven specimens were tested under the low-to-high amplitude block displacement histories; the geometric parameters that were varied in this test series included the beam depth (W14X38 and W8X21 sections), the flange angle thickness, and the bolt diameter. Two specimens were tested under high-to-low amplitude block histories; one was an 8-inch beam connection, the other was a W14X38 beam connection. Details of the test specimens are reported in Tables 2.2 and 2.3; the testing procedures are described in Section 2.3.2.

#### 3.2.2.1 Test Results

As discussed previously, all of the cyclic test specimens were subjected to complete displacement reversal to facilitate comparison of the hysteresis loops generated for beams of different depth. The tests were terminated when observed fatigue cracking had progressed partially across the faces of the flange angles. No test was extended to the point of complete rupture of a connection element. No slip was observed during the cyclic tests.

Figure 3.17a shows front and rear views of a top flange angle from specimen 14C1 after the test was stopped. It can be seen that cracking had progressed over most of the width at the toe of the fillet in the leg bolted to the column flange. (It should be noted that, for the majority of the cyclic test specimens, fatigue cracking initiated, in one or more of the flange angles, at the toe of the fillet in the leg bolted to the beam flange; otherwise, the appearance of the crack patterns is similar to that shown in Figure 3.17a).

After disassembly of test specimen 14C1 (and several of the other cyclic test specimens), it was discovered that significant cracking had progressed in the vicinity of the bolt hole under the washer. Although the formation of fatigue cracks had an observable effect on the load-displacement hysteresis loops, the decrease in maximum load was usually a small percentage of the maximum load for the stabilized

The permanent distortions shown in the flange and web angles of specimen 14C1, Figure 3.17b, give an indication of the large deformations experienced by the connection angles during the cyclic tests.

As mentioned previously, the specimens were intended to simulate, within reason, actual connections in situ. During the erection procedure, it would be natural to seat the beam on the bottom flange angle for support, thereby aligning the bottom angle as required at the expense of the top angle. As a consequence, the top angle would be subjected to the greater initial strains resulting from any lack of fit during the bolting procedure. This same erection sequence was followed in the test program, and is believed to explain the tendency of the top angle to form the first cracks in most of the cyclic tests. Also, the hysteresis loops tended to exhibit signs of stiffness degradation first in the negative moment region, corresponding to tension in the top flange angle.

Summaries of the cyclic test results are presented in Tables 3.4 through 3.8 for the W14X38 beam specimens, and in Tables 3.9 through 3.12 for the connections framed to the W8X21 sections. Complete hysteresis loop traces at each displacement amplitude for each of the nine test specimens are shown in Figures 3.18 through 3.26. The tables include the actuator displacement amplitude, the number of cycles imposed at each amplitude and test frequency, and the cumulative number of test cycles. For each displacement amplitude, the range of rotation (peak-to-peak) and the range of moment is given for the hysteresis loops. The area enclosed by a single hysteresis loop is given as well as the cumulative loop area. For the specimens tested in the initial study (14C1, 14C2, 8C1, 8C2) the areas of the hysteresis loops, other than for the single cycles reported in the tables, were calculated as the average of the first and last loop areas at a particular displacement amplitude and test frequency. For those specimens investigated in the present study (14C3, 14C4, 14B1, 8C3, 8B1), the areas of all of the hysteresis loops at each displacement amplitude were taken to be the same as the single reported area for purposes of calculating cumulative hysteretic energy.

### 3.2.2.2 Discussion of Test Results

In the variable amplitude cyclic test series, stable hysteresis loops were maintained, for the 14-inch beam specimens, within a few cycles after a change in amplitude was imposed relative to the preceding displacement under the block-type loading. For several of the 8-inch deep beam connections, a continual, though small, softening (loss of moment) was noted for each progressive cycle at a constant displacement amplitude; however, the succeeding hysteresis loops were otherwise similar in appearance. As seen in Figures 3.18 through 3.26, the moment-rotation behavior of the connections was characterized by hysteresis loops of continually decreasing slope for relatively small displacements in the non-linear range. In contrast, the loops exhibited a moderate "pinching" effect at larger amplitudes, the degree of pinching being more pronounced in the W14X38 beam connections than in the W8X21 members. This increase in stiffness observed toward the tip of each hysteresis hoop may be attributed, in large measure, to the changing geometry of the connection during each half cycle of loading; this behavior is explained in greater detail subsequently.

As noted earlier, each of the variable amplitude cyclic tests culminated in the formation and subsequent propagation of fatigue cracks originating at the toe of the fillet in one or more of the beam flange angles. The cracks generally initiated in the region of greatest restraint against displacement;

i.e., in the region between the bolt in the leg of the flange angle attached to the column and the first bolt from the end of the beam in the leg attached to the beam flange. The tests were terminated when cracking had progressed at least partially across the face of the angle at the fillet; no tests were extended to the point of rupture of a connection element. The connections maintained ductile behavior during the full extent of the cyclic tests, and exhibited only modest loss of maximum moment from the time fatigue cracking was noticed to the termination of a test. No slip was observed during the cyclic tests, nor was there any local buckling of the connection elements.

## Discussion of Moment-Rotation Hysteresis Loops

The shape of the hysteresis loops for the cyclic test specimens can be described in terms of the changes in the geometry of the connection as the moment is reversed. Consider one half of a typical loop, shown as a solid line in Figure 3.27. Point 1 in Figure 3.27 corresponds to one extreme of the actuator movement (Point 1 in Figure 3.28, actuator displacement vs. time). The portion of the moment-rotation curve that is generated as the actuator moves from Point 1 to Point 3 can be divided into three regions based on the configuration of the connection; these regions are labeled I, II, and III in Figure 3.27.

The initial loading of the connection in a cycle, culminating in the attainment of maximum negative moment, causes the connection to assume the configuration shown in Figure 3.29a. In this configuration the beam is pivoting about a point near BFA, the current compression flange angle. The remaining connection angles are pulled away from the column flange, generating the tension forces which establish the corresponding resisting moment at the beam-column interface. With the bottom angle in full bearing on the column flange, the stiffness of the connection is now at a relative maximum. The completion of this initial loading is indicated as Point 1 in Figure 3.27.

Reversal of the direction of actuator movement, with the specimen in the configuration shown in Figure 3.29a effects a period of essentially elastic unloading at a slope comparable to the initial slope of a statically loaded connection. This is identified as Region I in Figure 3.27.

Region II is a transition stage. During this time, the geometry of the connection is undergoing significant change. The compression force in BFA, which bears on the column face in Region I, decreases and eventually converts to a tension force as the moment is reversed; hence, the angle moves away from the column face (see Figure 3.29b).

The force in the top flange angle, TFA, changes from tension to compression in Region II, causing that angle to move toward the column face. As a result, the center of rotation of the connection moves (reflecting the redistribution of forces taking place) and eventually maintains a position near the top of the beam. During the time when both flange angles are temporarily bent away from the column face, the connection stiffness is at a minimum. The stiffness of Region II is not a constant for all loading histories. The initiation of yield in the flange angles is affected by the presence of residual stresses (and, later, fatigue cracks). The response of the connection in Region II is analogous to a rigid beam on an elastic-plastic foundation, where the foundation is represented by springs with changing stiffnesses. The relative stiffnesses of the springs depends on the magnitude of the connection rotation at the previous reversal of moment. As a result of this behavior, it is hypothesized that unloading from the central range of Region II will not be at a slope equal to that of Region I. Rather, the slope will lie between the limits established from the Region I response and the Region II slope immediately preceding unloading. (This has not been experimentally tested in the present investigation.) The end of Region II is reached when angle TFA has folded back upon the column face in compression. The behavior of the connection in Region II occurs only in cyclic loading, and hence cannot be compared to a monotonic static test.

Region III can be considered geometrically the reverse of the configuration existing in Region I. As shown in Figure 3.29c, the compression angle in bearing against the column face is now TFA, whereas flange angle BFA and the web angles are now pried in tension from the column. The center of rotation is again stationary, located near the top flange of the beam. The change in stiffness as the configuration changes from that of Figure 3.29b to the one in Figure 3.29c can be determined by noting the difference in the slope of the moment-rotation curve. The magnitude of this change depends on the connection details, as discussed below.

Comparing the change in slope between Regions II and III in specimens 14C1 and 14C2, for example, (Figures 3.18 and 3.19, respectively), it can be seen that the change is more pronounced in specimen 14C1. This difference can be attributed to the thicker flange angles of specimen 14C2, the web angles and bolt diameter being identical for the two specimens. Assuming the angles behave as beams, an analogy may be drawn between a span-to-depth ratio for a beam and the ratio of an "effective" gage length, $g - d_b$, to the thickness of the angle, t, for the leg of the flange angle mounted to the column flange. For specimen 14C1, $(g - d_b)/t$ is 4.7 and, for specimen 14C2, 3.5, indicating a stiffer beam in bending for the flange angles of specimen 14C2. During the transition phase of Region II the stiffer flange angles of specimen 14C2 offer more resistance to movement than the flange angles of specimen 14C1. Thus, when the compression flange angle goes into bearing, the change in stiffness is greater in specimen 14C1 than the corresponding change in stiffness of specimen 14C2. The same observations may be drawn by comparing the relative response of the other three 14-inch beam specimens, 14C3, 14C4, and 14B1. Specimens 14C3 and 14B1, with $(g - d_b)/t$ ratios of 3.25, exhibited very little evidence of pinching of the hysteresis loops, while 14C4, with a $(g - d_b)/t$ ratio of 4.3, exhibited perhaps a bit more prominent pinching than the other two members. (The pinching effect in specimen 14C4 was still considerably less pronounced than that of 14C1, however, as comparison of Figures 3.18 and 3.21 indicates).

By comparing the moment-rotation curves of specimens 8C1, 8C2, 8C3, and 8B1, the observations of the previous paragraph are again applicable. Specimen 8C1, with a $(g - d_b)/t$ ratio of 4.0, exhibited a more prominent change in slope from Region II to Region III than that of specimen 8C2, with a $(g - d_b)/t$ ratio of 3.3, or specimens 8C3 and 8B1, with identical ratios of 3.0. In fact, the latter three specimens are distinguished as having exhibited almost no consistent pinching behavior at all, even at large displacements.

## Connection Hysteretic Energy Capacity

The "average" hysteresis loop area at each displacement amplitude, and the total hysteretic energy accumulated at the termination of testing, is presented in Tables 3.4 through 3.12 for the nine variable amplitude test specimens. In general, for the low-to-high amplitude block tests, it was found that, with the exception of the first cycle following an increase in displacement amplitude, the hysteretic energy absorbed per cycle remained reasonably constant at each amplitude. Further, the ductile behavior of the connections was evident by the increase in hysteresis loop area with each succeeding increase in displacement amplitude (and connection rotation) through the full range of testing, even with pinching evident at the larger amplitudes.

As a consequence of the general stability of the connections at large rotations, and of the ductility of the connection elements, it is reasonable that the overall energy absorption capacities of like connections would increase directly with the depth of the beam sections to which they are attached. This is demonstrated, for example, by comparing the data for specimens 14C1 and 8C2, both of which contained 3/8-inch thick flange angles and were fastened with 3/4-inch diameter bolts. For specimen 14C1, the total accumulated hysteresis loop area was 520 k-in., more than twice the 243 k-in. achieved by specimen 8C2.

The hysteretic energy absorption performance of the specimens framed to a particular beam section, however, exhibited limited consistency. For example, specimen 14C4, fabricated with 3/8-inch thick angles and 7/8-inch diameter bolts, developed only 345 k-in. of hysteretic energy, well below the 520 k-in. of specimen 14C1 (3/8-inch flange angles, 3/4-inch bolts). It may be noted that fatigue cracking was observed during the block of cycles applied at a displacement amplitude of 1.6 inches for specimen 14C4; these cracks thereafter propagated continuously, and the test was discontinued after nine cycles were applied at a displacement amplitude of 1.8 inches. In contrast, fatigue cracking was not observed in specimen 14C1 until the twelfth cycle at a 2.0-inch displacement amplitude, enabling the latter member to accumulate considerable hysteretic energy at the large loop areas corresponding to that displacement.

Comparison of the behavior of specimens 14C1 and 14C4 serves to illustrate the sensitivity of total hysteretic energy absorption capacity to the formation and rate of propagation of fatigue cracks in the connection elements, particularly the flange angles. Fatigue crack initiation, in turn, is influenced by such factors as surface irregularities formed during the rolling or fabrication of the connection angles, residual stresses introduced during the erection process, and concentrations of stress resulting from the restraint against movement in the area adjacent to the bolts in each leg of the flange angle. Further illustration of the dependency of energy absorption on fatigue behavior is obtained by comparison of specimens 14C3 and 14B1. Geometrically the same, specimen 14C3 was tested under low-to-high amplitude loading, with displacement amplitudes increasing in blocks from 0.2 to 2.0 inches, and accumulated a 683 k-in. total hysteresis loop area. A fatigue crack was detected during the 1.6 inch displacement amplitude block, and progressed at a moderate rate until the test was stopped during cycling at an amplitude of 2.0 inches. Specimen 14B1, in a high-to-low amplitude test, exhibited fatigue cracking during the first block of cycles at a displacement amplitude of 1.8 inches; these cracks continued to grow, although at decreased rates, as the displacements were lowered progressively to 1.0 inches. At this point, a large crack had extended to the limit permitted in the other tests, and cycling of specimen 14B1 was discontinued. The total hysteretic energy achieved was 514 k-in., about 75 percent of that for the companion member, 14C3.

The influence of fatigue crack propagation on hysteretic energy absorption is further demonstrated by comparison of the behavior of specimen 14B1 with that of specimen 8B1. Although fatigue cracks were first detected in specimen 8B1 during the first block of cycles at its largest displacement amplitude, 1.2 inches, crack retardation (temporary cessation of crack growth) was observed at succeedingly smaller displacement amplitudes. At 0.2 inches, the crack lengths were still within the limits permitted in the cyclic test series; the amplitude was then increased again to 1.2 inches, and the crack extended rapidly during the first cycle at that amplitude. The total hysteretic eneregy accumulated by specimen 8B1 was 216 k-in., greater than that for its companion specimen, 8C3, (186 k-in.), which was tested under low-to-high amplitude block loading.

The consequences of fatigue crack acceleration or retardation on energy absorption capacity during variable amplitude cyclic loading are evident from the above comparisons. The differences in the crack growth rates between the low-to-high and the high-to-low amplitude tests also serve to illustrate the dependence of cyclic performance (and, correspondingly, damage accumulation models) on sequencing history as well as on amplitude of load or displacement. Thus, a linear damage rule of the form proposed by Miner (65), although simple to apply, cannot be expected to offer a consistently accurate prediction of damage accumulation for displacement histories more typical of a seismic event; this is discussed further in Section 4.3.

### 3.2.3 Fatigue Tests

Sixteen specimens were tested under constant amplitude cyclic (fatigue) displacement histories. The geometric parameters that were varied in this test series were the beam depth (W14X38 and W8X21 sections) and the flange angle thickness (3/8 inch and 1/2 inch for the 14-inch beam specimens, 5/16 inch and 3/8 inch for the W8X21 specimens). The bolt diameter was 7/8 inch for all specimens in this test series. Details of the test specimens are reported in Table 2.3; the testing procedures are described in Section 2.3.2.

#### 3.2.3.1 Test Results

A compilation of the fatigue test results for the sixteen specimens is presented in Table 3.13. The table includes the nominal chord rotation, the fatigue life, and the total accumulated hysteresis loop area for the specimens. The fatigue data for each of the specimens (except 8F6), including range of rotation, range of moment, and individual hysteresis loop area at selected percentages of the total fatigue life are presented in Tables 3.14 through 3.17. No hysteresis loop areas are available for specimen 8F6 because of a malfunction in the data recording equipment.

As discussed in Section 2.3.2.3, several of the fatigue test specimens were subjected to a number of initial "half" cycles before continuing with the full reversal displacements, in order to induce first cracking in the top flange angles, where inspection was easiest. Cracking did initiate in the top angles for these specimens, with the origin of cracking at the toe of the fillet, usually in the leg of the angles mounted to the beam flange. Fatigue "failure" was defined as the number of cycles at which the longest fatigue crack had extended over approximately three-fourths of the width of the flange angle. For some of the test specimens, this crack had grown through the thickness of the flange angle at one or more points by the time it had reached its limit length.

Complete hysteresis loop traces at selected cycles are shown in Figures 3.30 through 3.44 for the fifteen fatigue specimens for which data are available. For a few of the low amplitude tests (e.g., specimens 14F8, 14F4, and 8F2) the hysteresis loop traces shown in the figures appear somewhat erratic and non-coincidental. This is attributed to the sensitivity of the recorded data to slight self adjustments in the testing apparatus at low actuator loads corresponding to reversals in the direction of actuator movement. The irregular appearance of the tops of the hysteresis loops results from the limited number of digitized data points that could be recorded by each channel of the recording equipment, particularly in those specimens in which elastic displacements were prevalent. In general, however, it can be seen that the hysteretic response in specimens 14F3, 14F4, and 8F2 was reasonably consistent, with only small inelastic displacements evident during each cycle, and little degradation of moment carrying capability even toward the end of a test when fatigue cracking was quite extensive.

For the specimens tested at large displacement amplitudes, and which exhibited fatigue failures at the lower lives in the test program, it is apparent that the hysteresis loops were quite stable throughout each test, and that only nominal loss of moment occurred for the complete connection even toward the end of a test. Specimen 8F7, shown in Figure 3.40, typifies the response observed in the large displacement constant amplitude tests. The hysteresis loops are large and quite stable, with minor pinching evident toward the end of the loop. Note also the gradual, though rather nominal, loss of moment exhibited by the specimen toward the end of the test ($N_f$ = 67 cycles). This behavior was exhibited by the fatigue test specimens in spite of the fact that fatigue cracks had progressed to some depth through the thickness of the flange angle at the time they had reached the limit length at the surface. Because the crack was extending rapidly along the surface at the time testing was stopped, however, it was felt that the recorded fatigue life was very close to the total number of cycles that could be tolerated before complete rupture of one of the flange angles. The fatigue cracks were generally first visually detected as a series of fine hairline cracks which coincided with slight irregularities in the surface of the flange angle at the toe of the fillet. As cycling progressed, these individual cracks would eventually coalesce into a single crack, which then propagated more rapidly along the surface (and through the thickness, as the increasing width of the opening at the surface would indicate).

The appearance of the fatigue cracks in specimen 14F9 at 126, 136, 158, and 214 cycles is shown in Figure 3.45. Note the irregularity of the crack front, typical of that observed in all of the cyclic test specimens. Although cycle 126 is reported as the time at which a fatigue crack was first observed in specimen 14F9, the actual onset of visible cracking probably occurred slightly earlier, as the previous time the test had been stopped to examine for cracks was at 105 cycles. It should be noted, also, that the testing of specimen 14F9 was stopped at 230 cycles, at which time the crack shown in Figure 3.45 had a total surface length of about six inches.

### 3.2.3.2 Discussion of Test Results

The test data for the four sets of fatigue tests are plotted in Figures 3.46 through 3.49. Figures 3.46 and 3.47 present the data for the W14X38 beam specimens fabricated with flange angles of 3/8-inch and 1/2-inch thickness, respectively. The data in Figures 3.48 and 3.49 represent the W8X21 beam specimens with flange angle thicknesses of 5/16 inch and 3/8 inch,respectively. In the figures, the total fatigue lives (number of complete cycles of displacement, as identified in Figure 3.28) are plotted as a function of the total nominal range of rotation in an individual cycle, the range of rotation being calculated directly from the controlled actuator displacements. For each of the four sets of tests, the data generally are seen to follow a linear log-log relationship for the range of fatigue lives obtained. Using standard regression analysis, Manson-Coffin (66-68) type fatigue life relationships, with two empirically determined constants, have been generated for each of the four individual sets of data, and are shown in the figures.

In order to develop a single expression capable of predicting constant amplitude fatigue lives for specimens with varying geometries, a non-dimensionalized nominal flange angle chord rotation index was calculated for each of the sixteen specimens tested in this phase of the study. This chord rotation index may be considered representative, proportionally, of the surface strain in the tension flange angle of the test specimen at a particular displacement amplitude. The numerical values of the chord rotation index, R, are reported in Table 3.13 for each of the test specimens. The applicability of a relationship between R and $N_f$ as a model for predicting constant amplitude cyclic life expectancies is discussed in Section 4.2, where an analysis of the cyclic test data is apresented. The efficacy of using such a fatigue life relationship as a baseline for cumulative damage assessment under variable amplitude displacement excursions is explored also in Section IV.

Tables 3.14 through 3.17 include the total hysteretic energy (summation of moment-rotation hysteresis loop areas) accumulated by each of the specimens during fatigue testing. Typical of structural elements subjected to strain-based, low-cycle fatigue loading, the total accumulated hysteretic energy for a specific type of connection was not found to be constant over the range of fatigue lives considered in the investigation. From examination of the data in Tables 3.14 through 3.17, there appears to be a general trend toward increasing total hysteretic energy accumulation at the longer fatigue lifes corresponding to the smaller per cycle loop areas. For example, with the W8X21 specimens containing 3/8-inch thick flange angles (Table 3.16), the total hysteretic energy increases from 116.6 k-in. for specimen 8F1 (tested at a 1.5-inch actuator displacement amplitude, and exhibiting a fatigue life of 10 cycles) to approximately 308 k-in. for specimen 8F2 (which was tested as a displacement amplitude of 0.5 inches, and had a fatigue life of 560 cycles). This trend is not consistent, however, as the somewhat erratic pattern of energy accumulation in the 14-inch beam fatigue test specimens indicates (Tables 3.14, 3.15). It is apparent that additional data are required, covering a greater variety of specimen geometries, and for tests conducted over a broader range of fatigue lives, before any correlation between total energy absorption capacity and fatigue performance can be attempted. It may be noted here, however, that a linear log-log relationship between energy absorbed per cycle and fatigue life expectancy has been established for the specimens tested in this study; such a relationship offers promise as a means of predicting fatigue lives under constant amplitude testing, and as a baseline for use in damage accumulation models involving variable amplitude test excursions. The results of this analytical phase of the study are examined in Section IV.

As one element of the constant amplitude cyclic test program, it was intended that the separate stages of crack initiation and propagation be studied during each fatigue test. This turned out to be a rather formidable task because, as noted earlier, the fatigue cracks first appeared as a series of fine, hairline cracks separated from one another both along the width of the flange angle and in elevation from the toe of the fillet in the angle. These individual cracks would grow, at varying rates, until they eventually coalesced into a single, irregular crack similar in appearance to the one shown in Figure 3.45d. Beyond that point, the crack, usually not symmetrically positioned on the face of the flange angle, would extend quite rapidly to the limit length established for that test specimen. It was quite difficult, then, to define a representative crack growth history from among the several individual cracks that first appeared on the specimen surface.

The crack growth rate through the thickness of the affected flange angle was also difficult to determine. To obtain depth measurements, the fatigue test was stopped periodically with the top flange angle in the full tension position.

A 0.001-inch thick feeler gage was then inserted in the open crack to try to probe to the crack root.* The results of these measurements have been analyzed in a separate study (69), using a fracture mechanics crack growth model to predict the growth pattern. The results of that investigation are not reported here because it was felt that too few measurements were made to offer meaningful interpretations of the correlation between through-thickness crack growth and the observable surface crack growth behavior. Additional studies in this area have been proposed for consideration in a subsequent study.

---

*Because of the complex geometries of the test members and the loading apparatus, other potential non-destructive crack size measurement techniques, such as ultrasonic inspection, were not attempted.

# IV. ANALYTICAL INVESTIGATION

## 4.1 Static Tests

In the initial study (63) a number of analytical models were investigated for their ability to predict the moment-rotation characteristics of semi-rigid beam-to-column connections. It was determined that the initial stiffness of the connection could be reasonably predicted by a simple model which models the legs of the connecting angles as an assembly of beams. In addition, it was determined that the complete moment-rotation curve was best predicted by an empirical model which incorporates the physical and material characteristics of the connection as parameters. These models were utilized in this study in an attempt to predict the behavior of the specimens tested in the investigation. In addition to these models, a three dimensional finite element model using solid isoparametric elements was developed in an attempt to predict the moment-rotation curve for a typical connection.

### 4.1.1 Prediction of Moment-Rotation Behavior

#### 4.1.1.1 Beam Model for Initial Stiffness

The initial stiffness of the connections under study is assumed to correspond to the physical behavior indicated by Figure 4.1a; namely, that the center of rotation of the connection is located at the point of contact of the bottom flange of the beam with the compression flange angle at the end of the beam. Also, it is assumed that the material is linearly elastic and that displacements are small. From these assumptions, the horizontal displacement of the heel of the top flange angle, X, (Figure 4.1a) is:

$$X = \phi d \quad (4.1)$$

where:

$\phi$ = rotation of end of beam with respect to column face

It is assumed that the vertical leg of the flange angle can be represented by "stiff" beams and "flexible" beams as shown in Figures 4.1a, 4.2a, and Figure 4.3, where:

$\lambda$ = assumed beam length, flange angle leg adjacent to column face

$M_{AB}$ = moment at end A of beam AB

$M_{BA}$ = moment at end B of beam AB

F = shear force in beam (nominal bolt force)

It is assumed that the outstanding legs of the web angles can also be represented by "stiff" beams and "flexible" beams, as shown in Figures 4.1b, and 4.2b and Figure 4.4, where:

$\lambda_c$ = assumed beam length, web angle leg adjacent to column face

$p_c$ = pitch, center-to-center spacing of bolts in legs of web angle

$\Delta_i$ = $d_i\ \phi(i=1,2,3)$, displacement of heel of web angle for beam i

$d_i$ = distance from assumed center of rotation to beam i

$d_1 \quad = \quad d/2 + (n-1)p\ /2$

$d_2 \quad = \quad (n-2)d/2$

$d_3 \quad = \quad d/2 - (n-1)p\ /2$

$F_i \quad = \quad$ shear force in beam i

$(M_{CD})_i \quad = \quad$ moment at end C of beam i

$(M_{DC})_i \quad = \quad$ moment at end D of beam i

Neglecting the bending moment in the compression flange angle at the assumed center of rotation, and including both flexural and shear deformation, the total resisting moment of the connection is

$$M = M_f + M_c \tag{4.2}$$

$M_f \quad = \quad$ moment contributed by flange angle

$M_c \quad = \quad$ moment contributed by web angle

where

$M_c \quad = \quad M_c(\text{stiff}) + M_c(\text{flexible})$

$M_c(\text{stiff}) \quad = \quad$ moment contributed by stiff portion of web angle

$M_c$(flexible) = moment contributed by flexible portion of web angle

Considering equilibrium of the beam shown in Figure 4.2a and using the slope deflection equations, it can be shown (71) that

$$M_f = \left\{ \frac{6EI_1D}{b^2(1+r_1)}\left[\frac{2D}{b} + 1\right] + \frac{6EI_2D}{B^3(1+r_2)}\left[1 - \frac{2-r_2}{4+r_2}\right](D + B) \right\} \phi \qquad (4.3)$$

Similarly considering the beams in Figure 4.2b:

$$M_c(\text{stiff}) = \frac{24EI_3}{b_c^{\,3}(1+r_3)}\left[d_1^{\,2} + d_2^{\,2} + d_3^{\,2}\right]\phi$$

$$M_c(\text{flexible}) = \frac{12EI_4}{B_c^{\,3}(1+r_4)}\left[1 - \frac{2-r_4}{4+r_r}\right]\left[d_{e1}^{\,2} + d_{e2}^{\,2}\right]\phi + \frac{12EI_5}{B_c^{\,3}(1+r_5)}\left[1 - \frac{2-r_5}{4+r_5}\right]\left[d_{f1}^{\,2} + d_{f2}^{\,2}\right]\phi$$

where:

$$r_i = \frac{12EI_i}{A_{si}G\lambda_i^2}, \quad I_i = \frac{1}{12}p_it_i^2, \quad A_{si} = \frac{2}{3}p_it_i, \quad i = 1,2,3,4,5$$

| | | |
|---|---|---|
| $p_1$ = (no. of bolts) x $d_w$ | $\lambda_1 = b$ | $t_1 = t$ |
| $p_2 = L - p_1$ | $\lambda_2 = B$ | $t_2 = t$ |
| $p_3 = d_w$ | $\lambda_3 = b_c$ | $t_3 = t_c$ |
| $p_4 = 1/2[L_c - d_w - (n-1)p_c]$ | $\lambda_4 = B_c$ | $t_4 = t_c$ |
| $p_5 = p_c - d_w$ | $\lambda_5 = B_c$ | $t_5 = t_c$ |

$d_{e1} = [2d+(n-1)p_c+L_c+d_w]/4$

$d_{e2} = [2d-(n-1)p_c-L_c-d_2]/4$

$d_{f1} = d/2+(n-2)p_c/2$

$d_{f2} = (n-2)(d-p_c)/2$

n = number of bolts in beam web (2 or 3)

Equations 4.1 through 4.4 were evaluated for the specimens of this investigation which were tested statically. These equations were evaluated for both inclusion and exclusion of shear deformation; the results are compared in Table 4.1 with the corresponding test data. The test results presented in this table are taken from Tables 3.1 and 3.2, which include results from both the initial investigation and the current study.

#### 4.1.1.2 Empirical Model

In the initial study (63) an empirical model was developed to predict the moment-rotation behavior of semi-rigid beam to column connections of the type investigated herein. The resulting equation is:

$$\phi = C_1(KM) + C_2(KM)^3 + C_3(KM)^5 \qquad (4.5)$$

where

$\phi$ = rotation of beam with respect to column

M = moment developed by beam to column connection

$$K = P_1^{\alpha_1} P_2^{\alpha_2} P_3^{\alpha_3} P_4^{\alpha_4} P_5^{\alpha_5}$$

$P_1 = t \qquad \alpha_1 = -1.12808769$

$P_2 = d \qquad \alpha_2 = -1.2870455$

$P_3 = t_c \qquad \alpha_3 = -.41454097$

$P_4 = L \qquad \alpha_4 = -.69412158$

$P_5 = b+t/2 \qquad \alpha_5 = 1.34994572$

and:

$C_1 = .2232429 \times 10^{-4}$

$C_2 = .1850728 \times 10^{-7}$

$C_3 = .3188976 \times 10^{-11}$

Comparisons of Equation 4.5 with the results of the test investigations are presented in Figures 4.4 through 4.18.

4.1.1.3 Three Dimensional Finite Element Model - Flange Angles

Observations from all of the static tests indicated that a major portion of the connection deformation take place in the tension flange angle. Consequently, both analytical and experimental studies were carried out to determine its deformational characteristics. Pull tests were conducted to determine experimentally the behavior of the flange angle (see Appendix B.1) and a three dimensional finite element model of the flange angle was generated to analytically determine its behavior (see Appendix B.3). The moment-rotation characteristics for both the experimental and analytical studies were determined from the force-displacement relationships by assuming that the moment is calculated by multiplying the force in the angle by the depth of the beam, and that the rotation is calculated by dividing the flange angle displacement by the depth of the beam. A comparison of the pull test data with the finite element results is presented in Appendix B; a more detailed report of this study is given in Reference 69.

### 4.1.2 Discussion

Comparison of the test results with the predicted initial slopes, Table 4.1, indicates that slopes predicted by Equations 4.1 to 4.4 are reasonable, although not precise. The comparison also indicates that, in general, the predicted values are too low for the thinner angles and too high for the thicker angles for specimens using both the 3/4-inch diameter bolts and 7/8-inch diameter bolts. It also appears that inclusion of shear deformation in the prediction equations produces results that are generally more accurate.

Results obtained from the three-dimensional finite element analysis (see Figure B.10) for predicting the full moment-rotation curves were encouraging. The program and model developed in this investigation produced results far more accurate than the two-dimensional or three-dimensional models developed in the initial investigation (63). This appears to indicate that material nonlinearities are more significant than geometric nonlinearities in the behavior of the flange angle. In addition, it appears that solid elements are necessary to accurately model the behavior of the flange angles. Although the finite element analysis developed in this study is much more efficient than that of the initial study, the effort required to predict the full moment-rotation characteristics of the connections is still prohibitively large for design purposes.

Results presented in Figures 4.4 to 4.18 indicate that the empirical model, Equation 4.5, is a good predictor of the overall moment-rotation characteristics of connections of the type studied in this investigation. The equation is simple and suitable for incorporation into computer programs for design purposes or nonlinear analysis of frames with semi-rigid connections.

## 4.2 Fatigue Tests

### 4.2.1 Fatigue Life Predictions

This study employed the low cycle fatigue concept to generate baseline fatigue data in terms of two different parameters. In low cycle fatigue, the baseline fatigue data are usually expressed in terms of plastic strain. For most metals, the plot of plastic strain versus the number of cycles to failure produces a linear relationship on a log-log plot. This observation led Coffin (66, 67) and Manson (68) to propose the following equation:

$$\frac{\Delta\varepsilon_p}{2} = \varepsilon_f'(N_f)^c$$

where

$\frac{\Delta\varepsilon_p}{2}$ = plastic strain

$\varepsilon_f'$ = fatigue ductility

$N_f$ = total number of cycles to failure

$c$ = fatigue ductility exponent

A number of researchers have concluded that if the strain at critical locations in the structure could be measured, these measurements, together with Miner's Rule (65), baseline fatigue data, and an appropriate cycle counting method, could be used to make a reasonably good prediction of the life of structural components under random loading. Methods like that of Neuber's Rule (70) could be used to estimate local behavior if the external load is known for simple specimens. However, for complex systems such as connections, predicting strain at critical locations is not an easy task.

In order to establish baseline fatigue data in this study, four sets of constant amplitude tests were conducted, as discussed in Section III. Then, in order to develop a single expression for predicting fatigue lives for specimens of varying geometry, a parameter, R, representative of the degree of deformation in the tension flange angle, was considered. The parameter R, called the "nominal flange angle chord rotation index," is defined as

$$R = 2\left[\frac{(d+t)\tan\phi}{g-d_w/2-t}\right] \tag{4.6}$$

where:

$d$ = beam depth

$t$ = flange angle thickness

$\phi$ = rotation of end of beam with respect to column face

$d_w$ = diameter of washer

g = gage in the flange angle; distance from the heel of the angle to the center of the bolt hole in the leg of the flange angle attached to the column face

Referring to Figure 4.1(a) we can write

$$\tan\phi \simeq \frac{X}{d+t} \quad (4.7)$$

$$\tan\alpha = \frac{X}{(g-t_w/2-t)} \quad (4.8)$$

Since one complete reversal goes through the relative beam to column rotation twice, the total chord rotation index, R, is found as

$$R = 2\tan\alpha \quad (4.9)$$

Equations 4.7 to 4.9 are then combined to give Equation 4.6.

Figure 4.19 shows a plot of R versus the number of cycles to failure on a log-log scale for the constant amplitude cyclic tests. The least squares fit of a straight line through the data resulted in the following equation, which relates R to the number of cycles to failure, $N_f$:

$$N_f = 1.868(R)^{-3.2531} \quad (4.10)$$

At high displacement amplitudes, plastic strain is the predominant cause of energy dissipation in semi-rigid connections. In this study the amount of dissipated energy is approximated as the area of the hysteresis loop under the moment-rotation curve. To examine the effect of energy dissipation on fatigue life, the energy per cycle at approximately midlife, E, was plotted against the number of cycles to failure for all of the constant displacement amplitude cyclic tests on a log-log scale, as shown in Figure 4.20. This figure indicates that a linear relationship exists for each beam depth. Using a least squares fit, the following equations were obtained for beams of 14-inch depth and 8-inch depth, respectively:

$$N_f = 844.9(E)^{-1.20}$$

$$N_f = 298.65(E)^{-1.2639}$$

where:

$N_f$ = number of cycles to failure; fatigue life for constant displacement amplitude cyclic test

E = energy per cycle; area of single hysteresis loop

The parameter E becomes an alternative to the parameter R, so that the equations of Figure 4.20 could be considered as baseline fatigue relationships which could be used with Miner's Rule to calculate the life of a specimen under random loading.

## 4.3 Variable Amplitude Cyclic Tests

### 4.3.1 Prediction of Damage Accumulation

To predict the cumulative damage for the specimens tested under the low-to-high amplitude and high-to-low amplitude cyclic loadings, the chord rotation index, R, was calculated as described above for each test displacement. Equation 4.10 was then used to predict the number of cycles to failure, $N_f$, and the cumulative damage ratio, $n/N_f$, was calculated using the number of applied cycles, n, obtained from the test data. The results of this analysis are presented in Tables 4.2 and 4.3.

Cumulative damage in the variable amplitude cyclic tests was also predicted using energy dissipation. The average hysteresis loop area, obtained from the tests, was chosen to represent the dissipated energy, E, and Equations 4.11 and 4.12 were then used to predict the number of cycles to failure, $N_f$. The cumulative damage was then calculated. The results of this analysis are presented in Tables 4.4 and 4.5.

Comparison of Tables 4.3 and 4.4 with Tables 4.5 and 4.6 indicates that slightly better predictions of cumulative damage are obtained using energy dissipation, E, to predict fatigue life. Predictions based on the chord rotation index, R, are seen to be smaller than those obtained using E. Additional tests are needed, however, to further refine the proposed fatigue life relationships, for application to a linear cumulative damage model, as above, or to other models appropriate to the prediction of fatigue behavior under random loading conditions. Such tests have been proposed as an extension of the present investigation.

# V. SUMMARY AND CONCLUSIONS

## 5.1. Static Tests

In an initial investigation (63) and in the current study, a combined total of 18 bolted beam to column connections were tested under monotonic loading to generate static moment-rotation relationships. The connections consisted of top and seat angles bolted to the flanges of beam sections and a supporting stub column, together with double web angles bolted to the beam web and column flange. ASTM A36 steel was used for the members and connection elements; the fasteners were ASTM A325 high-strength bolts. Eight of the test connections were framed to W14X38 beam sections; of these, four were fastened with 3/4-inch diameter bolts, the remaining four with 7/8-inch diameter bolts. Ten connections were framed to W8X21 beam sections; seven of these were fabricated using 3/4-inch diameter bolts, the remainder with 7/8-inch diameter bolts. For the top and seat flange angles, the thickness, length, and gage (in the leg attached to the column flange) were varied, together with the beam depth and bolt diameter, to effect connections of varying stiffness. The thickness and length of the web angles were varied also.

In all of the static tests, the connections exhibited a moment-rotation response that became non-linear relatively early in the loading sequence. This is attributed, primarily, to local yielding and eventual plastic hinge formation at each toe of the fillet in the angle attached to the tension flange of the beam. Another hinge developed in the vicinity of the bolt line in the leg of the flange angle attached to the column, together with progressive plastic hinging in the outstanding legs of the web angles. Two of the specimens fastened with 3/4-inch diameter bolts, 8S2 and 14S2, and one specimen fastened with 7/8-inch bolts, 8S10, exhibited slip in the connection angles during testing. These were the stiffer connections for each beam size, developing the larger moments (and, correspondingly, larger bolt shear forces) in each test group.

With the exception of specimens 8S2, 8S10, and 14S2, all of the test connections were able to develop continually increasing moments through the full range of rotations imposed during the tests. (The maximum rotations corresponded to deflections exceeding four times the deflection, at allowable load, of simply supported beams having the same section and span as those in the test program). During the latter period of loading, a nearly constant or only very gradually decreasing positive slope of the moment-rotation curve was exhibited by each of the specimens (except 8S2). This nearly constant stiffness at large deformations has been attributed to material strain hardening, and to the consequences of progressive changes in the geometries of the connecting angles. The increasing deflection of the tension flange angle at large connection rotations produces a continuous change in the internal force distribution in the legs of the angle, with axial tension becoming an increasing factor as the angle progressively "flattens out." The gradual transition from a predominately flexural response to a combined flexural-axial response, with the accompanying strain hardening, can thus account for the ability of the connections to achieve considerably greater moment capacities, by a factor of at least two, than those predicted by a simple flexural plastic hinge mechanism.

From the static tests, it has been found that the geometric parameters that most significantly affect the static moment-rotation performance of the semi-rigid connections investigated are: the depth of the beam section to which the connection elements are framed; the thickness of the flange angles; and the gage in the leg of the flange angles attached to the column flange. Although the data are inconclusive, it appears that bolt diameter has a minimal effect on the initial stiffness of the connections; however, increasing the bolt diameter effects a corresponding increase in moment capacity at large rotations (beyond about $4X10^{-3}$ radians). Variations in the length of the flange angles, and in the length and thickness of the web angles, had a less pronounced effect on connection response than the other parameters.

An analytical model developed to predict the initial stiffness of the semi-rigid connections has been found to correlate reasonably well with the test results for the specimens considered in the investigation. The model represents the legs of the connection angles as an assembly of "stiff" and "flexible" beam elements, the stiff elements associated with the segments of the angles confined by the connecting bolts, and the flexible elements representing those segments between the bolt lines and at each end of the angles.

Using the results of the parametric test program, an empirical model has been generated to predict the complete non-linear moment-rotation behavior of the test connections. With the exception of the stiffest connections in both the W14X38 and W8X21 test series, this model offers reasonable approximations to the moment-rotation curves of the connections up to the limits of rotation examined in the test program. For the stiffest connections of each beam size, the model underestimates the moments developed at the larger connection rotations.

In a pilot study, tests were conducted of two specimens comprised of flange and web angles welded to W14X38 beam sections and bolted to the flanges of the supporting stub column. AWS E70 electrodes were used for the angle to beam welds; 7/8-inch diameter A325 bolts were used in the attachment of the angles to the stub column. For specimens of comparable geometry, the combined bolted-welded connections exhibited higher initial stiffnesses than the corresponding all-bolted specimens. This was attributed to the greater restraint against movement of the heel of the angle at the end of the beam flanges occasioned by the presence of the weld return on the top and seat angles. In addition to the higher initial stiffness, the bolted-welded specimens developed moderately larger moments than those in the all-bolted specimens at comparable rotations. These results are considered preliminary, however, and not necessarily indicative of expected relative performances when a more complete range of section depths, and flange and web angle sizes are considered. Such tests have been proposed as part of a continuation of the current investigation.

## 5.2 Cyclic Tests

### 5.2.1 Variable Amplitude Block Tests

Nine specimens, with geometries comparable to those of the static test series connections, were tested under variable amplitude cyclic loadings. Five of the specimens were framed to the W14X38 beam sections, the remaining four to the W8X21 beams. The other geometric parameters that were varied were the bolt diameter and the thickness of the top and seat flange angles.

Seven of the specimens were tested under low-to-high amplitude block displacement histories; the other two were subjected to high-to-low amplitude block loadings. The tests were conducted using full reversal of displacement to generate data indicative of the displacement extremes to which the connections could be subjected under seismic loading. The test procedure consisted of cycling sinusoidally between controlled limits of displacement, while monitoring the range in moment and the local displacements (rotations) developed during each cycle. The displacement-time histories followed a sequential block loading pattern, with a total of 12-15 cycles applied in each block before the amplitude was altered (increased in the low-to-high amplitude tests, decreased in the high-to-low amplitude tests).

Stable hysteresis loops were established, for the 14-inch test specimens, within a few cycles after an increase in amplitude was imposed relative to the preceding displacement under the low-to-high amplitude block loading pattern. For several of the 8-inch deep beam connections, a continual, though small, softening (loss of moment) was noted for each progressive cycle at a constant amplitude; however, the succeeding hysteresis loops were otherwise similar in appearance.

For each of the test specimens, the moment-rotation behavior was characterized by loops of continually decreasing slope for relatively small displacements in the non-linear range. In contrast, the hysteresis loops exhibited a moderate "pinching" effect at larger amplitudes, the degree of pinching being more pronounced in the W14X38 beam connections than in the W8X21 members. This increase in connection stiffness observed toward the tip of each hysteresis loop may be attributed, in large measure, to the changing geometry of the connection during each half cycle of loading. As rotation progresses, following a reversal in the direction of the moment at the connection, there is a period when both flange angles are drawn away from the column. With the connection in this configuration, the slope of the moment-rotation curve decreases as rotation proceeds. Eventually, the vertical leg of the compression flange angle folds back into full bearing on the column flange, with the connection exhibiting a concurrent increase in relative stiffness (pinching of the $M-\phi$ curve).

Each of the cyclic tests culminated in the formation and subsequent propagation of fatigue cracks at the toe of the fillet in one or more of the beam flange angles. The tests were terminated when cracking had progressed at least partially across the face of the angle at the fillet; no tests were extended to the point of rupture of a connection element. The connections maintained ductile behavior during the full extent of the cyclic tests, and exhibited only modest loss of maximum moment from the time fatigue cracking was noticed to the termination of the test. No slip was observed during the cyclic tests, nor was there any local buckling of the connection elements.

In general, for the low-to-high amplitude block tests, it was found that, with the exception of the first cycle following an increase in displacement amplitude, the hysteretic energy absorbed per cycle remained reasonably constant at each amplitude. Further, the ductile behavior of the connections was evident by the increase in hysteresis loop area with each succeeding increase in displacement amplitude, even with pinching evident at the larger amplitudes.

As a result of the general stability of the connections at large rotations, and of the ductility of the connection elements, it was found that the overall energy absorption of like connections increased directly with the depth of the beam sections to which they were attached. The hysteretic energy absorption performance of specimens framed to a particular beam section, however, exhibited limited consistency. This was attributed largely to the sensitivity of total energy absorption capacity to the time of formation, and rate of propagation of fatigue cracks in the connection elements, particularly the top and seat flange angles. Fatigue crack initiation, in turn, is influenced by such factors as surface irregularities formed during the rolling or fabrication of the connection angles, residual stresses introduced during the erection process, and stress concentrations at the toe of the fillet in each leg of the angles.

### 5.2.2 Constant Amplitude (Fatigue) Tests

Sixteen specimens were tested under constant displacement amplitude cyclic loading. Nine of the specimens were framed to the W14X38 beam sections, the remaining seven framed to the W8X21 beams. For each of the beam sizes, two thicknesses of the top and seat flange angles were used in the test members. The bolt diameter was 7/8 inch for all specimens in this test series. With the exception of several specimens which were initially subjected to a number of half cycles (null position to maximum displacement and return), the constant amplitude tests were conducted using full reversal of controlled displacement. The displacement amplitudes chosen resulted in fatigue lives ranging from nine to approximately 3500 cycles to "failure" (failure was defined as the number of cycles at which the longest fatigue crack had extended over approximately three-fourths of the width of the flange angle).

As with the variable amplitude tests, the specimens tested in the constant displacement amplitude series exhibited fatigue cracking that initated at the toe of the fillet in one or more of the beam flange angles. Again, the observed hysteresis loops remained quite stable throughout each test, with only nominal loss of moment evident even toward the end of a test, when fatigue cracks had progressed to some depth through the thickness of the flange angle.

For each of the four test sets in the constant amplitude series (two thicknesses of flange angle framed to both W14X38 and W8X21 beam sections), it was found that a linear log-log relationship exists between the cyclic range of rotation in the connection and the resultant total fatigue life. To develop a single expression capable of predicting constant amplitude fatigue lives for specimens of varying geometry, a nominal chord rotation index, R, indicative of the magnitude of the surface strain in the tension flange angle, was determined for each of the sixteen test specimens in the series. For the combined data, a linear log-log expression was generated relating the chord rotation index, R, to the total number of cycles to failure, $N_f$:

$$N_f = 1.868(R)^{-3.2531}$$

At large displacement amplitudes, plastic strain is the predominant means of energy dissipation in the semi-rigid connections. In this study, the amount of dissipated energy is approximated as the area of the hysteresis loops under the moment-rotation curve. To examine the effect of energy dissipation on fatigue life, the energy per cycle, E, measured at approximately mid-life, was compared to the number of cycles to failure for each of the constant amplitude test specimens. Again, a linear expression, on a log-log scale, was found to provide a reasonably good relationship between energy per cycle and total fatigue life, for each of the beams sizes individually:

$$N_f = 844.9(E)^{-1.20} \qquad \text{(14-inch beam section)}$$

$$N_f = 298.65(E)^{-1.2639} \qquad \text{(8-inch beam section)}$$

The low cycle, constant amplitude fatigue relationships between $N_f$ and R or E were then applied to Miner's linear damage accumulation model in an attempt to predict the behavior of the specimens subjected to the variable amplitude cyclic displacements. Cumulative damage summations for both the low-to-high amplitude and the high-to-low amplitude block cyclic tests ranged from 0.4279 to 1.2848. In general, slightly better predictions of cumulative damage were obtained using energy dissipation, E, to predict fatigue life, than were obtained from the fatigue relationship based on the chord rotation index. Additional data, leading to more refined fatigue life relationships, are needed to improve variable amplitude fatigue life predictions using Miner's Rule or other cumulative damage models; such tests have been proposed as a continuation of the present investigation.

REFERENCES


1. Takanashi, K., and Ohi, K., "Shaking Table Tests on 3-Story Braced and Unbraced Steel Frames," Proc. of the Eighth World Conference on Earthquake Engineering, Vol. VI, San Francisco, CA, U.S.A., July 1984.

2. Plugge, H.B., and Walpole, W.R., "The Tenacity of Bolted Beam End-Plate to Column Connections Under Simulated Seismic Loading." Report 83-2, Dept. of Civil Engineering, University of Canterbury, Christchurch, New Zealand, September 1983.

3. Kato, B., "Beam-to-Column Research in Japan," Journal of the Structural Division, ASCE, Vol. 108, No. ST2, Proc. Paper 16852, February 1982.

4. Krawinkler, H. and Popov, E.P., "Seismic Behavior of Moment Connections and Joints," Journal of the Structural Division, ASCE, Vol. 108, No. ST2, Proc. Paper 16865, February 1982.

5. Popov, E.P., "Seismic Steel Framing Systems for Tall Buildings," Engineering Journal, AISC, 3rd Quarter, Vol. 19, No. 3, 1982.

6. Rentschler, G.P., Chen, W.F., and Driscoll, G.C., "Beam-to-Column Web Connection Details," Journal of the Structural Division, ASCE, Vol. 108, No. ST2, Proc. Paper 16880, February 1982.

7. Whittaker, D., and Walpole, W.R., "Bolted End Plate Connections for Seismically Designed Steel Frames," Report 82-11, Dept. of Civil Engineering, University of Canterbury, Christchurch, New Zealand, June 1982.

8. Witteveen, J., Startk, J.W.B., Bijlaard, F.S.K., and Zoetemiejer, P., "Welded and Bolted Beam-to-Column Connections," Journal of the Structural Division, ASCE, Vol. 108, No.ST2, Proc. Paper 16873, February 1982.

9. Bijlaard, F.S.K., "Requirements for Welded and Bolted Beam-to-Column Connections in Non-Sway Frames," ed. Howlett, J.H., Jenkins, W.M., and Stainsby, R., Joints in Structural Steelwork, Proceedings of the International Conference, Teesside Polytechnic, Middlesbrough, England, April 1981.

10. Chen, W.F., and Patel, K.V., "Static Behavior of Beam-to-Column Moment Connections," Journal of the Structural Division, ASCE, Vol. 107, No. ST9, Proc. Paper 16512, September 1981.

11. Johnstone, N.D., and Walpole, W.R., "Bolted End Plate Beam to Connections Under Earthquake Type Loadings," Report 81-7, Dept. of Civil Engineering, University of Canterbury, Christchurch, New Zealand, September 1981.

12. Grundy, P., Thomas, I.R., and Bennetts, D., "Beam-to-Column Moment Connections," Journal of the Structural Division, ASCE, Vol. 106, No. ST1, Proc. Paper 15108, January 1980.

13. Popov, E.P., "An Update on Eccentric Seismic Bracing," Engineering Journal, AISC, 3rd Quarter, Vol. 17, No. 3, 1980.

14. Rentschler, G.P., Chen, W.F., and Driscoll, G.C., "Tests of Beam-to-Column Web Moment Connections," Journal of the Structural Division, ASCE, Vol. 106, No. ST5, Proc. Paper 15386, May 1980.

15. Krishnamurthy, N., Juang, H.-T., and Jeffrey, "Analytical M- $\phi$ Curves for End-Plate Connections., Journal of the Structural Division, ASCE, Vol. 105, No. ST1, Proc. Paper 14294, January 1979.

16. Roeder, C.W., and Popov, E.P., "Eccentrically Braced Steel Frames for Earthquakes," Journal of the Structural Division, ASCE, Vol. 105, No. ST11, Proc. Paper 14982, November 1979.

17. Krawinkler, H., "Shear in Beam-Column Joints in Seismic Design of Steel Frames, Engineering Journal, AISC, 3rd Quarter, Vol. 15, No. 3, 1978.

18. Krishnamurthy, N. "A Fresh Look at Bolted End-Plate Behavior and Design," Engineering Journal, AISC, 2nd Quarter, Vol. 15, No. 2, 1978.

19. Roeder, C.W., Popov, E.P., "Eccentrically Braced Steel Frames for Earthquakes," Journal of the Structural Division, ASCE, Vol. 104, No. ST3, Proc. Paper 13619, March 1978.

20. Krawinkler, H., Bertero, V.V., and Popov, E.P., "Inelastic Behavior of Steel Beam-to-Column Subassemblages, "Report No. UCB/EERC 71-7, University of California, Berkeley, California, 1977.

21. Parfitt, J., Jr., and Chen, W.F., "Tests of Welded Steel Beam-to-Column Moment Connections, "Journal of the Structural Division, ASCE, Vol. 102, No. ST1, Proc. Paper 11854, January 1976.

22. Hanson, R.D., "Characteristics of Steel Members and Connections," Proc. of the U.S. Nat. Conference on Earthquake Engineering, EERI, Ann Arbor, Michigan, June 1975.

23. Popov, E.P., Bertero, V.V. and Chandramouli, S., "Hysteretic Behavior of Steel Columns," Report No. UCB/EERC 75-11, University of California, Berkeley, California, September 1975.

24. Tarpy, T.S., and Lindsey, S.D., "Experimental Test Results on End-Plate Moment Connections," Report No. CE-AISE-1, Civil Engineering Department, Vanderbilt University, 1975.

25. Bertero, V.V., Krawinkler, H. and Popov, E.P., "Further Studies on Seismic Behavior of Steel Beam-Column Subassemblies," Report No. UBC/EERC 73-27, University of California, Berkeley, California, December 1973.

26. Carpenter, L.D., and Ly, L.-W., "Reversed and Repeated Load Tests of Full-Scale Steel Frames," Bulletin No. 24, AISI, April 1973.

27. Popov, E.P., and Bertero, V.V., "Cyclic Loading of Steel Beams and Connections," Journal of the Structural Division, ASCE, Vol. 99, No. ST6, Proc. Paper 9790, June 1973.

28. Bertero, V.V., Popov, E.P., and Krawinkler, H., "Beam-Column Subassemblages Under Repeated Loading," Journal of the Structural Division, ASCE, Vol. 98, Proc. Paper 8915, May 1972.

29. Popov, E.P., and Stephen, R.M., "Cyclic Loading of Full-Sized Steel Connections," Bulletin No. 21, AISI, February 1972.

30. Krawinkler, H., Bertero, V.V., and Popov, E.P., "Inelastic Behavior of Steel Beam-to-Column Subassemblies," Report No. UBC/EERC 71-7, University of California, Berkley, California, October 1971.

31. Ostrander, J.R., "An Experimental Investigation of End Plate Connections," Master's Thesis, University of Saskatchewan, Saskatoon, Saskatchewan, Canada, 1970.

32. Bertero, V.V., "Seismic Behavior of Steel Beam-to-Column Connection Subassemblages," Proc. of the Fourth World Conference on Earthquake Engineering, Vol. II, Santiago, Chile, January 1969.

33. Naka, T., Kato, B., Watabe, M., and Nakao, M., "Research on the Behavior of Steel Beam-to-Column Connections on Earthquake Engineering," Proc. of the Fourth World Conference on Earthquake Engineering, Vol. II, Santiago, Chile, January 1969.

34. Popov, E.P., and Pinkney, R.B., "Reliability of Steel Beam-to-Column Connections Under Cyclic Loading," Proc. of the Fourth World Conference on Earthquake Engineering, Vol. II, Santiago, Chile, January 1969.

35. Popov, E.P., and Pinkney, R.B., "Cyclic Yield Reversal in Steel Building Connections," Journal of the Structural Division, ASCE, Vol. 95, No. ST3, Proc. Paper 6441, March 1969.

36. Galambos, T.V., "Deformation and Energy Absorption Capacity of Steel Structures in the Inelastic Range," Bulletin No. 8, AISI, March 1968.

37. Hanson, R.D., "Comparison of Static and Dynamic Hysteresis Curves," Journal of the Engineering Mechanics Division, ASCE, Vol. 92, No. EM5, Proc. Paper 4949, October 1966.

38. Douty, R.T., and McGuire, W., "High Strength Bolted Moment

Connections," Journal of the Structural Division, ASCE, Vol. 91, No. ST2, Proc. Paper 4298, April 1965.

39. Beedle, L.S., and Christopher, R., "Tests of Steel Moment Connections," Engineering Journal, AISC, 3rd Quarter, Vol. 1, No. 3, October 1964.

40. Naka, T., Kato, B., Watabe, M., Tanaka, A., and Sasaki, T., "Research on the Behavior of Steel Beam-to-Column Connections Subjected to Lateral Force," Report No. 3, Trans. of the Architectural Inst. of Japan, Vol. 103, October 1964.

41. Pray, R.F., and Jensen, C.D., "Welded Top Plate Beam-Column Connections," Welding Journal, Vol. 35, No. 7, July 1956.

42. Brandes, J.L., and Mains, R.M., "Report of Tests of Welded Top-plate and Seat Connections," The Welding Journal, Vol. 24, No. 3, March 1944.

43. Johnson, B.G., and Deits, G.R., "Tests of Miscellaneous Welded Building Connections," Welding Journal, January 1942.

44. Rathbun, J.C., "Elastic Properties of Riveted Connections," Transactions, ASCE, Vol. 101, 1936.

45. "Second Report of the Steel Structures Research Committee," Great Britain, Dept. Sci. Ind. Res., London, 1934.

46. Chen, C.K., "Seismic Analysis of Building Frames With Semirigid Connections," Proc. of the Eighth World Conference on Earthquake Engineering, Vol. V, San Francisco, CA, U.S.A., July 1984.

47. Stelmack, T.W., "Analytical and Experimental Response of Flexibly-Connected Steel Frames," Report to AISI Under Project No. 199, Dept. of Civil, Environmental, and Architectural Engineering, University of Colorado, Boulder, Colorado, February 1983.

48. Wales, M.W., and Rossow, E.C., "Coupled Moment-Axial Force Behavior in Bolted Joints," Journal of the Structural Division, ASCE, Vol 109, No. 5, May 1983.

49. Ackroyd, M.H., and Gerstle, K.H., "Behavior of Type 2 Steel Frames, Journal of the Structural Division, ASCE, Vol. 108, No. ST7, Proc. Paper 17207, July 1982.

50. Marley, M.H., "Analysis and Tests of Flexibility-Connected Steel Frames," Report to AISI Under Project No. 199, Dept of Civil, Environmental, and Architectural Engineering, University of Colorado, Boulder, Colorado, March 1982.

51. Moncarz, P.D., and Gerstle, K.H., "Steel Frames With Nonlineaar Connections," Journal of the Structural Division, ASCE, Vol. 107, No. ST8, Proc. Paper 16440, August 1981.

52. Graves, R.W., Biggs, J.M., and Irvine, H.M., "The Effect of Connection Flexibility on the Seismic Response of Welded Open Steel Frames," Pub. No. R80-25, School of Engineering, Massachusetts Institute of Technology, Cambridge, Mass., June 1980.

53. Ackroyd, M., and Gerstle, K., "Strength and Stiffness of Type 2 Steel Frames," Report Prepared for the American Iron and Steel Institute Undner Projet No. 199, Department of Civil, Environmental and Architectural Engineering, University of Colorado, Boulder, Colorado, July 1977.

54. American Iron and Steel Institute, "Type 2 Construction With Wind Moment Connections: A Return to Simplicity," AISI, Washington, D.C., 1976.

55. Kahl, T.L., "Flexibility-Connected Steel Frames," Report Prepared for the American Iron and Steel Institute Under Project No. 199, Department of Civil, Environmental, and Architectural Engineering, University of Colorado, Boulder, Colorado, December 1976.

56. Frye, M.J., and Morris, G.A., "Analysis of Flexibility-Connected Steel Frames," Canadian Journal of Civil Engineering, Vol. 2, 1975.

57. Ronstad, K.M., and Sabramanian, C.V., "Analysis of Frames With Partial Connection Rigidity," Journal of the Structural Division, ASCE, Vol. 96, No. ST11, Proc. Paper 7664, November 1970.

58. Monforton, G.R., and Wu,T.S., "Matrix Analysis of Semi-Rigidly Connected Frames," Journal of Structural Division, ASCE, Vol. 89, No. ST6, Proc. Paper 3713, December 1963.

59. Kaneta, K., Kohzu, I., and Nishizawa, H., "Cumulative Damage of Welded Beam-to-Column Connections in Steel Structures Subjected to Destructive Earthquakes," Proc. of the Eighth World Conference on Earthquake Engineering, Vol. VI, San Francisco, CA, U.S.A., July 1984.

60. Krawinkler, H., "Damage Assessment in Steel Structures Subjected to Severe Earthquakes," Proc. of the Eighth World Conference on Earthquake Engineering, Vol. IV, San Francisco, CA, U.S.A., July 1984.

61. Nash, W.A., Chon, V.T., and Hutchinson, C.E., "Cumulative Damage Effects in Seismic Structures," Proc. of the Fifth World Conference on Earthquake Engineering, Vol. 2, Rome, Italy, June 1974.

62. Suidan, M.T., and Eubanks, R.A., "Cumulative Fatigue Damage in Seismic Structures," Journal of the Structural Division, ASCE, Vol. 99, No. ST5, Proc. Paper 9749, May 1973.

63. Altman, W.G., Jr., Azizinamini, A., Bradburn, J.H., and

Radziminski, J.B., "Moment-Rotation Characteristics of Semi-Rigid Steel Beam-Column Connections," Structural Research Studies, Department of Civil Engineering, University of South Carolina, Columbia, S.C., June 1982.

64. American Institute of Steel Construction, Manual of Steel Construction, Eighth Edition, AISC, Inc., Chicago, Illinois, 1980.

65. Miner, M.A., "Cumulative Damage in Fatigue," Transactions, ASME, Vol. 12, No. 3, September 1945.

66. Tavernelli, J.F., and Coffin, L.F., Jr., "Experimental Support for Generalized Equation Predicting Low Cycle Fatigue," Transactions, ASME, J. Basic Engr., Vol. 84, No. 4, December 1962.

67. Coffin, L.F., Jr., "A study of the Effects of Cyclic Thermal Stresses on a Ductile Metal," Transactions, ASME, Vol. 76, 1954.

68. Manson, S.S., "Behavior of Materials Under Conditions of Thermal Stress," NACA TN 2933, 1954.

69. Azizinamini, A., "Cyclic Characteristics of Bolted Semi-Rigid Steel Beam to Column Connections," Ph.D. Dissertation, University of South Carolina, Columbia, S.C., 1985.

70. Neuber, H., "Theory of Stress Concentration for Shear-Strained Prismatic Bodies with Arbitrary Non-Linear Stress-Strain Law," Journal of Applied Mechanics, Transactions, ASME, Vol. 83, 1961.

71. Azizinamini, A., "Monotonic Response of Semi-Rigid Steel Beam to Column Connections," M.S. Thesis, University of South Carolina, Columbia, S.C., July 1982.

# APPENDIX A

## NOMENCLATURE

# APPENDIX A

## NOMENCLATURE

Symbol

| | | |
|---|---|---|
| $A$ | = | cross-sectional area of flange angle, t X L |
| $B$ | = | $B' - t/2$ |
| $B'$ | = | overall length of leg of flange angle adjacent to column face |
| $B_c$ | = | $B'_c - t_c/2$ |
| $B'_c$ | = | overall length of leg of web angle adjacent to column face |
| $C_i$ | = | coefficients in empirical equation of static $M-\phi$ curve |
| $D$ | = | $d + t/2$ |
| $E$ | = | Modulus of Elasticity of steel, 29000 ksi |
| $E$ | = | energy per cycle; area of single hysteresis loop |
| $F$ | = | shear force in beam representative of angle leg |
| $G$ | = | shear modulus of steel |
| $K$ | = | $P_1^{\alpha_1} P_2^{\alpha_2} --- P_n^{\alpha_n}$ |
| $L$ | = | overall length of flange angle |
| $L_c$ | = | overall length of web angle |
| $M$ | = | resisting moment transferred from beam to column through connection |
| $M_b$ | = | moment in beam representing connection angle |
| $M_c$ | = | moment contribution of web angles |
| $M_{el}$ | = | moment in connection at elastic limit |
| $M_f$ | = | moment contribution of flange angle |
| $M_y$ | = | yield moment of connection |
| $N_f$ | = | fatigue life for constant displacement amplitude cyclic test |
| $P_i$ | = | parameters affecting relationship between M and $\phi$ |

Symbol

| | | |
|---|---|---|
| $R$ | = | nominal flange angle chord rotation index, $2\left[\frac{(d+t)\ \tan\phi}{g-dw/2-t}\right]$ |
| $S$ | = | elastic section modulus |
| $Z$ | = | plastic section modulus |
| $a$ | = | $g - k$ |
| $b$ | = | $g - d_b/2 - t/2$ |
| $b_c$ | = | $g_c - d_b/2 - t_c/2$ |
| $d$ | = | depth of beam |
| $d_b$ | = | diameter of bolt |
| $d_h$ | = | diameter of bolt hole |
| $d_w$ | = | diameter of washer |
| $g$ | = | gage in flange angle; from heel of angle to center of bolt hole in leg adjacent to column face |
| $g_c$ | = | gage in web angle; from heel of angle to center of bolt hole |
| $k$ | = | distance from heal of angle to toe of fillet, flange angle |
| $k_c$ | = | distance from heel of angle to toe of fillet, web angle |
| $n$ | = | number of applied constant amplitude displacement cycles |
| $n$ | = | number of bolts in beam web |
| $p$ | = | pitch, center-to-center spacing of bolts in leg of flange angle adjacent to column face |
| $p_c$ | = | pitch, center-to-center spacing of bolts in each leg of web angle |
| $t$ | = | thickness of flange angle |
| $t_c$ | = | thickness of web angle |
| $\alpha_i$ | = | exponents in empirical equation of static $M-\phi$ curve |
| $\gamma$ | = | length of flange angle used in finite element analysis |
| $\Delta$ | = | displacement of heel of flange angle |

Symbol

$\varepsilon_y$ = strain at initial yieldng in connection angles

$\lambda$ = length of beam representative of flange angle leg adjacent to column face

$\lambda_c$ = length of beam representative of web angle leg adjacent to column face

$\sigma_y$ = stress at initial yielding in connection angles

$\phi$ = rotation of end of beam with respect to column face

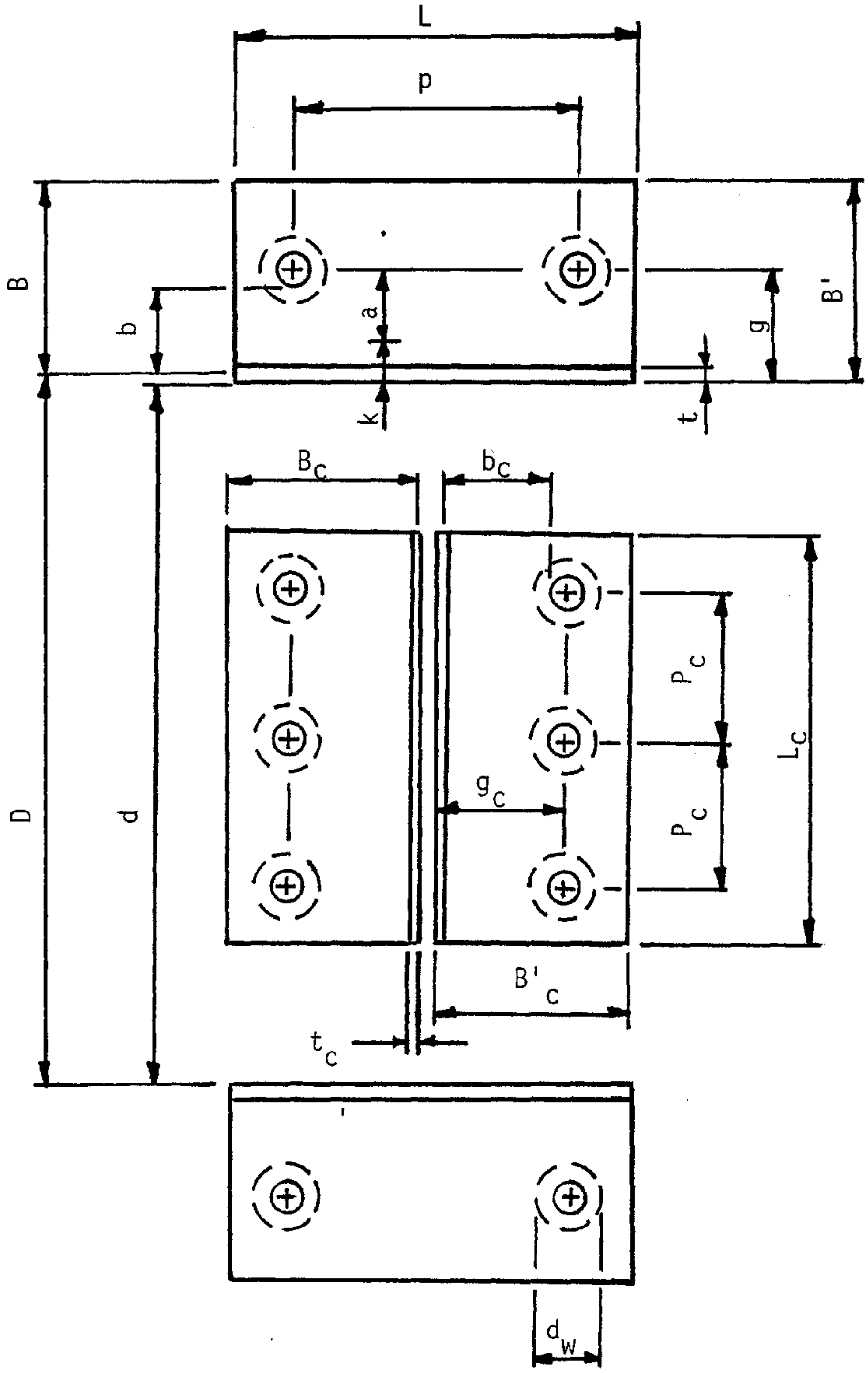


FIG. A1 NOMENCLATURE FOR CONNECTION ELEMENTS

# APPENDIX B

## THREE DIMENSIONAL FINITE ELEMENT ANALYSIS OF DOUBLE ANGLE PULL TEST SPECIMENS

# APPENDIX B

## B.1 Pull Tests

The main objective of the pull tests was to investigate the behavior of the flange angle only. A total of two pull tests was conducted. The general configuration of these specimens is shown in Figure B.1.

Flange angle thicknesses of 1/2-inch and 3/8-inch were investigated. An imposed displacement rate of 0.624 inch/minute was applied to the specimens through the actuator ram, which was attached to the center plate, as shown in Figure B.1. Figure B.2 shows the load vs. the average displacement obtained from the LVDTs attached to the two flange angles for specimens with a flange angle thickness of 1/2-inch. For the purpose of analysis, the experimentally obtained load-deformation curve was approximated by the smooth curve. It should be noted that Figure B.2 depicts the load-deformation curve for two flange angles attached as shown in Figure B.1. The assumption was made that the actuator load was evenly carried by the two flange angles, allowing for the load displacement curve for one flange angle to be obtained as shown in Figure B.4.

Figure B.3 shows the actuator load vs. the average of the two LVDT displacements for specimens with 3/8-inch thick flange angles, together with a smooth approximated curve for the purpose of analysis. Because of actuator load limitations, the test was discontinued when a load of approximately 50 kips had been applied to the specimen. Again, the assumption was made that each flange angle carries half the actuator load, to obtain the load-displacement curve for one flange angle as in Figure B.4.

## B.2 Specimens With Top and Bottom Flange Angles

In addition to the pulltests, tests were conducted of two specimens comprised of top and seat angles attached to W14X38 beam sections. The purpose of these tests was to study the ability of the results of the pull tests, and of a finite element analysis (discussed in Section B.3), to predict the moment-rotation characteristics of a connection with top and seat flange angles only. The test configuration for the specimens with top and bottom flange angles was identical to the specimens tested in the present investigation, Figure 2.2a, except that the web angles were omitted.

The results of tests for moment-rotation obtained for specimens with 1/2-inch thick flange angles and 3/8-inch flange angles are shown in Figures B.9 and B.10, respectively.

### B.3 Three Dimensional Finite Element Analysis

The finite element analysis program used in the analytical study is described in Reference 69. The model used in the analysis was developed from a portion of the flange angle, as shown in Figure B.5, by considering approximate boundary conditions and conditions of symmetry. Instead of modeling the entire length of the horizontal leg, only 1.75 inches of the 1/2-inch thick flange angle, and 1.625 inch of the 3/8-inch thick flange angle was modeled, since test observations indicated no appreciable deformation in the remainder of the horizontal leg.

A model was generated for both the 1/2-inch thick and 3/8-inch thick angles, each model consisting of 150 twenty-node isoparametric elements producing a total of 993 nodes, as shown in Figure B.6. For simplicity, the bolt hole in the vertical leg was modeled as a square with an area equivalent to that of a circular hole having a 15/16-inch diameter.

Symmetry conditions were imposed on Face A by restraining displacements in the Y direction on this face. Bolt head restraint was simulated by restraining all displacements for nodes at the intersection of the bolt hole and the front face of the angle. Displacements in the Z direction were restrained along line B-B and displacements in the X direction were restrained along line A-A.

Loading on the model was created by imposing uniform displacement of Face B in the X direction, as shown in Figure B.7, in small increments.

The stress-strain relation used in the analysis was obtained by conducting tension tests on sample coupons of flange angles used in the pull tests. The results were approximated by the bi-linear relationship indicated by Figure B.8.

Comparisons of the moment-rotation diagrams obtained from the pull tests, the finite element analysis, and the connection tests are shown for 1/2-inch and 3/8-inch thick flange angles in Figures B.9 and B.10, respectively, for a 14X38 beam section. For the 1/2-inch thick flange angles, the initial slopes from the finite element analysis, pull test, and connection test are 430,000, 365,000, and 840,000 k.-in./radian, respectively, while for the 3/8-inch thick flange angles, the slopes were 209,000, 338,000, and 135,000 k.-in./radian, respectively.

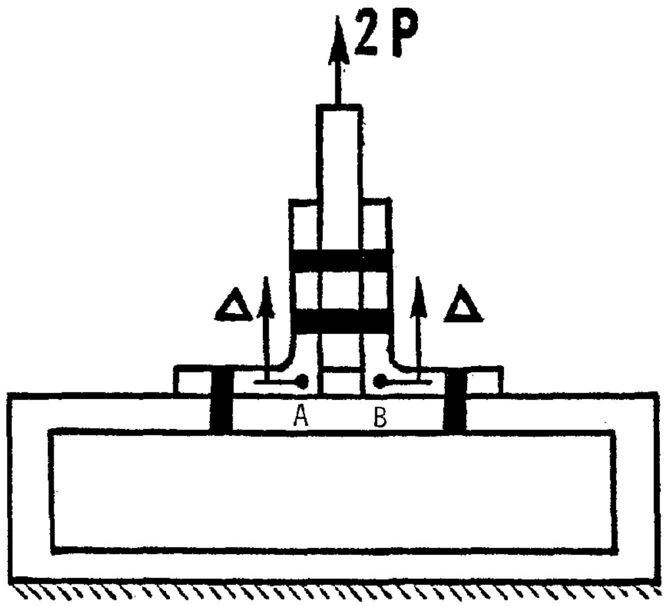


FIG. B.1 GENERAL CONFIGURATION OF PULL TEST SPECIMEN

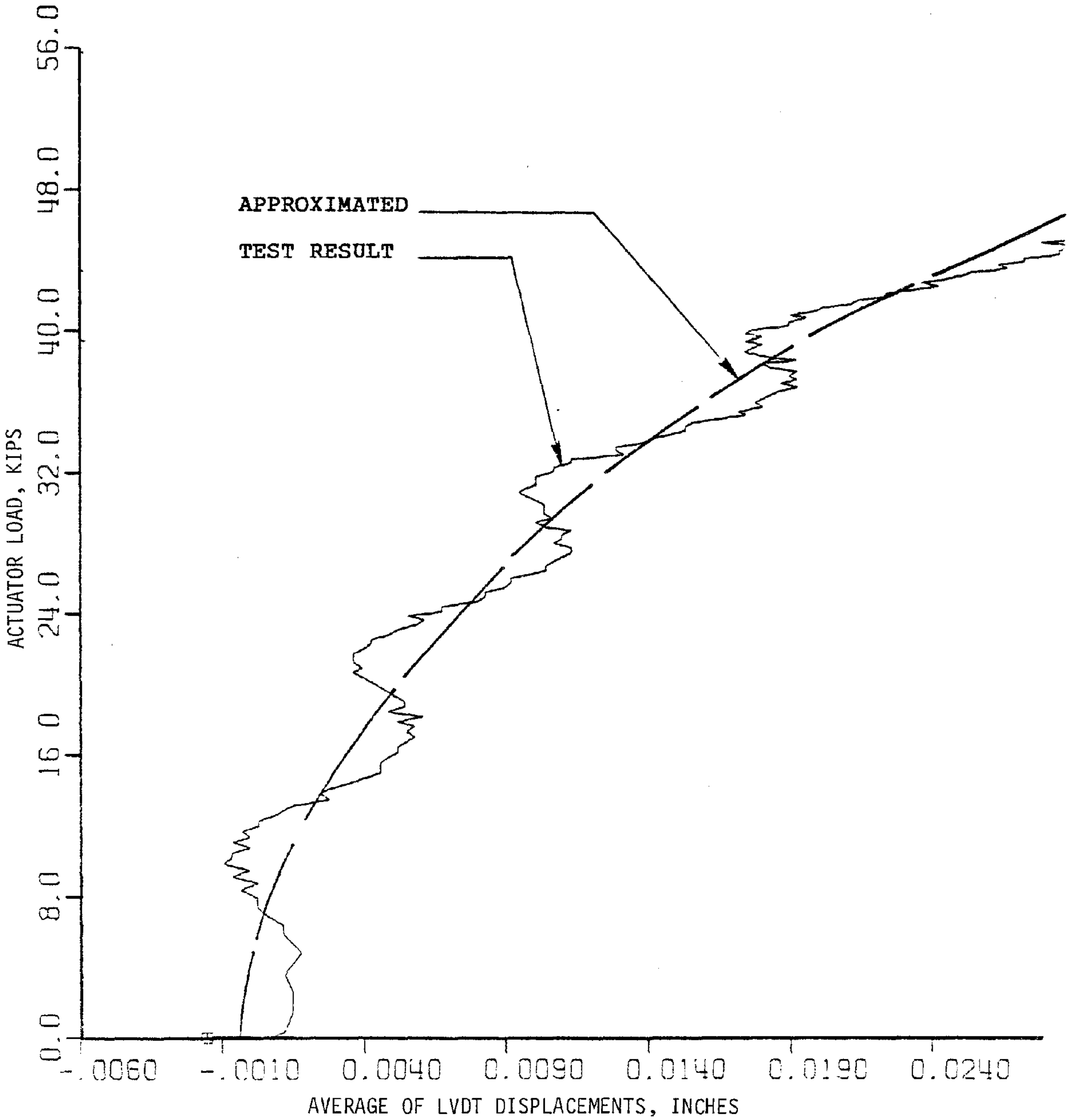


FIG. B.2 LOAD DEFORMATION CHARACTERISTICS OF PULL TEST SPECIMEN (FLANGE ANGLE THICKNESS OF ½-INCH)

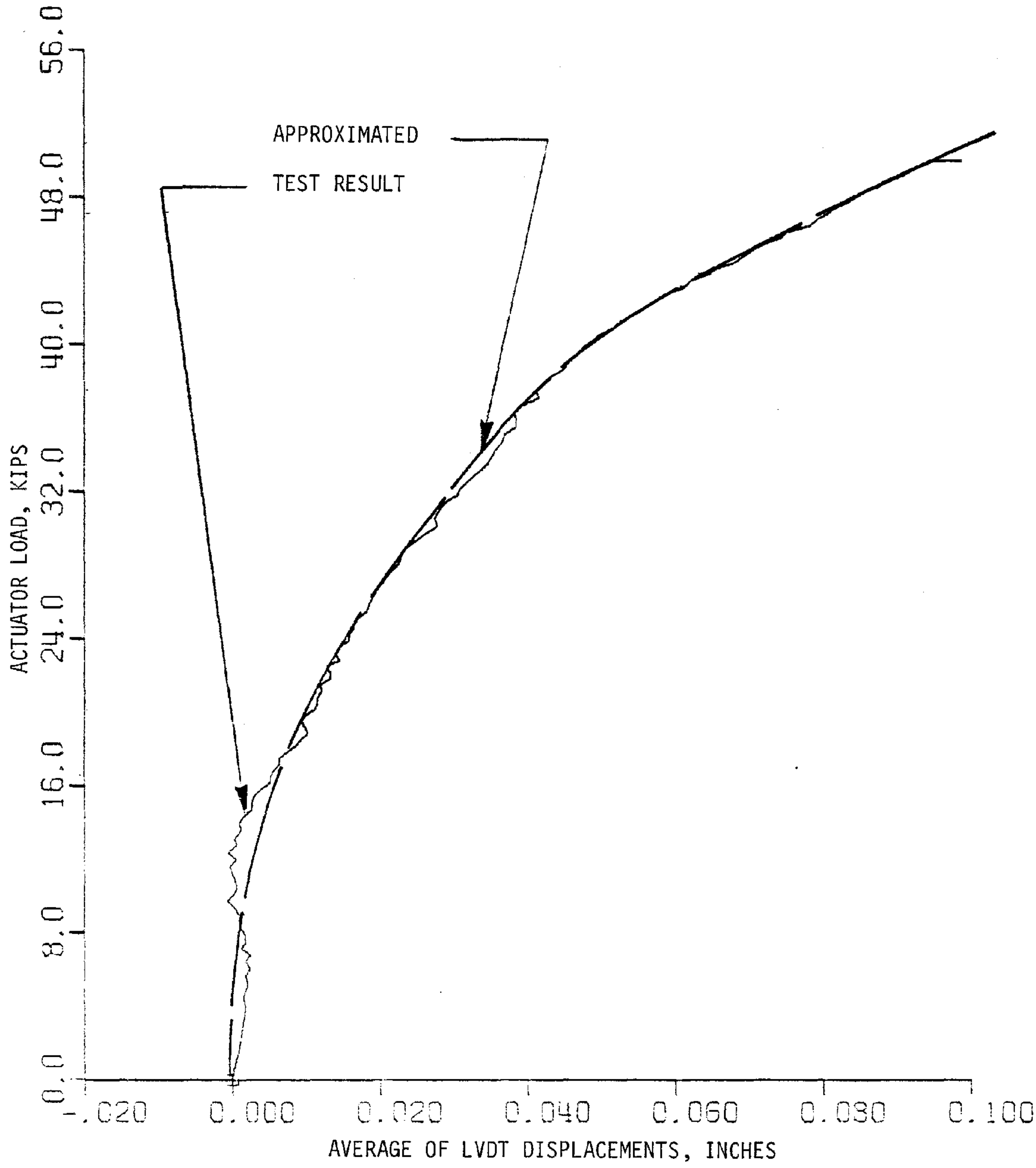


FIG. B.3 LOAD DEFORMATION CHARACTERISTICS OF PULL TEST SPECIMEN (FLANGE ANGLE THICKNESS OF ⅜-INCH)

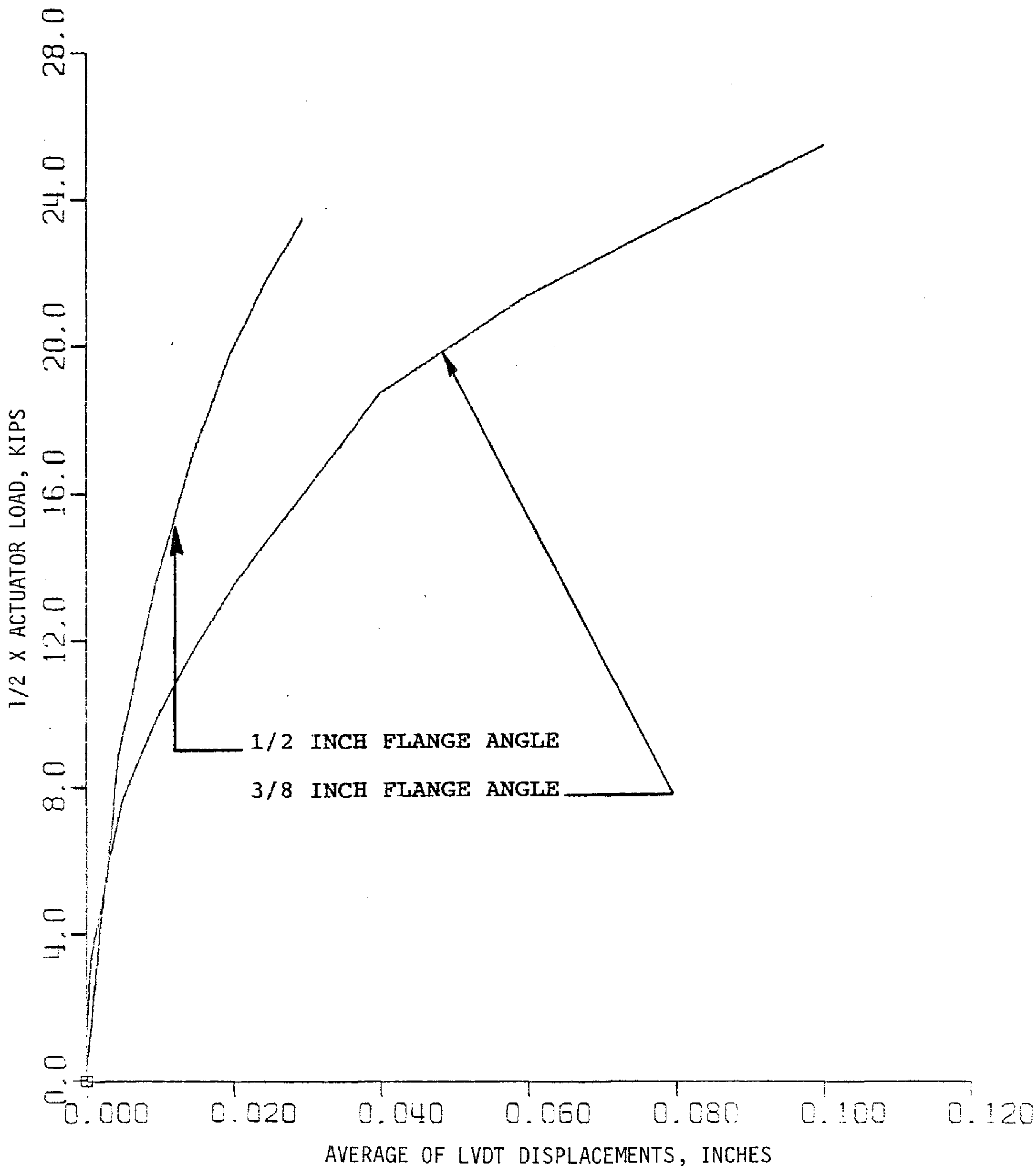


FIG. B.4 LOAD DEFORMATION CHARACTERISTICS OF PULL TEST SPECIMENS.

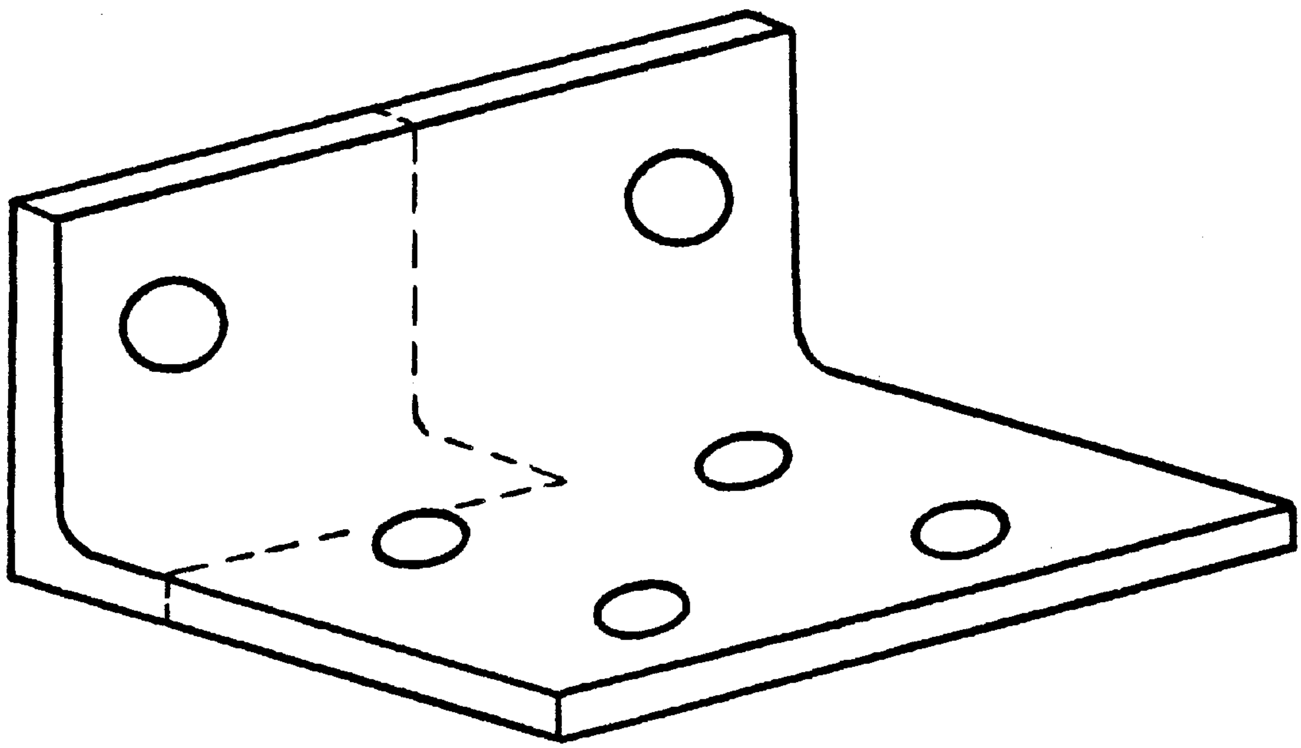

FIG. B.5 PORTION OF THE FLANGE ANGLE MODELED FOR FINITE ELEMENT ANALYSIS

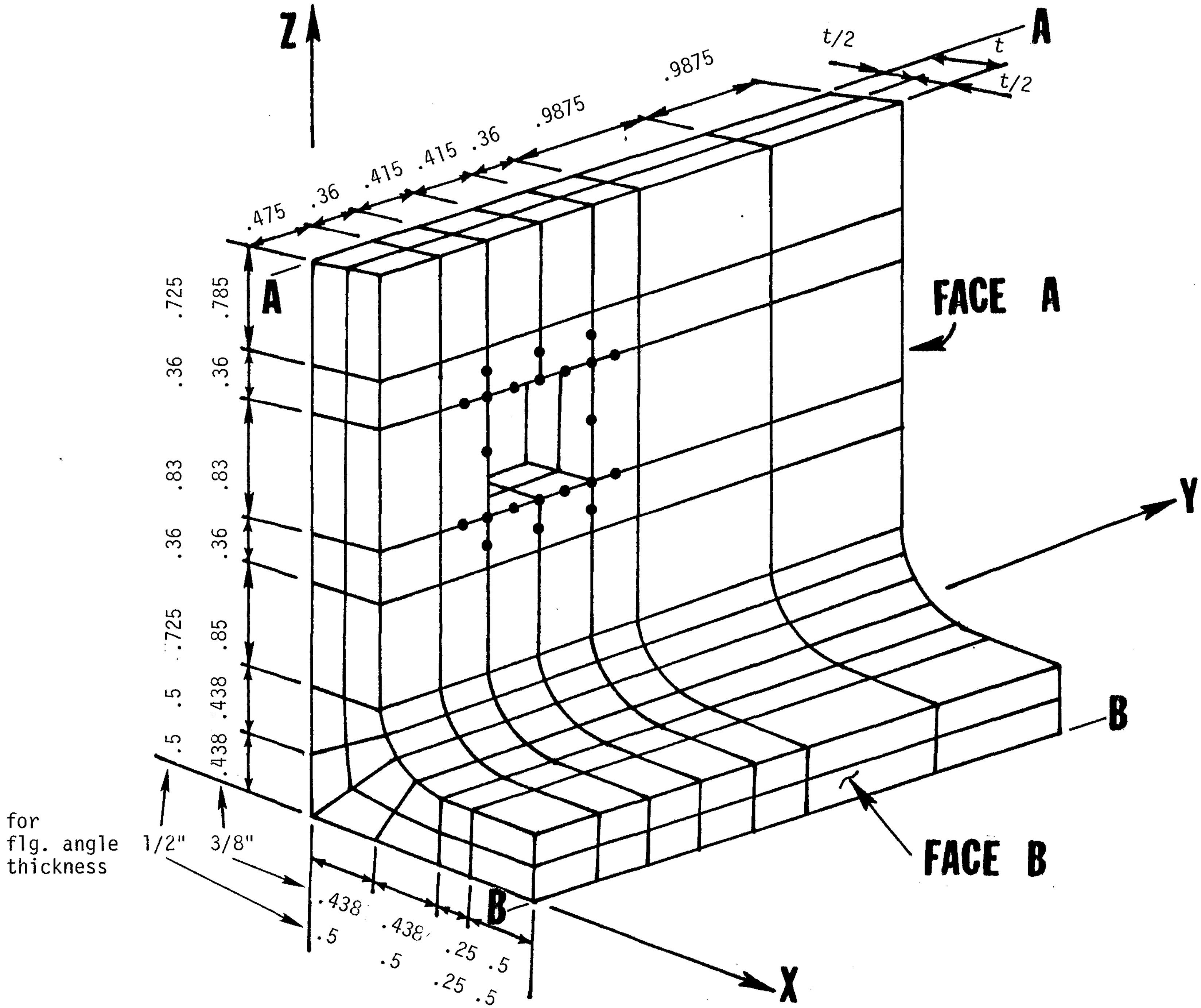


FIG. B.6 FINITE ELEMENT MODEL OF FLANGE ANGLE FOR ½ AND ⅜ INCH THICK FLANGE ANGLE

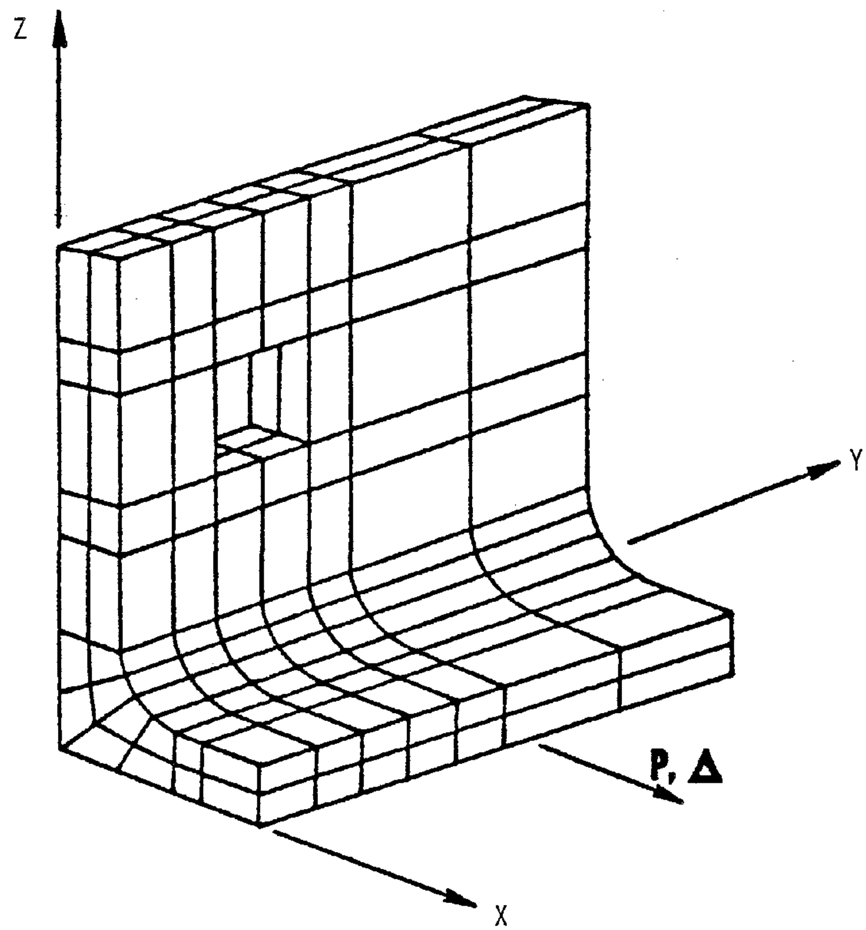


FIG. B.7 LOADING DIRECTION FOR FINITE ELEMENT MODEL

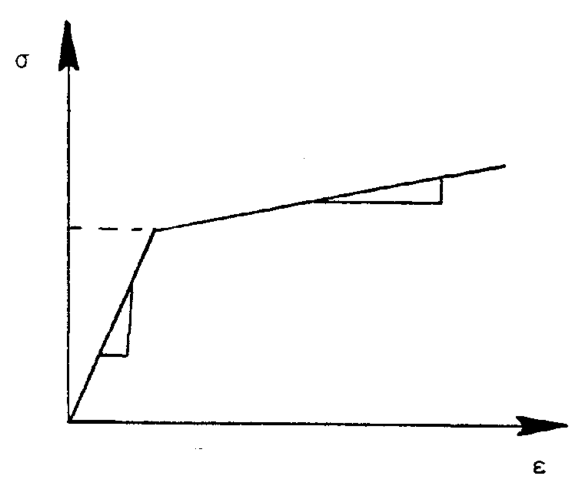


FIG. B.8 STRESS-STRAIN DIAGRAM OBTAINED FROM COUPON TEST USED IN FINITE ELEMENT ANALYSIS OF FLANGE ANGLE

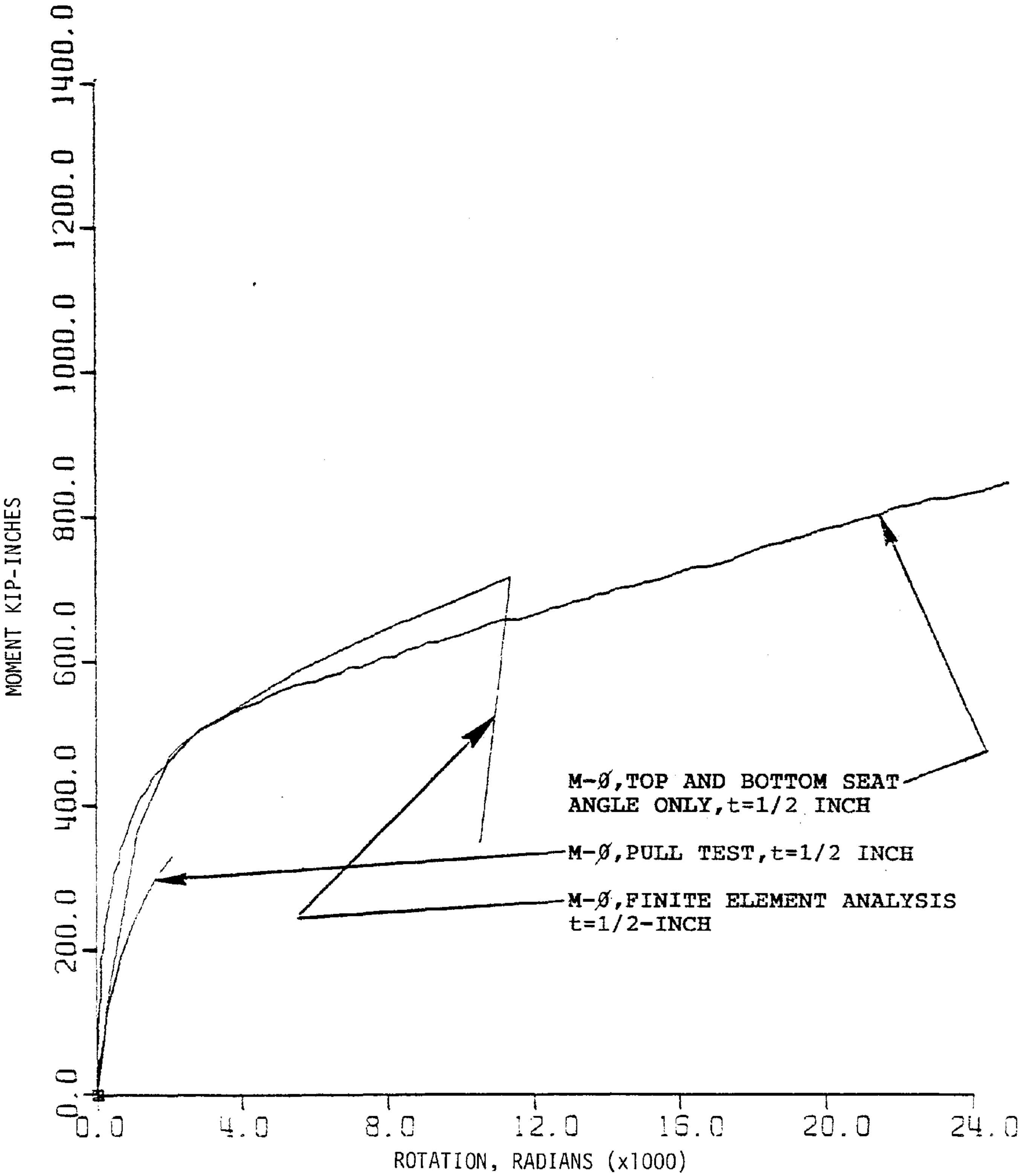


FIG. B.9 COMPARISON OF MOMENT—ROTATION CURVES FOR CONNECTION WITH TOP AND BOTTOM FLANGE ANGLE ONLY, T= ½-inch

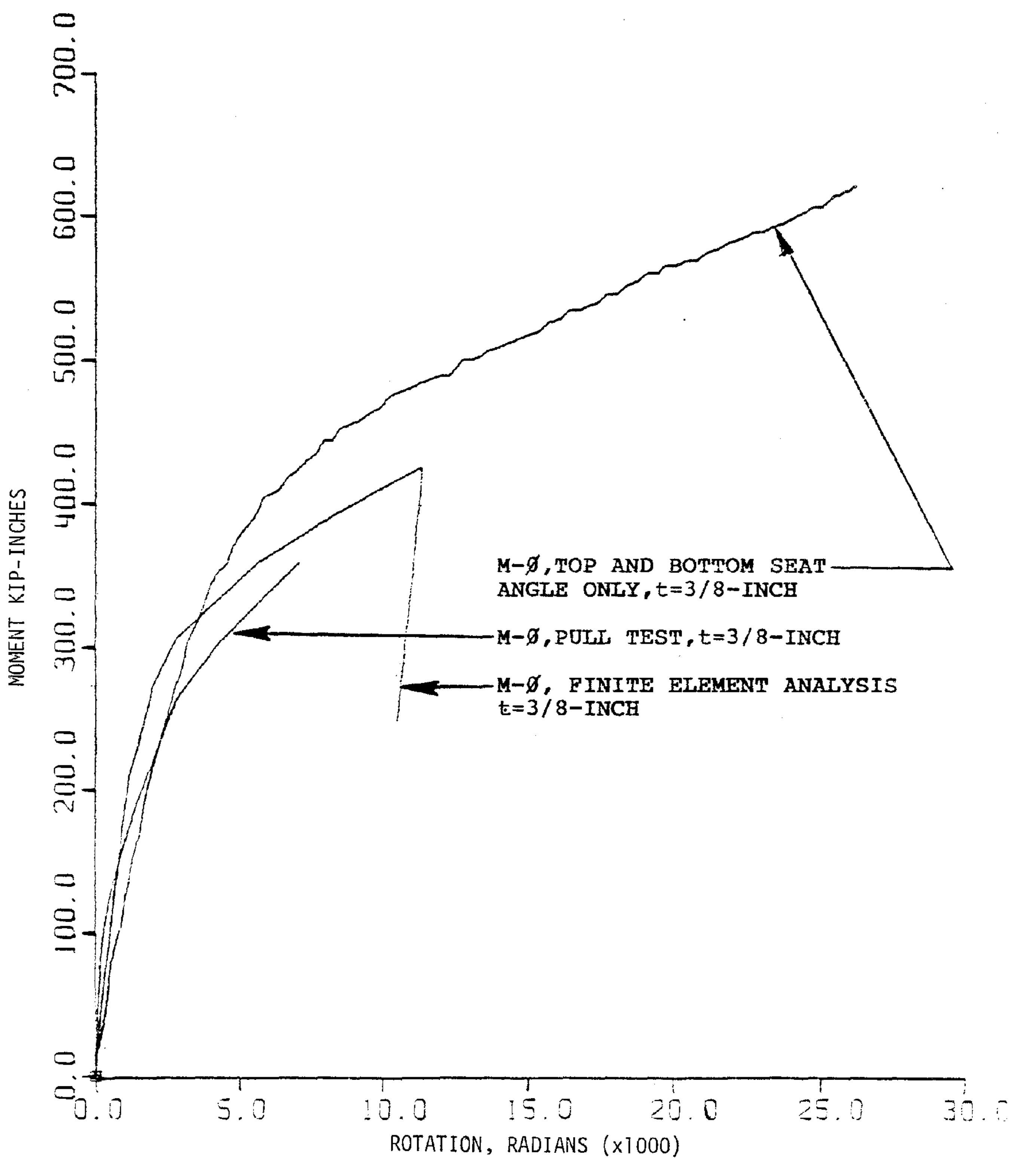


FIG. B.10 COMPARISON OF MOMENT-ROTATION CURVES FOR CONNECTION WITH TOP AND BOTTOM FLANGE ONLY, T=⅜-INCH

# TABLES

TABLE 2.1

MECHANICAL PROPERTIES OF TEST MATERIAL

| Designation | Mechanical Properties* | | |
|---|---|---|---|
| | Yield Stress (ksi) | Ultimate Strength (ksi) | Elongation in 2-inch Gage Length (percent) |
| ASTM A36 | 42.8 | 69.9 | 23.8 |
| | 42.9 | 67.9 | 22.9 |
| | 39.3 | 68.0 | 32.5 |
| | 37.6 | 67.9 | 31.9 |
| | 53** | 80** | - - |
| | 36.5 | 71.9 | 31.3 |
| | 43.7 | 69.9 | 31.3 |
| | 40.0 | 64.0 | 34.4 |
| | 38.0 | 66.0 | 37.5 |

* Top five entries represent stock used in fabrication of specimens in initial study (with 3/4" dia. bolts); bottom four entries represent stock used in fabrication of specimens in current study (with 7/8" dia. bolts, welds).

** Flange angle material, specimen 14S2.

TABLE 2.2

SCHEDULE OF BOLTED TEST SPECIMENS

3/4 - INCH DIAMETER BOLTS

| Specimen Number | Type of Test * | Beam Section | Top and Bottom Flange Angles ** | | | | Web Angles ** | |
|---|---|---|---|---|---|---|---|---|
| | | | Angle | Length "L" (inches) | Gage in Leg on Column Flange "g" (inches) | Bolt Spacing in Leg on Column Flange, "p" (inches) | Angle | Length, "$L_c$" (inches) |
| 14S1 | Static | W14X38 | L6X4X3/8 | 8 | 2½ | 5½ | 2L4X3½X¼ | 8½ |
| 14S2 | Static | W14X38 | L6X4x½ | 8 | 2½ | 5½ | 2L4X3½X¼ | 8½ |
| 14S3 | Static | W14X38 | L6X4X3/8 | 8 | 2½ | 5½ | 2L4X3½X¼ | 5½ † |
| 14S4 | Static | W14X38 | L6X4X3/8 | 8 | 2½ | 5½ | 2L4X3½X3/8 | 8½ |
| 8S1 | Static | W8X21 | L6X3½X5/16 | 6 | 2 | 3½ | 2L4X3½X¼ | 5½ |
| 8S2 | Static | W8X21 | L6X3½X3/8 | 6 | 2 | 3½ | 2L4X3½X¼ | 5½ |
| 8S3 | Static | W8X21 | L6X3½X5/16 | 8 | 2 | 3½ | 2L4X3½X¼ | 5½ |
| 8S4 | Static | W8X21 | L6X6X3/8 | 6 | 4½ | 3½ | 2L4X3½X¼ | 5½ |
| 8S5 | Static | W8X21 | L6X4X3/8 | 8 | 2½ | 5½ | 2L4X3½X¼ | 5½ |
| 8S6 | Static | W8X21 | L6X4X5/16 | 6 | 2½ | 3½ | 2L4X3½X¼ | 5½ |
| 8S7 | Static | W8X21 | L6X4X3/8 | 6 | 2½ | 3½ | 2L4X3½X¼ | 5½ |
| 14C1 | Cyclic-LH | W14X38 | L6X4X3/8 | 8 | 2½ | 5½ | 2L4X3½X¼ | 8½ |
| 14C2 | Cyclic-LH | W14X38 | L6X4½ | 8 | 2½ | 5½ | 2L4X3½X¼ | 8½ |
| 8C1 | Cyclic-LH | W8X21 | L6X3½X5/16 | 6 | 2 | 3½ | 2L4X3½X¼ | 5½ |
| 8C2 | Cyclic-LH | W8X21 | L6X3½X3/8 | 6 | 2 | 3½ | 2L4X3½X¼ | 5½ |

* Cyclic - LH: Low to high amplitude block loading, Fig. 2.11a
Cyclic - CF: Constant amplitude (fatigue) loading, Fig. 2.11b
Cyclic - HL: High to low amplitude block loading, Fig. 2.11c

** See Nomenclature, Appendix A

† Two bolts at 3-inch spacing, mounted on top two holes on stub column, Fig. 2.2a

TABLE 2.3

SCHEDULE OF BOLTED TEST SPECIMENS

7/8 - INCH DIAMETER BOLTS

| Specimen Number | Type of Test * | Beam Section | Top and Bottom Flange Angles ** | | | | Web Angles ** | |
|---|---|---|---|---|---|---|---|---|
| | | | Angle | Length "L" (inches) | Gage in Leg on Column Flange "g" (inches) | Bolt Spacing in Leg on Column Flange, "p" (inches) | Angle | Length, "$L_c$" (inches) |
| 14S5 | Static | W14X38 | L6X4X3/8 | 8 | 2½ | 5½ | 2L4X3½X¼ | 8½ |
| 14S6 | Static | W14X38 | L6X4X½ | 8 | 2½ | 5½ | 2L4X3½X¼ | 8½ |
| 14S8 | Static | W14X38 | L6X4X5/8 | 8 | 2½ | 5½ | 2L4X3½X¼ | 8½ |
| 14S9 | Static | W14X38 | L6X4X½ | 8 | 2½ | 5½ | 2L4X3½X¼ | 8½ |
| 14F1 | Cyclic-CF | W14X38 | L6X4X3/8 | 8 | 2½ | 5½ | 2L4X3½X¼ | 8½ |
| 14F2 | Cyclic-CF | W14X38 | L6X4X3/8 | 8 | 2½ | 5½ | 2L4X3½X¼ | 8½ |
| 14F3 | Cyclic-CF | W14X38 | L6X4X3/8 | 8 | 2½ | 5½ | 2L4X3½X¼ | 8½ |
| 14F4 | Cyclic-CF | W14X38 | L6X4X3/8 | 8 | 2½ | 5½ | 2L4X3½X¼ | 8½ |
| 14F5 | Cyclic-CF | W14X38 | L6X4X½ | 8 | 2½ | 5½ | 2L4X3½X¼ | 8½ |
| 14F6 | Cyclic-CF | W14X38 | L6X4X½ | 8 | 2½ | 5½ | 2L4X3½X¼ | 8½ |
| 14F7 | Cyclic-CF | W14X38 | L6X4X½ | 8 | 2½ | 5½ | 2L4X3½X¼ | 8½ |
| 14F8 | Cyclic-CF | W14X38 | L6X4X½ | 8 | 2½ | 5½ | 2L4X3½X¼ | 8½ |
| 14F9 | Cyclic-CF | W14X38 | L6X4X3/8 | 8 | 2½ | 5½ | 2L4X3½X¼ | 8½ |
| 14C3 | Cyclic-LH | W14X38 | L6X4X½ | 8 | 2½ | 5½ | 2L4X3½X¼ | 8½ |
| 14C4 | Cyclic-LH | W14X38 | L6X4X3/8 | 8 | 2½ | 5½ | 2L4X3½X¼ | 8½ |

* Cyclic - LH: Low to high amplitude block loading, Fig. 2.11a
Cyclic - CF: Constant amplitude (fatigue) loading, Fig. 2.11b
Cyclic - HL: High to low amplitude block loading, Fig. 2.11c

** See Nomenclature, Appendix A

TABLE 2.3 (CONTINUED)

SCHEDULE OF BOLTED TEST SPECIMENS

7/8 - INCH DIAMETER BOLTS

| Specimen Number | Type of Test * | Beam Section | Top and Bottom Flange Angles ** | | | | Web Angles ** | |
|---|---|---|---|---|---|---|---|---|
| | | | Angle | Length "L" (inches) | Gage in Leg on Column Flange "g" (inches) | Bolt Spacing in Leg on Column Flange, "p" (inches) | Angle | Length, "$L_c$" (inches) |
| 14B1 | Cyclic-HL | W14X38 | L6X4X½ | 8 | 2½ | 5½ | 2L4X3½X¼ | 8½ |
| 8S8 | Static | W8X21 | L6X3½X5/16 | 6 | 2 | 3½ | 2L4X3½X¼ | 5½ |
| 8S9 | Static | W8X21 | L6X3½X3/8 | 6 | 2 | 3½ | 2L4X3½X¼ | 5½ |
| 8S10 | Static | W8X21 | L6X3½X½ | 6 | 2 | 3½ | 2L4X3½X¼ | 5½ |
| 8F1 | Cyclic-CF | W8X21 | L6X3½X3/8 | 6 | 2 | 3½ | 2L4X3½X¼ | 5½ |
| 8F2 | Cyclic-CF | W8X21 | L6X3½X3/8 | 6 | 2 | 3½ | 2L4X3½X¼ | 5½ |
| 8F3 | Cyclic-CF | W8X21 | L6X3½X3/8 | 6 | 2 | 3½ | 2L4X3½X¼ | 5½ |
| 8F4 | Cyclic-CF | W8X21 | L6X3½X3/8 | 6 | 2 | 3½ | 2L4X3½X¼ | 5½ |
| 8F6 | Cyclic-CF | W8X21 | L6X3½X5/16 | 6 | 2 | 3½ | 2L4X3½X¼ | 5½ |
| 8F7 | Cyclic-CF | W8X21 | L6X3½X5/16 | 6 | 2 | 3½ | 2L4X3½X¼ | 5½ |
| 8F8 | Cyclic-CF | W8X21 | L6X3½X5/16 | 6 | 2 | 3½ | 2L4X3½X¼ | 5½ |
| 8C3 | Cyclic-LH | W8X21 | L6X3½X3/8 | 6 | 2 | 3½ | 2L4X3½X¼ | 5½ |
| 8B1 | Cyclic-HL | W8X21 | L6X3½X3/8 | 6 | 2 | 3½ | 2L4X3½X¼ | 5½ |

* Cyclic - LH: Low to high amplitude block loading, Fig. 2.11a
Cyclic - CF: Constant amplitude (fatigue) loading, Fig. 2.11b
Cyclic - HL: High to low amplitude block loading, Fig. 2.11c

** See Nomenclature, Appendix A

TABLE 2.4

SCHEDULE OF BOLTED-WELDED TEST SPECIMENS
7/8-INCH DIAMETER BOLTS

| Specimen Number | Type of Test | Beam Section | Top and Bottom Flange Angles* | | | | | Web Angles* | | |
|---|---|---|---|---|---|---|---|---|---|---|
| | | | Angle | Length "L" (inches) | Gage in Leg On Col Flange "g" (inches) | Bolt Spacing in Leg on Column Flange "p" (inches) | Weld size (inches) | Angle | Length "$L_c$" (inches) | Weld size (inches) |
| 14WS1 | Static | W14X38 | L6X4X3/8 | 8 | 2½ | 5½ | 5/16 | 2L4X3½X¼ | 8½ | 3/16 |
| 14WS2 | Static | W14X38 | L6X4X½ | 8 | 2½ | 5½ | 5/16 | 2L4X3½X¼ | 8½ | 3/16 |

*See Nomenclature, Appendix A
For weld details, see Fig. 2.3

TABLE 3.1

SUMMARY OF STATIC TEST RESULTS - BOLTED SPECIMENS
3/4-INCH DIAMETER BOLTS

| Specimen Number | Initial Slope of M-$\phi$ Curve (k-in./radian) | Slope of Secant Line to M-$\phi$ Curve at $4.0X10^{-3}$ radians (k-in./radian) | Moment at $4.0X10^{-3}$ radians (k-in.) | Slope of M-$\phi$ Curve at $24X10^{-3}$ radians (k-in./radian) | Moment at $24X10^{-3}$ radians (k-in.) | Remarks |
|---|---|---|---|---|---|---|
| 14S1 | $195.0X10^{+3}$ | $108.7X20^{+3}$ | 435 | $5.8X10^{+3}$ | 688 | |
| 14S2 | 295.0 | 151.8 | 607 | 12.6 | (947) | Major slip at $12X10^{-3}$ & $20X10^{-3}$ radians |
| 14S3 | 115.9 | 88.8 | 355 | 7.2 | 652 | |
| 14S4 | 221.9 | 124.0 | 496 | 8.3 | 822 | |
| 8S1 | 66.7 | 44.3 | 177 | 4.1 | 329 | |
| 8S2 | 123.4 | 69.0 | 276 | 1.5 | (384) | Major slip at $16X10^{-3}$ radians |
| 8S3 | 104.7 | 64.3 | 257 | 4.0 | 422 | |
| 8S4 | 15.3 | 14.4 | 57.5 | 2.2 | 165 | |
| 8C5 | 76.7 | 47.9 | 191.5 | 2.7 | 337 | |
| 8S6 | 39.5 | 30.0 | 120 | 3.2 | 244 | |
| 8S7 | 48.0 | 40.8 | 163 | 3.2 | 381 | |

TABLE 3.2

SUMMARY OF STATIC TEST RESULTS - BOLTED SPECIMENS
(7/8-INCH DIAMETER BOLTS)

| Specimen Number | Initial Slope of M-$\phi$ Curve (k-in./radian) | Slope of Secant Line to M-$\phi$ Curve and $4.0X10^{-3}$ radians (k-in./radian) | Moment at $4.0X10^{-3}$ radians (k-in.) | Slope of M-$\phi$ Curve at $24X10^{-3}$ radians (k-in./radian) | Moment at $24X10^{-3}$ radians (k-in.) | Remarks |
|---|---|---|---|---|---|---|
| 14S5 | $247X10^{+3}$ | $117.4X10^{+3}$ | 467 | $10.8X10^{+3}$ | 763 | |
| 14S6 | 286 | 146.9 | 589 | 10.3 | 1053 | |
| 14S8 | 579 | 256.9 | 1027 | 15.0 | 1561 | |
| 14S9 | 258 | 154.1 | 624 | 9.3 | 1024 | |
| 8S8 | 70 | 44.4 | 183 | 3.8 | 380 | |
| 8S9 | 104 | 54.5 | 226 | 4.4 | 423 | |
| 8S10 | 427 | 104.1 | 434 | 6.9 | (634) | Major slip at $5.3X10^{-3}$ radians |

TABLE 3.3

SUMMARY OF STATIC TEST RESULTS - BOLTED-WELDED SPECIMENS

| Specimen Number | Initial Slope of M-$\phi$ Curve (k-in./radian) | Slope of Secant Line to M-$\phi$ Curve at $4.0 \times 10^{-3}$ radians (k-in./radian) | Moment at $4.0 \times 10^{-3}$ radians (k-in.) | Slope of M-$\phi$ Curve at $24 \times 10^{-3}$ radians (k-in./radian) | Moment at $24 \times 10^{-3}$ radians (k-in.) |
|---|---|---|---|---|---|
| 14WS1 | $200 \times 10^{+3}$ | $119.4 \times 10^{+3}$ | 486 | 12.1 | 923 |
| 14WS2 | 456 | 188.5 | 773 | 11.5 | 1235 |

TABLE 3.4

SUMMARY OF CYCLIC TEST RESULTS - SPECIMEN 14C1

| Actuator Displacement Amplitude (inches) | Frequency (Hz) | Number of Cycles | Range of Rotation (radians X 1000) | Range of Moment (kip-inches) | Area of a Single Hysteresis Loop* (kip-inches) | Cumulative Area of Hysteresis Loops (kip-inches) | Cumulative Number of Cycles | Remarks |
|---|---|---|---|---|---|---|---|---|
| 0.2 | .05 | 4 | - | - | - | - | 4 | No Data |
| | .1 | 1 | 2.20 | 435.8 | 0 | 0 | 5 | |
| | | 1 | 2.08 | 441.5 | 0 | 0 | 6 | |
| | .5 | 1 | 2.10 | 428.5 | 0 | 0 | 7 | |
| | | 10 | 2.34 | 439.2 | 0 | 0 | 17 | |
| 0.4 | .1 | 1 | 4.75 | 745.0 | .296 | .296 | 18 | |
| | | 1 | 4.87 | 738.5 | .123 | .419 | 19 | |
| | | 1 | 4.89 | 741.5 | .111 | .530 | 20 | |
| | .25 | 1 | 4.91 | 742.5 | .069 | .599 | 21 | |
| | | 1 | 4.77 | 737.1 | .064 | .663 | 22 | |
| | | 10 | 5.04 | 751.7 | .069 | 1.353 | 32 | |
| 0.6 | .1 | 1 | 7.84 | 931.3 | .734 | 2.087 | 33 | |
| | | 1 | 7.77 | 934.9 | .419 | 2.506 | 34 | |
| | | 1 | 7.85 | 933.2 | .320 | 2.826 | 35 | |
| | .25 | 1 | 7.78 | 924.9 | .283 | 3.109 | 36 | |
| | | 1 | 7.88 | 922.0 | .279 | 3.388 | 37 | |
| | | 10 | 8.08 | 932.2 | .282 | 6.208 | 47 | |
| 0.8 | .1 | 1 | 11.10 | 1068 | 1.608 | 7.816 | 48 | |
| | | 1 | 10.99 | 1046 | .998 | 8.814 | 49 | |
| | | 1 | 10.86 | 1031 | .824 | 9.638 | 50 | |
| | .25 | 1 | 10.95 | 1032 | .812 | 10.450 | 51 | |
| | | 1 | 11.03 | 1034 | .831 | 11.281 | 52 | |
| | | 10 | 11.23 | 1042 | .829 | 19.571 | 62 | |
| 1.0 | .1 | 1 | 14.44 | 1142 | 2.45 | 22.021 | 63 | |
| | | 1 | 14.32 | 1105 | 1.912 | 23.933 | 64 | |
| | | 1 | 14.37 | 1102 | 1.875 | 25.808 | 65 | |
| | .25 | 1 | 14.49 | 1095 | 1.818 | 27.626 | 66 | |
| | | 1 | 14.28 | 1094 | 1.83 | 29.456 | 67 | |
| | | 10 | 14.70 | 1109 | 1.78 | 47.256 | 77 | |

*For multiple cycles, the area of one loop is computed as the average of the first and last loop areas.

Continued -

TABLE 3.4 (CONTINUED)

SUMMARY OF CYCLIC TEST RESULTS - SPECIMEN 14C1

| Actuator Displacement Amplitude (inches) | Frequency (Hz) | Number of Cycles | Range of Rotation (radians X 1000) | Range of Moment (kip-inches) | Area of a Single Hysteresis Loop* (kip-inches) | Cumulative Area of Hysteresis Loops (kip-inches) | Cumulative Number of Cycles | Remarks |
|---|---|---|---|---|---|---|---|---|
| 1.2 | .1 | 1 | 17.73 | 1185 | 3.747 | 51.003 | 78 | |
| | | 1 | 17.64 | 1146 | 3.372 | 54.38 | 79 | |
| | | 1 | 17.78 | 1142 | 3.39 | 57.77 | 80 | |
| | .25 | 1 | 17.67 | 1139 | 3.278 | 61.04 | 81 | |
| | | 1 | 17.70 | 1140 | 3.241 | 64.28 | 82 | |
| | | 10 | 17.94 | 1140 | 3.193 | 96.21 | 92 | |
| 1.4 | .1 | 1 | 21.12 | 1207 | 5.480 | 101.69 | 93 | |
| | | 1 | 21.17 | 1183 | 5.230 | 106.9 | 94 | |
| | | 1 | 21.36 | 1173 | 5.232 | 112.2 | 95 | |
| | .25 | 1 | 21.22 | 1171 | 5.09 | 117.2 | 96 | |
| | | 1 | 21.18 | 1169 | 5.033 | 122.3 | 97 | |
| | | 10 | 21.73 | 1170 | 4.98 | 172.1 | 107 | |
| 1.6 | .1 | 1 | 24.51 | 1276 | 7.092 | 179.2 | 108 | |
| | | 1 | 24.65 | 1250 | 6.704 | 185.9 | 109 | |
| | | 1 | 24.68 | 1238 | 6.577 | 192.5 | 110 | |
| | | 1 | 24.83 | 1230 | 6.594 | 199.0 | 111 | |
| | .25 | 1 | 24.52 | 1217 | 6.58 | 205.6 | 112 | |
| | | 1 | 24.60 | 1219 | 6.537 | 212.2 | 113 | |
| | | 10 | 25.11 | 1217 | 6.507 | 277.2 | 123 | |
| 1.8 | .1 | 1 | 28.30 | 1261 | 9.0 | 286.2 | 124 | |
| | | 1 | 28.42 | 1232 | 8.912 | 295.1 | 125 | |
| | | 1 | 28.31 | 1213 | 8.734 | 303.9 | 126 | |
| | .25 | 1 | 28.17 | 1213 | 8.615 | 312.5 | 127 | |
| | | 1 | 28.22 | 1203 | 8.60 | 321.1 | 128 | |
| | | 10 | 28.55 | 1206 | 8.415 | 405.2 | 138 | |
| 2.0 | .1 | 1 | 31.81 | 1257 | 11.0 | 416.2 | 139 | |
| | | 1 | 31.76 | 1225 | 10.87 | 427.1 | 140 | |
| | | 1 | 32.17 | 1220 | 10.775 | 437.9 | 141 | |
| | .25 | 1 | ---- | ---- | ---- | ---- | ---- | half cycle |
| | | 1 | 31.85 | 1193 | 10.55 | 448.4 | 142 | |
| | | 1 | 31.90 | 1198 | 10.474 | 458.9 | 143 | |
| | | 6 | 32.46 | 1197 | 10.26 | 520.5 | 149 | cracks detected-6th cycle |

*For multiple cycles, the area of one loop is computed as the average of the first and last loop areas.

TABLE 3.5

SUMMARY OF CYCLIC TEST RESULTS - SPECIMEN 14C2

| Actuator Displacement Amplitude (inches) | Frequency (Hz) | Number of Cycles | Range of Rotation (radians X 1000) | Range of Moment (kip-inches) | Area of a Single Hysteresis Loop* (kip-inches) | Cumulative Area of Hysteresis Loops (kip-inches) | Cumulative Number of Cycles | Remarks |
|---|---|---|---|---|---|---|---|---|
| 0.2 | .1 | 1 | 2.16 | 472.3 | 0 | | 1 | |
| | .25 | 1 | 2.12 | 478.1 | 0 | | 2 | |
| | | 1 | 2.09 | 474.2 | 0 | | 3 | |
| | | 10 | 2.37 | 488.7 | 0 | 0 | 13 | |
| .4 | .1 | 1 | 4.47 | 850.7 | .238 | .238 | 14 | |
| | .25 | 1 | 4.45 | 831.1 | .152 | .390 | 15 | |
| | | 1 | 4.54 | 857.0 | .135 | .525 | 16 | |
| | | 10 | 4.43 | ** | .211** | 2.635 | 26 | |
| .6 | .1 | 1 | 7.07 | 1132 | .725 | 3.360 | 27 | Inverted cycle*** |
| | .25 | 1 | 7.0 | 1143 | .404 | 3.764 | 28 | Inverted cycle |
| | | 1 | 7.1 | 1139 | .310 | 4.074 | 29 | Inverted cycle |
| | | 10 | 7.31 | 1154 | .304 | 7.114 | 39 | |
| .8 | .1 | 1 | 10.12 | 1357 | 1.469 | 8.583 | 40 | |
| | | 1 | 9.95 | 1345 | .878 | 9.461 | 41 | Inverted cycle |
| | | 1 | 9.87 | 1345 | 1.038 | 10.499 | 42 | Inverted cycle |
| | .25 | 1 | 10.08 | 1334 | .748 | 11.247 | 43 | |
| | | 1 | 9.82 | 1331 | .928 | 12.175 | 44 | |
| | | 10 | 10.09 | 1332 | .919 | 21.365 | 54 | |
| 1.0 | .1 | 1 | 13.12 | 1490 | 2.809 | 24.174 | 55 | |
| | .25 | 1 | 12.98 | 1477 | 2.437 | 26.611 | 56 | |
| | | 1 | 13.26 | 1466 | 2.262 | 28.873 | 57 | |
| | | 10 | 13.43 | 1465 | 2.197 | 50.843 | 67 | |
| 1.2 | .1 | 1 | 16.28 | 1571 | 4.563 | 55.406 | 68 | |
| | .25 | 1 | 16.31 | 1548 | 4.237 | 59.643 | 69 | |
| | | 1 | 16.18 | 1541 | 4.101 | 63.744 | 70 | |
| | | 10 | 16.70 | 1536 | 4.012 | 103.86 | 80 | |

*For multiple cycles, the area of one loop is computed as the average of the first and last loop areas.
**Questionable data.
***Load cycle inverted from normal sine wave, Fig. 3.28.

Continued -

TABLE 3.5 (CONTINUED)

SUMMARY OF CYCLIC TEST RESULTS - SPECIMEN 14C2

| Actuator Displacement Amplitude (inches) | Frequency (Hz) | Number of Cycles | Range of Rotation (radians X 1000) | Range of Moment (kip-inches) | Area of a Single Hysteresis Loop* (kip-inches) | Cumulative Area of Hysteresis Loops (kip-inches) | Cumulative Number of Cycles | Remarks |
|---|---|---|---|---|---|---|---|---|
| 1.4 | .1 | 1 | 19.79 | 1637 | 6.837 | 110.70 | 81 | |
| | .25 | 1 | 19.96 | 1608 | 6.481 | 117.18 | 82 | |
| | | 1 | 19.80 | 1590 | 6.389 | 123.57 | 83 | |
| 0.5 | .1 | 1 | 6.92 | 660.4 | .451 | 124.02 | 84 | Inspection for cracks |
| 0.5 | | 1 | 6.83 | 662 | .234 | 124.26 | 85 | |
| 1.4 | .1 | 1 | 19.80 | 1579 | 6.206 | 130.46 | 86 | |
| | | 1 | 19.89 | 1577 | 6.428 | 136.89 | 87 | |
| | | 1 | 20.15 | 1560 | 4.595 | 141.49 | 88 | Inverted cycle** |
| | | 1 | 19.95 | 1559 | 6.363 | 147.85 | 89 | Inverted cycle |
| | .25 | 10 | 20.21 | 1562 | 6.24 | 210.25 | 99 | Inverted cycle |
| 1.6 | .1 | 1 | 23.39 | 1653 | 7.933 | 218.18 | 100 | |
| | | 1 | 23.52 | 1622 | 9.069 | 227.25 | 101 | |
| | .25 | 1 | 23.44 | 1615 | 8.79 | 236.04 | 102 | |
| | | 1 | 23.30 | 1613 | 8.749 | 244.79 | 103 | |
| | | 10 | 23.78 | 1606 | 8.559 | 330.38 | 113 | |
| 1.8 | .1 | 1 | 26.78 | 1670 | 11.487 | 341.87 | 114 | |
| | .25 | 1 | 26.86 | 1647 | 11.296 | 353.16 | 115 | |
| | | 1 | 27.05 | 1636 | 11.113 | 364.28 | 116 | |
| | | 10 | 27.20 | 1633 | 10.777 | 472.05 | 126 | Crack detected |
| 2.0 | .1 | 1 | 30.48 | 1687 | 14.032 | 486.08 | 127 | |
| | | 1 | 30.37 | 1659 | 13.871 | 499.95 | 128 | |
| | | 1 | 30.54 | 1643 | 13.722 | 513.67 | 129 | |
| | | 1 | 30.60 | 1623 | 13.529 | 527.20 | 130 | |

*For multiple cycles, the area of one loop is computed as the average of the first and last loop areas.
**Load cycle inverted from normal sine wave, Fig. 3.28.

TABLE 3.6

SUMMARY OF CYCLIC TEST RESULTS - SPECIMEN 14C3

| Actuator Displacement Amplitude (inches) | Frequency (Hz) | Number of Cycles | Range of Rotation (radians x 1000) | Range of Moment (kip-inches) | Area of a Single Hysteresis Loop (kip-inches) | Cumulative Area of Hysteresis Loops* (kip-inches) | Cumulative Number of Cycles | Remarks |
|---|---|---|---|---|---|---|---|---|
| 0.2 | .25 | 2 | - - | - - | - - | .064 | 2 | |
| | | 1 | 2.25 | 486.5 | .032 | .096 | 3 | |
| | | 9 | - - | - - | - - | .384 | 12 | |
| 0.4 | .25 | 2 | - - | - - | - - | .567 | 14 | |
| | | 1 | 4.2 | 935 | .092 | .659 | 15 | |
| | | 11 | - - | - - | - - | 1.666 | 26 | |
| 0.6 | .25 | 2 | - - | - - | - - | 2.806 | 28 | |
| | | 1 | 6.7 | 1272 | .570 | 3.376 | 29 | |
| | | 9 | - - | - - | - - | 8.506 | 38 | |
| 0.8 | .25 | 2 | - - | - - | - - | 11.78 | 40 | |
| | | 1 | 9.7 | 1503 | 1.637 | 13.42 | 41 | |
| | | 9 | - - | - - | - - | 28.15 | 50 | |
| 1.0 | .25 | 2 | - - | - - | - - | 35.12 | 52 | |
| | | 1 | 12.8 | 1666 | 3.484 | 38.60 | 53 | |
| | | 9 | - - | - - | - - | 69.96 | 62 | |
| 1.2 | .25 | 2 | - - | - - | - - | 82.55 | 64 | |
| | | 1 | 16.0 | 1740 | 6.297 | 88.85 | 65 | |
| | | 9 | - - | - - | - - | 145.5 | 74 | |
| 1.4 | .25 | 3 | - - | - - | - - | 172.4 | 77 | |
| | | 1 | 19.0 | 1825 | 8.954 | 181.2 | 79 | |
| | | 9 | - - | - - | - - | 261.9 | 87 | |
| 1.6 | .25 | 2 | - - | - - | - - | 286.0 | 89 | |
| | | 1 | 22.4 | 1909 | 12.015 | 298.0 | 90 | |
| | | 9 | - - | - - | - - | 406.1 | 99 | Crack detected |

* At each displacement amplitude, the area of all hysteresis loops is assumed constant.

Continued -

TABLE 3.6 (CONTINUED)

SUMMARY OF CYCLIC TEST RESULTS - SPECIMEN 14C3

| Actuator Displacement Amplitude (inches) | Frequency (Hz) | Number of Cycles | Range of Rotation (radians x 1000) | Range of Moment (kip-inches) | Area of a Single Hysteresis Loop (kip-inches) | Cumulative Area of Hysteresis Loops* (kip-inches) | Cumulative Number of Cycles | Remarks |
|---|---|---|---|---|---|---|---|---|
| 1.8 | .25 | 4 | - - | - - | - - | 466.0 | 103 | |
| | | 1 | 26.1 | 1909 | 14.967 | 480.9 | 104 | |
| | | 9 | - - | - - | - - | 615.6 | 113 | |
| 2.0 | .25 | 2 | - - | - - | - - | 649.1 | 115 | |
| | | 1 | 30.3 | 1780 | 16.732 | 665.8 | 116 | |
| | | 1 | - - | - - | - - | 682.6 | 117 | Large cracks - all flange angles |

* At each displacement amplitude, the area of all hysteresis loops is assumed constant.

TABLE 3.7

SUMMARY OF CYCLIC TEST RESULTS - SPECIMEN 14C4

| Actuator Displacement Amplitude (inches) | Frequency (Hz) | Number of Cycles | Range of Rotation (radians x 1000) | Range of Moment (kip-inches) | Area of a Single Hysteresis Loop (kip-inches) | Cumulative Area of Hysteresis Loops* (kip-inches) | Cumulative Number of Cycles | Remarks |
|---|---|---|---|---|---|---|---|---|
| 0.2 | .25 | 2 | - - | - - | - - | .040 | 2 | |
| | | 1 | 2.6 | 356 | .020 | .060 | 3 | |
| | | 9 | - - | - - | - - | .240 | 12 | |
| 0.4 | .25 | 2 | - - | - - | - - | .447 | 14 | |
| | | 1 | 5.1 | 657 | .103 | .550 | 15 | |
| | | 9 | - - | - - | - - | 1.481 | 24 | |
| 0.6 | .25 | 2 | - - | - - | - - | 2.292 | 26 | |
| | | 1 | 7.8 | 902 | .405 | 2.697 | 27 | |
| | | 9 | - - | - - | - - | 6.346 | 36 | |
| 0.8 | .25 | 2 | - - | - - | - - | 8.397 | 38 | |
| | | 1 | 10.9 | 1072 | 1.026 | 9.423 | 39 | |
| | | 9 | - - | - - | - - | 18.65 | 48 | |
| 1.0 | .25 | 2 | - - | - - | - - | 22.84 | 50 | |
| | | 1 | 14.2 | 1191 | 2.093 | 24.93 | 51 | |
| | | 9 | - - | - - | - - | 43.76 | 60 | |
| 1.2 | .25 | 2 | - - | - - | - - | 51.05 | 62 | |
| | | 1 | 17.4 | 1268 | 3.644 | 54.70 | 63 | |
| | | 9 | - - | - - | - - | 87.49 | 72 | |
| 1.4 | .25 | 2 | - - | - - | - - | 98.79 | 74 | |
| | | 1 | 20.9 | 1291 | 5.650 | 104.4 | 75 | |
| | | 9 | - - | - - | - - | 155.3 | 84 | |
| 1.6 | .25 | 2 | - - | - - | - - | 171.3 | 86 | |
| | | 1 | 24.7 | 1318 | 7.986 | 179.2 | 87 | |
| | | 9 | - - | - - | - - | 251.1 | 96 | Crack detected |

* At each displacement amplitude, the area of all hysteresis loops is assumed constant.

Continued -

TABLE 3.7 (CONTINUED)

SUMMARY OF CYCLIC TEST RESULTS - SPECIMEN 14C4

| Actuator Displacement Amplitude (inches) | Frequency (Hz) | Number of Cycles | Range of Rotation (radians x 1000) | Range of Moment (kip-inches) | Area of a Single Hysteresis Loop (kip-inches) | Cumulative Area of Hysteresis Loops* (kip-inches) | Cumulative Number of Cycles | Remarks |
|---|---|---|---|---|---|---|---|---|
| 1.8 | .25 | 2 | - - | - - | - - | 272.0 | 98 | |
| | | 1 | 27.9 | 1311 | 10.442 | 282.4 | 99 | |
| | | 6 | - - | - - | - - | 345.1 | 105 | Large crack - test stopped |

* At each displacement amplitude, the area of all hysteresis loops is assumed constant.

TABLE 3.8

SUMMARY OF CYCLIC TEST RESULTS - SPECIMEN 14B1

| Actuator Displacement Amplitude (inches) | Frequency (Hz) | Number of Cycles | Range of Rotation (radians x 1000) | Range of Moment (kip-inches) | Area of a Single Hysteresis Loop (kip-inches) | Cumulative Area of Hysteresis Loops* (kip-inches) | Cumulative Number of Cycles | Remarks |
|---|---|---|---|---|---|---|---|---|
| 1.8 | .25 | 2 | - - | - - | - - | 32.16 | 2 | |
| | | 1 | 26.0 | 1863 | 16.078 | 48.23 | 3 | |
| | | 9 | - - | - - | - - | 192.9 | 12 | Crack detected |
| 1.6 | .25 | 2 | - - | - - | - - | 214.4 | 14 | |
| | | 1 | 23.5 | 1648 | 10.711 | 225.1 | 15 | |
| | | 9 | - - | - - | - - | 321.5 | 24 | |
| 1.4 | .25 | 2 | - - | - - | - - | 336.8 | 26 | |
| | | 1 | 20.4 | 1472 | 7.642 | 344.4 | 27 | Extensive cracks-two flange angles |
| | | 9 | - - | - - | - - | 413.2 | 36 | |
| 1.2 | .25 | 2 | - - | - - | - - | 423.5 | 38 | |
| | | 1 | 17.5 | 1299 | 5.163 | 428.7 | 39 | |
| | | 9 | - - | - - | - - | 475.1 | 48 | |
| 1.0 | .25 | 2 | - - | - - | - - | 481.6 | 50 | |
| | | 1 | 14.4 | 1101 | 3.241 | 484.8 | 51 | |
| | | 9 | - - | - - | - - | 514.0 | 60 | Large crack-test stopped |

* At each displacement amplitude, the area of all hysteresis loops is assumed constant.

TABLE 3.9

SUMMARY OF CYCLIC TEST RESULTS - SPECIMEN 8C1

| Actuator Displacement Amplitude (inches) | Frequency (Hz) | Number of Cycles | Range of Rotation (radians X 1000) | Range of Moment * (kip-inches) | Area of a Single Hysteresis Loop** (kip-inches) | Cumulative Area of Hysteresis Loops (kip-inches) | Cumulative Number of Cycles | Remarks |
|---|---|---|---|---|---|---|---|---|
| 0.2 | .1 | 1 | 4.33 | 231.2 | .045 | .045 | 1 | |
| | .25 | 10 | 4.27 | 233.8 | .037 | .415 | 11 | |
| .4 | .1 | 1 | 9.11 | 399.7 | .370 | .785 | 12 | |
| | | 1 | 8.96 | 394.9 | .247 | 1.032 | 13 | |
| | .25 | 10 | 9.54 | 422.2 | .162 | 2.652 | 23 | |
| .6 | .1 | 1 | 13.81 | 495.9 | 1.089 | 3.741 | 24 | |
| | | 1 | 13.98 | 488.4 | .871 | 4.612 | 25 | |
| | | 1 | 14.11 | 485.3 | .821 | 5.433 | 26 | |
| | .25 | 10 | 14.50 | 484.0 | .774 | 13.173 | 36 | |
| .8 | .1 | 1 | 20.22 | 538.6 | 2.303 | 15.476 | 37 | |
| | | 1 | 19.80 | 523.5 | 2.299 | 17.775 | 38 | |
| | | 1 | 19.98 | 500.2 | 2.342 | 20.117 | 39 | |
| | | 1 | 20.18 | 495.9 | 2.417 | 22.534 | 40 | |
| | .25 | 10 | 20.5 | 490.1 | 2.361 | 46.144 | 50 | |
| 1.0 | .1 | 1 | 26.03 | 511.6 | 4.188 | 50.332 | 51 | |
| | | 1 | 26.36 | 516.2 | 4.222 | 54.554 | 52 | |
| | | 1 | 26.23 | 490.8 | 4.154 | 58.708 | 53 | |
| | | 1 | 27.20 | 490.9 | 4.431 | 63.139 | 54 | |
| | .25 | 10 | 28.00 | 499.7 | 4.283 | 105.969 | 64 | |
| 1.2 | .1 | 1 | 32.35 | 521.3 | 6.130 | 112.10 | 65 | |
| | | 1 | 32.71 | 513.9 | 6.320 | 118.42 | 66 | |
| | .25 | 5 | 32.82 | 505.7 | 6.118 | 149.01 | 71 | |
| | | 5 | 32.55 | 480.5 | 6.004 | 179.03 | 76 | |
| 1.4 | .1 | 1 | 38.94 | 498.2 | 7.923 | 186.95 | 77 | |
| | | 1 | 39.05 | 478.6 | 7.626 | 194.58 | 78 | |
| | | — | — | — | — | — | — | Half cycle, abrupt crack formation |

*Extreme values reported.

**For multiple cycles, the area of one loop is computed as the average of the first and last loop areas.

TABLE 3.10

SUMMARY OF CYCLIC TEST RESULTS - SPECIMEN 8C2

| Actuator Displacement Amplitude (inches) | Frequency (Hz) | Number of Cycles | Range of Rotation (radians X 1000) | Range of Moment* (kip-inches) | Area of a Single Hysteresis Loop** (kip-inches) | Cumulative Area of Hysteresis Loops (kip-inches) | Cumulative Number of Cycles | Remarks |
|---|---|---|---|---|---|---|---|---|
| 0.2 | .1 | 1 | 4.13 | 252.2 | .062 | .062 | 1 | |
| | .25 | 10 | 4.39 | 268.9 | .317 | 3.232 | 11 | |
| .4 | .1 | 1 | 8.39 | 439.3 | .454 | 3.686 | 12 | |
| | | 1 | 8.05 | 454.0 | .307 | 3.993 | 13 | |
| | .25 | 10 | 8.49 | 453.8 | .254 | 6.533 | 23 | |
| .6 | .1 | 1 | 13.43 | 564.3 | 1.438 | 7.971 | 24 | |
| | | 1 | 13.29 | 556.0 | 1.272 | 9.243 | 25 | |
| | .25 | 10 | 13.85 | 554.5 | 1.265 | 21.89 | 35 | |
| .8 | .1 | 1 | 19.00 | 605.2 | 3.112 | 25.01 | 36 | |
| | | 1 | 19.12 | 601.5 | 3.039 | 28.04 | 37 | |
| | | 1 | 18.80 | 589.6 | 2.886 | 30.93 | 38 | |
| | .25 | 10 | 19.89 | 592.9 | 2.903 | 59.96 | 48 | |
| 1.0 | .1 | 1 | 25.02 | 616.0 | 5.202 | 65.16 | 49 | |
| | | 1 | 25.32 | 619.4 | 5.22 | 70.38 | 50 | |
| | .25 | 10 | 25.75 | 611.1 | 4.956 | 119.9 | 60 | |
| 1.2 | .1 | 1 | 30.78 | 635.0 | 7.265 | 127.2 | 61 | |
| | | 1 | 31.12 | 637.1 | 7.303 | 134.5 | 62 | |
| | .25 | 10 | 32.17 | 650.2 | 7.063 | 205.1 | 72 | Cracks detected-btm. angle |
| 1.4 | .1 | 1 | 37.29 | 663.7 | 9.704 | 214.8 | 73 | |
| | | 1 | 36.89 | 659.1 | 9.647 | 224.5 | 74 | |
| | .25 | 2 | 37.21 | 653.2 | 9.449 | 243.4 | 76 | Cracks detected-top angles |

*Extreme values reported

**For multiple cycles, the area of one loop is computed as the average of the first and last loop areas.

TABLE 3.11

SUMMARY OF CYCLIC TEST RESULTS - SPECIMEN 8C3

| Actuator Displacement Amplitude (inches) | Frequency (Hz) | Number of Cycles | Range of Rotation (radians x 1000) | Range of Moment (kip-inches) | Area of a Single Hysteresis Loop (kip-inches) | Cumulative Area of Hysteresis Loops* (kip-inches) | Cumulative Number of Cycles | Remarks |
|---|---|---|---|---|---|---|---|---|
| 0.2 | .25 | 2 | - - | - - | - - | .040 | 2 | |
| | | 1 | 3.5 | 316.8 | .020 | .060 | 3 | |
| | | 9 | - - | - - | - - | .240 | 12 | |
| 0.4 | .25 | 2 | - - | - - | - - | .730 | 14 | |
| | | 1 | 7.6 | 541.6 | .245 | .975 | 15 | |
| | | 9 | - - | - - | - - | 3.180 | 24 | |
| 0.6 | .25 | 2 | - - | - - | - - | 5.280 | 26 | |
| | | 1 | 12.1 | 681.4 | 1.050 | 6.329 | 27 | |
| | | 9 | - - | - - | - - | 15.78 | 36 | |
| 0.8 | .25 | 2 | - - | - - | - - | 21.11 | 38 | |
| | | 1 | 17.3 | 735.4 | 2.666 | 23.77 | 39 | |
| | | 9 | - - | - - | - - | 47.77 | 48 | |
| 1.0 | .25 | 2 | - - | - - | - - | 57.84 | 50 | |
| | | 1 | 23.9 | 764.8 | 5.037 | 62.88 | 51 | |
| | | 9 | - - | - - | - - | 108.2 | 60 | Cracks detected |
| 1.2 | .25 | 2 | - - | - - | - - | 123.9 | 62 | |
| | | 1 | 29.8 | 750.3 | 7.835 | 131.7 | 63 | |
| | | 7 | - - | - - | - - | 186.5 | 70 | Large cracks - test stopped |

* At each displacement amplitude, the area of all hysteresis loops is assumed constant.

TABLE 3.12

SUMMARY OF CYCLIC TEST RESULTS - SPECIMEN 8B1

| Actuator Displacement Amplitude (inches) | Frequency (Hz) | Number of Cycles | Range of Rotation (radians x 1000) | Range of Moment (kip-inches) | Area of a Single Hysteresis Loop (kip-inches) | Cumulative Area of Hysteresis Loops* (kip-inches) | Cumulative Number of Cycles | Remarks |
|---|---|---|---|---|---|---|---|---|
| 1.2 | .25 | 2 | - - | - - | - - | 16.46 | 2 | |
| | | 1 | 29.9 | 775.5 | 8.228 | 24.63 | 3 | |
| | | 9 | - - | - - | - - | 93.74 | 12 | Cracks detected |
| 1.0 | .25 | 2 | - - | - - | - - | 103.7 | 14 | |
| | | 1 | 24.9 | 660.4 | 4.961 | 113.6 | 15 | |
| | | 9 | - - | - - | - - | 158.3 | 24 | |
| 0.8 | .25 | 2 | - - | - - | - - | 163.7 | 26 | |
| | | 1 | 19.7 | 572.5 | 2.694 | 166.4 | 27 | |
| | | 9 | - - | - - | - - | 190.6 | 36 | |
| 0.6 | .25 | 2 | - - | - - | - - | 193.0 | 38 | |
| | | 1 | 14.2 | 461.5 | 1.196 | 194.2 | 39 | |
| | | 9 | - - | - - | - - | 205.0 | 48 | |
| 0.4 | .25 | 2 | - - | - - | - - | 205.6 | 50 | |
| | | 1 | 9.2 | 343.5 | .347 | 206.0 | 51 | |
| | | 9 | - - | - - | - - | 209.1 | 60 | |
| 0.2 | .25 | 2 | - - | - - | - - | 209.2 | 62 | |
| | | 1 | 4.6 | 195.2 | .029 | 209.2 | 63 | |
| | | 9 | - - | - - | - - | 209.5 | 72 | |
| 1.2 | .25 | 1 | 30.7 | 668.2 | 6.623 | 216.1 | 73 | Large crack - test stopped |

* At each displacement amplitude, the area of all hysteresis loops is assumed constant.

TABLE 3.13

COMPILATION OF CONSTANT AMPLITUDE CYCLIC (FATIGUE) TEST RESULTS
ALL TEST SPECIMENS

| Specimen Number | Beam Section | Thickness of Flange Angle (inches) | Fatigue Test Results | | | | |
|---|---|---|---|---|---|---|---|
| | | | Actuator Displacement Amplitude (inches) | Nominal Range of Rotation* (radiansX1000) | Nominal Flange Angle Chord Rotation Index, R** | Fatigue Life Cycle | Total Accumulated Hysteresis Loop Area (kip-inches) |
| 14F3 | W14X38 | 3/8 | 2.8 | 49.1 | 0.569 | 9 | 232.05 |
| 14F2 | W14X38 | 3/8 | 2.0 | 35.1 | 0.407 | 58 | ~800 |
| 14F1 | W14X38 | 3/8 | 1.6 | 28.1 | 0.325 | 72 | 589.41 |
| 14F9 | W14X38 | 3/8 | 1.0 | 17.5 | 0.203 | 230 | 515.76 |
| 14F4 | W14X38 | 3/8 | 0.5 | 8.8 | 0.102 | 3450 | 763.57 |
| 14F7 | W14X38 | ½ | 2.5 | 43.9 | 0.570 | 26 | 648.82 |
| 14F5 | W14X38 | ½ | 1.5 | 26.3 | 0.341 | 59 | 515.84 |
| 14F6 | W14X38 | ½ | 1.0 | 17.5 | 0.227 | 316 | 924.00 |
| 14F8 | W14X38 | ½ | 0.7 | 12.3 | 0.160 | 1031 | 911.30 |
| 8F8 | W8X21 | 5/16 | 1.5 | 45.5 | 0.481 | 16 | 153.98 |
| 8F7 | W8X21 | 5/16 | 1.0 | 30.3 | 0.320 | 62 | 231.87 |
| 8F6 | W8X21 | 5/16 | 0.7 | 21.2 | 0.224 | 173 | No data |
| 8F1 | W8X21 | 3/8 | 1.5 | 45.5 | 0.525 | 10 | 116.57 |
| 8F4 | W8X21 | 3/8 | 1.0 | 30.3 | 0.350 | 56 | 263.46 |
| 8F3 | W8X21 | 3/8 | 0.7 | 21.2 | 0.245 | 147 | 257.76 |
| 8F2 | W8X21 | 3/8 | 0.5 | 15.2 | 0.175 | 560 | 307.99 |

* Twice actuator displacement amplitude divided by distance from support to column face.

** $R = 2\left[\frac{(d+t)\tan\phi}{g-dw/2-t}\right]$ . See Nomenclature, Appendix A.

TABLE 3.14

SUMMARY OF CONSTANT AMPLITUDE CYCLIC TEST RESULTS
W14X38 SPECIMENS WITH ½-INCH THICK FLANGE ANGLES

| Specimen Number | Actuator Displacement Amplitude (inches) | Frequency (Hz) | Cycle Number | Percent of Total Fatigue Life | Range of Rotation (radians x 1000) | Range of Moment (kip-inches) | Area of a Single Hysteresis Loop (kip-inches) | Cumulative Area of Hysteresis Loops* (kip-inches) | Remarks |
|---|---|---|---|---|---|---|---|---|---|
| 14F7 | 2.5 | 0.025 | 1 | 3.8 | 19.0 | 1601 | 1.830 | 1.83 | Cycles 1,2 - half cycles |
| | | 0.025 | 3 | 11.5 | 38.4 | 2054 | 35.264 | 38.92 | |
| | | 0.25 | 7 | 26.9 | 38.6 | 1877 | 27.139 | 159.67 | |
| | | 0.10 | 12 | 46.2 | 38.9 | 1852 | 26.063 | 292.14 | Cycle 20 - cracks detected |
| | | 0.10 | 18 | 69.2 | 39.2 | 1829 | 25.639 | 447.03 | |
| | | 0.10 | 25 | 96.2 | 39.2 | 1806 | 24.975 | 623.85 | |
| | | 0.10 | 26 | 100 | - - | - - | - - | 648.82 | End of test |
| 14F5 | 1.5 | 0.25 | 6 | 10.2 | 21.5 | 1729 | 8.968 | 53.81 | |
| | | | 12 | 20.3 | 21.7 | 1703 | 8.832 | 107.14 | |
| | | | 18 | 30.5 | 21.6 | 1692 | 8.874 | 160.28 | |
| | | | 24 | 40.7 | 21.8 | 1674 | 8.550 | 212.39 | |
| | | | 30 | 50.8 | 21.7 | 1663 | 8.898 | 264.91 | Cycle 33 - crack detected |
| | | | 36 | 61.0 | 21.8 | 1648 | 8.533 | 317.02 | |
| | | | 42 | 71.2 | 21.7 | 1653 | 8.728 | 368.90 | |
| | | | 48 | 81.4 | 21.6 | 1637 | 8.718 | 421.23 | |
| | | | 54 | 91.5 | 21.9 | 1678 | 8.566 | 473.01 | |
| | | | 59 | 100 | - - | - - | - - | 515.84 | End of test |

* For cycles between those reported, the area of a single hysteresis loop is calculated as the average of the preceding and succeeding reported loop areas.

Continued -

TABLE 3.14 (CONTINUED)

SUMMARY OF CONSTANT AMPLITUDE CYCLIC TEST RESULTS
W14X38 SPECIMENS WITH ½-INCH THICK FLANGE ANGLES

| Specimen Number | Actuator Displacement Amplitude (inches) | Frequency (Hz) | Cycle Number | Percent of Total Fatigue Life | Range of Rotation (radians x 1000) | Range of Moment (kip-inches) | Area of a Single Hysteresis Loop (kip-inches) | Cumulative Area of Hysteresis Loops* (kip-inches) | Remarks |
|---|---|---|---|---|---|---|---|---|---|
| 14F6 | 1.0 | 0.25 | 1 | 0.3 | 6.2 | 1051 | 2.180 | 2.18 | Cycles 1-10, half cycles |
| | | | 13 | 4.1 | 13.1 | 1571 | 2.996 | 30.79 | |
| | | | 18 | 5.7 | 12.9 | 1568 | 2.849 | 45.33 | |
| | | | 200 | 63.3 | 13.1 | 1537 | 2.909 | 569.33 | Cycle 199 - cracks detected |
| | | | 267 | 84.5 | 13.4 | 1434 | 3.179 | 773.42 | |
| | | | 287 | 90.8 | 13.7 | 1318 | 3.093 | 836.09 | |
| | | | 297 | 94.0 | 14.1 | 1313 | 3.155 | 867.36 | |
| | | | 307 | 97.2 | 14.1 | 1265 | 2.927 | 897.66 | |
| | | | 316 | 100 | - - | - - | - - | 924.00 | End of test |
| 14F8 | 0.7 | 0.25 | 1 | 0.1 | 1.1 | 795 | 0.165 | 0.17 | Cycles 1-25, half cycles |
| | | | 27 | 2.6 | 8.3 | 1342 | 0.823 | 5.77 | |
| | | | 31 | 3.0 | 8.4 | 1327 | 0.827 | 9.07 | |
| | | | 36 | 3.5 | 8.5 | 1308 | 0.879 | 13.36 | |
| | | | 83 | 8.1 | 8.6 | 1280 | 0.881 | 54.72 | |
| | | | 481 | 46.7 | 8.3 | 1200 | 0.896 | 408.36 | |
| | | | 806 | 78.2 | 8.4 | 1197 | 0.878 | 696.62 | Cycle 795 - cracks detected |
| | | | 906 | 87.9 | 8.5 | 1202 | 0.893 | 785.18 | |
| | | | 956 | 92.7 | 8.8 | 1173 | 1.052 | 833.88 | |
| | | | 1031 | 100 | 8.9 | 1174 | 1.013 | 911.30 | End of test |

* For cycles between those reported, the area of a single hysteresis loop is calculated as the average of the preceding and succeeding reported loop areas.

TABLE 3.15

SUMMARY OF CONSTANT AMPLITUDE CYCLIC TEST RESULTS
W14X38 SPECIMENS WITH 3/8-INCH THICK FLANGE ANGLES

| Specimen Number | Actuator Displacement Amplitude (inches) | Frequency (Hz) | Cycle Number | Percent of Total Fatigue Life | Range of Rotation (radians x 1000) | Range of Moment (kip-inches) | Area of a Single Hysteresis Loop (kip-inches) | Cumulative Area of Hysteresis Loops* (kip-inches) | Remarks |
|---|---|---|---|---|---|---|---|---|---|
| 14F3 | 2.8 | 0.25 | 1 | 11.1 | 44.6 | 1648 | 31.48 | 31.48 | |
| | | | 2 | 22.2 | 44.6 | 1538 | 26.92 | 58.40 | |
| | | | 3 | 33.3 | 45.2 | 1508 | 25.97 | 84.37 | |
| | | | 4 | 44.4 | 45.3 | 1470 | 25.50 | 109.87 | |
| | | | 5 | 55.6 | 45.7 | 1454 | 25.15 | 134.99 | |
| | | | 6 | 66.7 | 45.5 | 1449 | 24.67 | 159.66 | Sudden crack |
| | | | 7 | 77.8 | 45.6 | 1435 | 24.39 | 184.05 | formation in |
| | | | 8 | 88.9 | 45.4 | 1409 | 24.00 | 208.05 | 9th cycle |
| | | | 9 | 100 | - - | - - | - - | 232.06 | End of test |
| 14F2 | 2.0 | 0.25 | 1 | 1.7 | 30.7 | 1510 | 19.38 | 19.38 | |
| | | | 5 | 8.6 | 31.5 | 1315 | 14.62 | 85.00 | |
| | | | 10 | 17.2 | 31.8 | 1267 | 13.94 | 156.06 | |
| | | | 20 | 34.5 | 31.9 | 1210 | 13.47 | 292.87 | |
| | | | 25 | 43.1 | 32.0 | 1176 | 13.13 | 359.20 | |
| | | | 30 | 51.7 | 31.9 | 1166 | 13.20 | 425.06 | |
| | | | 58 | 100 | - - | - - | - - | ∿800 | End of test |
| 14F1 | 1.6 | 0.25 | 4 | 5.6 | 24.5 | 1172 | 9.14 | 36.56 | |
| | | | 13 | 18.1 | 23.9 | 1000 | 8.64 | 116.32 | |
| | | | 23 | 31.9 | 24.2 | 991.5 | 8.38 | 201.32 | |
| | | | 33 | 45.8 | 25.2 | 1008 | 8.26 | 284.43 | |
| | | | 43 | 59.7 | 25.7 | 995 | 7.87 | 364.88 | Cycle 43 - |
| | | | 53 | 73.6 | 25.4 | 904 | 7.79 | 443.14 | cracks de- |
| | | | 63 | 87.5 | 24.7 | 901 | 7.67 | 520.38 | tected |
| | | | 72 | 100 | - - | - - | - - | 589.41 | End of test |

* For cycles between those reported, the area of a single hysteresis loop is calculated as the average of the preceding and succeeding reported loop areas.

Continued -

TABLE 3.15 (CONTINUED)

SUMMARY OF CONSTANT AMPLITUDE CYCLIC TEST RESULTS
W14X38 SPECIMENS WITH 3/8-INCH THICK FLANGE ANGLES

| Specimen Number | Actuator Displacement Amplitude (inches) | Frequency (Hz) | Cycle Number | Percent of Total Fatigue Life | Range of Rotation (radians x 1000) | Range of Moment (kip-inches) | Area of a Single Hysteresis Loop (kip-inches) | Cumulative Area of Hysteresis Loops* (kip-inches) | Remarks |
|---|---|---|---|---|---|---|---|---|---|
| 14F9 | 1.0 | 0.025 | 1-11 | 4.8 | - - | - - | - - | - - | No data** |
| | | 0.25 | 23 | 10.0 | 14.3 | 1169 | 2.052 | 24.62 | Cycles 12-23 |
| | | | 46 | 20.0 | 14.6 | 1124 | 2.189 | 73.46 | assumed equal |
| | | | 66 | 28.7 | 14.6 | 1125 | 2.295 | 118.36 | area |
| | | | 86 | 37.4 | 14.5 | 1109 | 2.382 | 165.17 | |
| | | | 106 | 46.1 | 14.5 | 1068 | 2.375 | 212.74 | Cycle 126 - |
| | | | 138 | 60.0 | 14.5 | 1063 | 2.497 | 290.75 | cracks de- |
| | | | 159 | 69.1 | 14.8 | 1056 | 2.476 | 342.76 | tected |
| | | | 175 | 76.1 | 14.9 | 1038 | 2.482 | 382.62 | |
| | | | 205 | 89.1 | 14.8 | 1012 | 2.428 | 456.24 | |
| | | | 225 | 97.8 | 15.0 | 964 | 2.365 | 504.14 | |
| | | | 227 | 98.7 | 15.1 | 949 | 2.319 | 508.80 | |
| | | | 230 | - - | - - | - - | - - | 515.76 | End of test |
| 14F4 | 0.5 | 0.25 | 1 | 0.03 | 7.0 | 603 | 0.439 | 0.44 | |
| | | | 3 | 0.09 | 6.8 | 630 | 0.239 | 1.02 | |
| | | | 101 | 2.9 | 6.8 | 622 | 0.175 | 21.27 | |
| | | | 251 | 7.2 | 6.8 | 612 | 0.165 | 46.77 | |
| | | | 801 | 23.2 | 7.0 | 622 | 0.211 | 150.19 | |
| | | | 826 | 23.9 | 7.2 | 633 | 0.224 | 155.63 | |
| | | | 1451 | 42.1 | 7.0 | 623 | 0.188 | 284.36 | |
| | | | 2101 | 60.9 | 7.2 | 638 | 0.249 | 426.42 | Cycle 2680 - |
| | | | 2876 | 83.4 | 7.1 | 617 | 0.256 | 622.11 | crack de- |
| | | | 2976 | 86.3 | 7.1 | 613 | 0.235 | 646.85 | tected |
| | | | 3276 | 95.0 | 7.1 | 607 | 0.251 | 719.56 | |
| | | | 3401 | 98.6 | 7.4 | 607 | 0.254 | 751.12 | |
| | | | 3450 | 100 | - - | - - | - - | 763.57 | End of test |

* For cycles between those reported, the area of a single hysteresis loop is calculated as the average of the preceding and succeeding reported loop areas.

** Cycles 1-11 are half cycles - no data recorded.

TABLE 3.16

SUMMARY OF CONSTANT AMPLITUDE CYCLIC TEST RESULTS
W8X21 SPECIMENS WITH 3/8-INCH THICK FLANGE ANGLES

| Specimen Number | Actuator Displacement Amplitude (inches) | Frequency (Hz) | Cycle Number | Percent of Total Fatigue Life | Range of Rotation (radians x 1000) | Range of Moment (kip-inches) | Area of a Single Hysteresis Loop (kip-inches) | Cumulative Area of Hysteresis Loops* (kip-inches) | Remarks |
|---|---|---|---|---|---|---|---|---|---|
| 8F1 | 1.5 | 0.025 | 1 | 10.0 | 17.4 | 699 | 6.499 | 6.50 | Cycles 1,2 - half cycles |
| | | 0.25 | 3 | 30.0 | 37.6 | 891.2 | 13.809 | 26.81 | |
| | | | 5 | 50.0 | 38.7 | 824.4 | 13.121 | 53.39 | |
| | | | 7 | 70.0 | 39.3 | 791.6 | 12.581 | 78.82 | Cycle 9-large cracks observed |
| | | | 10 | 100 | - - | - - | - - | 116.57 | End of test |
| 8F4 | 1.0 | 0.025 | 1 | 1.8 | - - | - - | - - | | No data - cycles 1, 2 half cycles |
| | | 0.25 | 7 | 12.5 | 24.9 | 654.4 | 5.196 | 25.98 | |
| | | | 11 | 19.6 | 24.4 | 621.5 | 4.999 | 46.27 | |
| | | | 16 | 28.6 | 24.8 | 615.4 | 4.884 | 70.92 | |
| | | | 21 | 37.5 | 24.6 | 611 | 4.934 | 95.49 | |
| | | | 25 | 44.6 | 24.9 | 605.1 | 4.909 | 115.16 | Cycle 30-cracks detected |
| | | | 31 | 55.4 | 24.4 | 591 | 4.772 | 144.14 | |
| | | | 36 | 64.3 | 24.9 | 604.9 | 4.904 | 168.40 | |
| | | | 41 | 73.2 | 24.9 | 599.6 | 4.831 | 192.70 | |
| | | | 45 | 80.4 | 24.9 | 593 | 4.868 | 211.66 | |
| | | | 51 | 91.1 | 25.0 | 590.3 | 4.818 | 240.24 | |
| | | | 55 | 98.2 | 25.2 | 575.1 | 4.571 | 258.89 | |
| | | | 56 | 100 | - - | - - | - - | 263.46 | End of test |

* For cycles between those reported, the area of a single hysteresis loop is calculated as the average of the preceding and succeeding reported loop areas.

Continued -

TABLE 3.16 (CONTINUED)

SUMMARY OF CONSTANT AMPLITUDE CYCLIC TEST RESULTS
W8X21 SPECIMENS WITH 3/8-INCH THICK FLANGE ANGLES

| Specimen Number | Actuator Displacement Amplitude (inches) | Frequency (Hz) | Cycle Number | Percent of Total Fatigue Life | Range of Rotation (radians x 1000) | Range of Moment (kip-inches) | Area of a Single Hysteresis Loop (kip-inches) | Cumulative Area of Hysteresis Loops* (kip-inches) | Remarks |
|---|---|---|---|---|---|---|---|---|---|
| 8F3 | 0.7 | 0.25 | 1 | 0.7 | 7.5 | 462 | 1.154 | 1.15 | Cycles 1-5 half cycles |
| | | | 7 | 4.8 | 15.5 | 688.8 | 1.922 | 9.61 | |
| | | | 15 | 10.2 | 15.1 | 652.8 | 1.738 | 24.16 | |
| | | | 29 | 19.7 | 15.7 | 640.7 | 1.700 | 48.21 | |
| | | | 43 | 29.3 | 14.7 | 602.9 | 1.804 | 72.79 | |
| | | | 57 | 38.8 | 16.0 | 605.9 | 1.738 | 97.55 | |
| | | | 71 | 48.3 | 15.8 | 601 | 1.714 | 121.70 | Cycle 86 - crack detected |
| | | | 99 | 67.3 | 16.1 | 603.7 | 1.785 | 170.72 | |
| | | | 113 | 76.9 | 16.1 | 596.6 | 1.832 | 196.07 | |
| | | | 126 | 85.7 | 16.4 | 577.9 | 1.815 | 219.76 | |
| | | | 141 | 95.9 | 16.3 | 573.4 | 1.828 | 247.09 | |
| | | | 145 | 98.6 | 16.6 | 565.6 | 1.762 | 254.24 | |
| | | | 147 | 100 | - - | - - | - - | 257.76 | End of test |
| 8F2 | 0.5 | 0.25 | 1 | 0.18 | 4.8 | 334 | 0.364 | 0.36 | Cycles 1-10 - half cycles |
| | | | 21 | 3.8 | 9.9 | 581.3 | 0.606 | 10.31 | |
| | | | 57 | 10.2 | 9.9 | 578.5 | 0.427 | 28.81 | |
| | | | 113 | 20.2 | 10.4 | 559.5 | 0.488 | 54.46 | |
| | | | 225 | 40.2 | 10.4 | 546.7 | 0.501 | 109.85 | Cycle 280 - cracks detected |
| | | | 281 | 50.2 | 10.9 | 534.2 | 0.605 | 140.87 | |
| | | | 341 | 60.9 | 10.7 | 532.5 | 0.670 | 179.15 | |
| | | | 393 | 70.2 | 10.8 | 522.8 | 0.613 | 212.48 | |
| | | | 449 | 80.2 | 10.9 | 598.6 | 0.604 | 246.55 | |
| | | | 505 | 90.2 | 10.9 | 477.9 | 0.560 | 279.12 | |
| | | | 559 | 99.8 | 11.5 | 437.8 | 0.491 | 307.47 | |
| | | | 560 | 100 | 11.4 | 430 | 0.519 | 307.99 | End of test |

* For cycles between those reported, the area of a single hysteresis loop is calculated as the average of the preceding and succeeding reported loop areas.

TABLE 3.17

SUMMARY OF CONSTANT AMPLITUDE CYCLIC TEST RESULTS
W8X21 SPECIMENS WITH 5/16-INCH THICK FLANGE ANGLES

| Specimen Number | Actuator Displacement Amplitude (inches) | Frequency (Hz) | Cycle Number | Percent of Total Fatigue Life | Range of Rotation (radians x 1000) | Range of Moment (kip-inches) | Area of a Single Hysteresis Loop* | Cumulative Area of Hysteresis Loops (kip-inches) | Remarks |
|---|---|---|---|---|---|---|---|---|---|
| 8F8 | 1.5 | 0.025 | 1 | 6.3 | 21.2 | 578.8 | 6.381 | 6.38 | Cycle 1-half cycle |
| | | 0.25 | 3 | 18.8 | 39.1 | 724 | 10.950 | 28.28 | |
| | | | 6 | 37.5 | 39.7 | 703.2 | 10.087 | 59.40 | Cycle 8-cracks detected |
| | | | 9 | 56.3 | 39.7 | 690.5 | 9.789 | 89.07 | |
| | | | 13 | 81.3 | 39.9 | 655.4 | 9.339 | 127.10 | |
| | | | 15 | 93.8 | 40.8 | 610.9 | 8.885 | 145.10 | |
| | | | 16 | 100 | - - | - - | - - | 153.98 | End of test |
| 8F7 | 1.0 | 0.25 | 1 | 1.6 | 2.0 | 473.0 | 2.746 | 2.75 | Cycles 1-5-half cycles |
| | | | 9 | 14.5 | 24.6 | 631.7 | 4.065 | 29.99 | |
| | | | 19 | 30.6 | 25.6 | 617.1 | 3.989 | 70.22 | |
| | | | 31 | 50.0 | 25.4 | 609.4 | 3.922 | 117.65 | Cycle 30-cracks detected |
| | | | 43 | 69.4 | 25.4 | 595.9 | 3.825 | 164.09 | |
| | | | 56 | 90.3 | 25.7 | 529.3 | 3.608 | 212.29 | |
| | | | 61 | 98.4 | 26.9 | 496.0 | 3.090 | 228.78 | |
| | | | 67 | 100 | - - | - - | - - | 231.87 | End of test |
| 8F6 | 0.7 | 0.25 | 1-169 | - - | - - | - - | - - | - - | No data** |
| | | | 170 | 98.3 | 17.5 | 431.8 | 1.377 | - - | Cycle 95-cracks detected |
| | | | 171 | 98.8 | 17.3 | 417.8 | 1.182 | - - | |
| | | | 172 | 99.4 | 17.7 | 430.3 | 1.251 | - - | |
| | | | 173 | 100 | - - | - - | - - | - - | End of test |

* For cycles between those reported, the area of a single hysteresis loop is calculated as the average of the preceding and succeeding reported loop areas.
** Malfunction of recording system.

TABLE 4.1

COMPARISON OF PREDICTED INITIAL CONNECTION STIFFNESS
WITH TEST RESULTS

| Specimen Number | Initial Slope (k.-in./radian) | | |
|---|---|---|---|
| | Test | Predicted | |
| | | Including Shear | Excluding Shear |
| 14S1 | 195,000 | 152,900 | 172,000 |
| 14S2 | 295,000 | 328,700 | 409,800 |
| 14S3 | 115,900 | 150,000 | 169,500 |
| 14S4 | 221,900 | 212,200 | 240,900 |
| 14S5 | 247,000 | 191,000 | 217,000 |
| 14S6 | 286,000 | 408,800 | 518,900 |
| 14S8 | 579,000 | 748,000 | 1,093,000 |
| 14S9 | 258,000 | 408,800 | 518,900 |
| 8S1 | 66,700 | 62,100 | 72,300 |
| 8S2 | 123,400 | 103,200 | 129,000 |
| 8S3 | 104,700 | 63,300 | 73,500 |
| 8S4 | 15,300 | 12,500 | 13,000 |
| 8S5 | 76,700 | 52,900 | 59,700 |
| 8S6 | 39,500 | 31,700 | 34,500 |
| 8S7 | 48,000 | 51,400 | 58,200 |
| 8S8 | 70,000 | 80,100 | 94,500 |
| 8S9 | 104,000 | 132,700 | 169,400 |
| 8S10 | 427,000 | 292,600 | 453,500 |

TABLE 4.2
PREDICTION OF CUMULATIVE DAMAGE
USING FATIGUE RELATIONSHIP BASED ON NOMINAL CHORD ROTATION INDEX
W14X38 BEAM SPECIMENS

| Specimen Number | Actuator Displacement Amplitude (inches) | Nominal Range of Rotation, $\phi$ (radians x 1000) | Nominal Flange Angle Chord Rotation Index, R* | Nominal Applied Cycles, n, at Displacement Amplitude | Predicted Constant Amplitude Fatigue Life, $N_f$** | $n/N_f$ | $\Sigma n/N_f$ |
|---|---|---|---|---|---|---|---|
| 14C1 | 0.2 | 3.5 | 0.037 | 17 | 84,949 | 0.0002 | 0.0002 |
| | 0.4 | 7.0 | 0.074 | 15 | 8,910 | 0.0017 | 0.0019 |
| | 0.6 | 10.5 | 0.111 | 15 | 2,383 | 0.0063 | 0.0082 |
| | 0.8 | 14.0 | 0.148 | 15 | 935 | 0.0160 | 0.0242 |
| | 1.0 | 17.5 | 0.185 | 15 | 452 | 0.0332 | 0.0574 |
| | 1.2 | 21.1 | 0.222 | 15 | 250 | 0.0600 | 0.1174 |
| | 1.4 | 24.6 | 0.259 | 15 | 151 | 0.0993 | 0.2167 |
| | 1.6 | 28.1 | 0.296 | 16 | 98 | 0.1633 | 0.3800 |
| | 1.8 | 31.6 | 0.332 | 15 | 67.5 | 0.2222 | 0.6022 |
| | 2.0 | 35.1 | 0.369 | 12 | 48 | 0.2500 | 0.8522 |
| 14C2 | 0.2 | 3.5 | 0.041 | 13 | 60,832 | 0.0002 | 0.0002 |
| | 0.4 | 7.0 | 0.082 | 13 | 6,380 | 0.0020 | 0.0022 |
| | 0.5 | 8.8 | 0.103 | 2 | 3,039 | 0.0007 | 0.0029 |
| | 0.6 | 10.5 | 0.123 | 13 | 1,706 | 0.0076 | 0.0105 |
| | 0.8 | 14.0 | 0.164 | 15 | 669 | 0.0224 | 0.0329 |
| | 1.0 | 17.5 | 0.205 | 13 | 324 | 0.0401 | 0.0730 |
| | 1.2 | 21.1 | 0.246 | 13 | 179 | 0.0726 | 0.1456 |
| | 1.4 | 24.6 | 0.287 | 17 | 108 | 0.1574 | 0.3030 |
| | 1.6 | 28.1 | 0.328 | 14 | 70 | 0.2000 | 0.5030 |
| | 1.8 | 31.6 | 0.369 | 13 | 48 | 0.2708 | 0.7738 |
| | 2.0 | 35.1 | 0.410 | 4 | 34 | 0.1176 | 0.8914 |

$$*R = 2\left[\frac{(d+t)\tan\phi}{g-d_w/2-t}\right]$$

**From Equation: $N_f = 1.868(R)^{-3.2531}$ (see Fig. 4.19)

Continued -

TABLE 4.2 (CONTINUED)
PREDICTION OF CUMULATIVE DAMAGE
USING FATIGUE RELATIONSHIP BASED ON NOMINAL CHORD ROTATION INDEX
W14X38 BEAM SPECIMENS

| Specimen Number | Actuator Displacement Amplitude (inches) | Nominal Range of Rotation, $\phi$ (radians x 1000) | Nominal Flange Angle Chord Rotation Index, R* | Nominal Applied Cycles, n, at Displacement Amplitude | Predicted Constant Amplitude Fatigue Life, $N_f$** | $n/N_f$ | $\Sigma n/N_f$ |
|---|---|---|---|---|---|---|---|
| 14C3 | 0.2 | 3.5 | 0.046 | 12 | 41,837 | 0.0003 | 0.0003 |
| | 0.4 | 7.0 | 0.091 | 14 | 4,547 | 0.0031 | 0.0034 |
| | 0.6 | 10.5 | 0.137 | 12 | 1,201 | 0.0100 | 0.0134 |
| | 0.8 | 14.0 | 0.182 | 12 | 477 | 0.0252 | 0.0386 |
| | 1.0 | 17.5 | 0.227 | 12 | 232 | 0.0517 | 0.0903 |
| | 1.2 | 21.1 | 0.273 | 12 | 128 | 0.0938 | 0.1841 |
| | 1.4 | 24.6 | 0.319 | 13 | 77 | 0.1688 | 0.3529 |
| | 1.6 | 28.1 | 0.364 | 12 | 50 | 0.2400 | 0.5929 |
| | 1.8 | 31.6 | 0.410 | 14 | 34 | 0.4118 | 1.0047 |
| | 2.0 | 35.1 | 0.455 | 4 | 24 | 0.1667 | 1.1714 |
| 14C4 | 0.2 | 3.5 | 0.041 | 12 | 60,832 | 0.0002 | 0.0002 |
| | 0.4 | 7.0 | 0.081 | 12 | 6,640 | 0.0018 | 0.0020 |
| | 0.6 | 10.5 | 0.122 | 12 | 1,752 | 0.0068 | 0.0088 |
| | 0.8 | 14.0 | 0.163 | 12 | 683 | 0.0176 | 0.0264 |
| | 1.0 | 17.5 | 0.203 | 12 | 334 | 0.0359 | 0.0623 |
| | 1.2 | 21.1 | 0.244 | 12 | 184 | 0.0652 | 0.1275 |
| | 1.4 | 24.6 | 0.284 | 12 | 112 | 0.1071 | 0.2346 |
| | 1.6 | 28.1 | 0.325 | 12 | 72 | 0.1667 | 0.4013 |
| | 1.8 | 31.6 | 0.366 | 9 | 49 | 0.1837 | 0.5850 |
| 14B1 | 1.8 | 31.6 | 0.410 | 12 | 34 | 0.3529 | 0.3529 |
| | 1.6 | 28.1 | 0.364 | 12 | 50 | 0.2400 | 0.5929 |
| | 1.4 | 24.6 | 0.319 | 12 | 77 | 0.1558 | 0.7487 |
| | 1.2 | 21.1 | 0.273 | 12 | 128 | 0.0938 | 0.8425 |
| | 1.0 | 17.5 | 0.227 | 12 | 232 | 0.0517 | 0.8942 |

$$*R = 2\left[\frac{(d+t)\tan\phi}{g-d_w/2-t}\right]$$

**From Equation: $N_f = 1.868(R)^{-3.2531}$ (see Fig. 4.19)

TABLE 4.3
PREDICTION OF CUMULATIVE DAMAGE
USING FATIGUE RELATIONSHIP BASED ON NOMINAL CHORD ROTATION INDEX
W8X21 BEAM SPECIMENS

| Specimen Number | Actuator Displacement Amplitude (inches) | Nominal Range of Rotation, $\phi$ (radians x 1000) | Nominal Flange Angle Chord Rotation Index, R* | Nominal Applied Cycles, n, at Displacement Amplitude | Predicted Constant Amplitude Fatigue Life, $N_f$** | $n/N_f$ | $\Sigma n/N_f$ |
|---|---|---|---|---|---|---|---|
| 8C1 | 0.2 | 6.1 | 0.056 | 11 | 22,062 | 0.0005 | 0.0005 |
| | 0.4 | 12.1 | 0.111 | 12 | 2,383 | 0.0050 | 0.0055 |
| | 0.6 | 18.2 | 0.167 | 13 | 631 | 0.0206 | 0.0261 |
| | 0.8 | 24.2 | 0.222 | 14 | 250 | 0.0560 | 0.0821 |
| | 1.0 | 30.3 | 0.278 | 14 | 120 | 0.1167 | 0.1988 |
| | 1.2 | 36.4 | 0.333 | 12 | 67 | 0.1791 | 0.3799 |
| | 1.4 | 42.4 | 0.389 | 2 | 40 | 0.0500 | 0.4279 |
| 8C2 | 0.2 | 6.1 | 0.060 | 11 | 17,627 | 0.0006 | 0.0006 |
| | 0.4 | 12.1 | 0.120 | 12 | 1,848 | 0.0065 | 0.0071 |
| | 0.6 | 18.2 | 0.180 | 12 | 494 | 0.0243 | 0.0314 |
| | 0.8 | 24.2 | 0.240 | 13 | 194 | 0.0670 | 0.0984 |
| | 1.0 | 30.3 | 0.300 | 12 | 94 | 0.1277 | 0.2261 |
| | 1.2 | 36.4 | 0.360 | 12 | 52 | 0.2308 | 0.4569 |
| | 1.4 | 42.4 | 0.420 | 4 | 31.5 | 0.1270 | 0.5839 |
| 8C3 | 0.2 | 6.1 | 0.070 | 12 | 10,676 | 0.0011 | 0.0011 |
| | 0.4 | 12.1 | 0.140 | 12 | 1,120 | 0.0107 | 0.0118 |
| | 0.6 | 18.2 | 0.210 | 12 | 299 | 0.0401 | 0.0519 |
| | 0.8 | 24.2 | 0.280 | 12 | 117 | 0.1026 | 0.1545 |
| | 1.0 | 30.3 | 0.350 | 12 | 57 | 0.2105 | 0.3650 |
| | 1.2 | 36.4 | 0.420 | 10 | 31.5 | 0.3175 | 0.6825 |

$$*R = 2\left[\frac{(d+t)\tan\phi}{g-d_w/2-t}\right]$$

**From Equation: $N_f = 1.868(R)^{-3.2531}$ (see Fig. 4.19)

Continued -

TABLE 4.3 (CONTINUED)
PREDICTION OF CUMULATIVE DAMAGE
USING FATIGUE RELATIONSHIP BASED ON NOMINAL CHORD ROTATION INDEX
W8X21 BEAM SPECIMENS

| Specimen Number | Actuator Displacement Amplitude (inches) | Nominal Range of Rotation, $\phi$ (radians x 1000) | Nominal Flange Angle Chord Rotation Index, R* | Nominal Applied Cycles, n, at Displacement Amplitude | Predicted Constant Amplitude Fatigue Life, $N_f$** | $n/N_f$ | $\Sigma n/N_f$ |
|---|---|---|---|---|---|---|---|
| 8B1 | 1.2 | 36.4 | 0.420 | 12 | 31.5 | 0.3810 | 0.3810 |
| | 1.0 | 30.3 | 0.350 | 12 | 57 | 0.2105 | 0.5915 |
| | 0.8 | 24.2 | 0.280 | 12 | 117 | 0.1026 | 0.6941 |
| | 0.6 | 18.2 | 0.210 | 12 | 299 | 0.0401 | 0.7341 |
| | 0.4 | 12.1 | 0.140 | 12 | 1,120 | 0.0107 | 0.7449 |
| | 0.2 | 6.1 | 0.070 | 12 | 10,676 | 0.0011 | 0.7460 |
| | 1.2 | 36.4 | 0.420 | 1 | 31.5 | 0.0317 | 0.7777 |

$$*R = 2\left[\frac{(d+t)\tan\phi}{g-d_w/2-t}\right]$$

**From Equation: $N_f = 1.868(R)^{-3.2531}$ (see Fig. 4.19)

TABLE 4.4

PREDICTION OF CUMULATIVE DAMAGE
USING FATIGUE RELATIONSHIP BASED ON HYSTERETIC ENERGY

W14X38 BEAM SPECIMENS

| Specimen Number | Actuator Displacement Amplitude (inches) | Average Hysteresis Loop Area (kip-inches) | Number of Applied Cycles, n, at Displacement Amplitude | Predicted Constant Amplitude Fatigue Life, $N_f$* | $n/N_f$ | $\Sigma n/N_f$ |
|---|---|---|---|---|---|---|
| 14C1 | 0.2 | - | 17 | - | - | - |
| | 0.4 | 0.09 | 15 | 15,195 | .0010 | .0010 |
| | 0.6 | 0.32 | 15 | 3,317 | .0045 | .0055 |
| | 0.8 | 0.89 | 15 | 972 | .0154 | .0209 |
| | 1.0 | 1.35 | 15 | 404 | .0371 | .0580 |
| | 1.2 | 3.26 | 15 | 205 | .0732 | .1312 |
| | 1.4 | 5.06 | 15 | 121 | .1240 | .2552 |
| | 1.6 | 6.57 | 16 | 88 | .1818 | .4370 |
| | 1.8 | 8.53 | 15 | 64.5 | .2326 | .6696 |
| | 2.0 | 10.48 | 12 | 50.5 | .2376 | .9072 |
| 14C2 | 0.2 | - | 13 | - | - | - |
| | 0.4 | 0.18 | 13 | 6,614 | .0020 | .0020 |
| | 0.5 | 0.34 | 2 | 3,083 | .0007 | .0027 |
| | 0.6 | 0.34 | 13 | 3,083 | .0042 | .0069 |
| | 0.8 | 0.95 | 15 | 899 | .0167 | .0236 |
| | 1.0 | 2.27 | 13 | 316 | .0411 | .0647 |
| | 1.2 | 4.08 | 13 | 156 | .0833 | .1480 |
| | 1.4 | 6.22 | 17 | 94 | .1809 | .3289 |
| | 1.6 | 8.58 | 14 | 64 | .2188 | .5477 |
| | 1.8 | 10.90 | 13 | 48 | .2708 | .8185 |
| | 2.0 | 13.79 | 4 | 36 | .1111 | .9296 |

*From Equation: $N_f = 844.9(E)^{-1.20}$ (see Fig. 4.20)

Continued -

TABLE 4.4 (CONTINUED)
PREDICTION OF CUMULATIVE DAMAGE
USING FATIGUE RELATIONSHIP BASED ON HYSTERETIC ENERGY
W14X38 BEAM SPECIMENS

| Specimen Number | Actuator Displacement Amplitude (inches) | Average Hysteresis Loop Area (kip-inches) | Number of Applied Cycles, n, at Displacement Amplitude | Predicted Constant Amplitude Fatigue Life, $N_f$* | $n/N_f$ | $\Sigma n/N_f$ |
|---|---|---|---|---|---|---|
| 14C3 | 0.2 | 0.03 | 12 | 56,788 | .0002 | .0002 |
| | 0.4 | 0.09 | 14 | 15,195 | .0009 | .0011 |
| | 0.6 | 0.57 | 12 | 1,659 | .0072 | .0083 |
| | 0.8 | 1.64 | 12 | 467 | .0257 | .0340 |
| | 1.0 | 3.48 | 12 | 189 | .0635 | .0975 |
| | 1.2 | 6.30 | 12 | 92.5 | .1297 | .2272 |
| | 1.4 | 8.95 | 13 | 61 | .2131 | .4403 |
| | 1.6 | 12.02 | 12 | 42.5 | .2824 | .7227 |
| | 1.8 | 14.97 | 14 | 33 | .4242 | 1.1469 |
| | 2.0 | 16.73 | 4 | 29 | .1379 | 1.2848 |
| 14C4 | 0.2 | 0.02 | 12 | 92,378 | .0001 | .0001 |
| | 0.4 | 0.10 | 12 | 13,391 | .0009 | .0010 |
| | 0.6 | 0.41 | 12 | 2,463 | .0049 | .0058 |
| | 0.8 | 1.03 | 12 | 815 | .0147 | .0206 |
| | 1.0 | 2.09 | 12 | 349 | .0344 | .0550 |
| | 1.2 | 3.64 | 12 | 179 | .0670 | .1220 |
| | 1.4 | 5.65 | 12 | 106 | .1132 | .2352 |
| | 1.6 | 7.99 | 12 | 69.5 | .1727 | .4079 |
| | 1.8 | 10.44 | 9 | 50.5 | .1782 | .5861 |

*From Equation: $N_f = 844.9(E)^{-1.20}$ (see Fig. 4.20)

Continued -

TABLE 4.4 (CONTINUED)
PREDICTION OF CUMULATIVE DAMAGE
USING FATIGUE RELATIONSHIP BASED ON HYSTERETIC ENERGY
W14X38 BEAM SPECIMENS

| Specimen Number | Actuator Displacement Amplitude (inches) | Average Hysteresis Loop Area (kip-inches) | Number of Applied Cycles, n, at Displacement Amplitude | Predicted Constant Amplitude Fatigue Life, $N_f$* | $n/N_f$ | $\Sigma n/N_f$ |
|---|---|---|---|---|---|---|
| 14B1 | 1.8 | 16.08 | 12 | 30 | .4000 | .4000 |
| | 1.6 | 10.71 | 12 | 49 | .2449 | .6449 |
| | 1.4 | 7.64 | 12 | 73.5 | .1633 | .8082 |
| | 1.2 | 5.16 | 12 | 118 | .1017 | .9099 |
| | 1.0 | 3.24 | 12 | 206 | .0583 | .9682 |

*From Equation: $N_f = 844.9(E)^{-1.20}$ (see Fig. 4.20)

TABLE 4.5
PREDICTION OF CUMULATIVE DAMAGE
USING FATIGUE RELATIONSHIP BASED ON HYSTERETIC ENERGY
W8X21 BEAM SPECIMENS

| Specimen Number | Actuator Displacement Amplitude (inches) | Average Hysteresis Loop Area (kip-inches) | Number of Applied Cycles, n, at Displacement Amplitude | Predicted Constant Amplitude Fatigue Life, $N_f$* | $n/N_f$ | $\Sigma n/N_f$ |
|---|---|---|---|---|---|---|
| 8C1 | 0.2 | 0.04 | 11 | 17,465 | .0006 | .0006 |
| | 0.4 | 0.19 | 12 | 2,437 | .0049 | .0055 |
| | 0.6 | 0.81 | 13 | 390 | .0333 | .0388 |
| | 0.8 | 2.36 | 14 | 101 | .1386 | .1774 |
| | 1.0 | 4.27 | 14 | 47.5 | .2947 | .4721 |
| | 1.2 | 6.09 | 12 | 30 | .4000 | .8721 |
| | 1.4 | 7.77 | 2 | 22.5 | .0889 | .9610 |
| 8C2 | 0.2 | 0.29 | 11 | 1,429 | .0077 | .0077 |
| | 0.4 | 0.28 | 12 | 1,493 | .0080 | .0157 |
| | 0.6 | 1.28 | 12 | 219 | .0548 | .0705 |
| | 0.8 | 2.93 | 13 | 76.5 | .1699 | .2404 |
| | 1.0 | 5.00 | 12 | 39 | .3077 | .5481 |
| | 1.2 | 7.10 | 12 | 25 | .4800 | 1.0281 |
| | 1.4 | 9.56 | 4 | 17 | .2353 | 1.2634 |

*From Equation: $N_f = 298.65(E)^{-1.2639}$ (see Fig. 4.20)

Continued -

TABLE 4.5 (CONTINUED)
PREDICTION OF CUMULATIVE DAMAGE
USING FATIGUE RELATIONSHIP BASED ON HYSTERETIC ENERGY
W8X21 BEAM SPECIMENS

| Specimen Number | Actuator Displacement Amplitude (inches) | Average Hysteresis Loop Area (kip-inches) | Number of Applied Cycles, n, at Displacement Amplitude | Predicted Constant Amplitude Fatigue Life, $N_f$* | $n/N_f$ | $\Sigma n/N_f$ |
|---|---|---|---|---|---|---|
| 8C3 | 0.2 | 0.02 | 12 | 41,943 | .0003 | .0003 |
| | 0.4 | 0.25 | 12 | 1,723 | .0070 | .0073 |
| | 0.6 | 1.05 | 12 | 281 | .0427 | .0500 |
| | 0.8 | 2.67 | 12 | 86 | .1395 | .1895 |
| | 1.0 | 5.04 | 12 | 38.5 | .3117 | .5012 |
| | 1.2 | 7.84 | 10 | 22 | .4546 | .9558 |
| 8B1 | 1.2 | 8.23 | 12 | 20.5 | .5854 | .5854 |
| | 1.0 | 4.96 | 12 | 39.5 | .3038 | .8892 |
| | 0.8 | 2.69 | 12 | 85.5 | .1404 | 1.0296 |
| | 0.6 | 1.20 | 12 | 237 | .0506 | 1.0802 |
| | 0.4 | 0.35 | 12 | 1,126 | .0107 | 1.0909 |
| | 0.2 | 0.03 | 12 | 25,124 | .0005 | 1.0914 |
| | 1.2 | 6.62 | 1 | 27.5 | .0364 | 1.1278 |

*From Equation: $N_f = 298.65(E)^{-1.2639}$ (see Fig. 4.20)

FIGURES

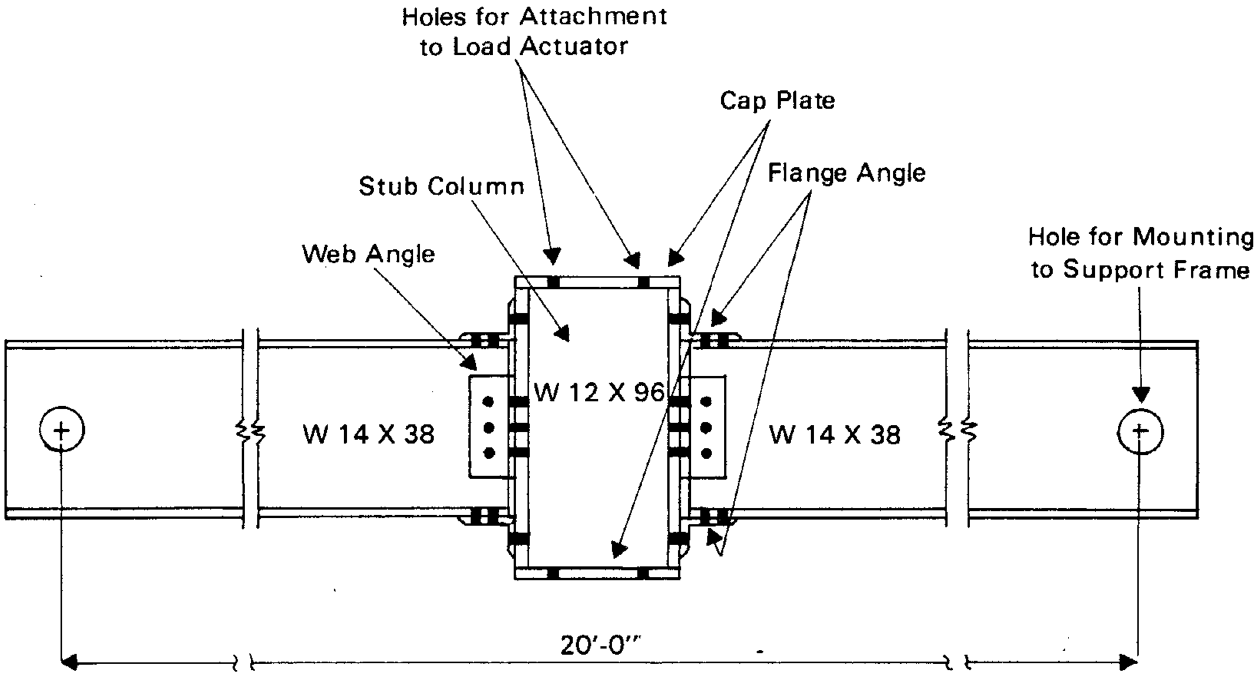


a. W 14 X 38 BEAM TEST SPECIMEN

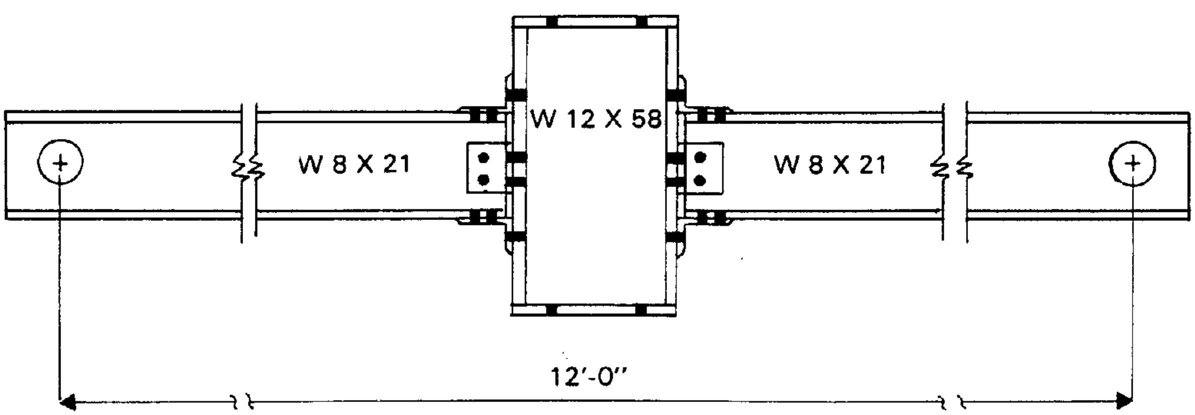


b. W 8 X 21 BEAM TEST SPECIMEN

FIG. 2.1 GENERAL CONFIGURATIONS OF TEST SPECIMENS

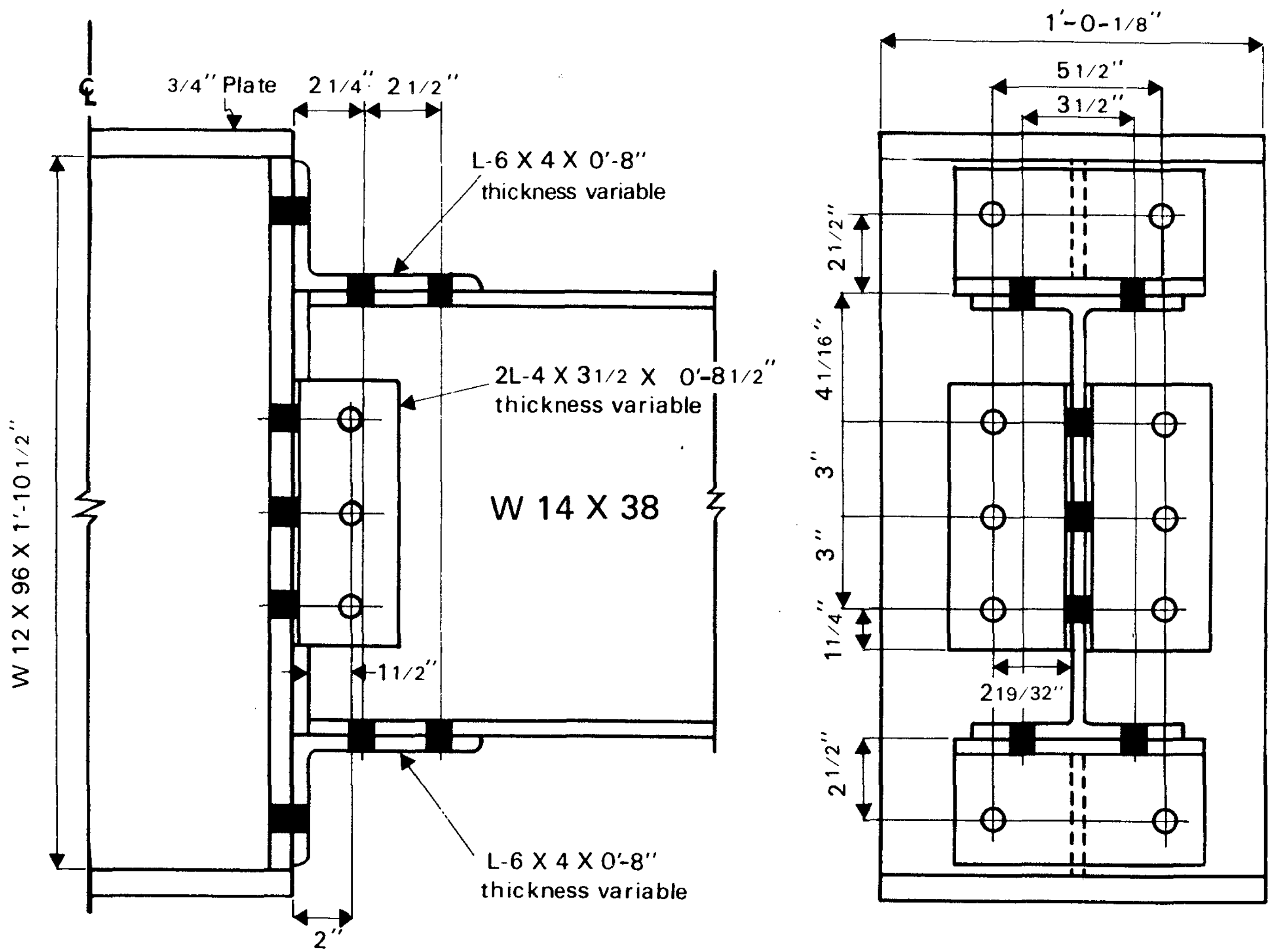


FIG. 2.2a DETAILS OF CONNECTION FOR W14X38 BEAM — BOLTED SPECIMENS

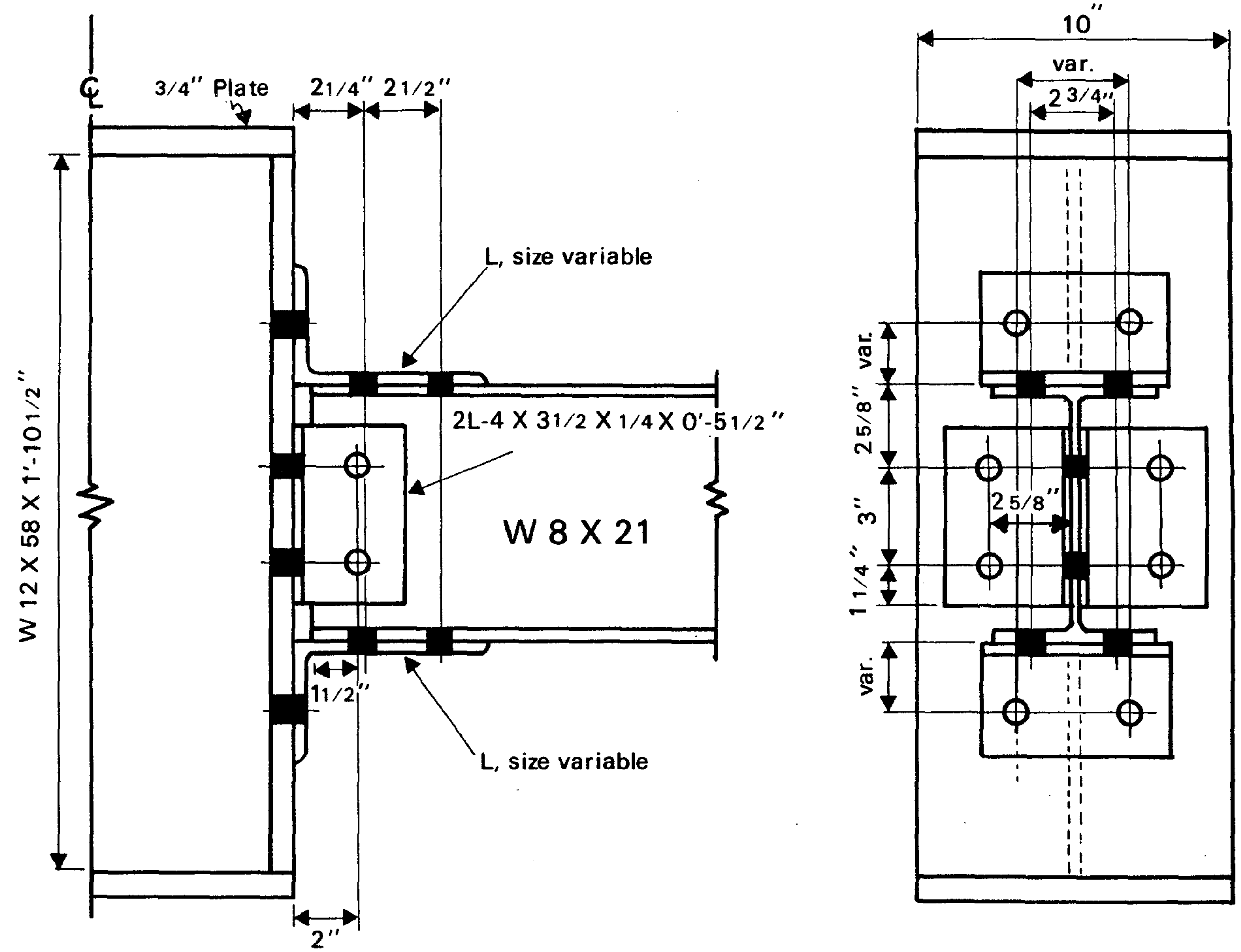


FIG. 2.2b DETAILS OF CONNECTION FOR W8X21 BEAM — BOLTED SPECIMENS

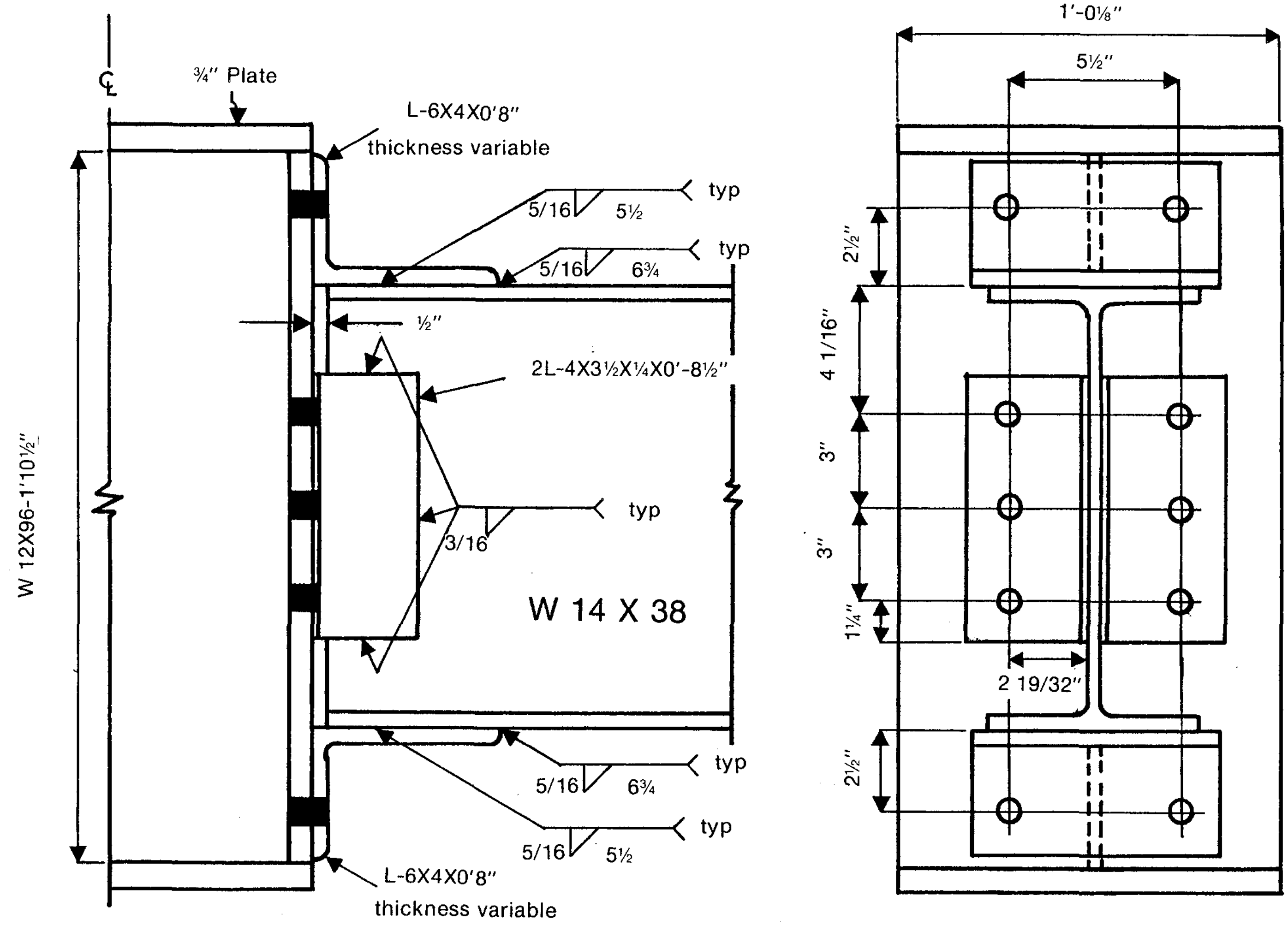


FIG. 2.3 DETAILS OF CONNECTION FOR W14X38 BEAM — BOLTED — WELDED SPECIMENS

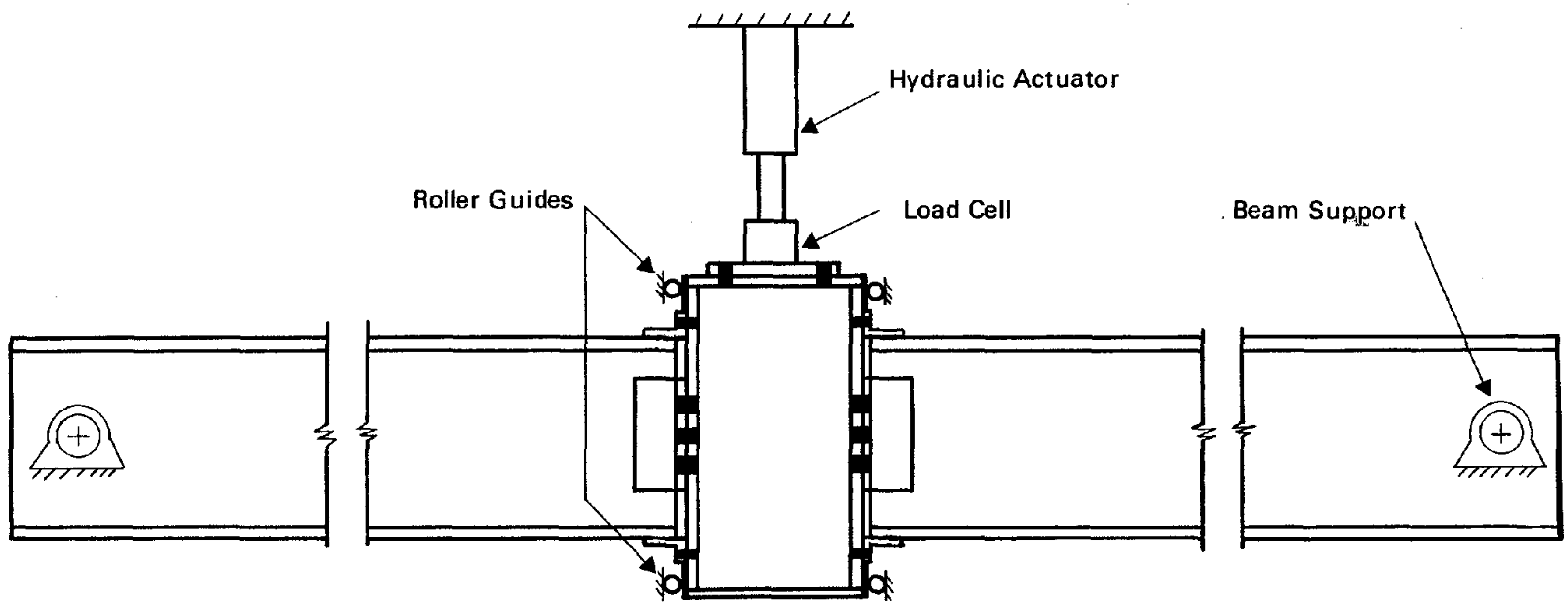


FIG. 2.4 SCHEMATIC OF LOADING SYSTEM FOR TEST BEAMS

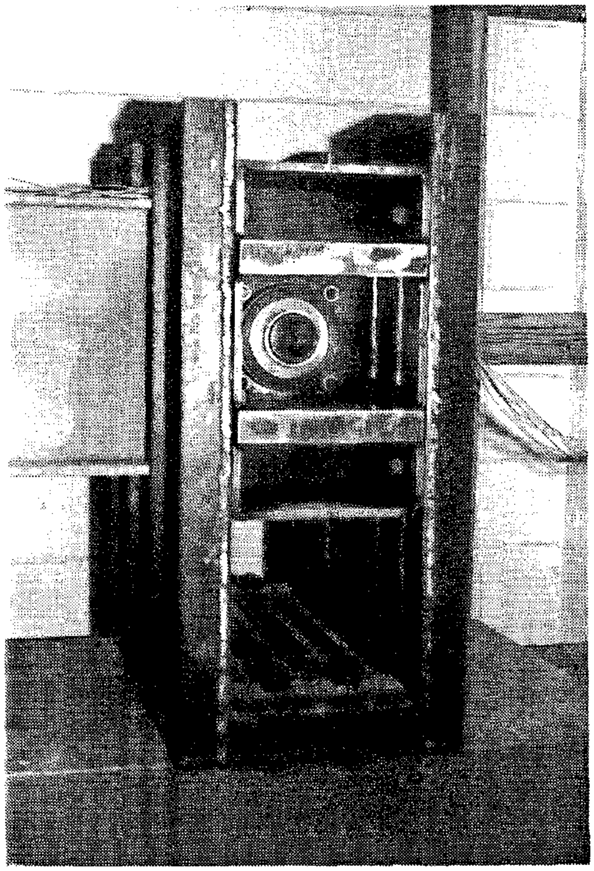

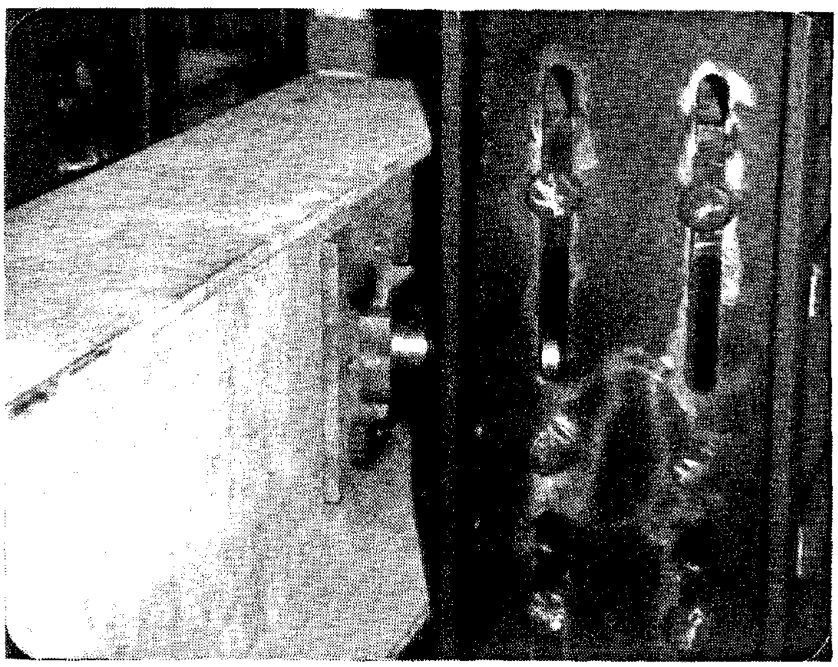

FIG. 2.5 BEAM SUPPORTS FOR TEST SPECIMENS

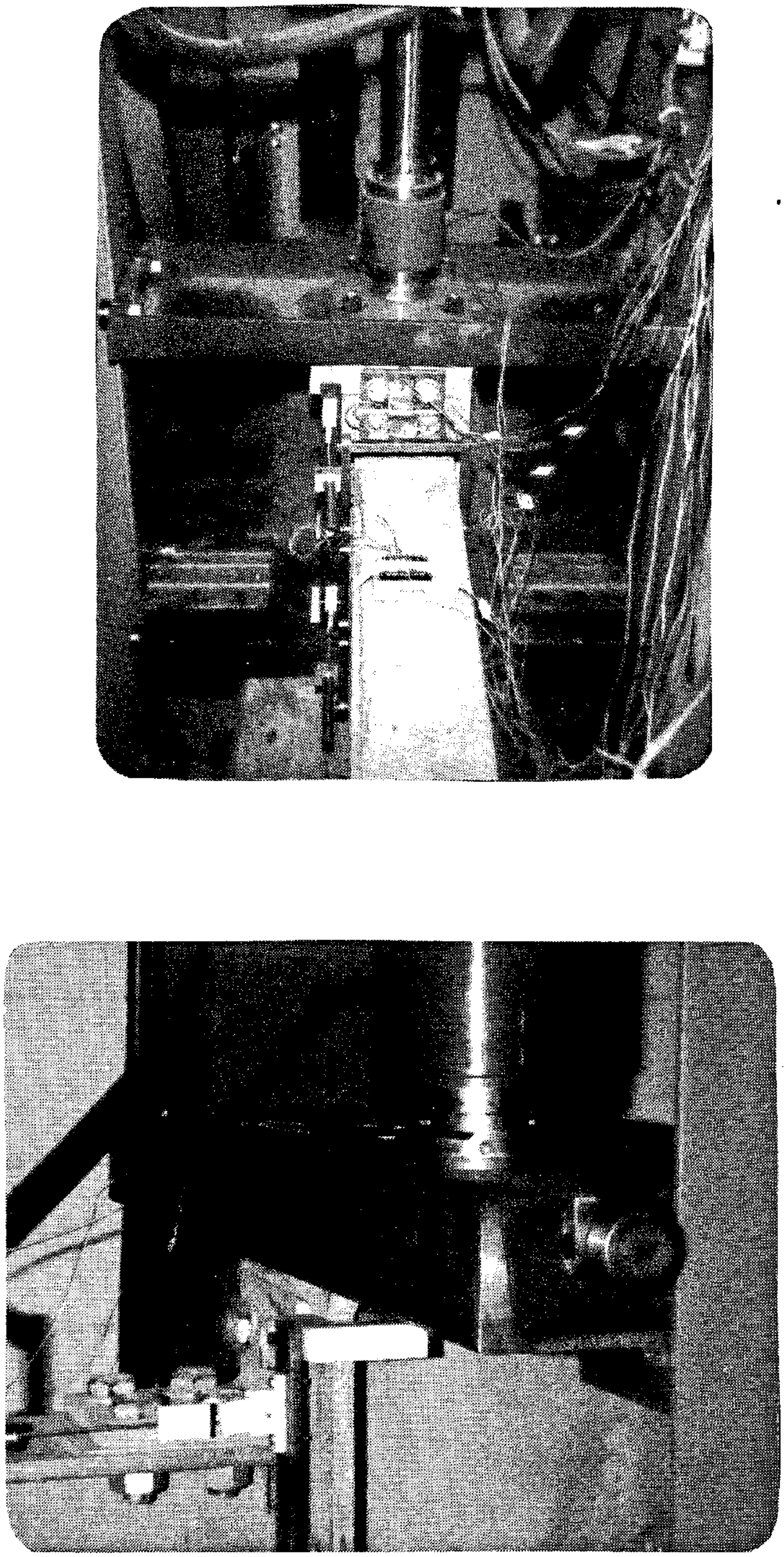

FIG. 2.6 LATERAL SUPPORT SYSTEM FOR TEST SPECIMENS

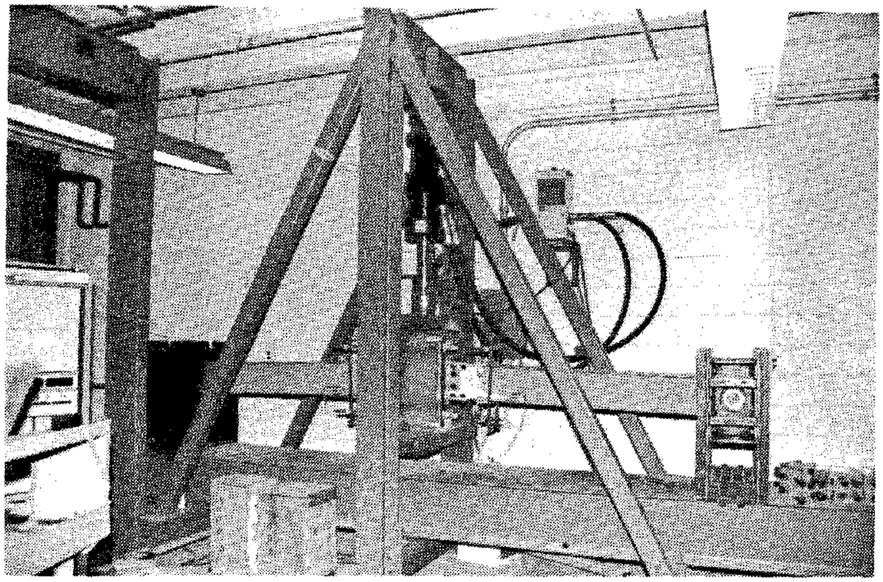

FIG. 2.7 LOADING FRAME AND TEST SET-UP

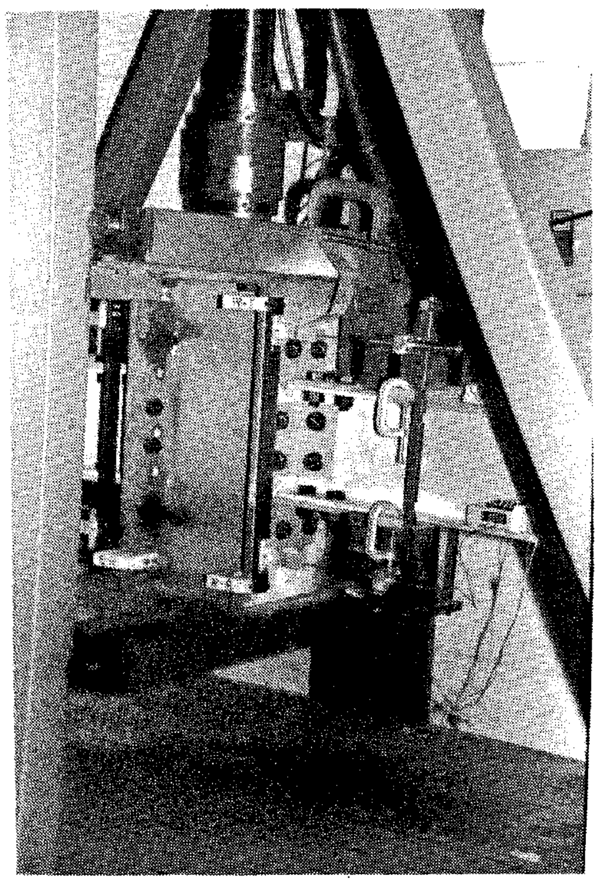

FIG. 2.8 CLOSE-UP OF TEST CONNECTION

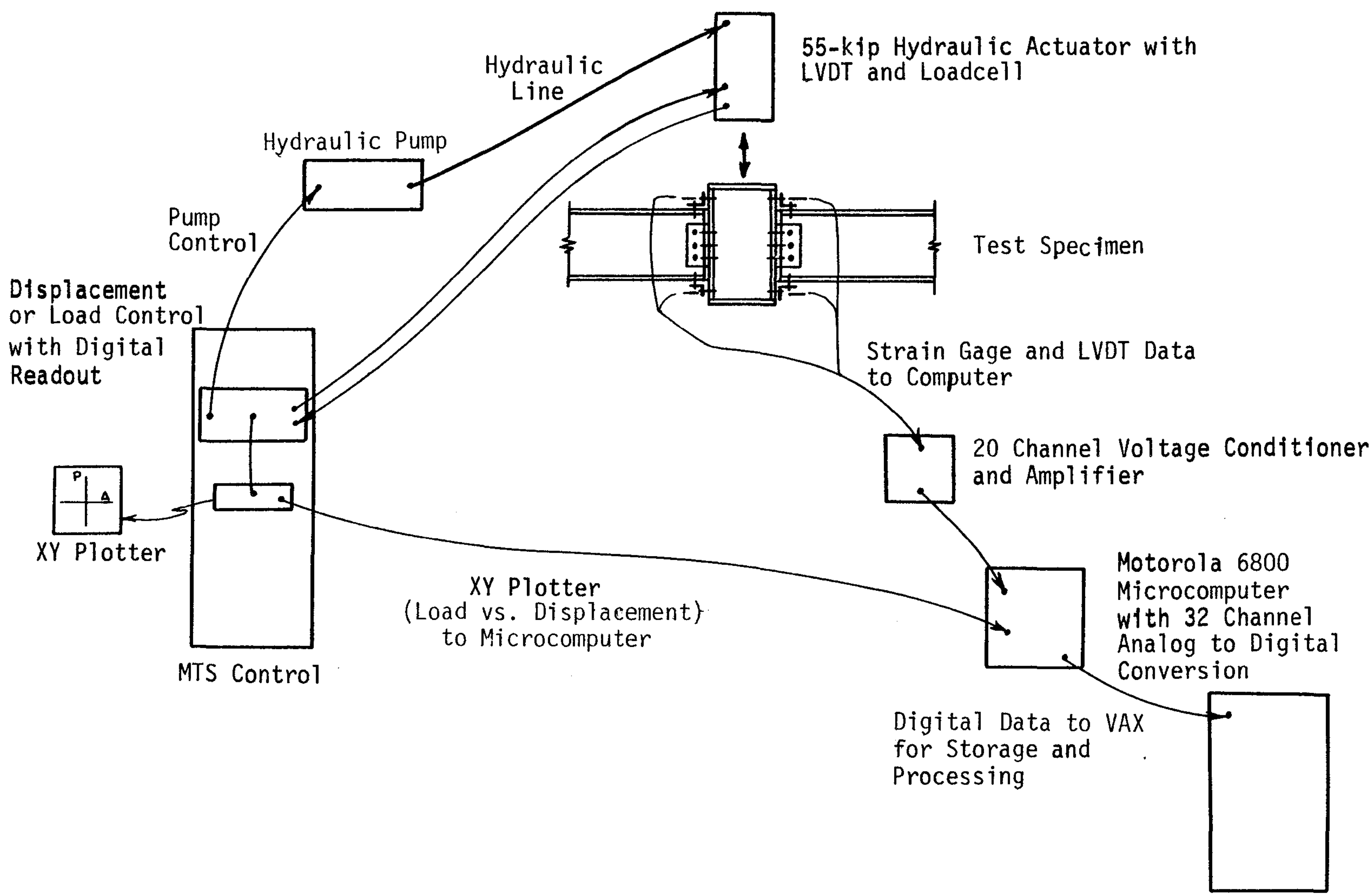


FIG. 2.9 **SCHEMATIC OF TESTING AND RECORDING EQUIPMENT**

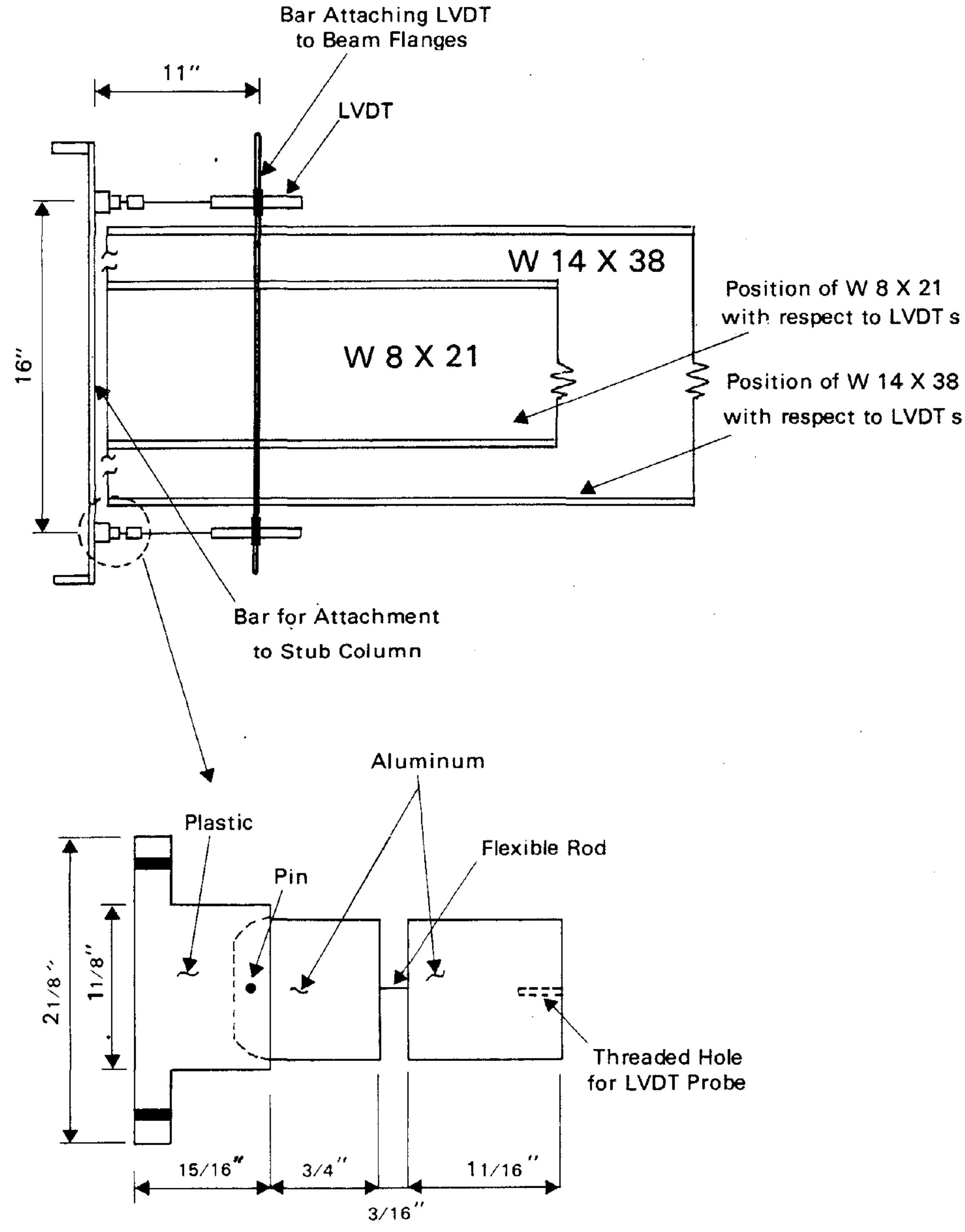


FIG. 2.10 LVDT MOUNTING APPARATUS

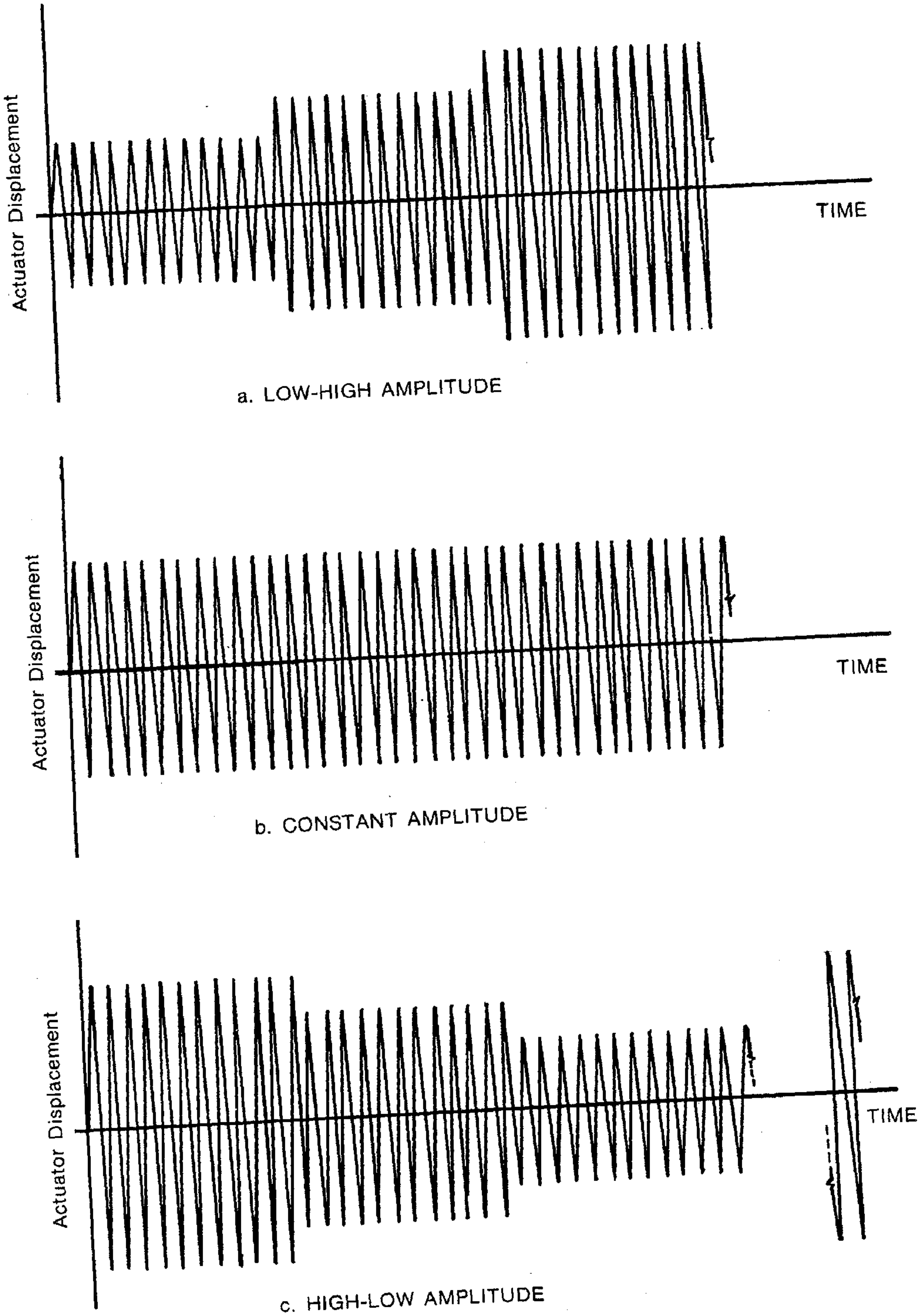


FIG. 2.11 TYPICAL TIME-DISPLACEMENT HISTORIES

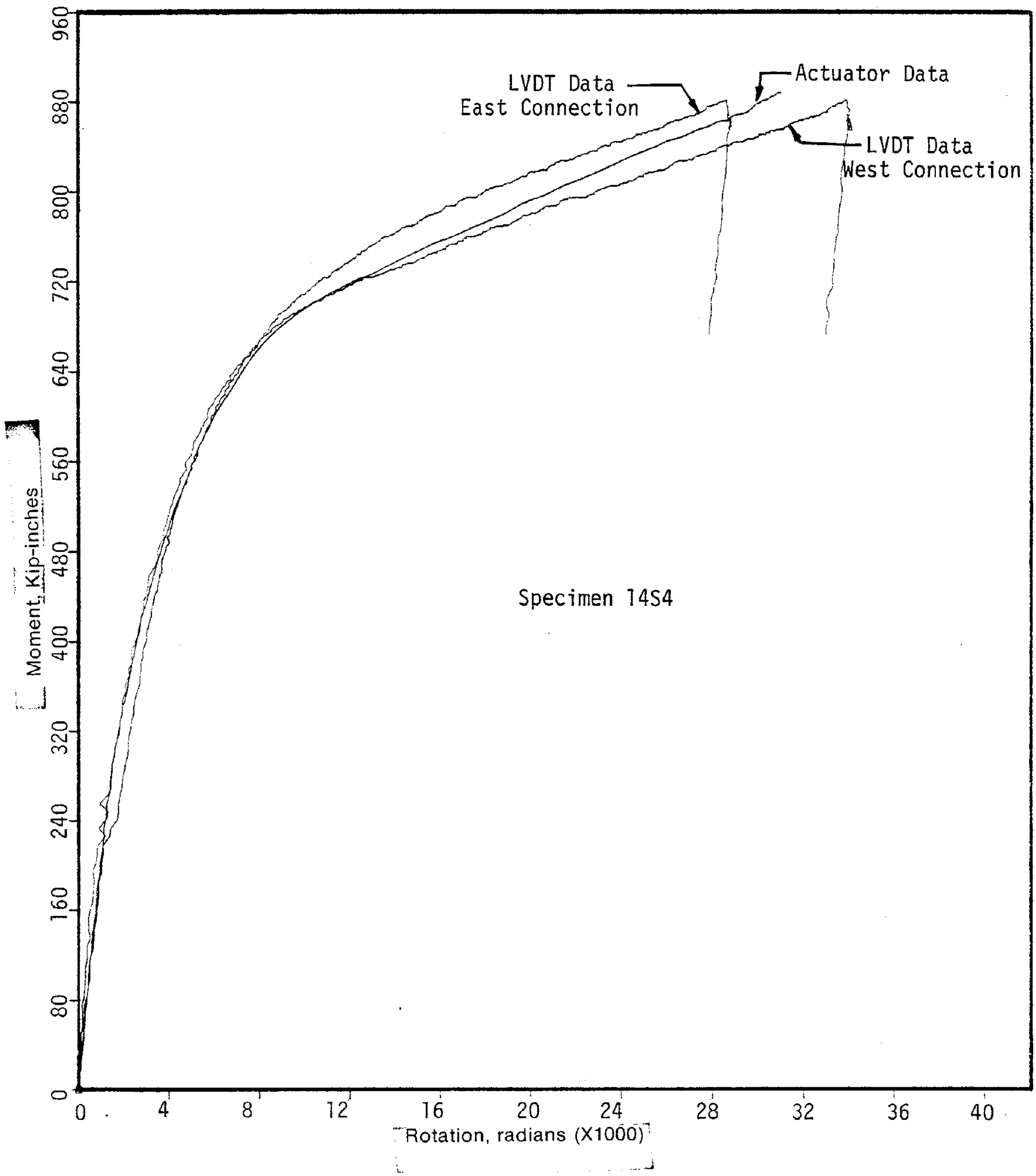


FIG. 3.1 COMPARISON OF MOMENT-ROTATION CURVES OBTAINED FROM LVDT MEASUREMENTS WITH CURVE OBTAINED FROM ACTUATOR DISPLACEMENTS

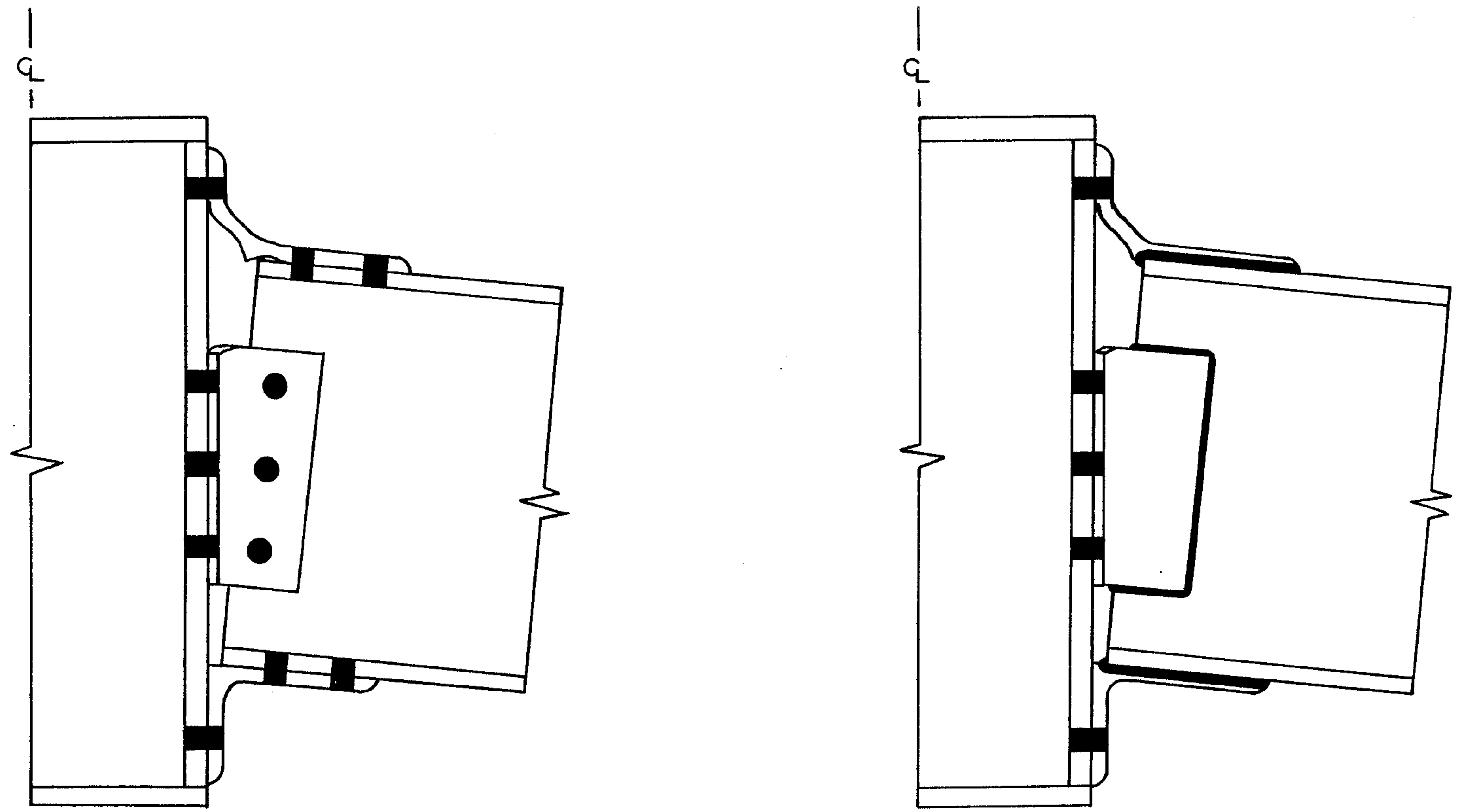


a. ALL-BOLTED CONNECTION

b. BOLTED-WELDED CONNECTION

FIG. 3.2 DEFORMATION PATTERNS IN BEAM-COLUMN CONNECTION ELEMENTS

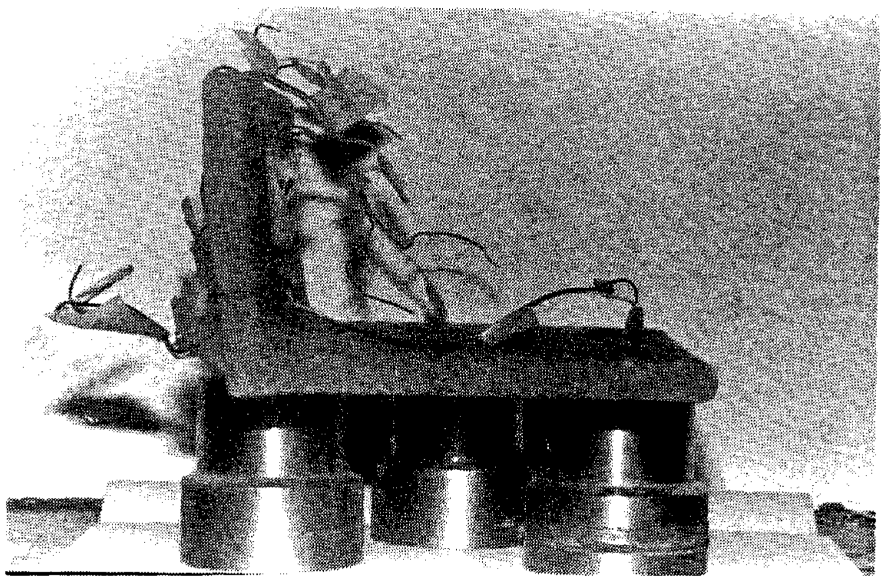

FIG. 3.3 FLANGE ANGLE FROM SPECIMEN 14S2 AFTER TEST

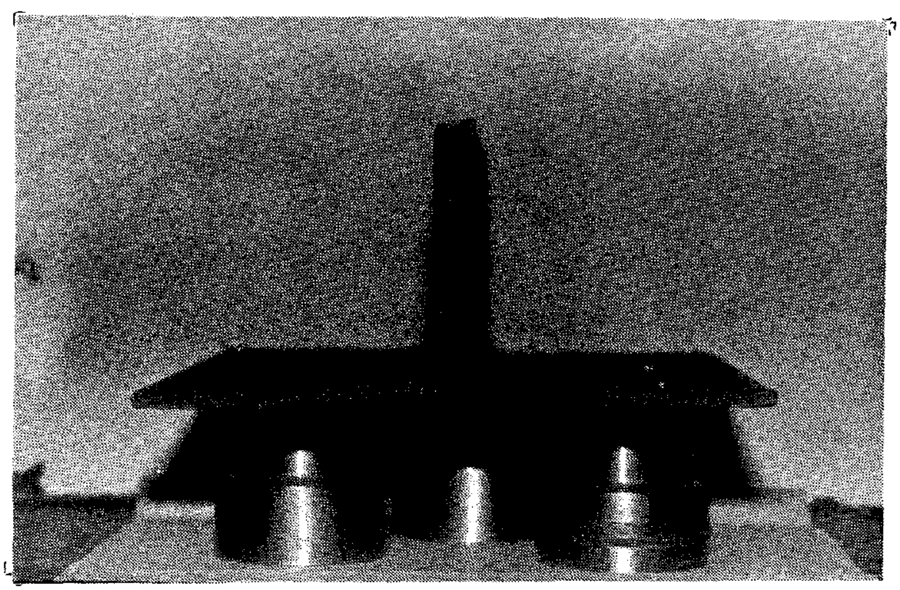

FIG. 3.4 WEB ANGLES FROM SPECIMEN 14S2 AFTER TEST

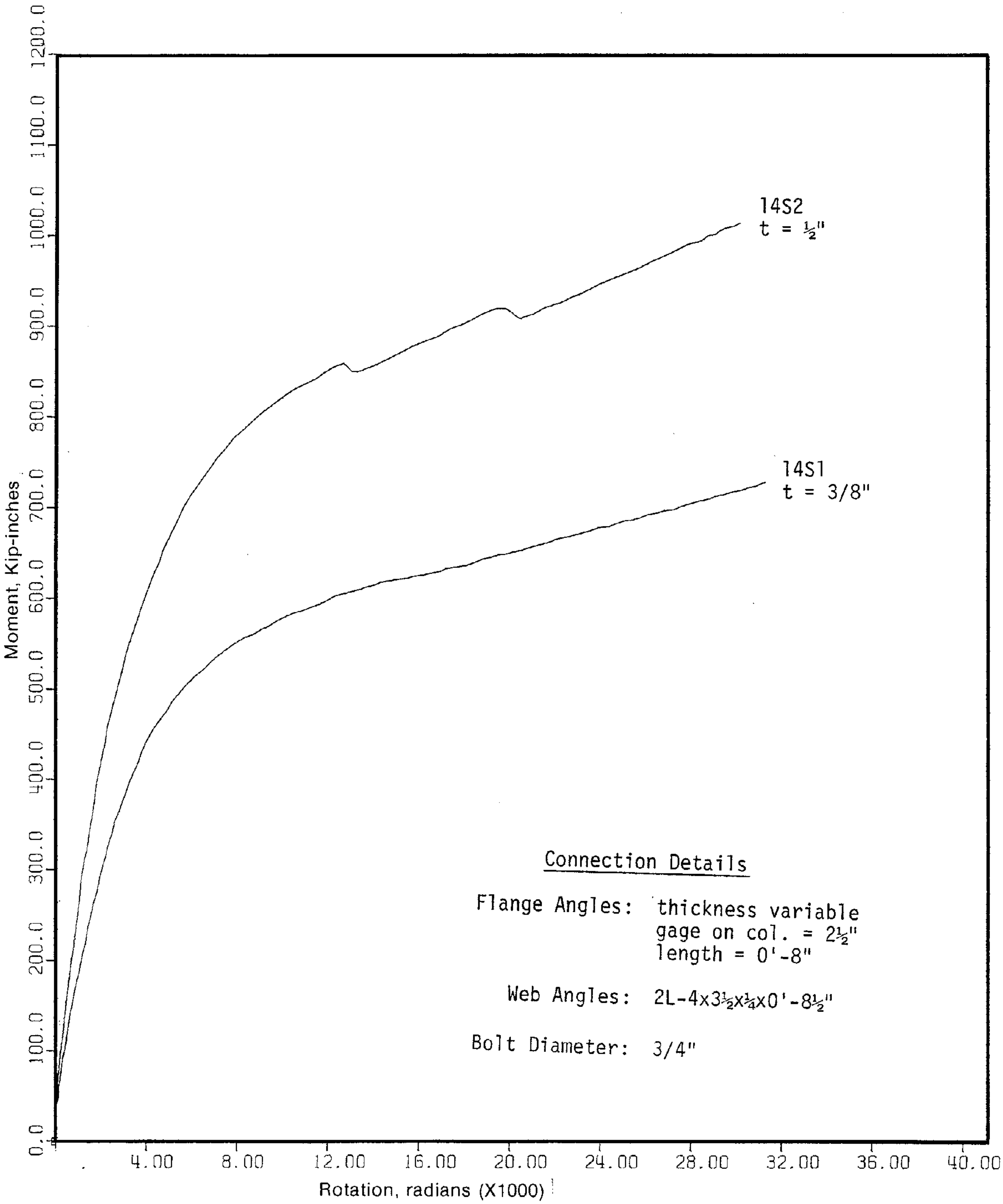


FIG. 3.5 EFFECT OF FLANGE ANGLE THICKNESS ON STATIC MOMENT-ROTATION BEHAVIOR — W14X38 BEAM CONNECTION (BOLT DIAMETER = ¾")

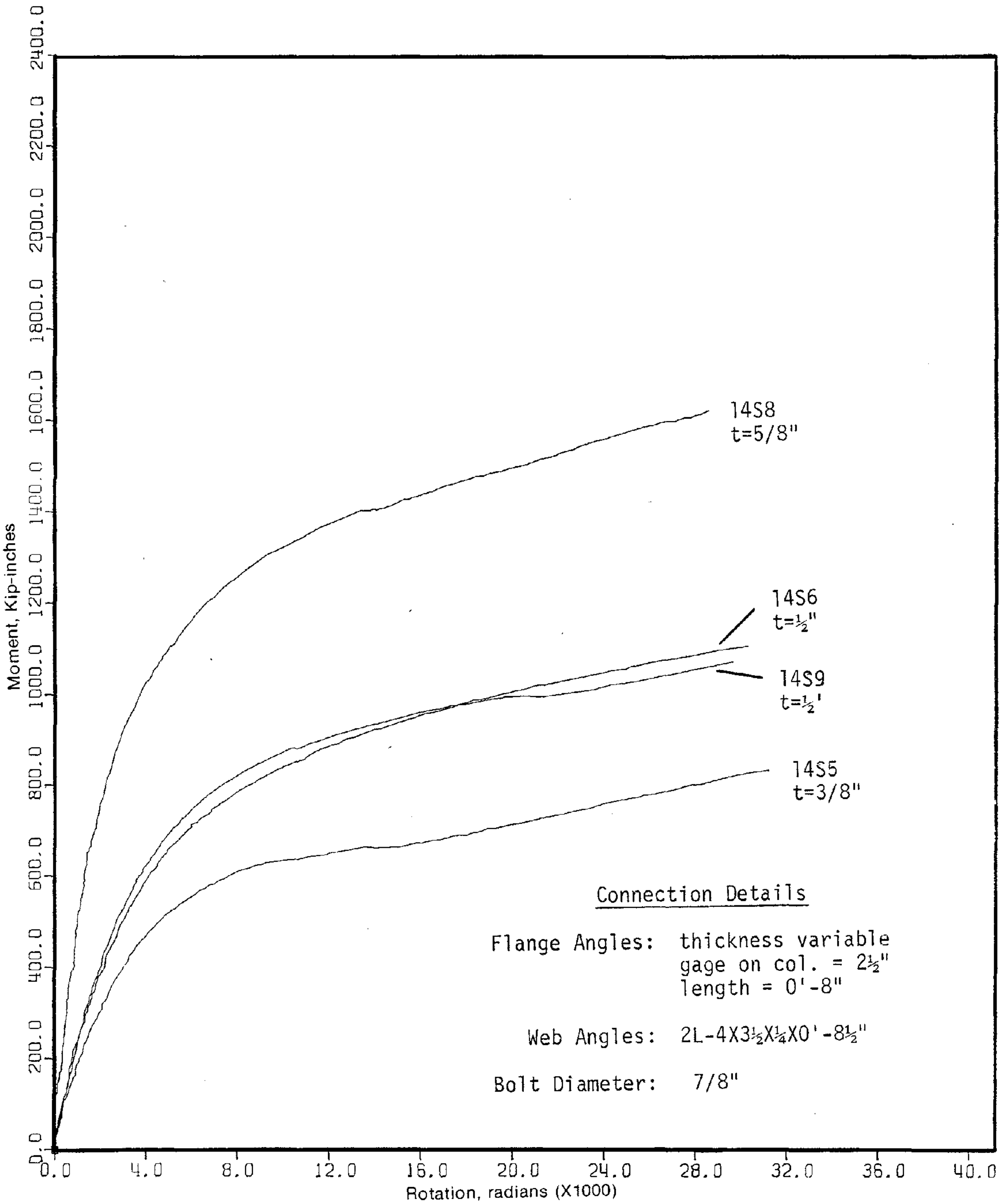


FIG. 3.6 EFFECT OF FLANGE ANGLE THICKNESS ON STATIC MOMENT-ROTATION BEHAVIOR — W14X38 BEAM CONNECTION (BOLT DIAMETER = ⅞")

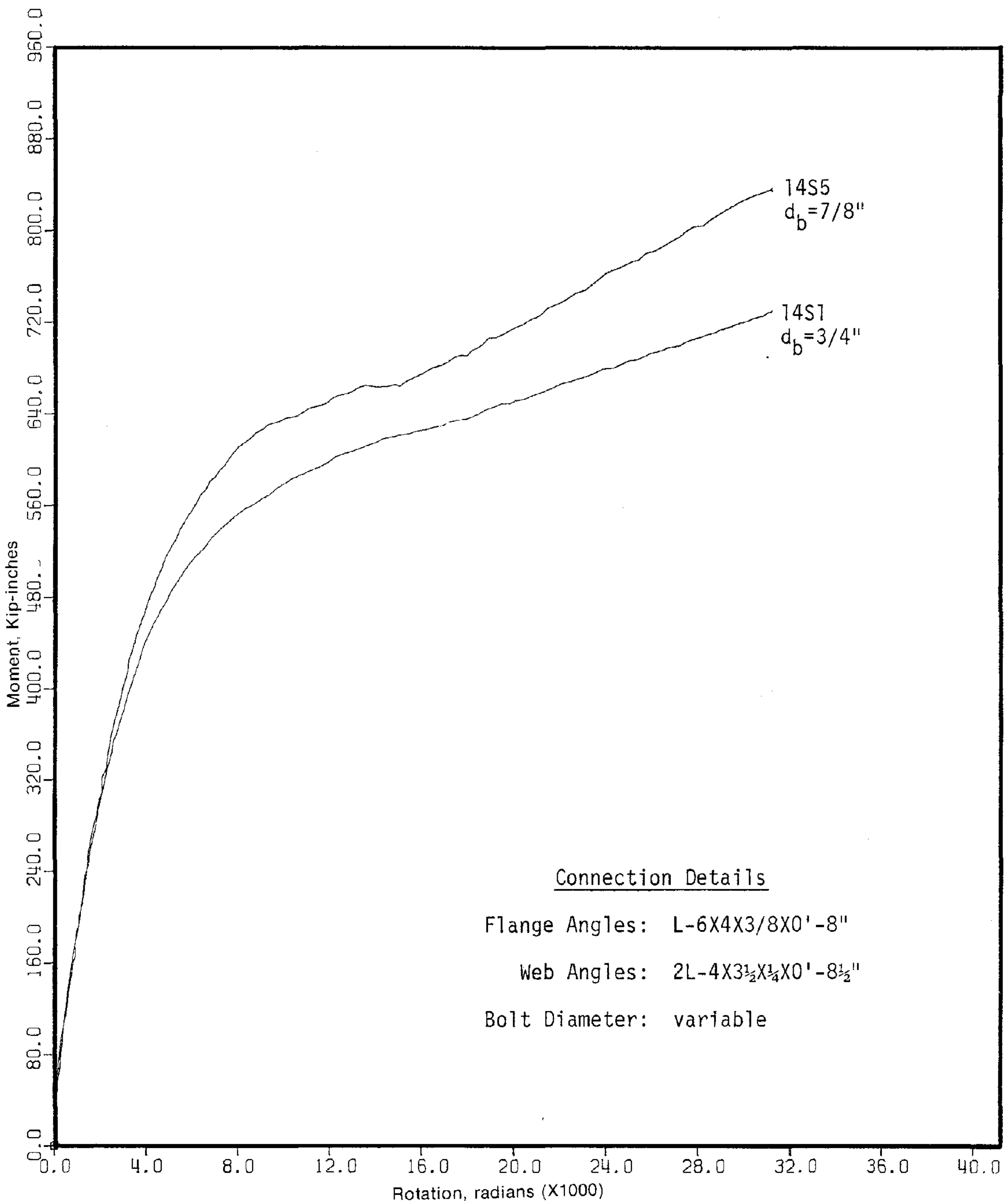


FIG. 3.7a EFFECT OF BOLT DIAMETER ON STATIC MOMENT-ROTATION BEHAVIOR — W14X38 BEAM CONNECTION (FLANGE ANGLE THICKNESS = ⅜")

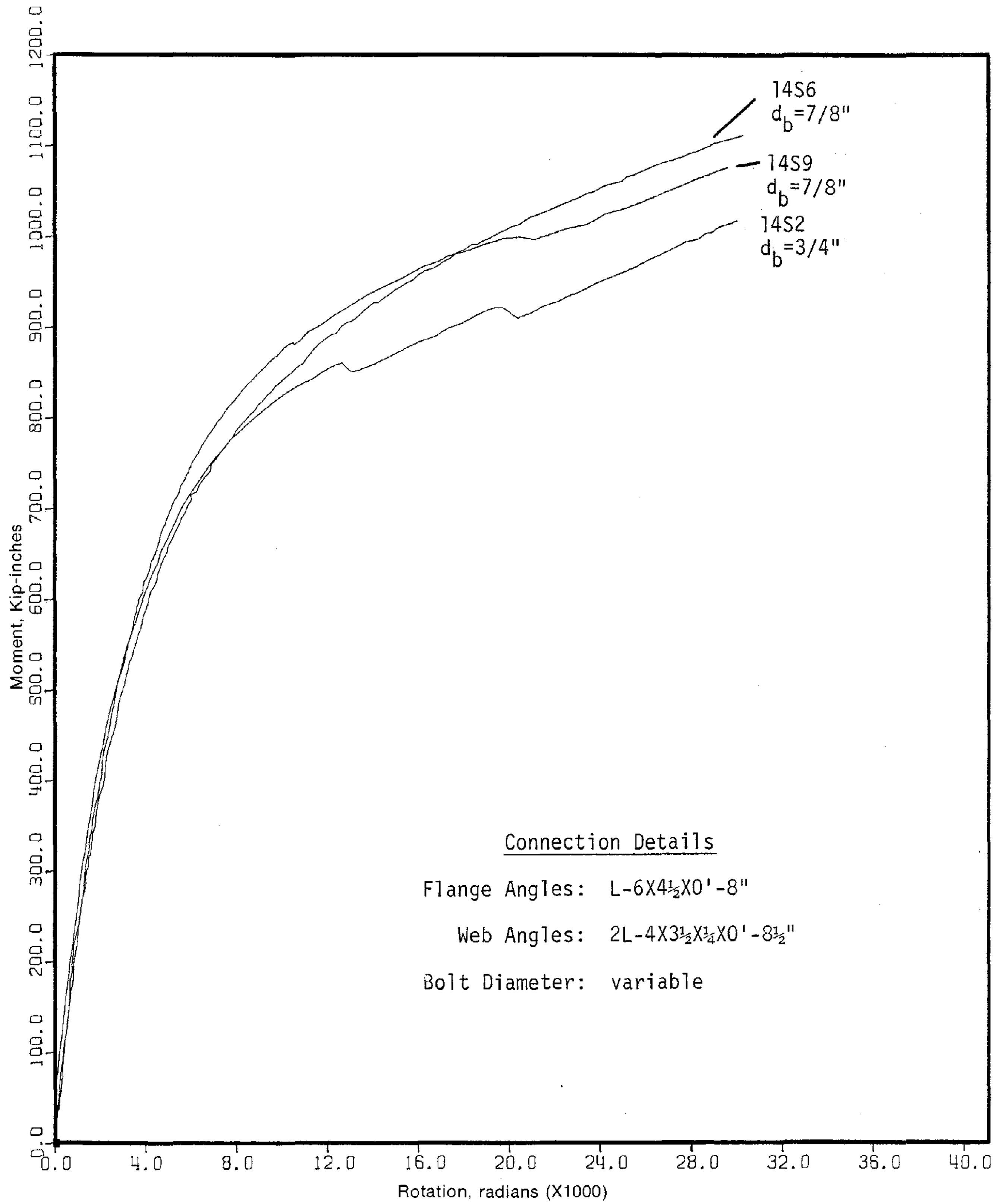


FIG. 3.7b EFFECT OF BOLT DIAMETER ON STATIC MOMENT-ROTATION BEHAVIOR — W14X38 BEAM CONNECTION (FLANGE ANGLE THICKNESS = ½")

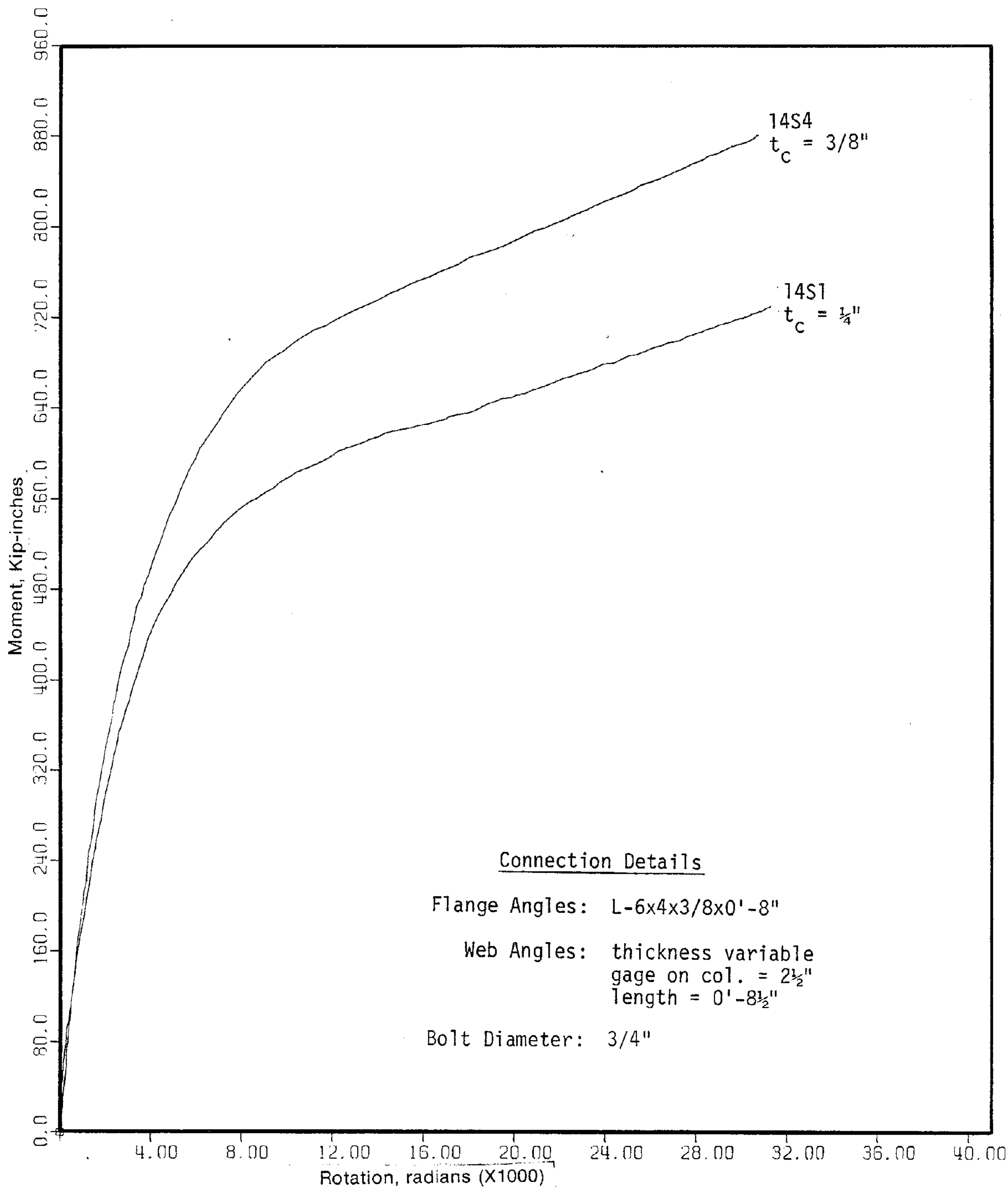


FIG. 3.8 EFFECT OF WEB ANGLE THICKNESS ON STATIC MOMENT-ROTATION BEHAVIOR — W14X38 BEAM CONNECTION

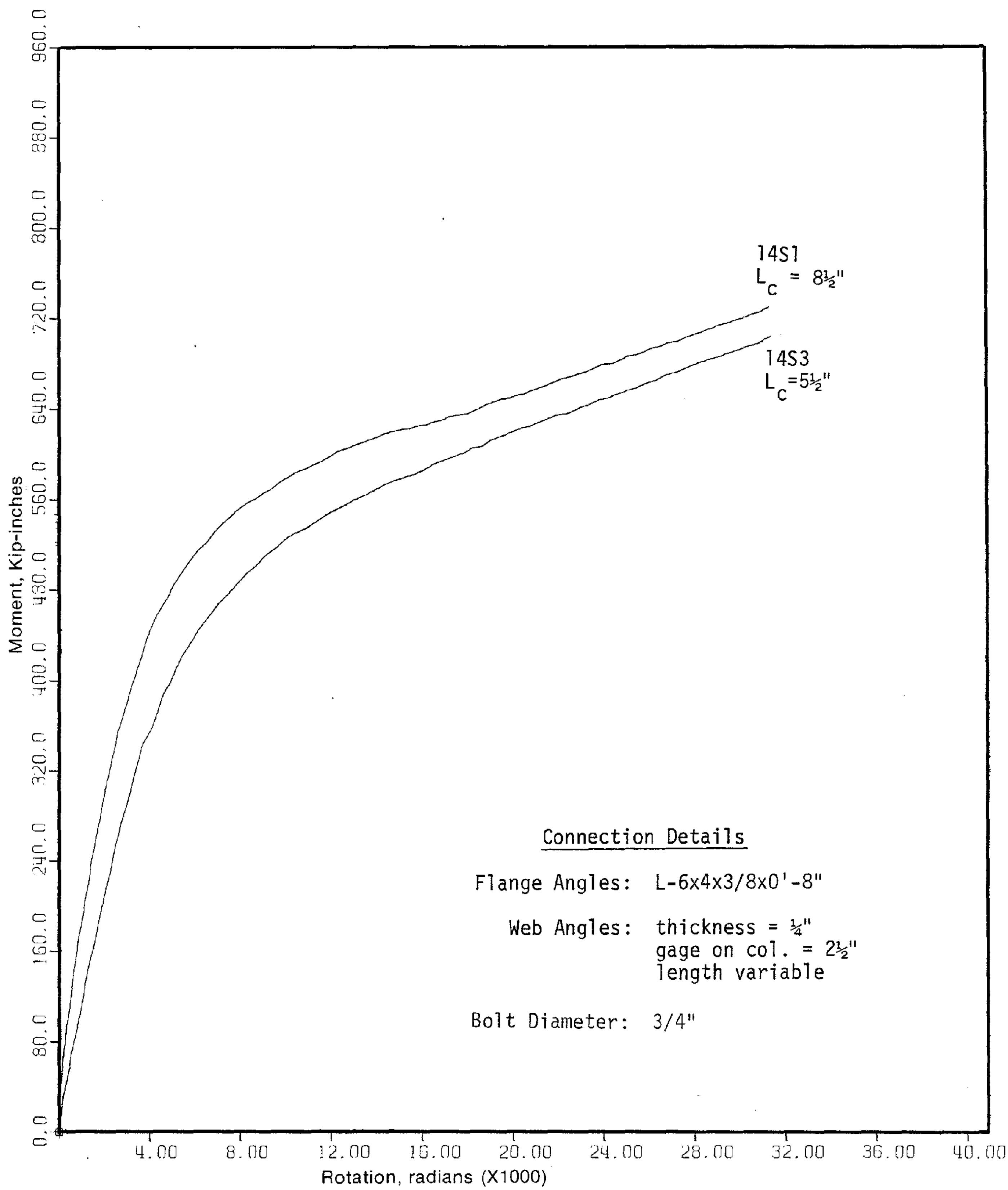


FIG. 3.9 EFFECT OF WEB ANGLE LENGTH ON STATIC MOMENT-ROTATION BEHAVIOR — W14X38 BEAM CONNECTION

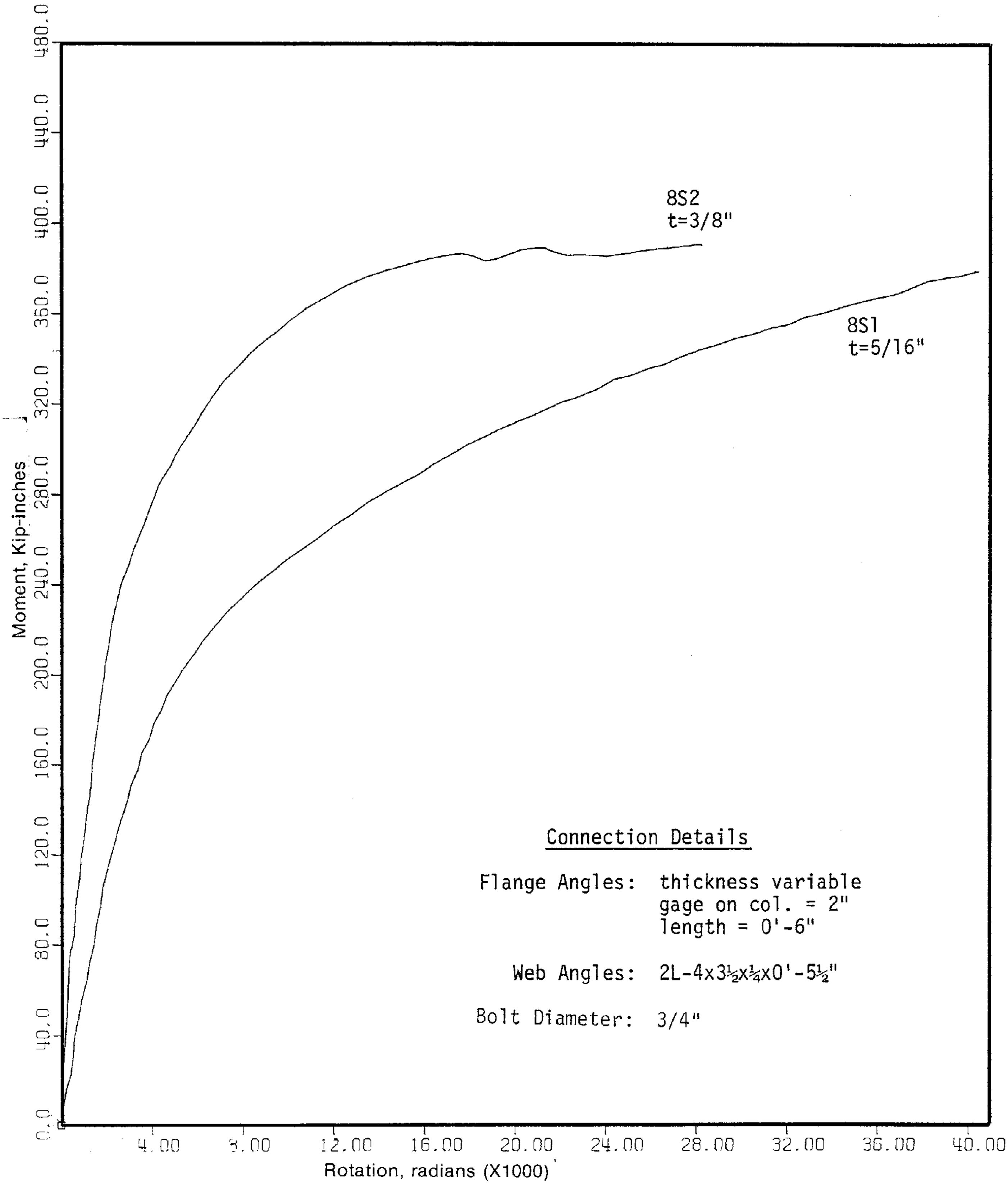


FIG. 3.10a EFFECT OF FLANGE ANGLE THICKNESS ON STATIC MOMENT-ROTATION BEHAVIOR — W8X21 BEAM CONNECTION (BOLT DIAMETER = ¾", ANGLE GAGE = 2")

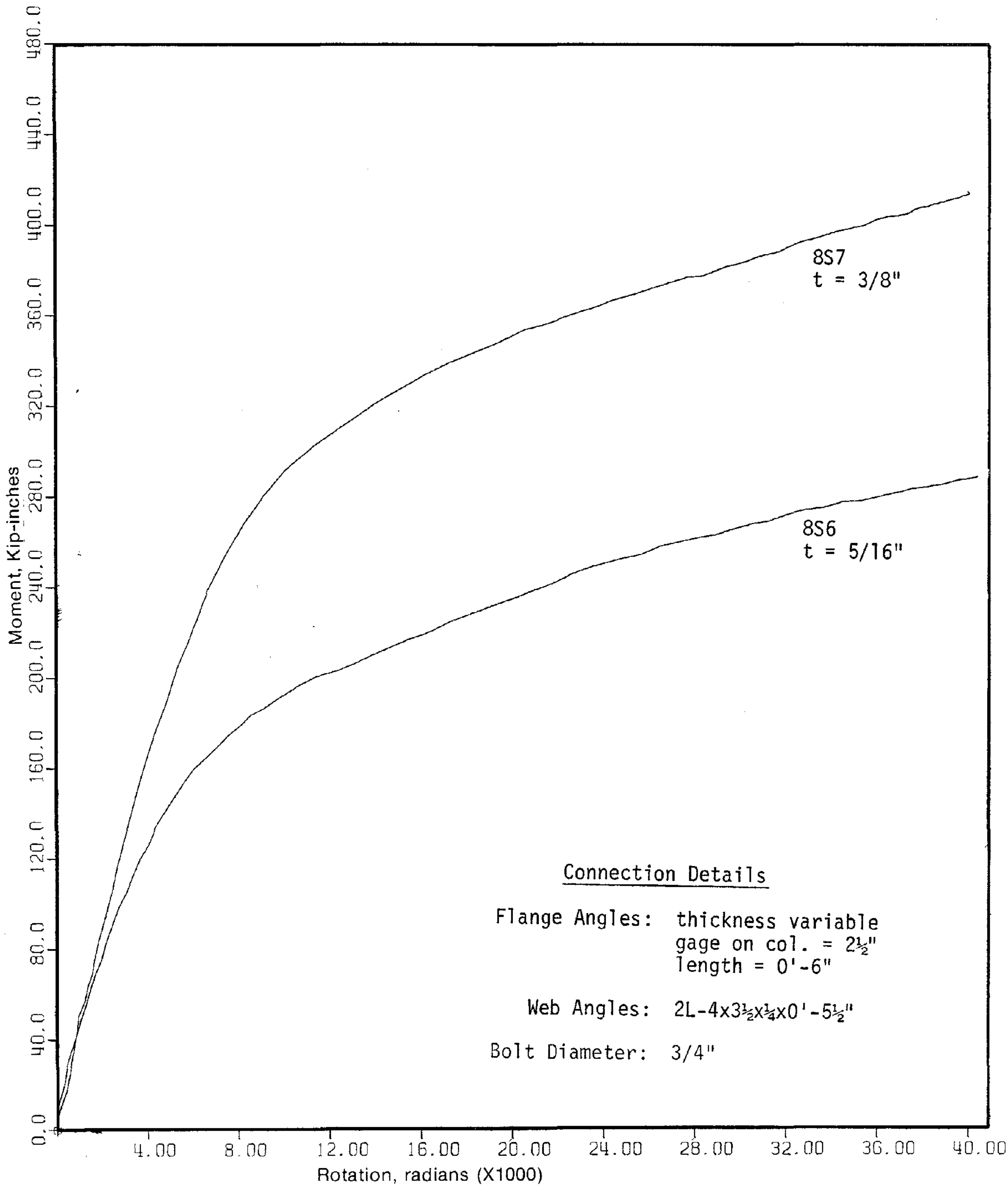


FIG. 3.10b EFFECT OF FLANGE ANGLE THICKNESS ON STATIC MOMENT-ROTATION BEHAVIOR — W8X21 BEAM CONNECTION (BOLT DIAMETER = ¾", ANGLE GAGE = 2½")

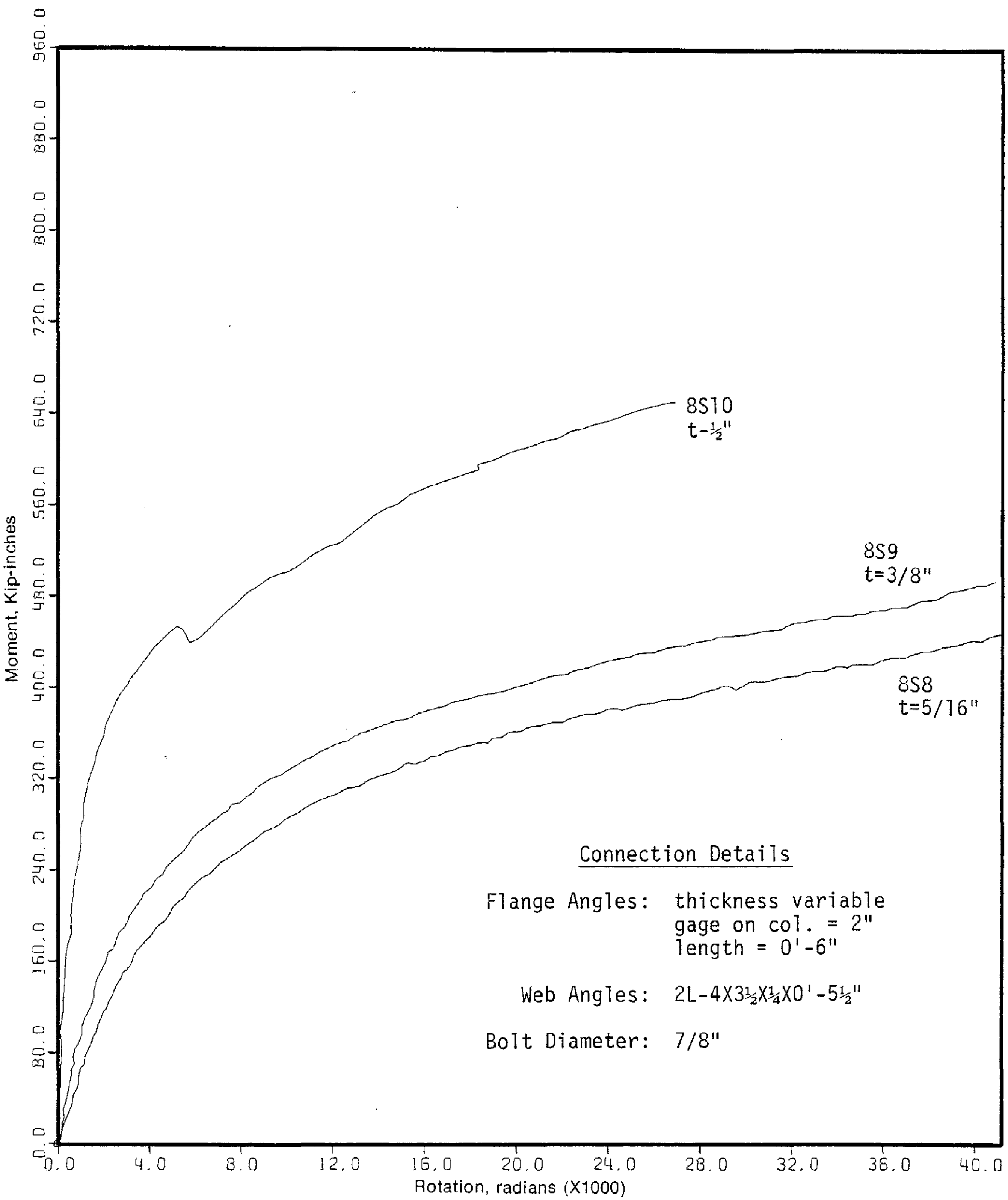


FIG. 3.11 EFFECT OF FLANGE ANGLE THICKNESS ON STATIC MOMENT-ROTATION BEHAVIOR — W8X21 BEAM CONNECTIONS (BOLT DIAMETER = ⅞", ANGLE GAGE = 2")

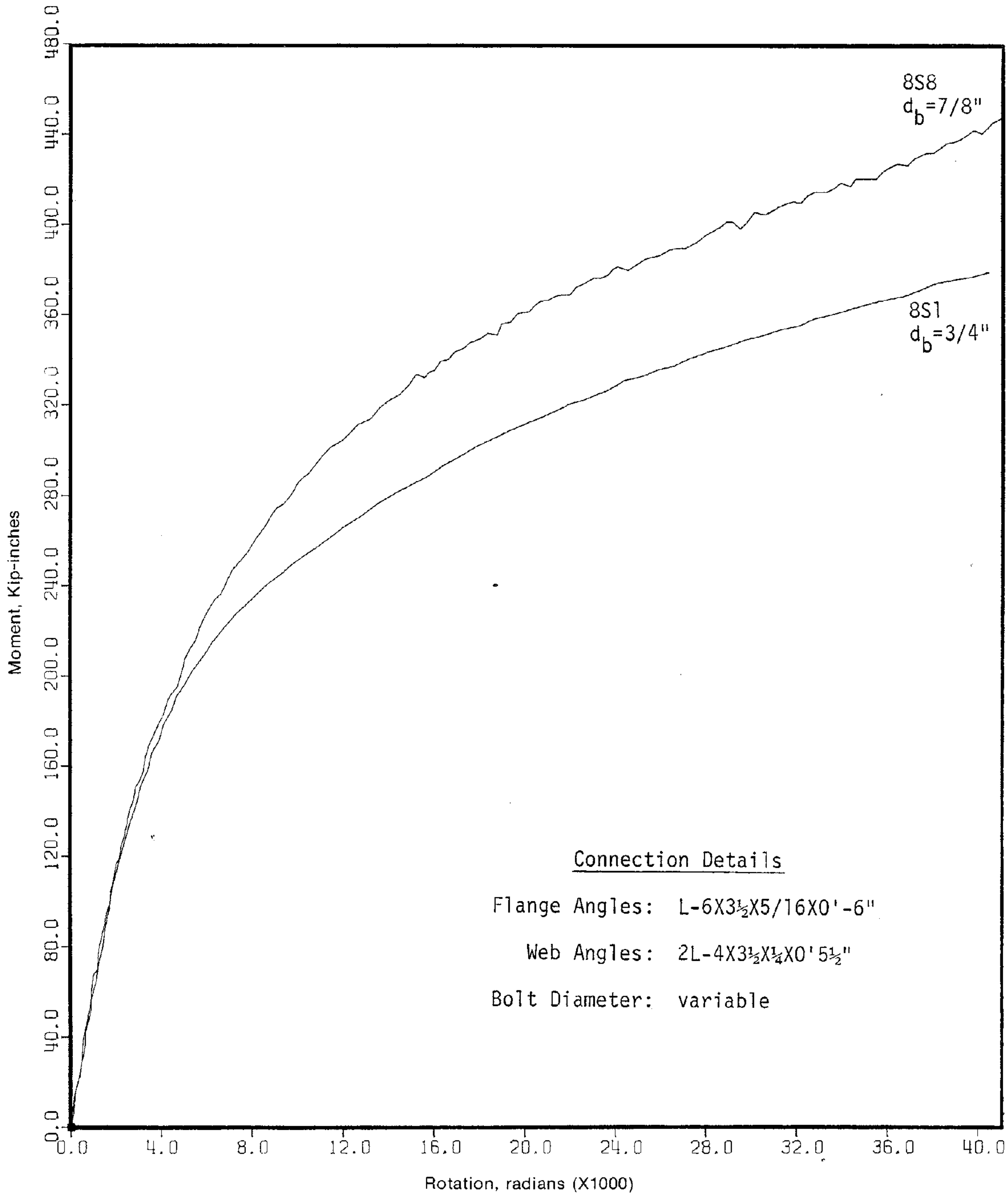


FIG. 3.12a EFFECT OF BOLT DIAMETER ON STATIC MOMENT-ROTATION BEHAVIOR — W8X21 BEAM CONNECTION (FLANGE ANGLE THICKNESS = 5/16")

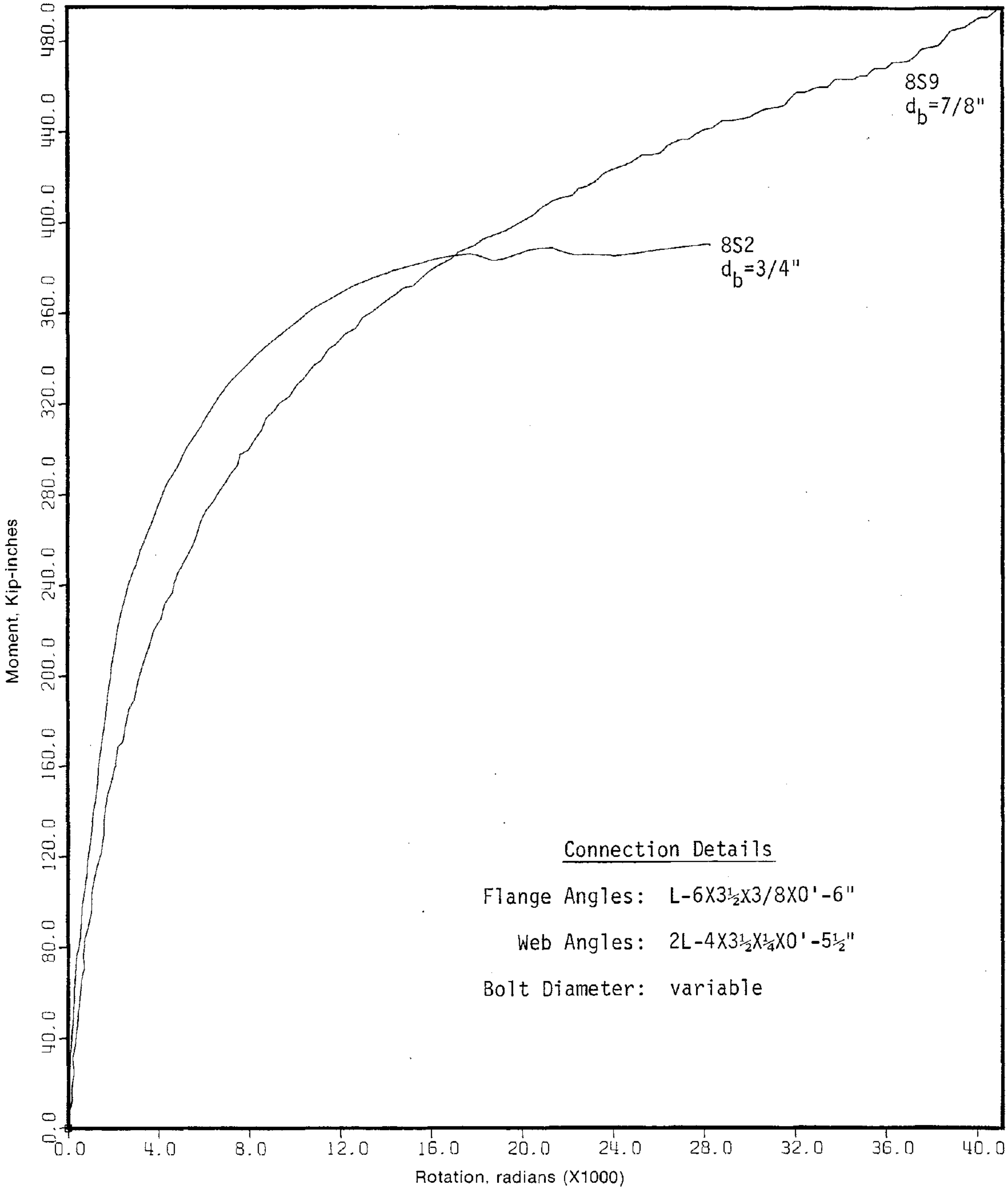


FIG. 3.12b EFFECT OF BOLT DIAMETER ON STATIC MOMENT-ROTATION BEHAVIOR — W8X21 BEAM CONNECTION (FLANGE ANGLE THICKNESS = ⅜")

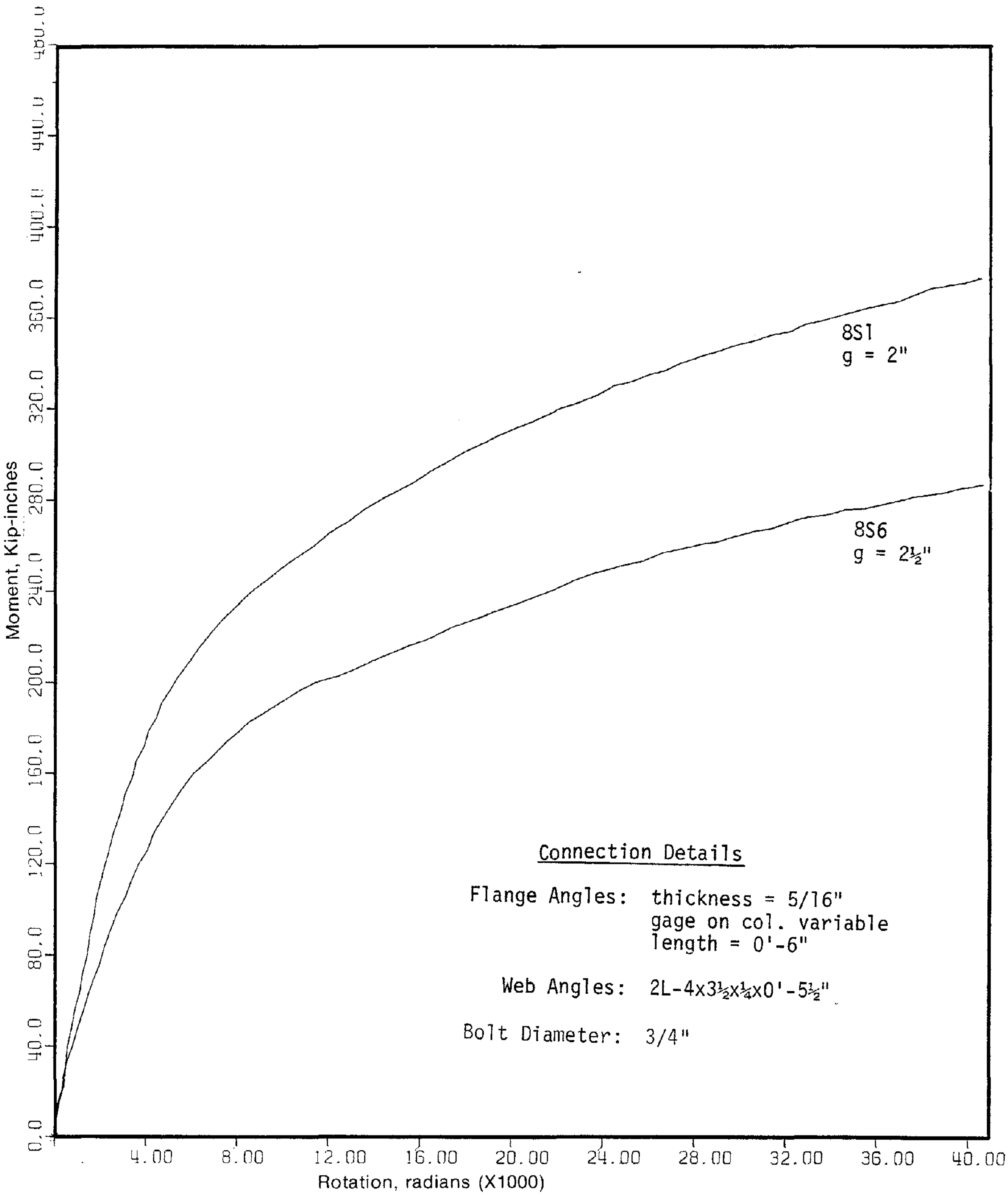


FIG. 3.13a EFFECT OF FLANGE ANGLE GAGE ON STATIC MOMENT-ROTATION BEHAVIOR — W8X21 BEAM CONNECTION (ANGLE THICKNESS — 5/16")

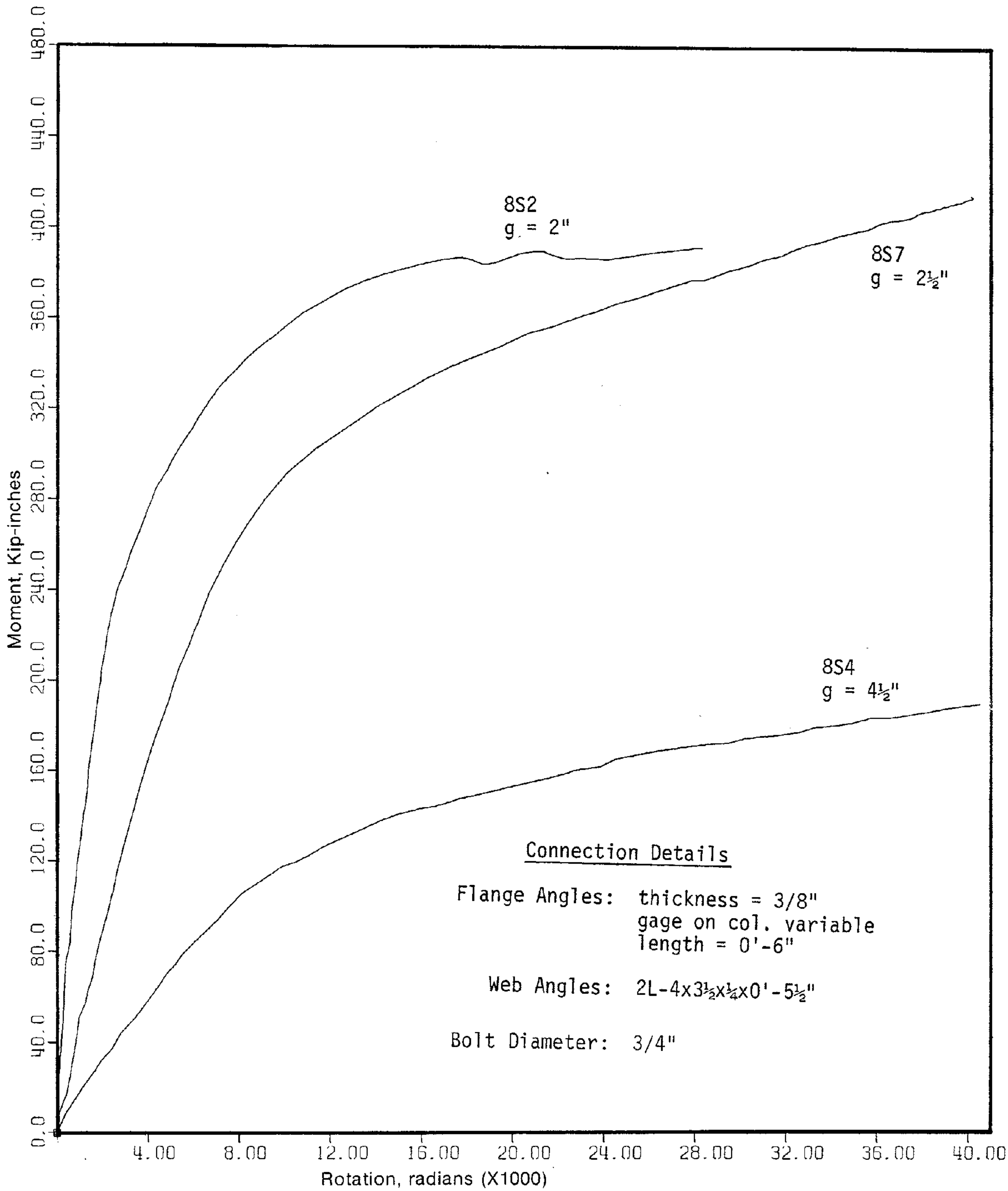


FIG. 3.13b EFFECT OF FLANGE ANGLE GAGE ON STATIC MOMENT-ROTATION BEHAVIOR — W8X21 BEAM CONNECTION (ANGLE THICKNESS = ⅜")

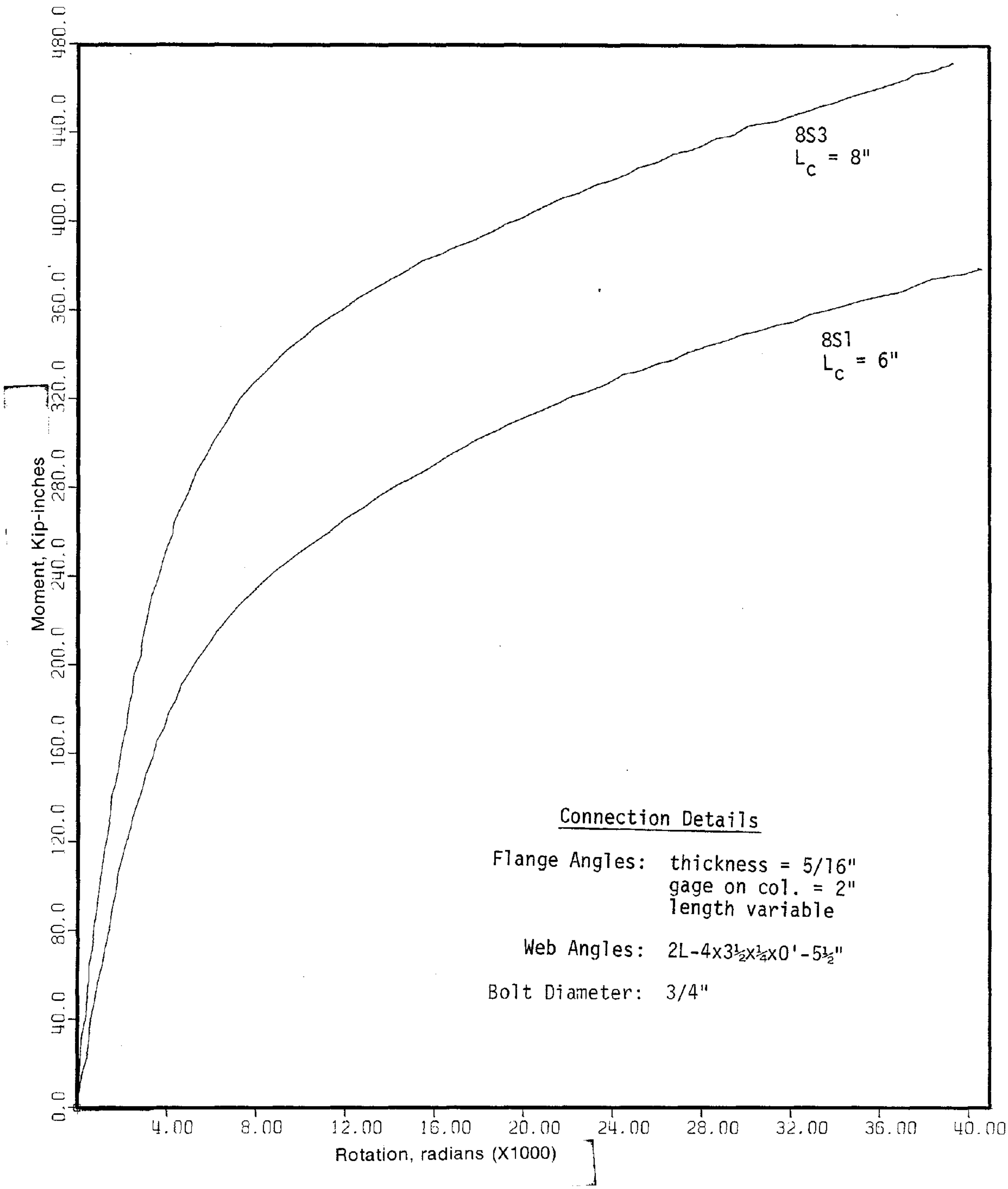


FIG. 3.14 EFFECT OF FLANGE ANGLE LENGTH ON STATIC MOMENT-ROTATION BEHAVIOR — W8X21 BEAM CONNECTION

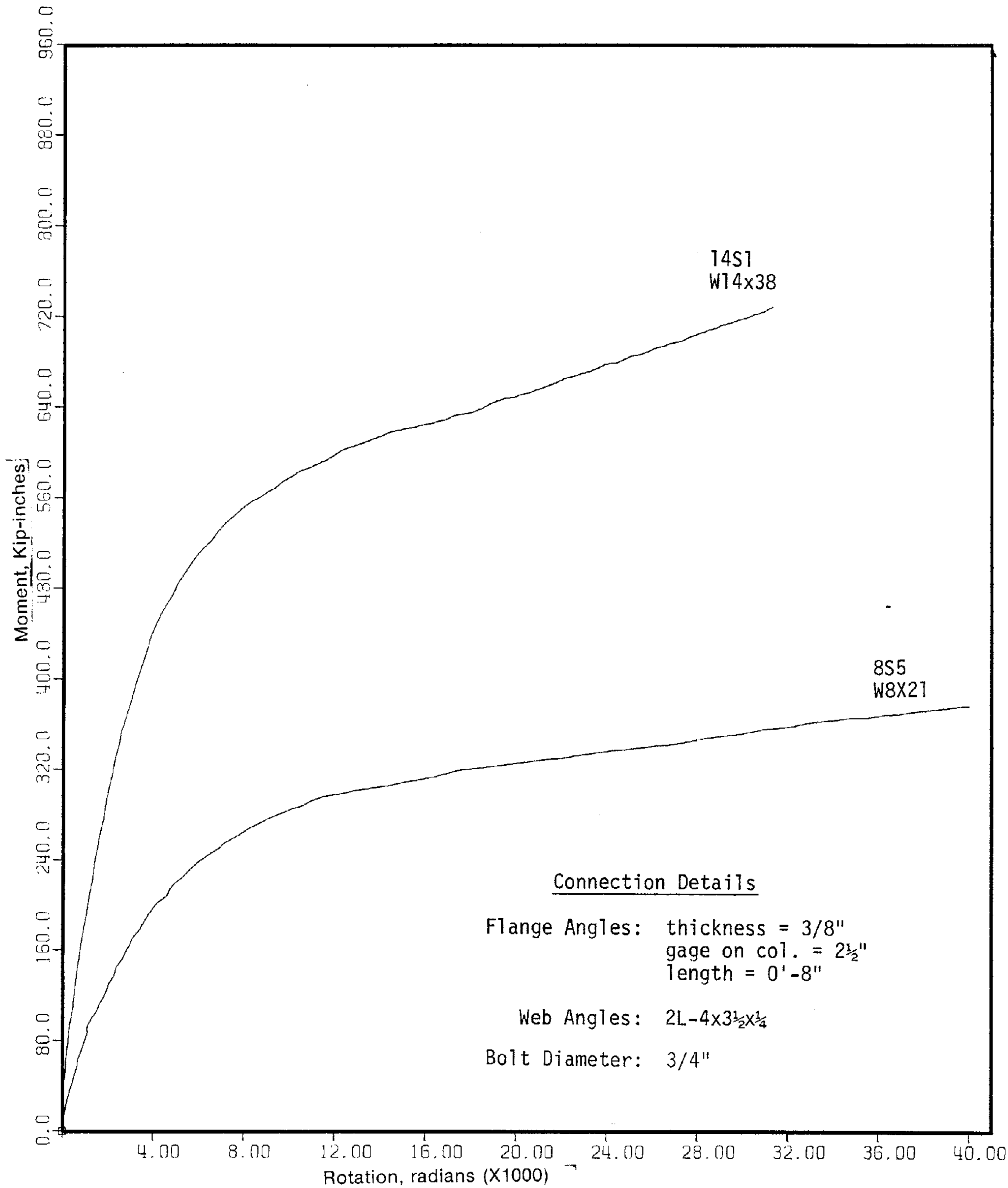


FIG. 3.15 COMPARISON OF STATIC MOMENT-ROTATION BEHAVIOR OF W14X38 and W8X21 BEAM CONNECTIONS

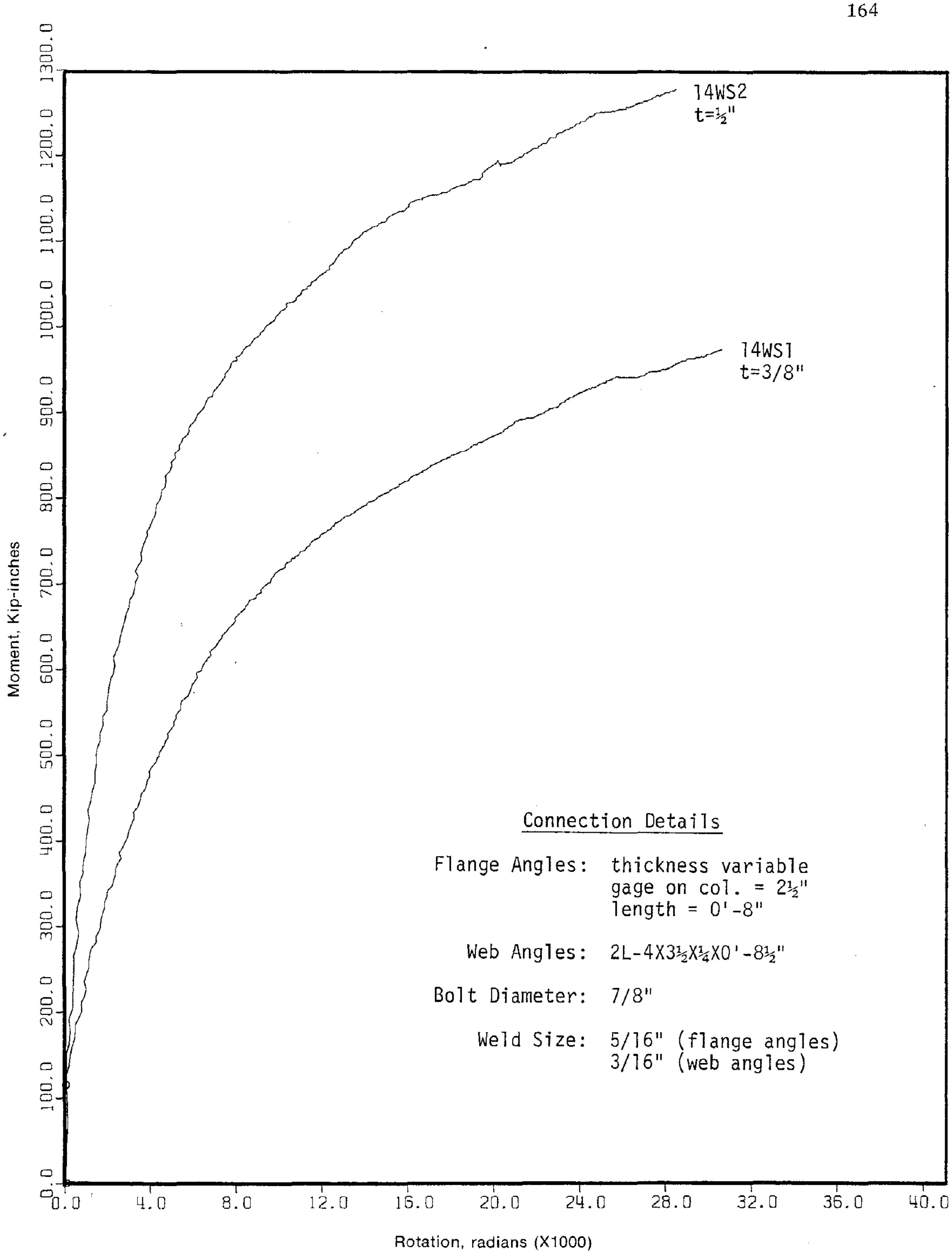


FIG. 3.16 EFFECT OF FLANGE ANGLE THICKNESS ON STATIC MOMENT-ROTATION BEHAVIOR OF W14 X 38 BEAM CONNECTIONS - BOLTED-WELDED SPECIMENS

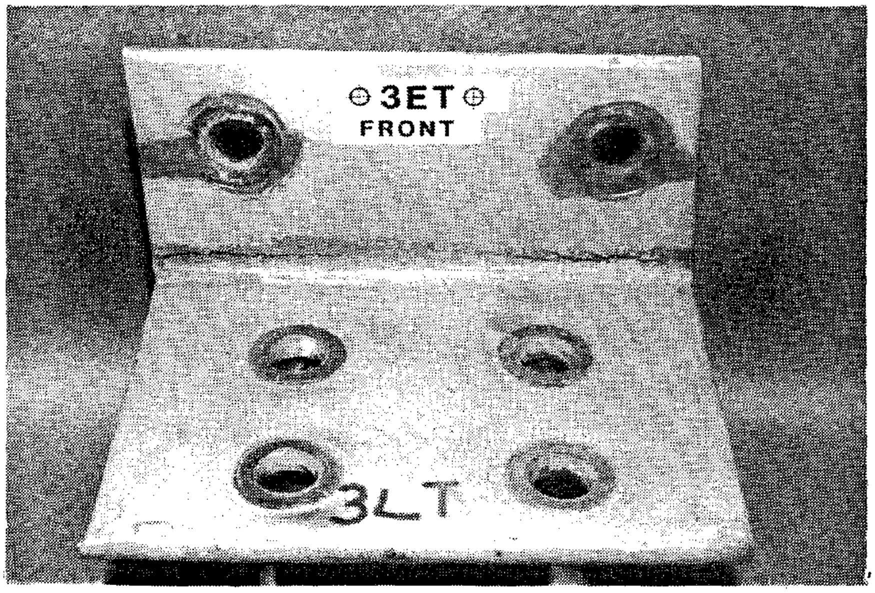


a. FRONT VIEW

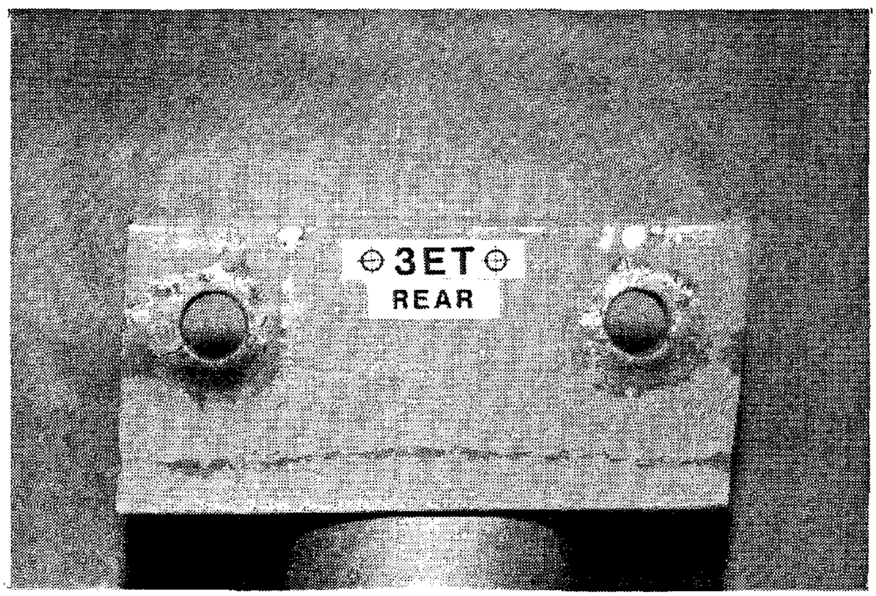


b. REAR VIEW

FIG. 3.17a FLANGE ANGLE FROM SPECIMEN 14CI AFTER CYCLIC TEST

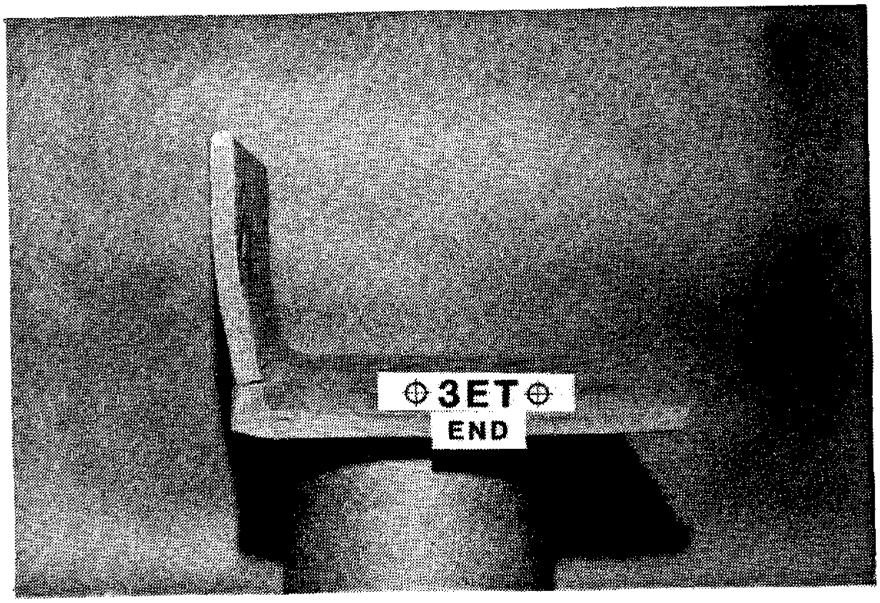


a. FLANGE ANGLE — END VIEW

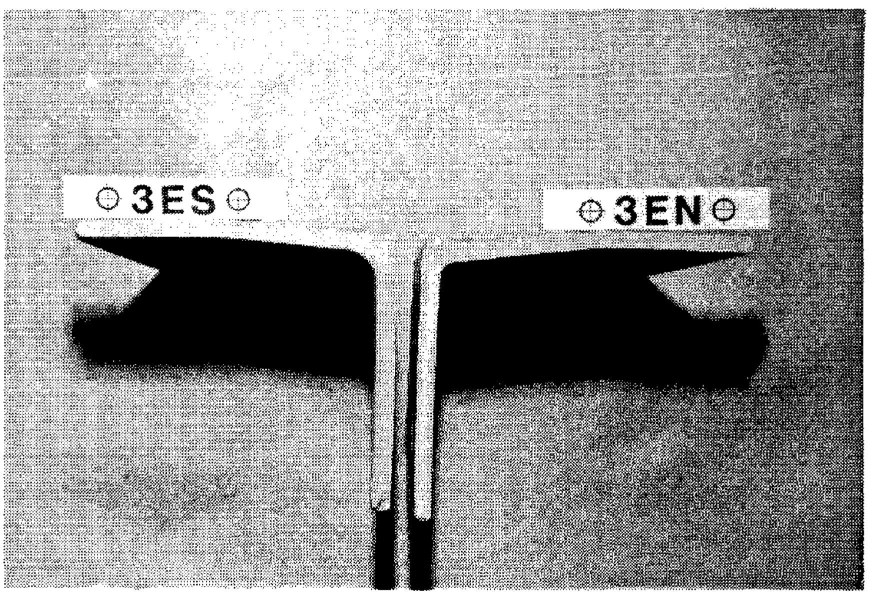


b. WEB ANGLES — END VIEW

FIG. 3.17b FLANGE AND WEB ANGLES FROM SPECIMEN 14CI AFTER CYCLIC TEST

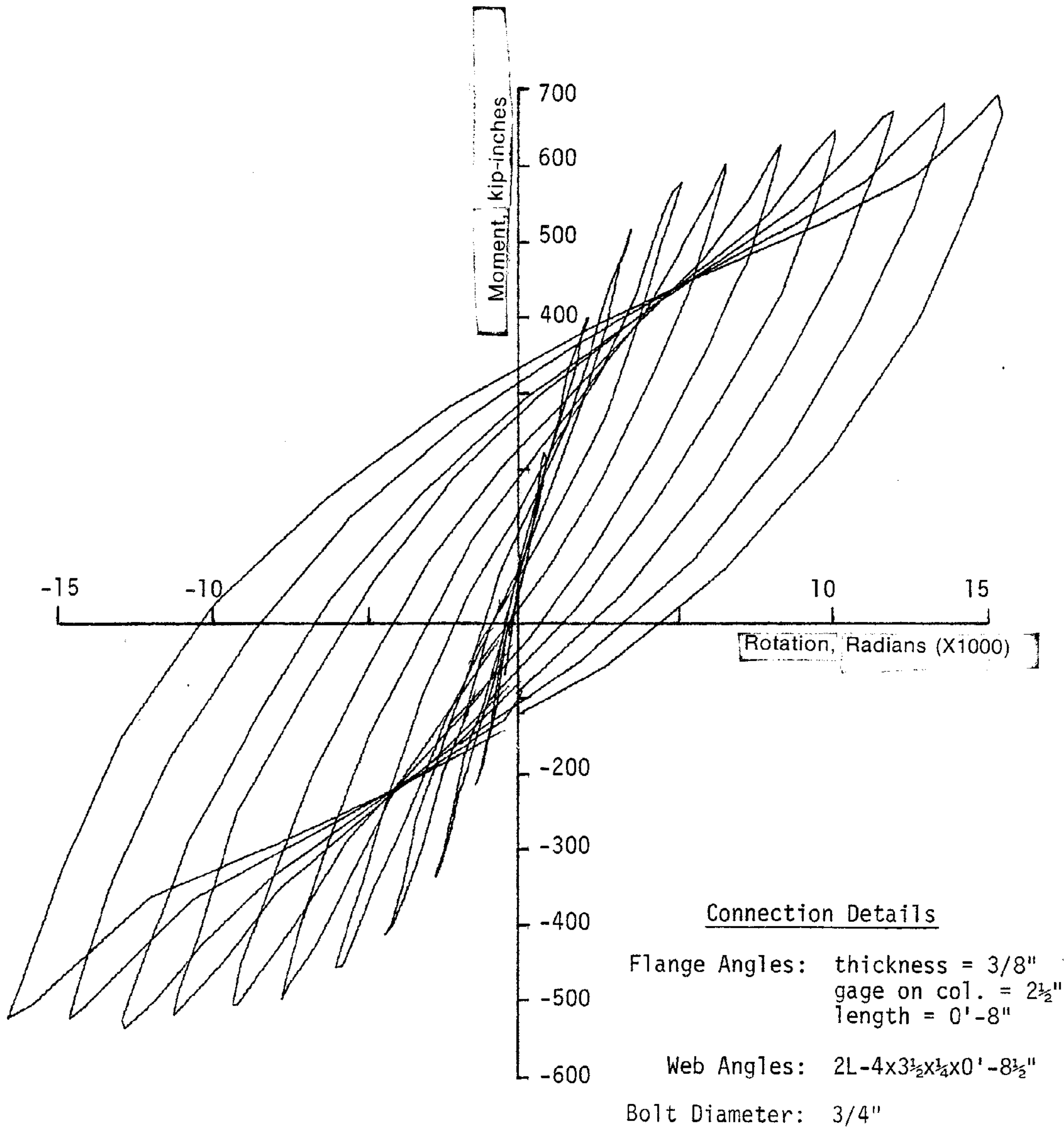


FIG. 3.18 STABLE HYSTERESIS LOOPS FOR SPECIMEN 14C1

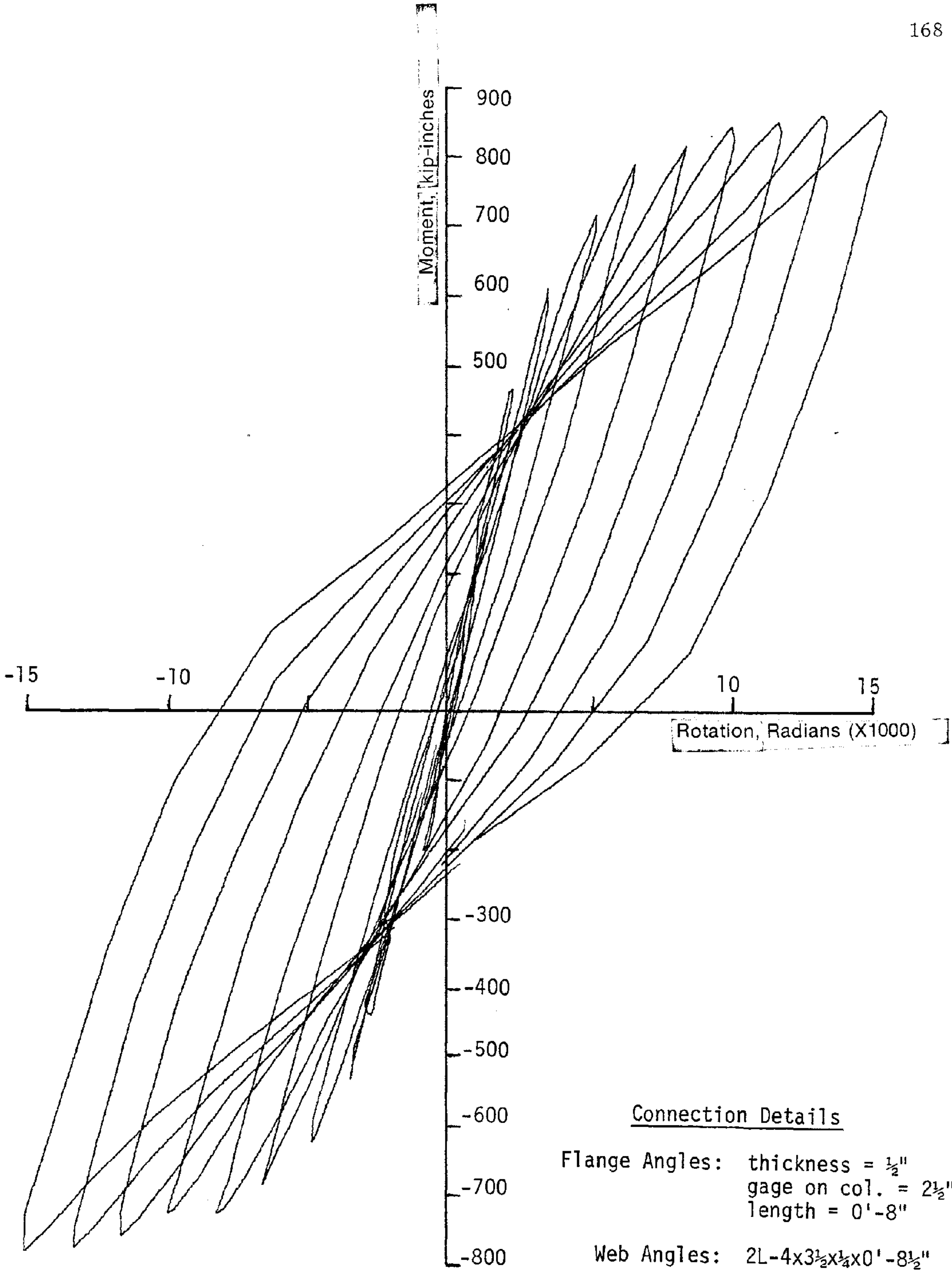


Connection Details

Flange Angles: thickness = ½"
gage on col. = 2½"
length = 0'-8"

Web Angles: 2L-4x3½x¼x0'-8½"

Bolt Diameter: 3/4"

FIG. 3.19 STABLE HYSTERESIS LOOPS FOR SPECIMEN 14C2

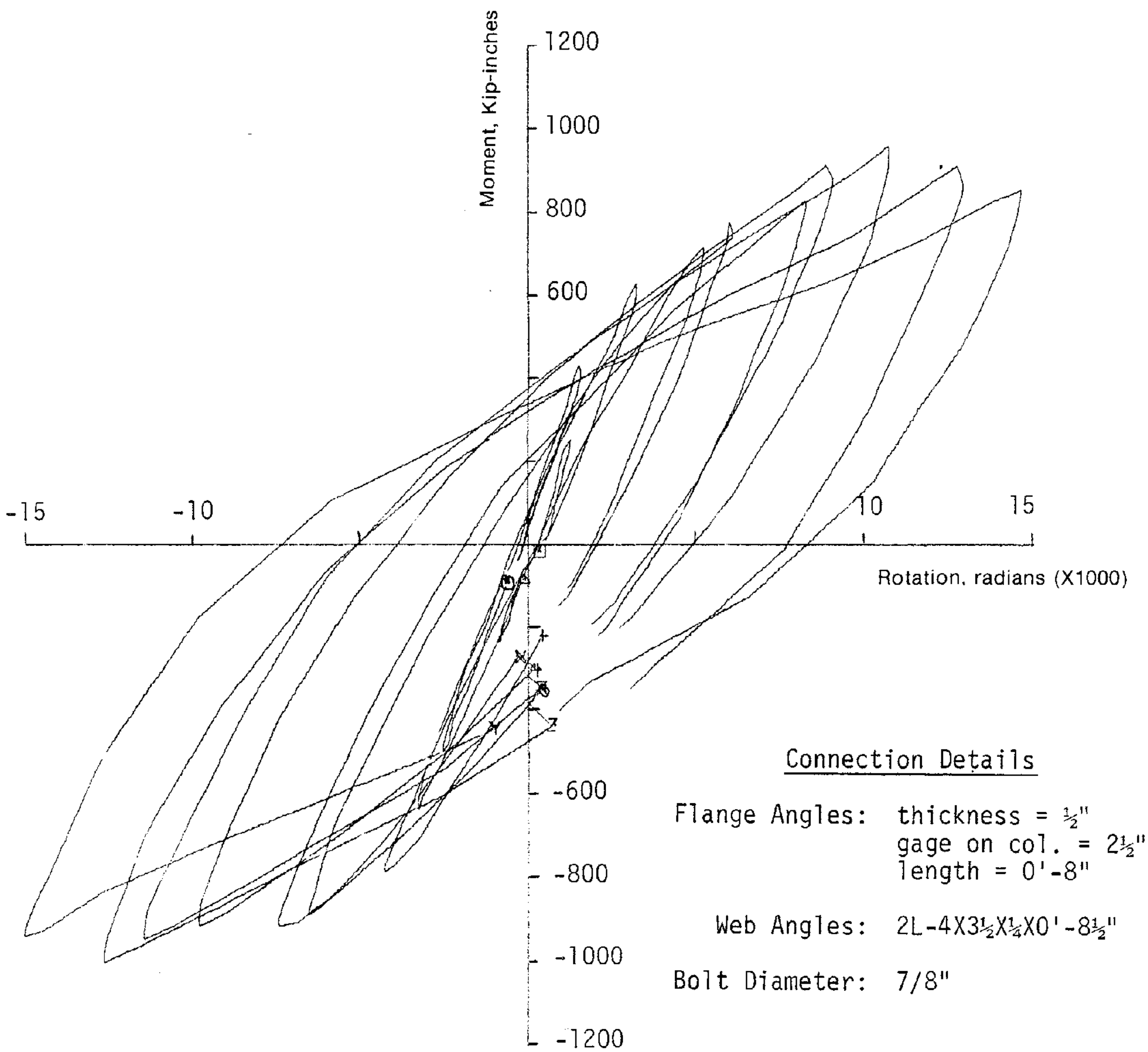


FIG. 3.20 STABLE HYSTERESIS LOOPS FOR SPECIMEN 14C3

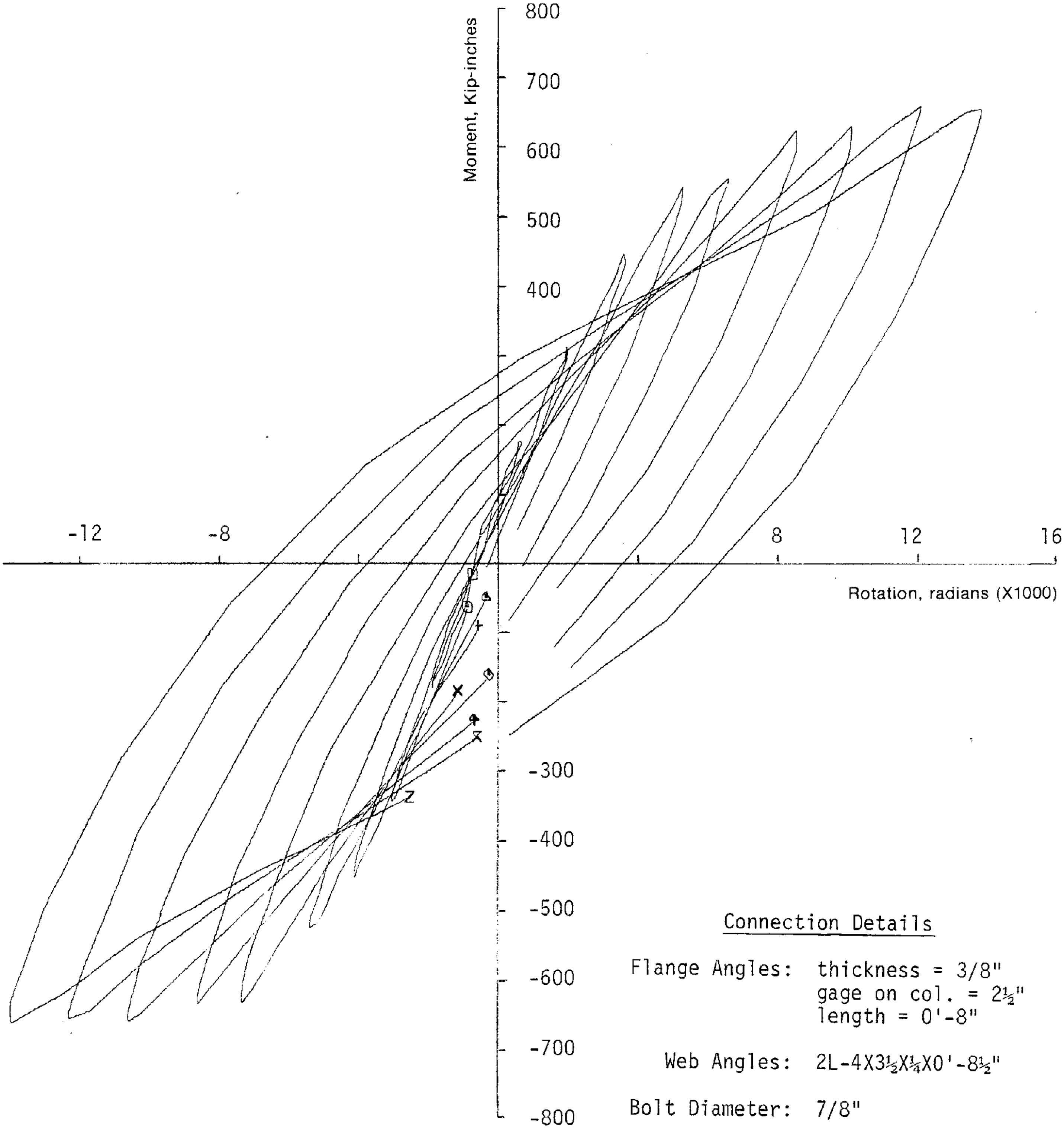


FIG. 3.21 STABLE HYSTERESIS LOOPS FOR SPECIMEN 14C4

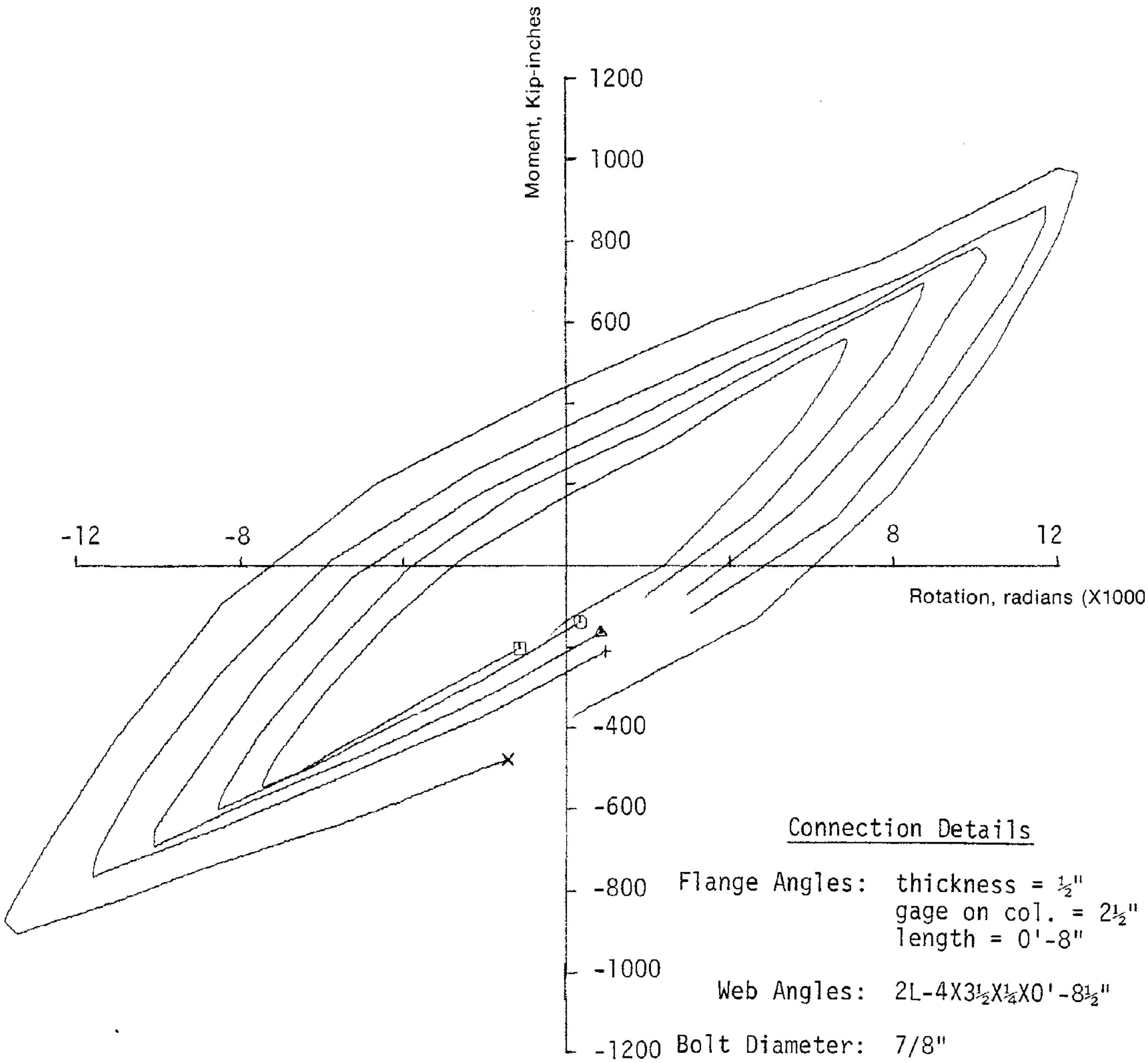


FIG. 3.22 STABLE HYSTERESIS LOOPS FOR SPECIMEN 14B1

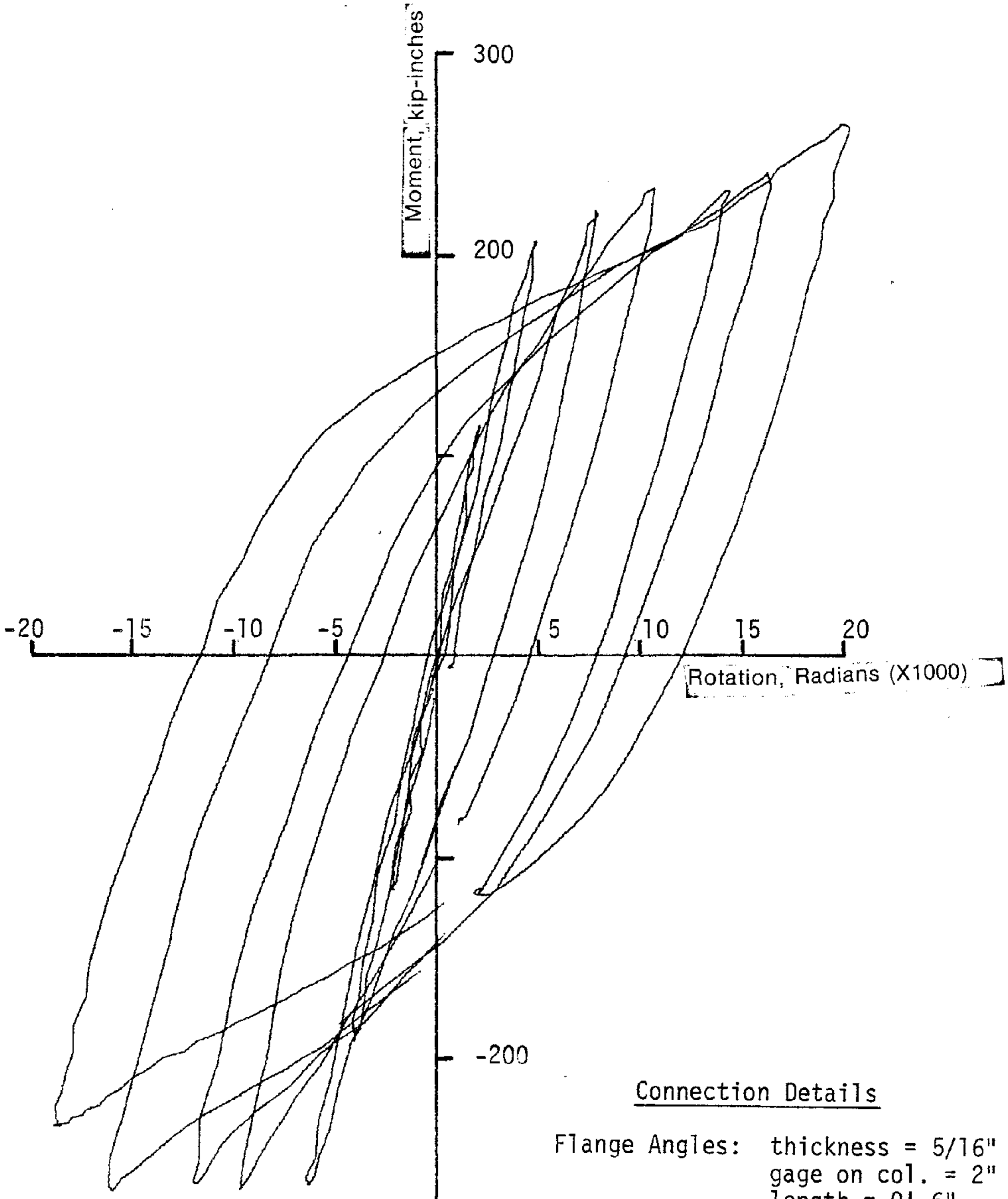


### Connection Details

Flange Angles: thickness = 5/16"
gage on col. = 2"
length = 0'-6"

Web Angles: 2L-4x3½x¼x0'-5½"

Bolt Diameter: 3/4"

FIG. 3.23 STABLE HYSTERESIS LOOPS FOR SPECIMEN 8C1

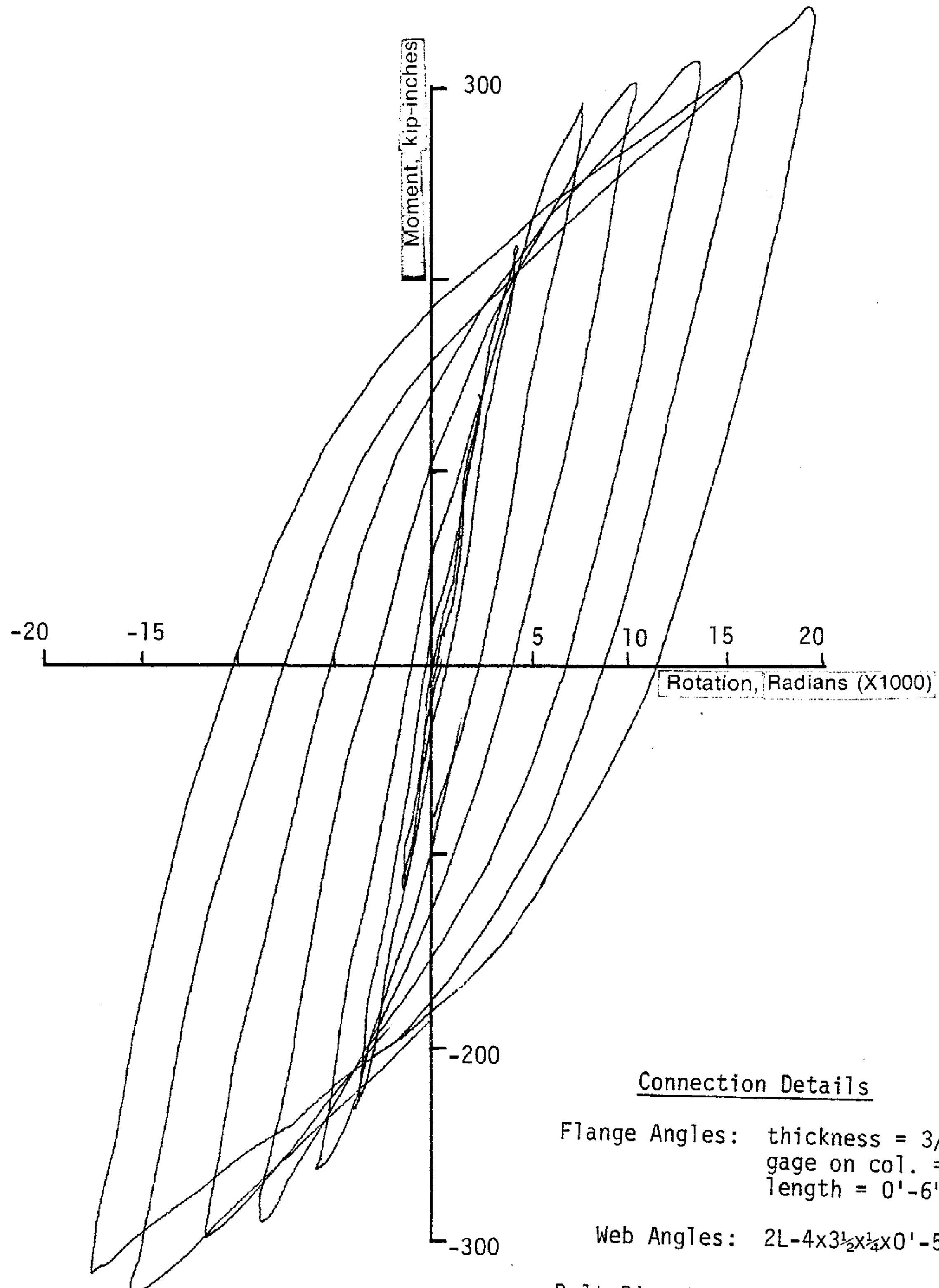


Connection Details

Flange Angles: thickness = 3/8"
gage on col. = 2"
length = 0'-6"

Web Angles: 2L-4x3½x¼x0'-5½"

Bolt Diameter: 3/4"

FIG. 3.24 STABLE HYSTERESIS LOOPS FOR SPECIMEN 8C2

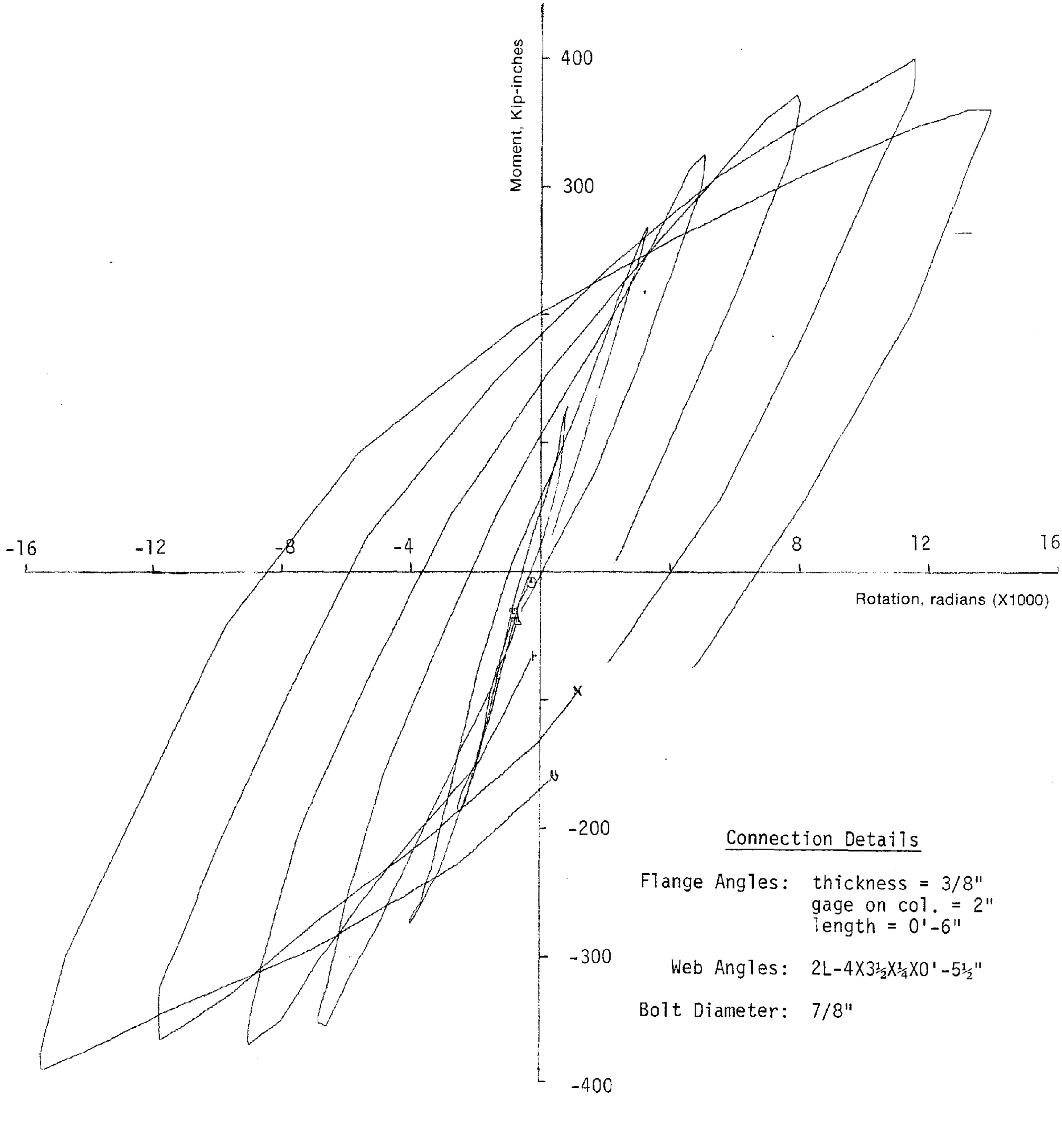


FIG. 3.25 STABLE HYSTERESIS LOOPS FOR SPECIMEN 8C3

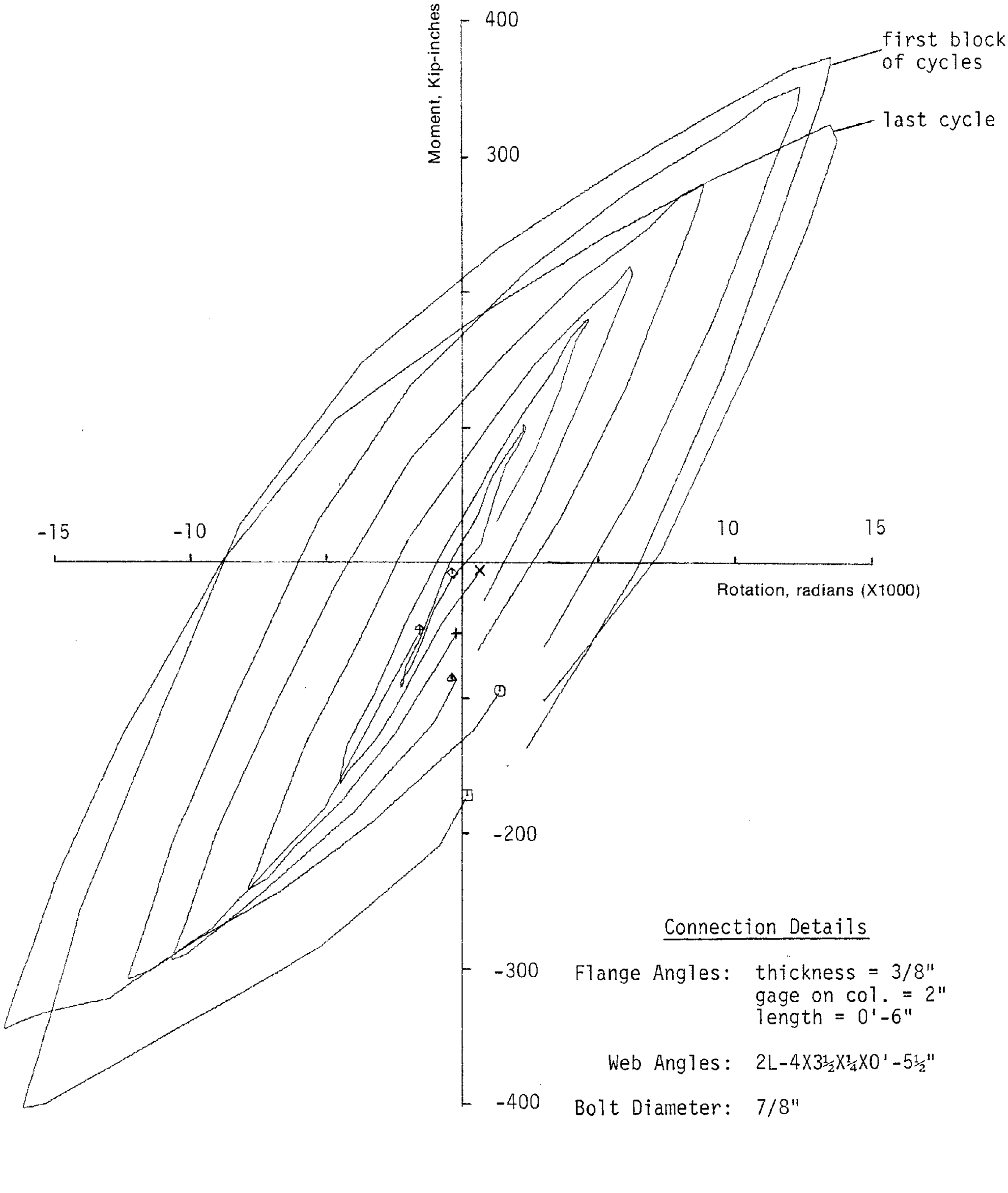


FIG. 3.26 STABLE HYSTERESIS LOOPS FOR SPECIMEN 8B1

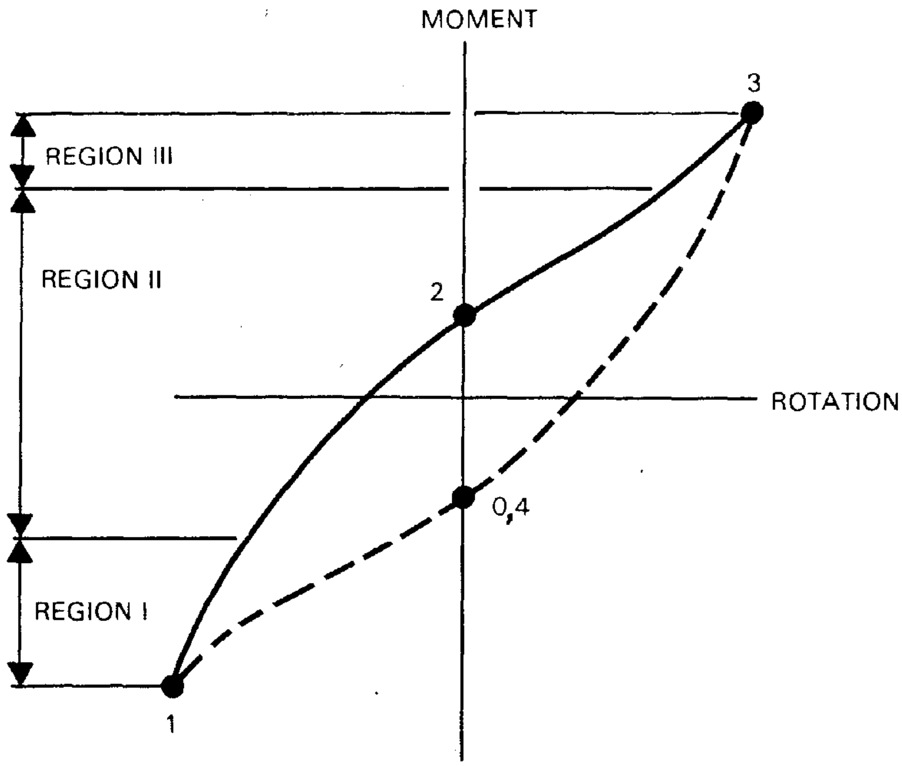


FIG. 3.27 TYPICAL MOMENT-ROTATION HYSTERESIS LOOP — CYCLIC TESTS

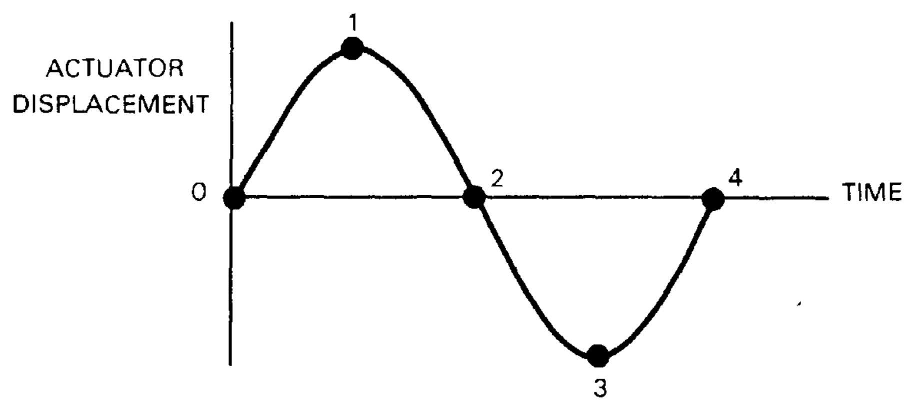


FIG. 3.28 TYPICAL TIME-ACTUATOR DISPLACEMENT CYCLE

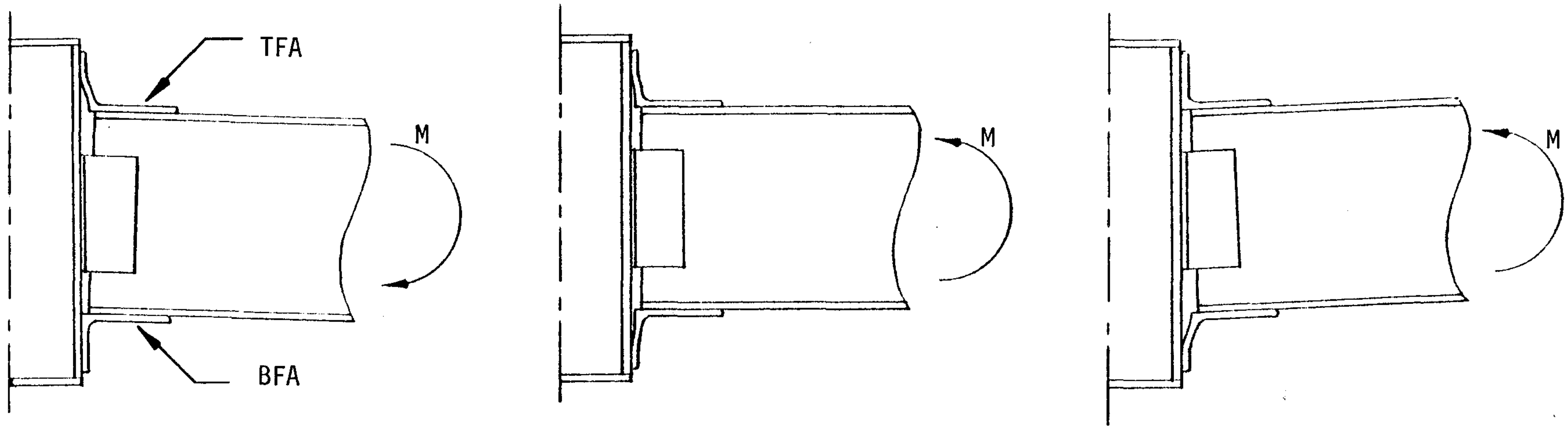


a. REGION I CONFIGURATION

b. REGION II CONFIGURATION

c. REGION III CONFIGURATION

FIG. 3.29 CONFIGURATIONS OF CONNECTION DURING ONE-HALF CYCLE

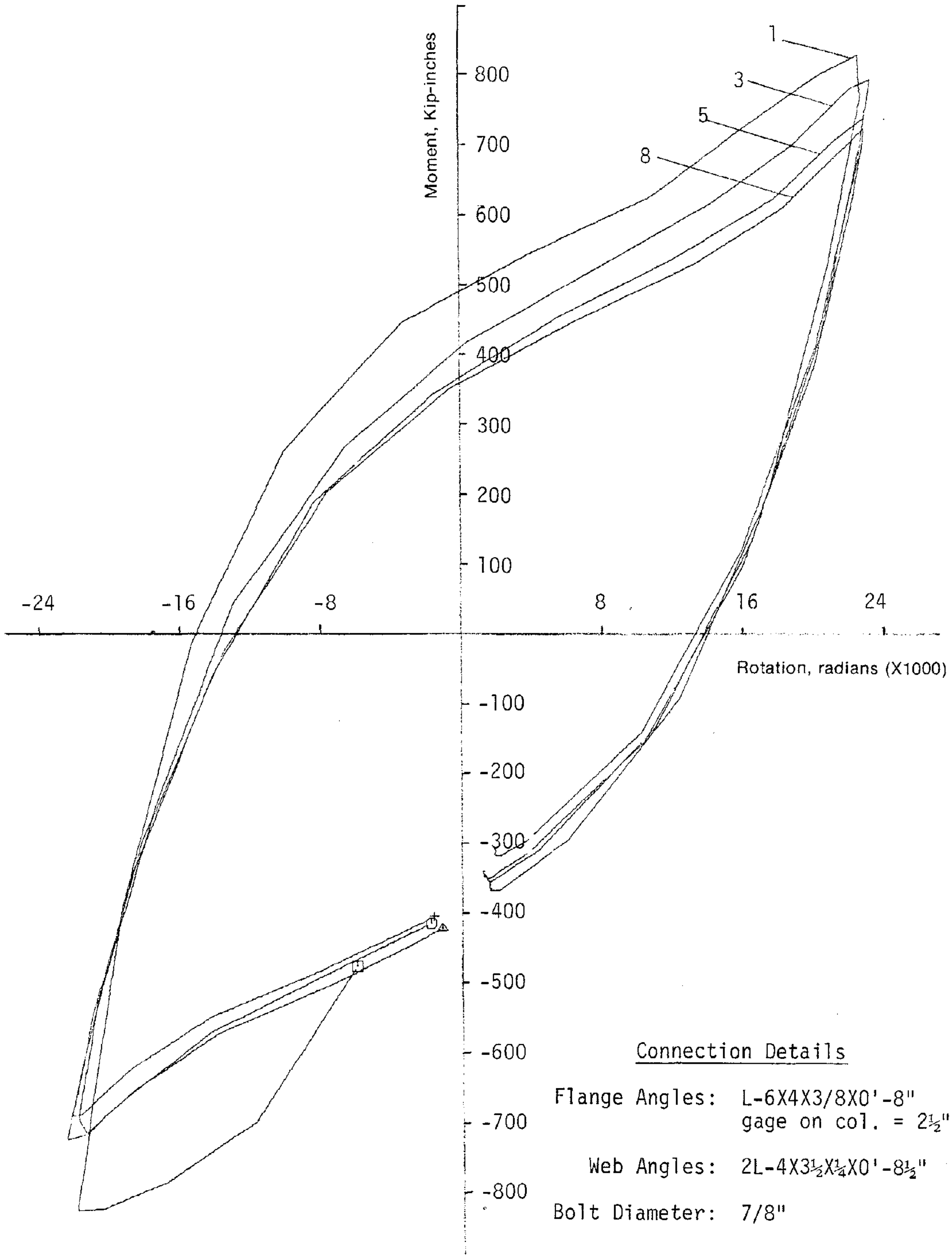


FIG. 3.30 SELECTED HYSTERESIS LOOPS FOR SPECIMEN 14F3

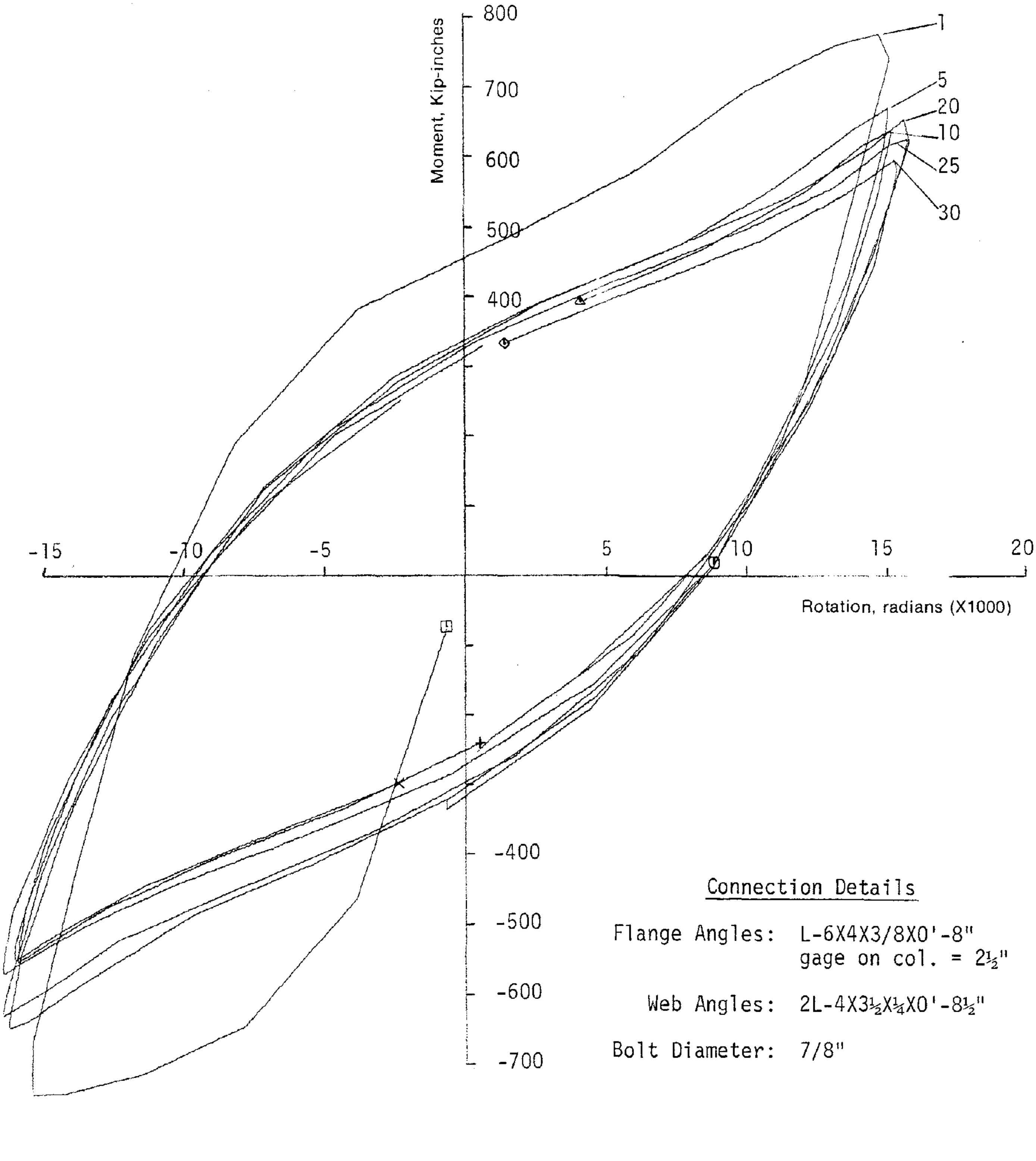


FIG. 3.31 SELECTED HYSTERESIS LOOPS FOR SPECIMEN 14F2

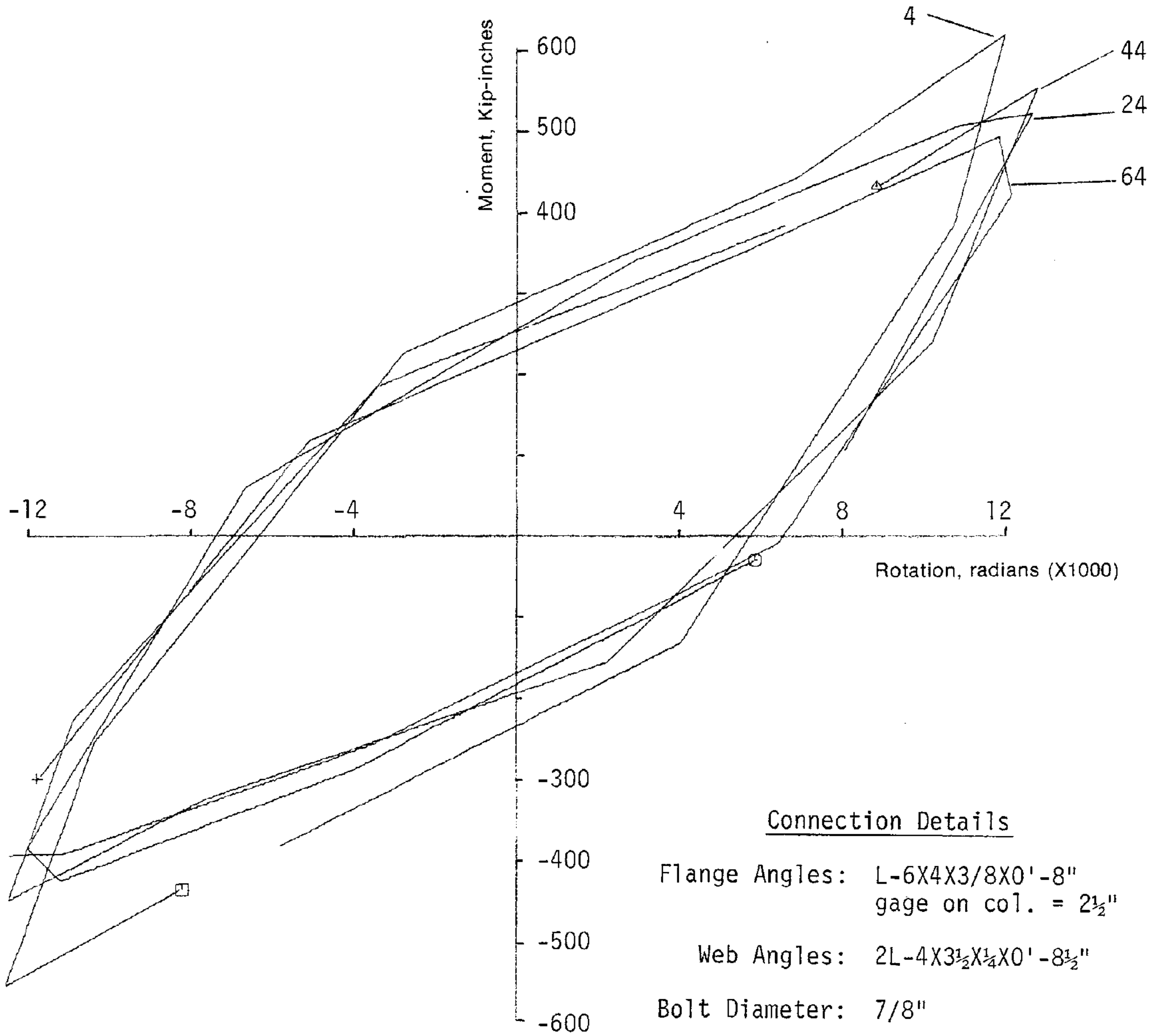


FIG. 3.32 SELECTED HYSTERESIS LOOPS FOR SPECIMEN 14F1

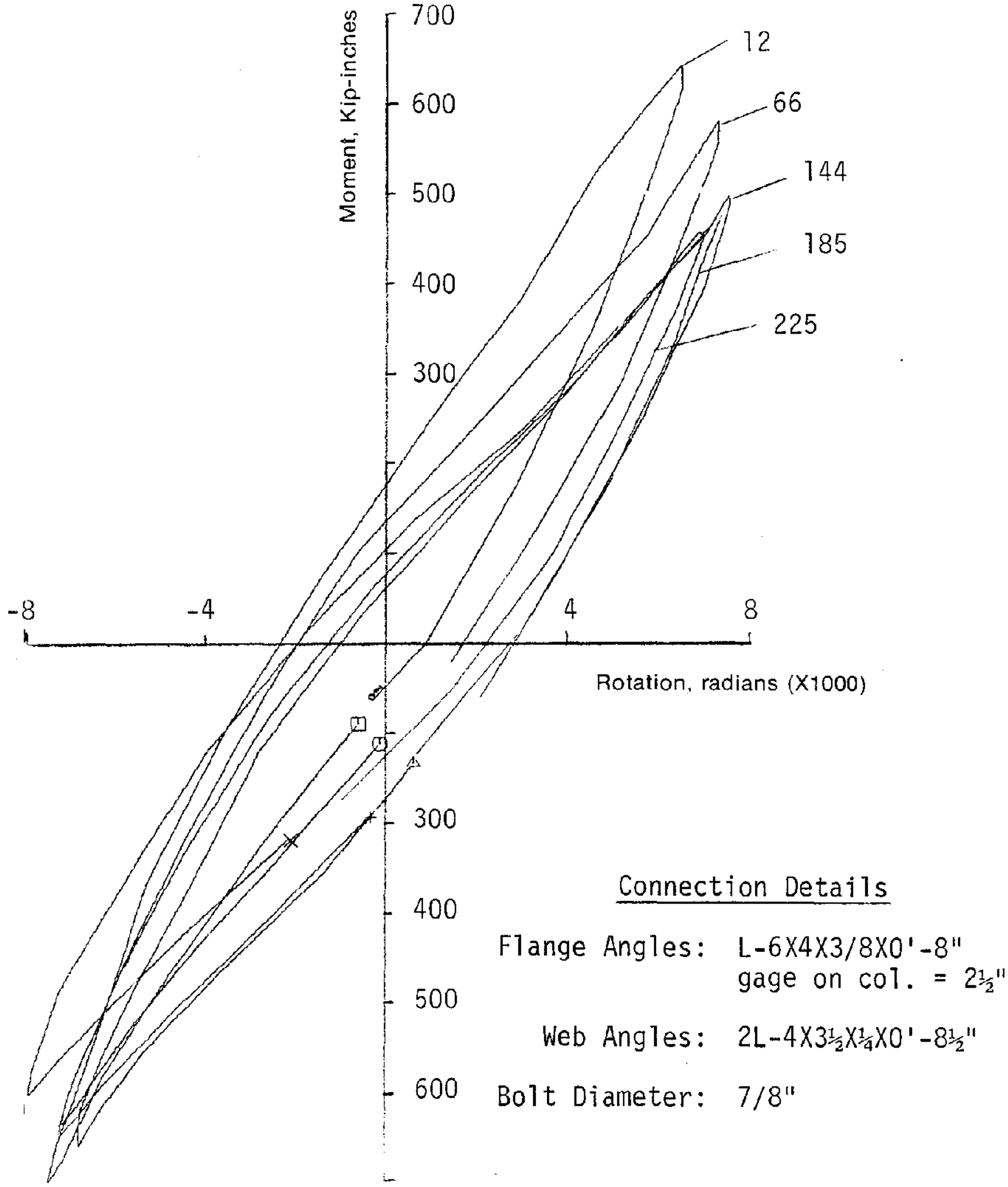


FIG. 3.33 SELECTED HYSTERESIS LOOPS FOR SPECIMEN 14F9

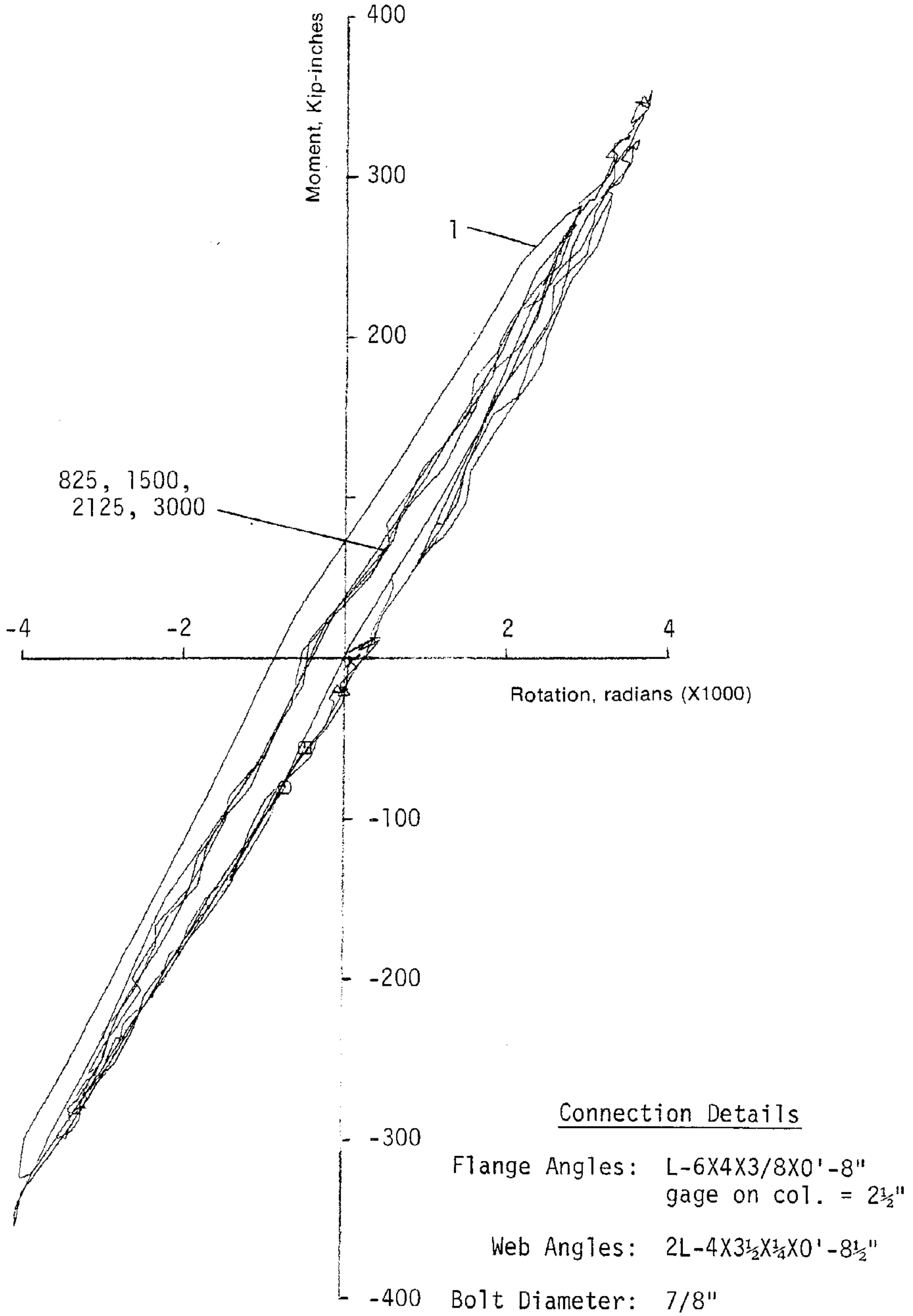


FIG. 3.34 SELECTED HYSTERESIS LOOPS FOR SPECIMEN 14F4

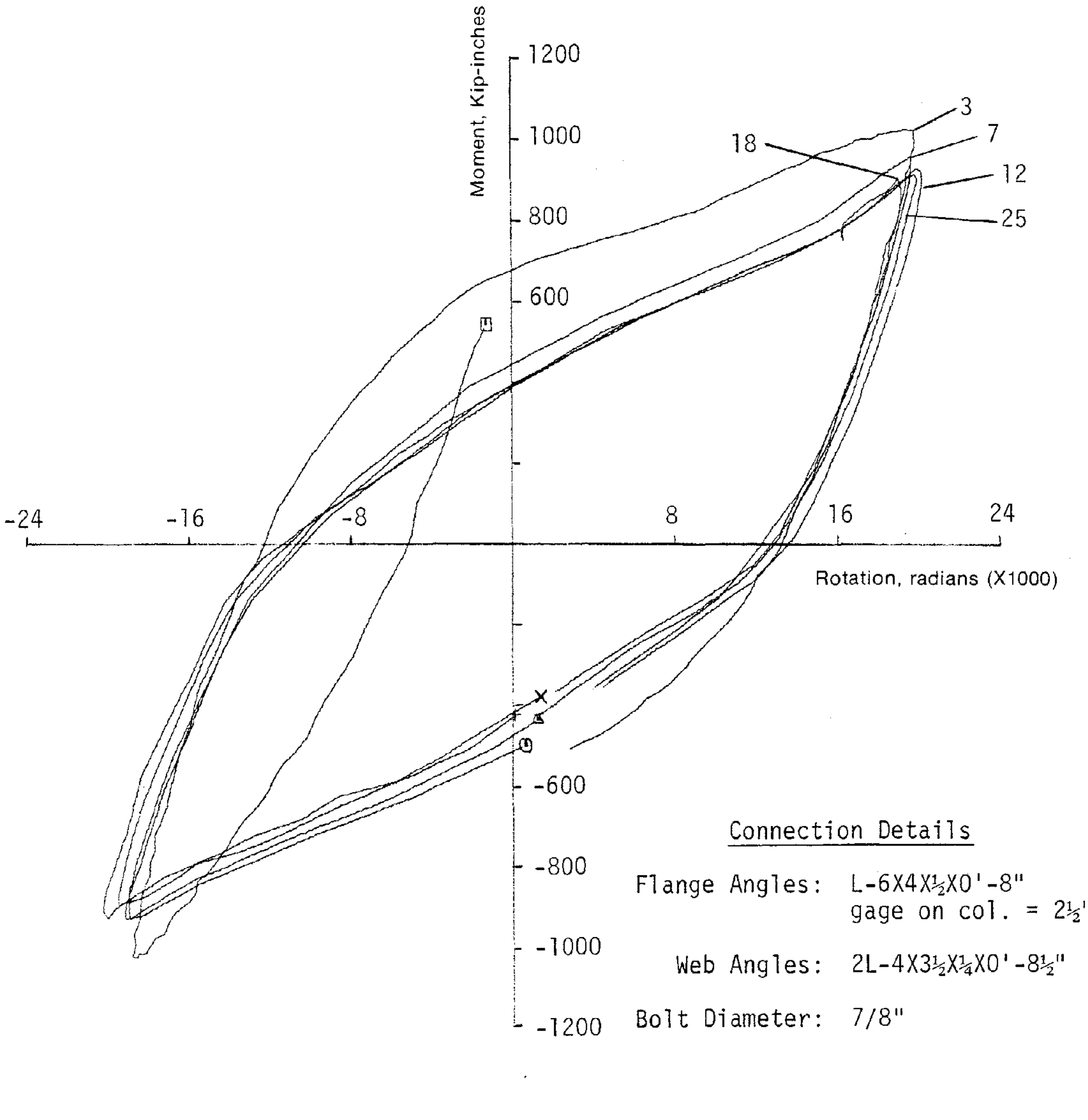


FIG. 3.35 SELECTED HYSTERESIS LOOPS FOR SPECIMEN 14F7

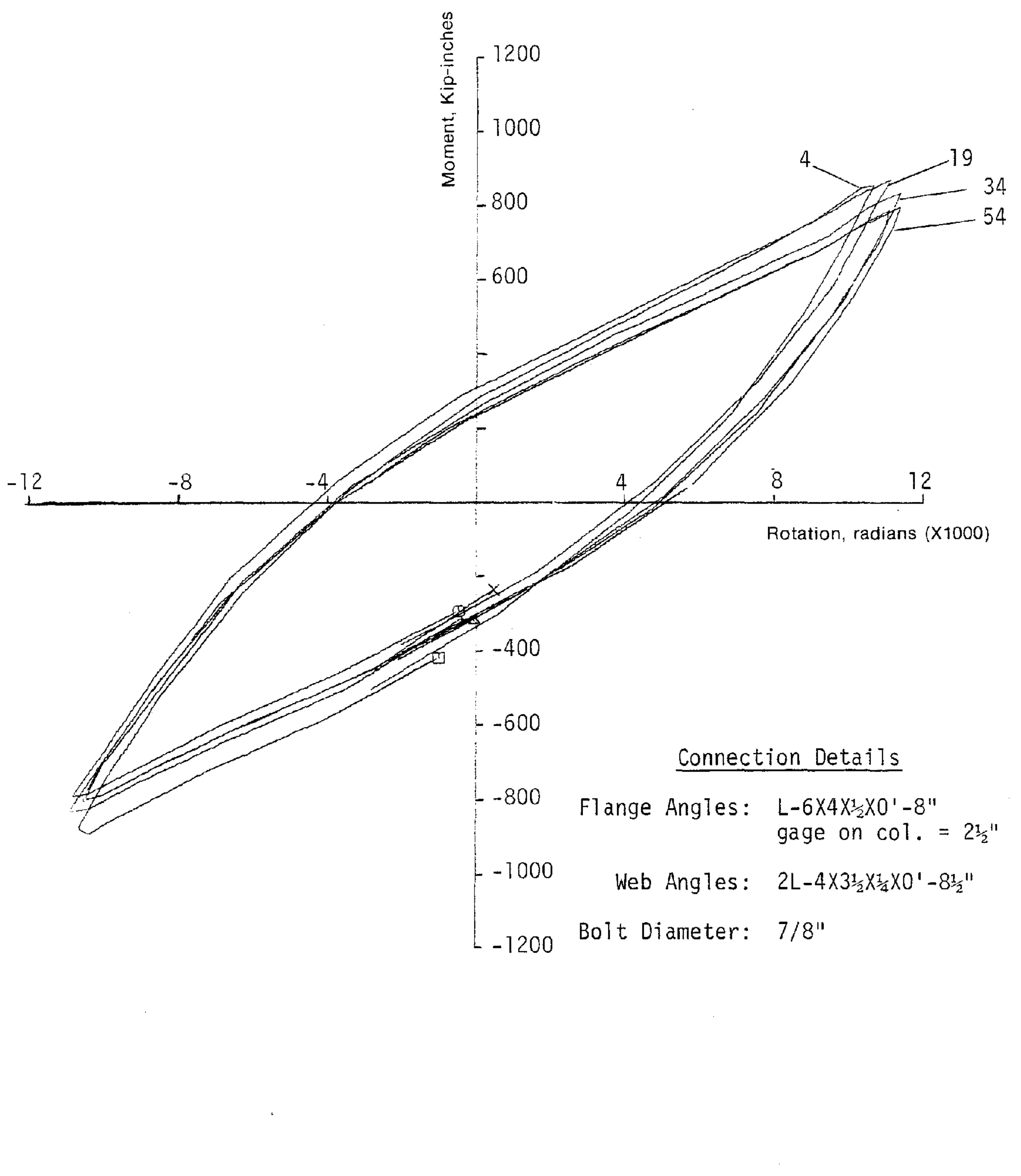


FIG. 3.36 SELECTED HYSTERESIS LOOPS FOR SPECIMEN 14F5

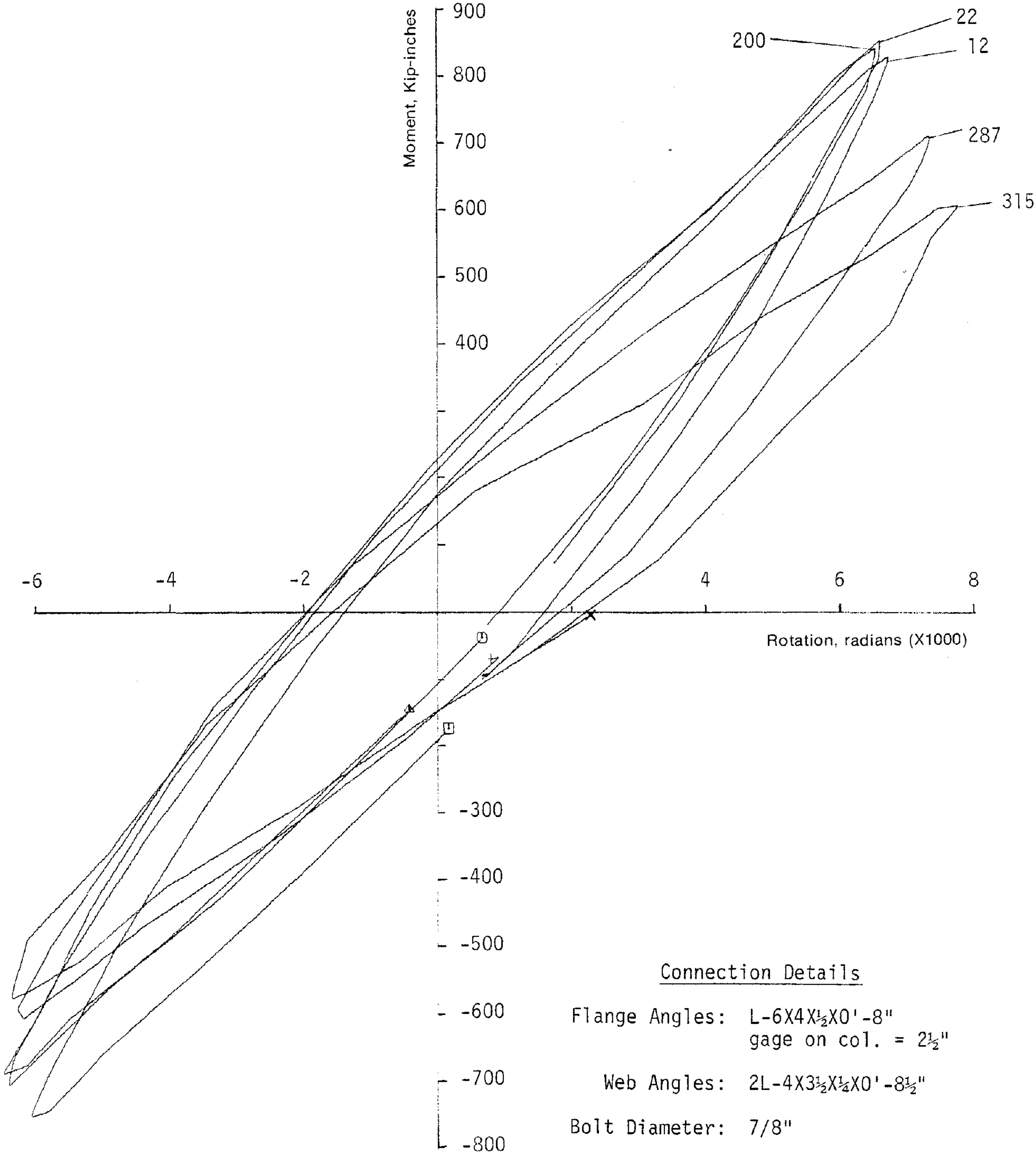


FIG. 3.37 SELECTED HYSTERESIS LOOPS FOR SPECIMEN 14F6

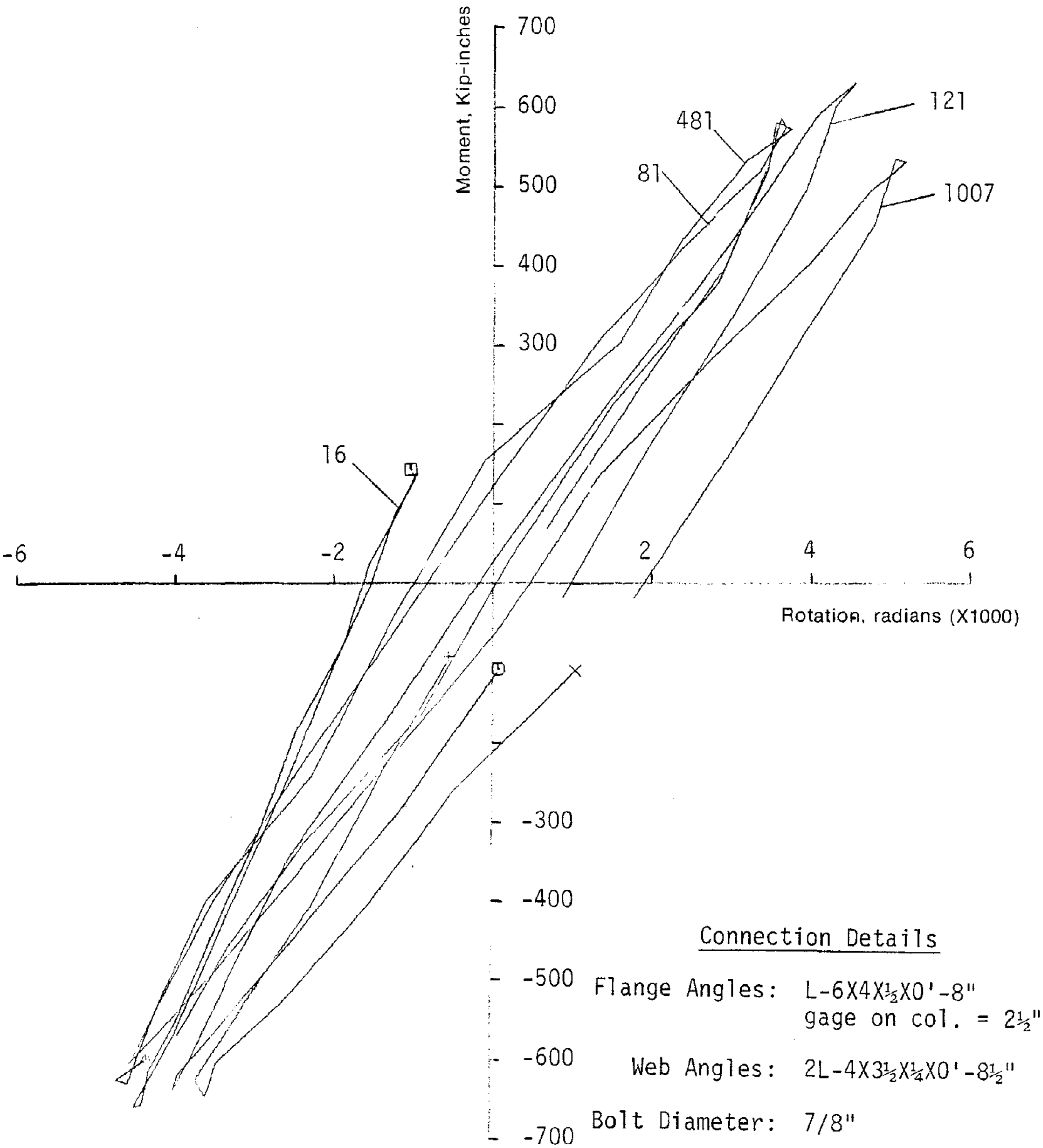


FIG. 3.38 SELECTED HYSTERESIS LOOPS FOR SPECIMEN 14F8

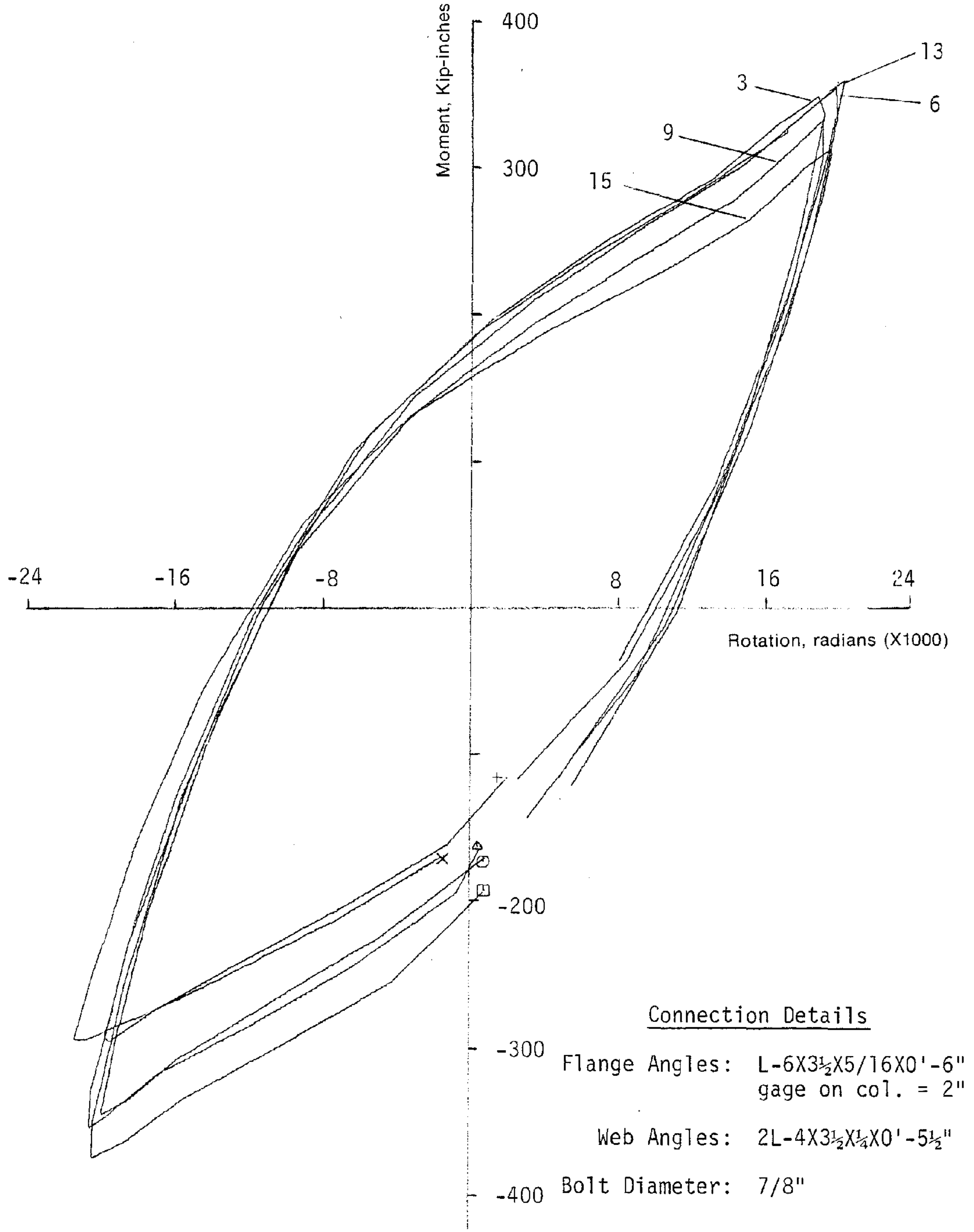


FIG. 3.39 SELECTED HYSTERESIS LOOPS FOR SPECIMEN 8F8

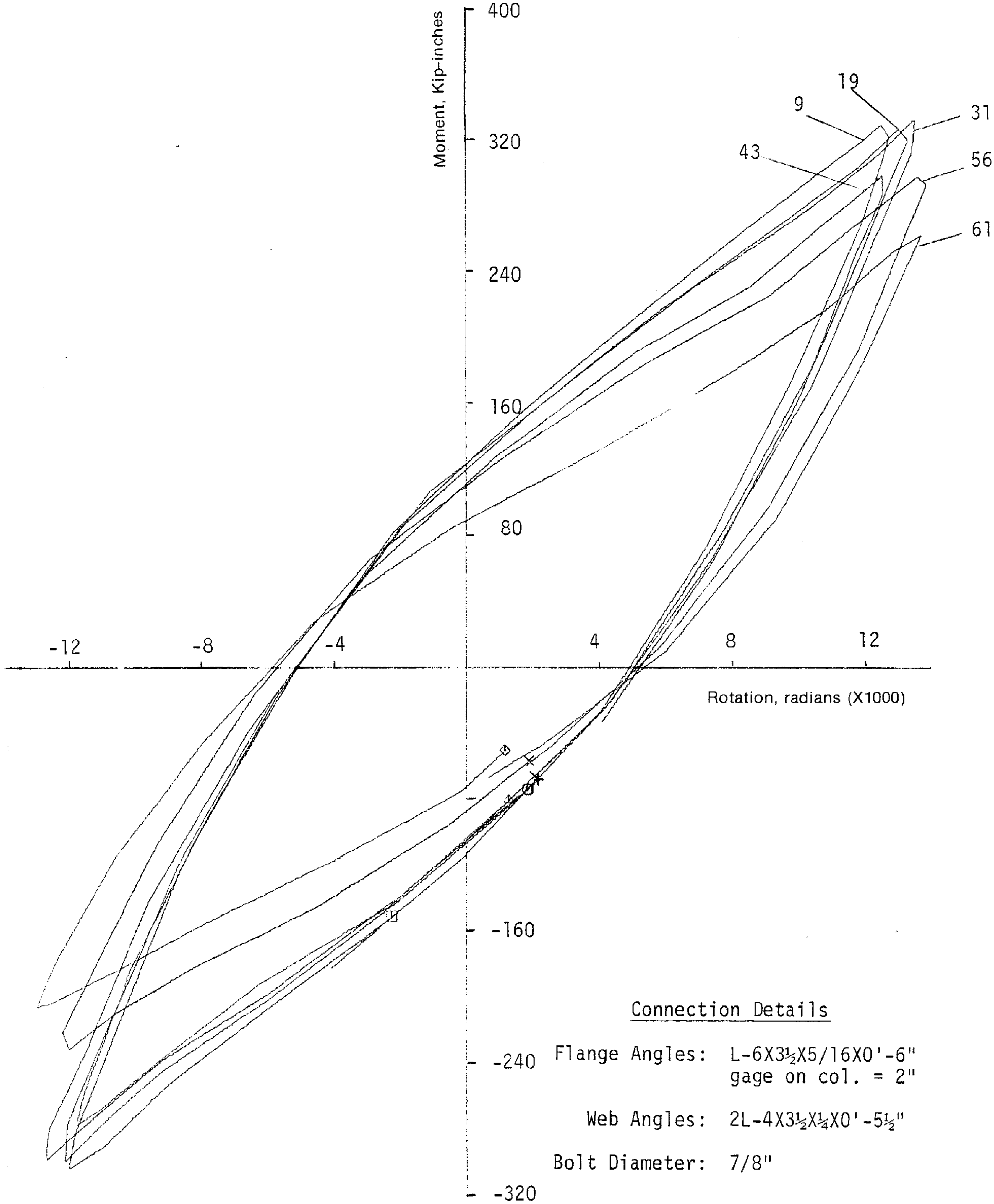


FIG. 3.40 SELECTED HYSTERESIS LOOPS FOR SPECIMEN 8F7

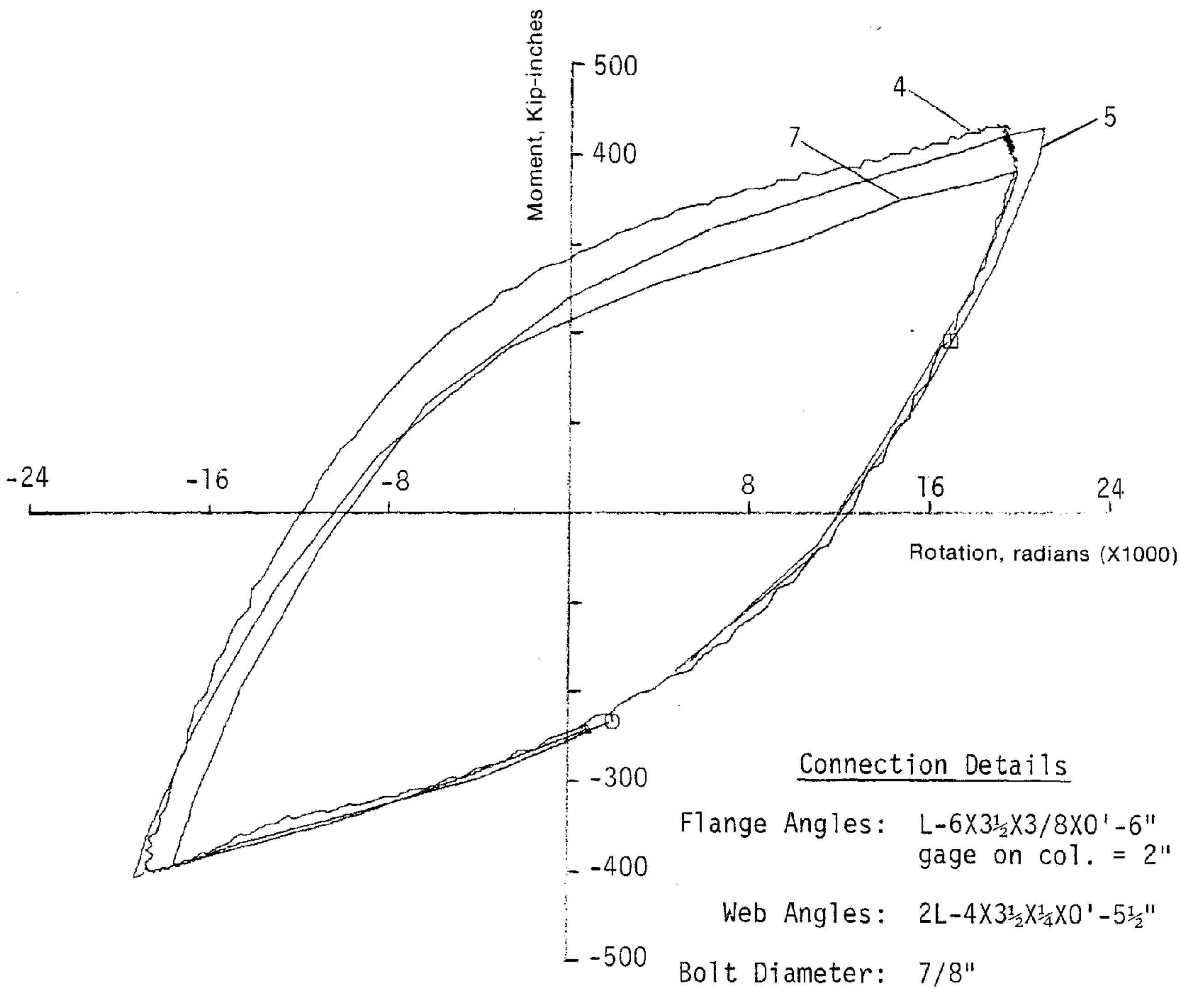


FIG. 3.41 SELECTED HYSTERESIS LOOPS FOR SPECIMEN 8F1

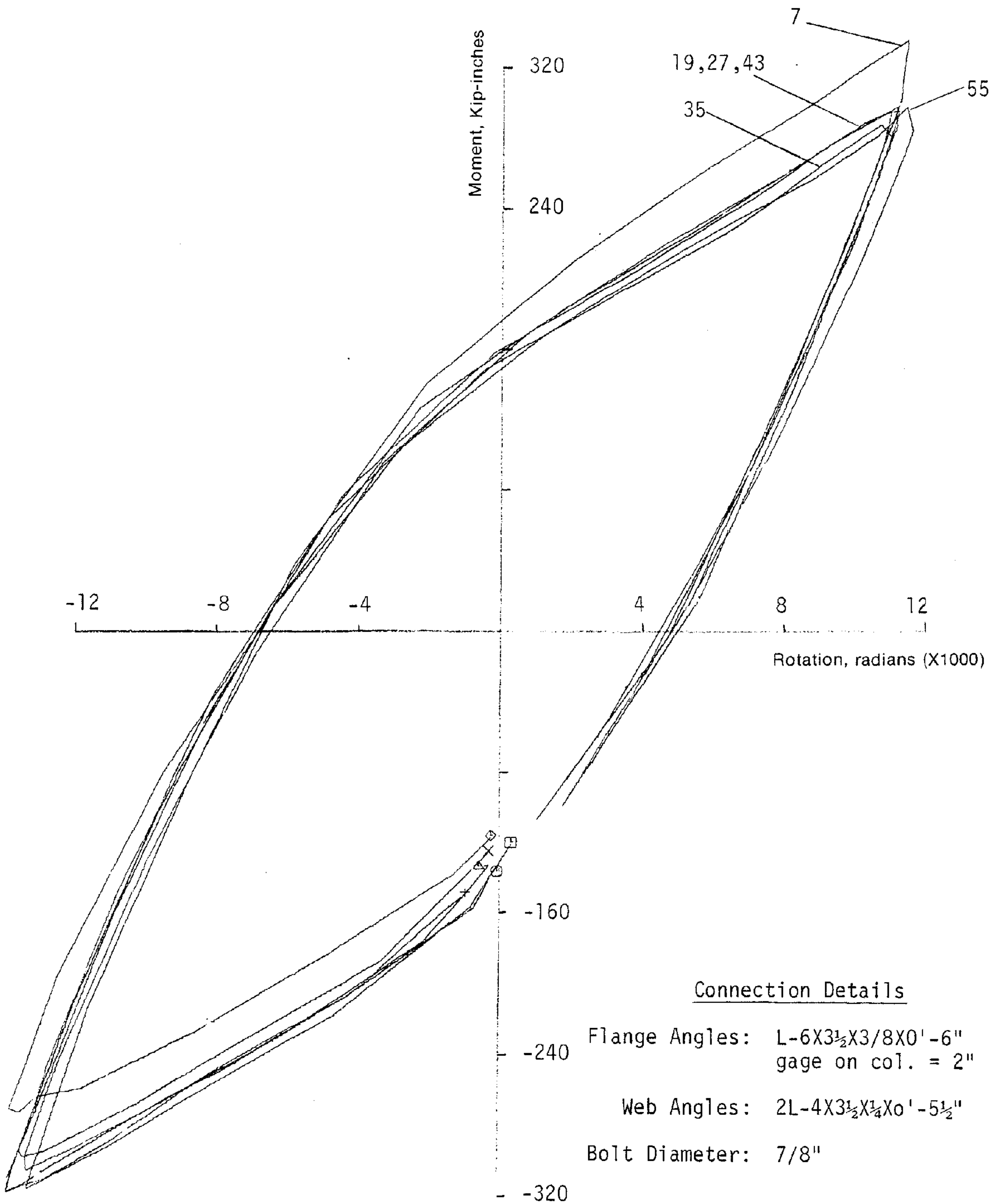


FIG. 3.42 SELECTED HYSTERESIS LOOPS FOR SPECIMEN 8F4

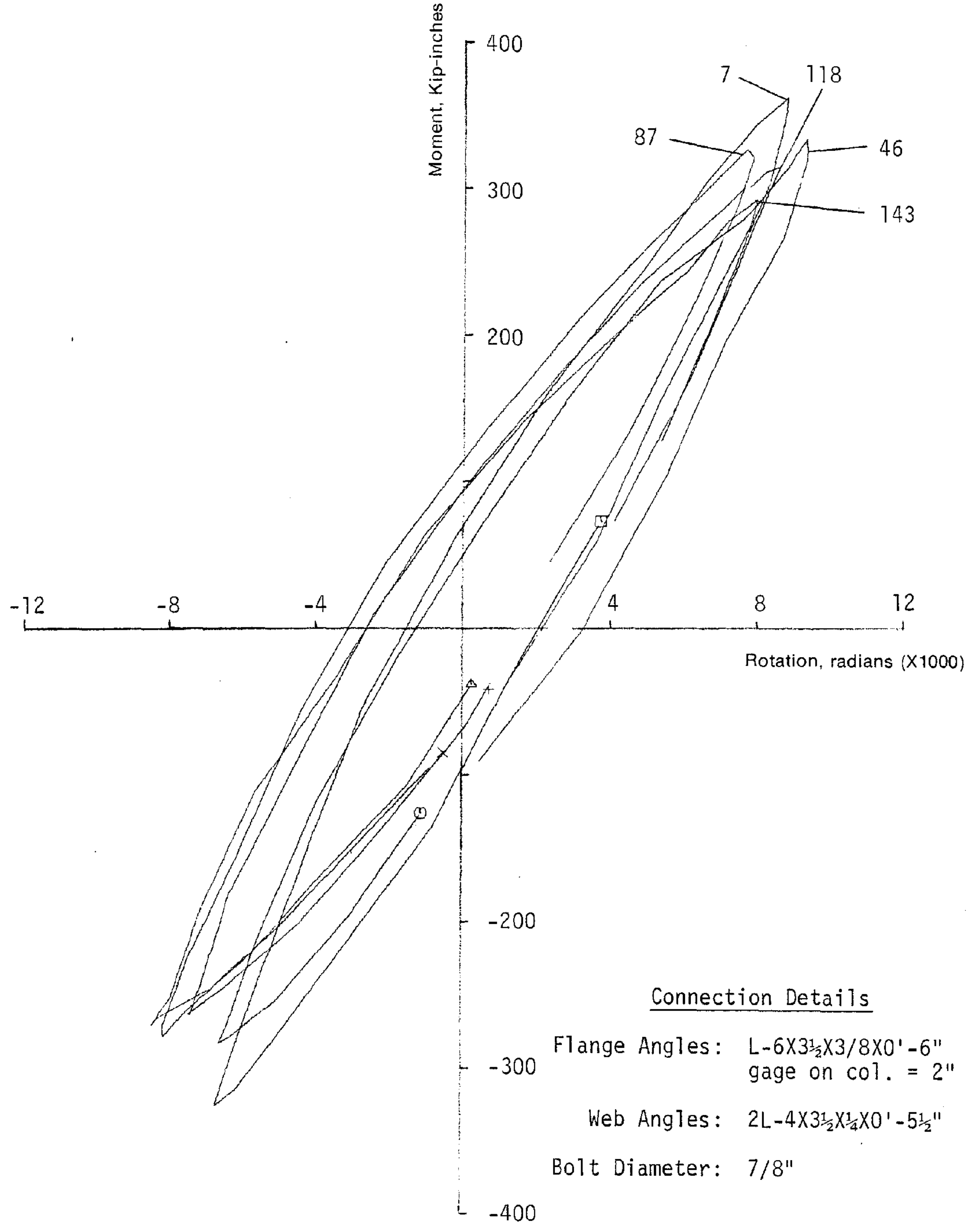


FIG. 3.43 SELECTED HYSTERESIS LOOPS FOR SPECIMEN 8F3

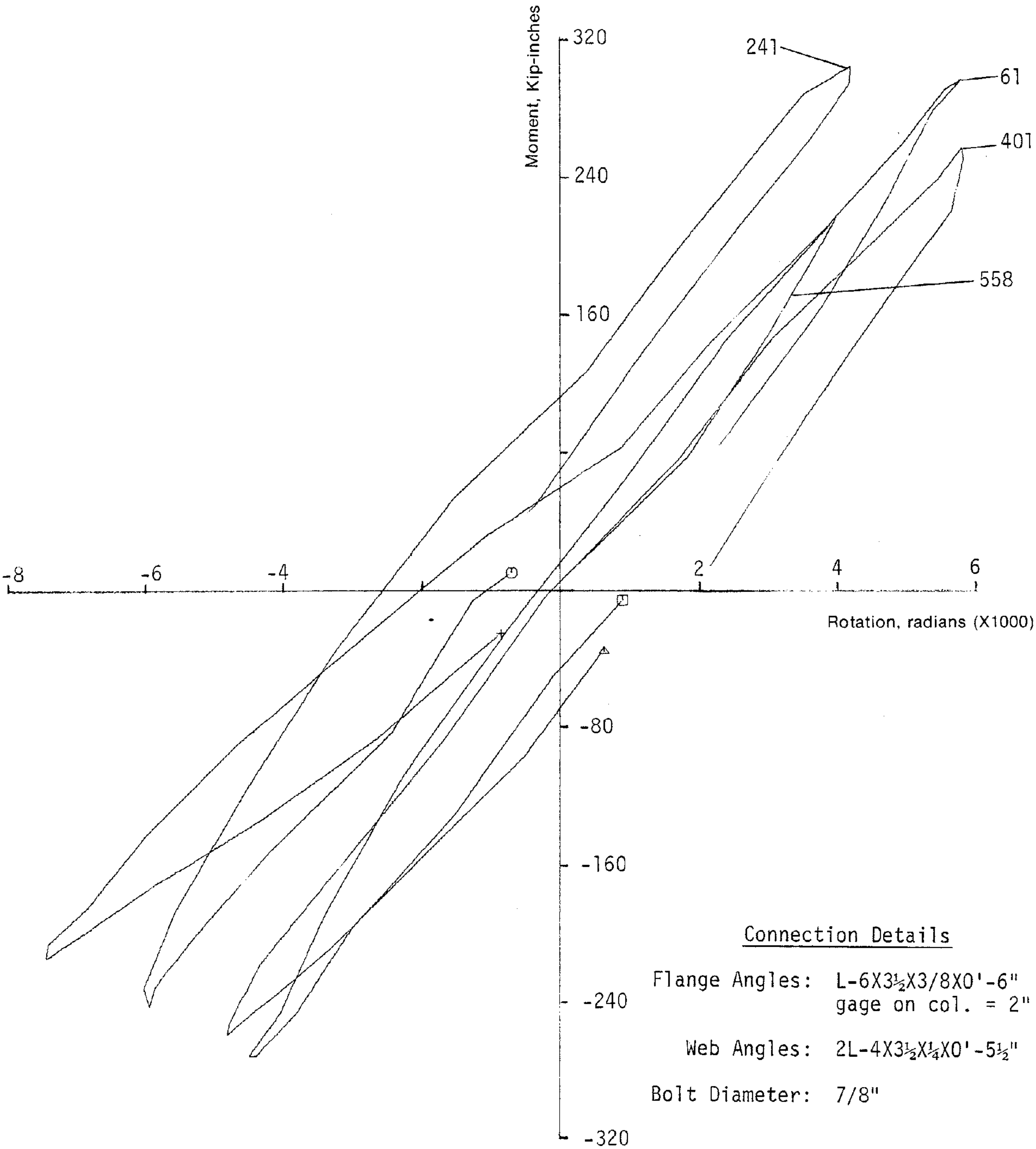


<u>Connection Details</u>

Flange Angles: L-6X3½X3/8X0'-6"
gage on col. = 2"

Web Angles: 2L-4X3½X¼X0'-5½"

Bolt Diameter: 7/8"

FIG. 3.44 SELECTED HYSTERESIS LOOPS FOR SPECIMEN 8F2

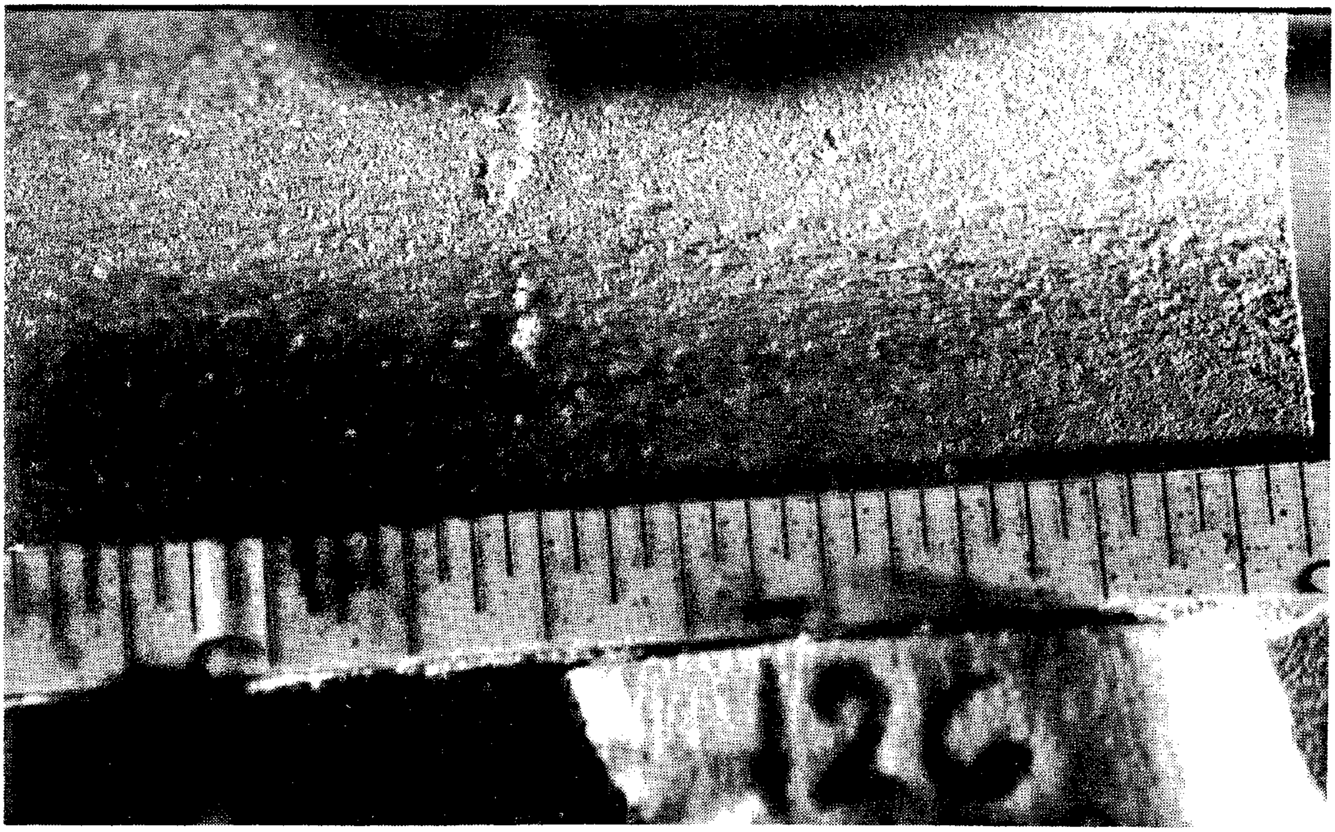


a. CRACK PATTERN AT 126 CYCLES

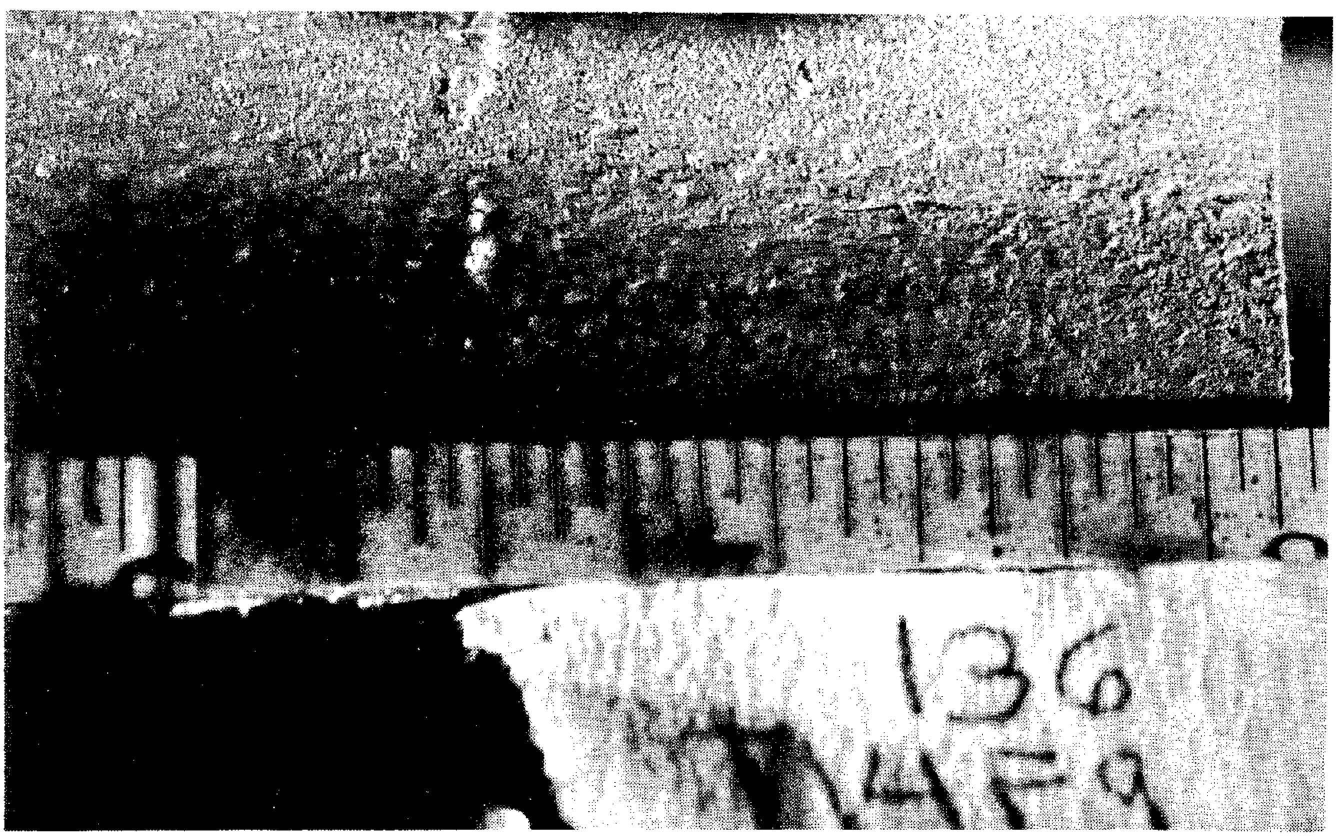


b. CRACK PATTERN AT 136 CYCLES

FIG. 3.45 FATIGUE CRACK PATTERN FOR SPECIMEN 14F9

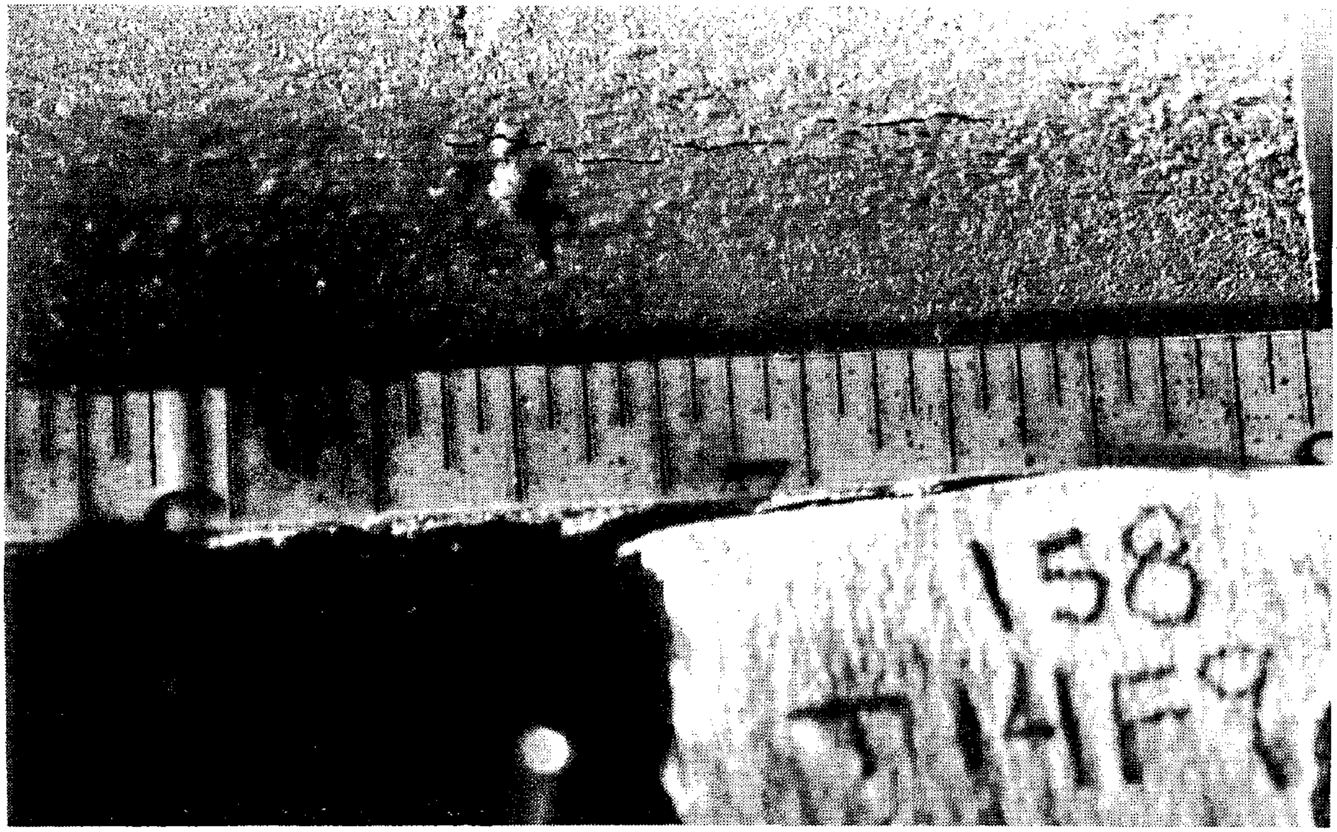


c. CRACK PATTERN AT 158 CYCLES

d. CRACK PATTERN AT 214 CYCLES

FIG. 3.45 FATIGUE CRACK PATTERN FOR SPECIMEN 14F9

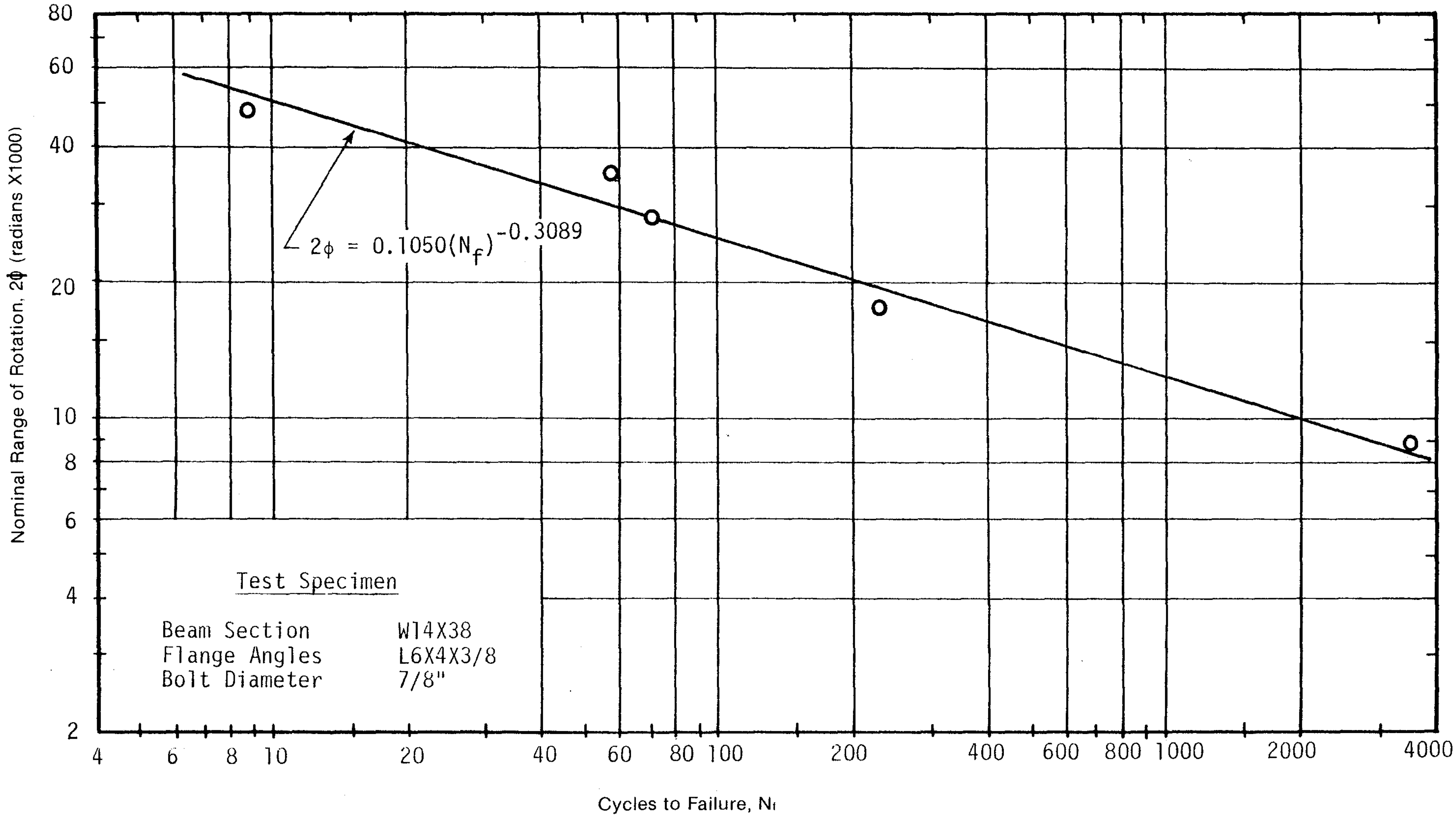


FIG. 3.46 CONSTANT AMPLITUDE CYCLIC TEST BEHAVIOR — W14X38 BEAM CONNECTIONS (FLANGE ANGLE THICKNESS = 3/8")

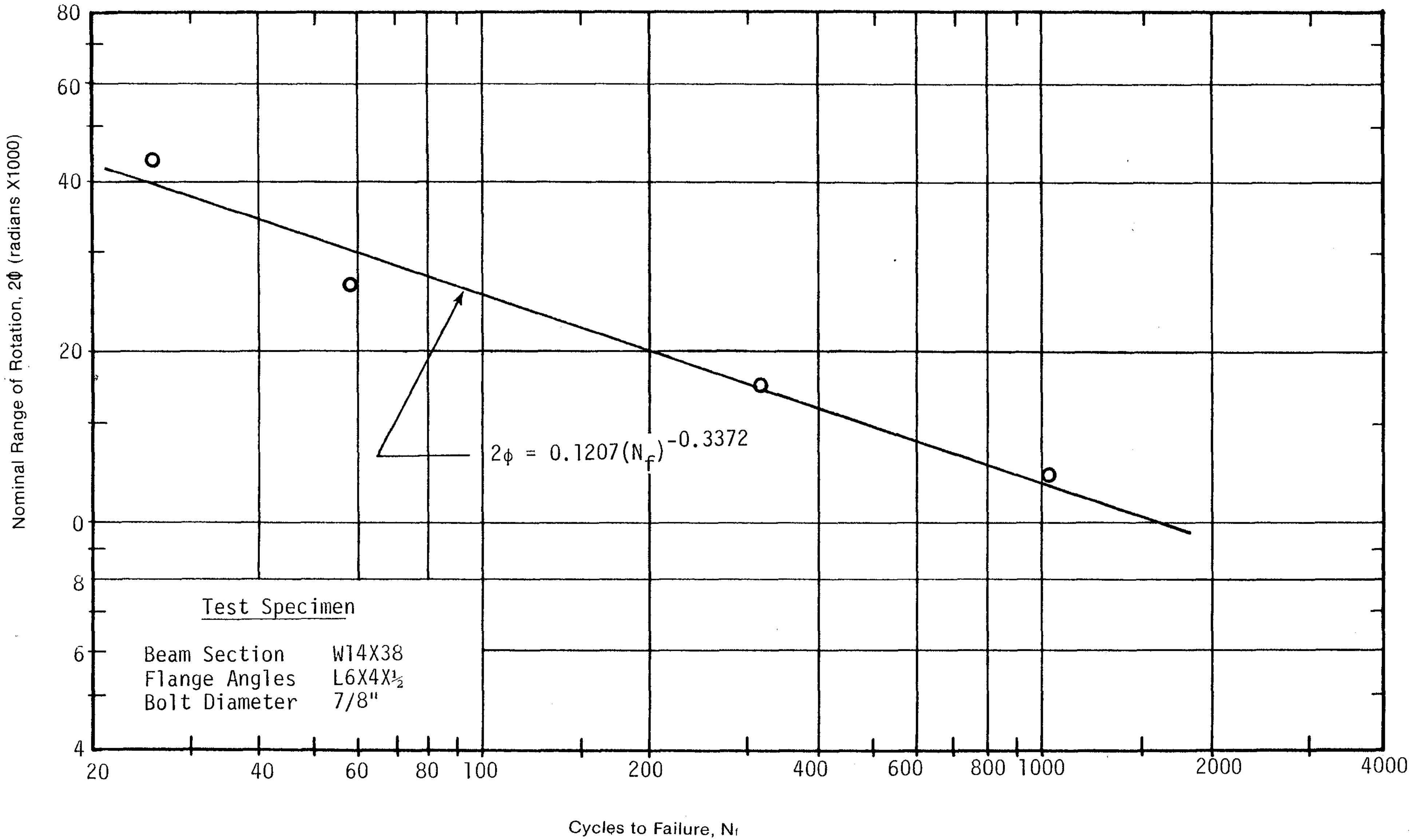


FIG. 3.47 CONSTANT AMPLITUDE CYCLIC TEST BEHAVIOR —W14X38 BEAM CONNECTIONS (FLANGE ANGLE THICKNESS = ½")

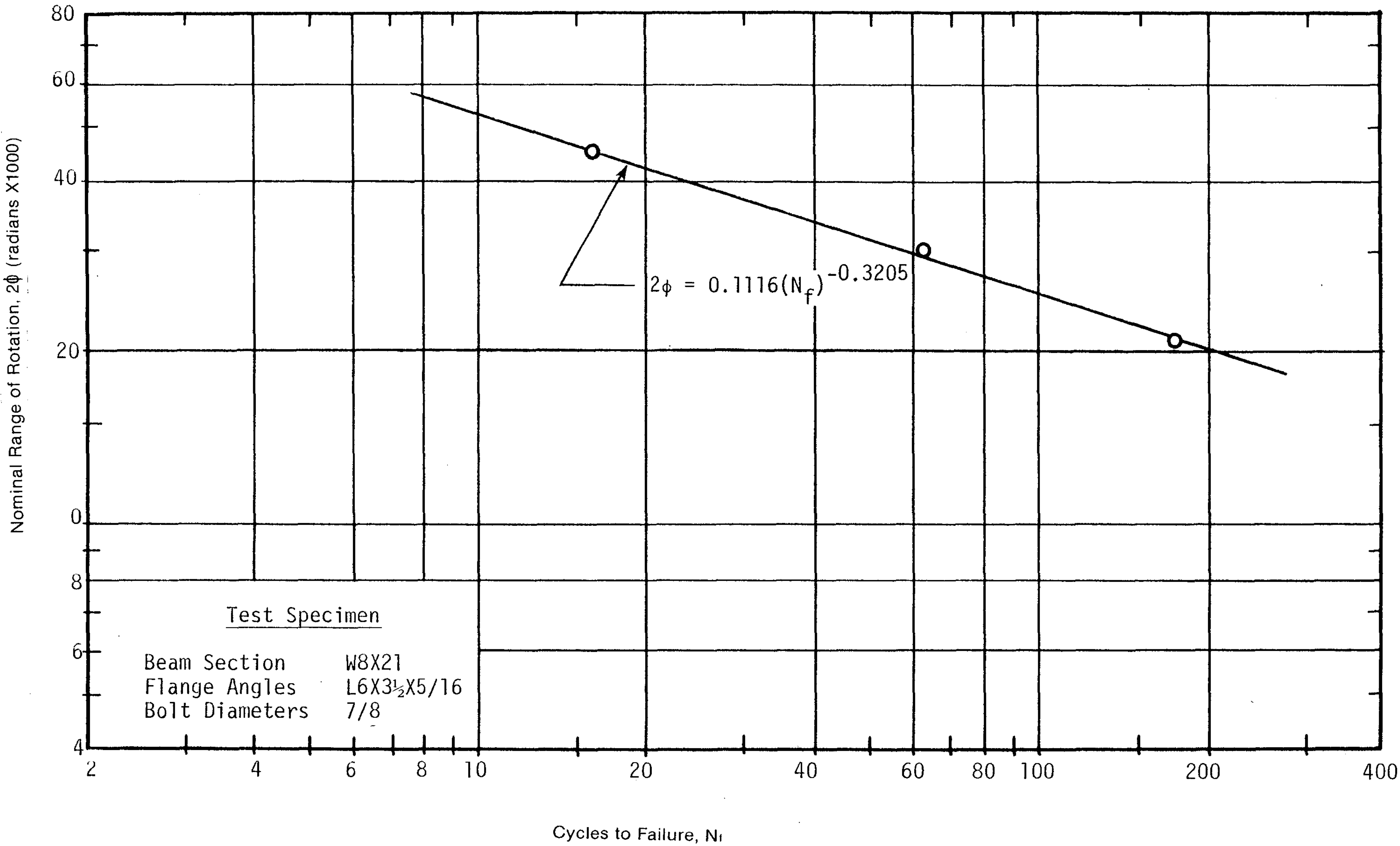


FIG. 3.48 CONSTANT AMPLITUDE CYCLIC TEST BEHAVIOR — W8X21 BEAM CONNECTIONS (FLANGE ANGLE THICKNESS = 5/16")

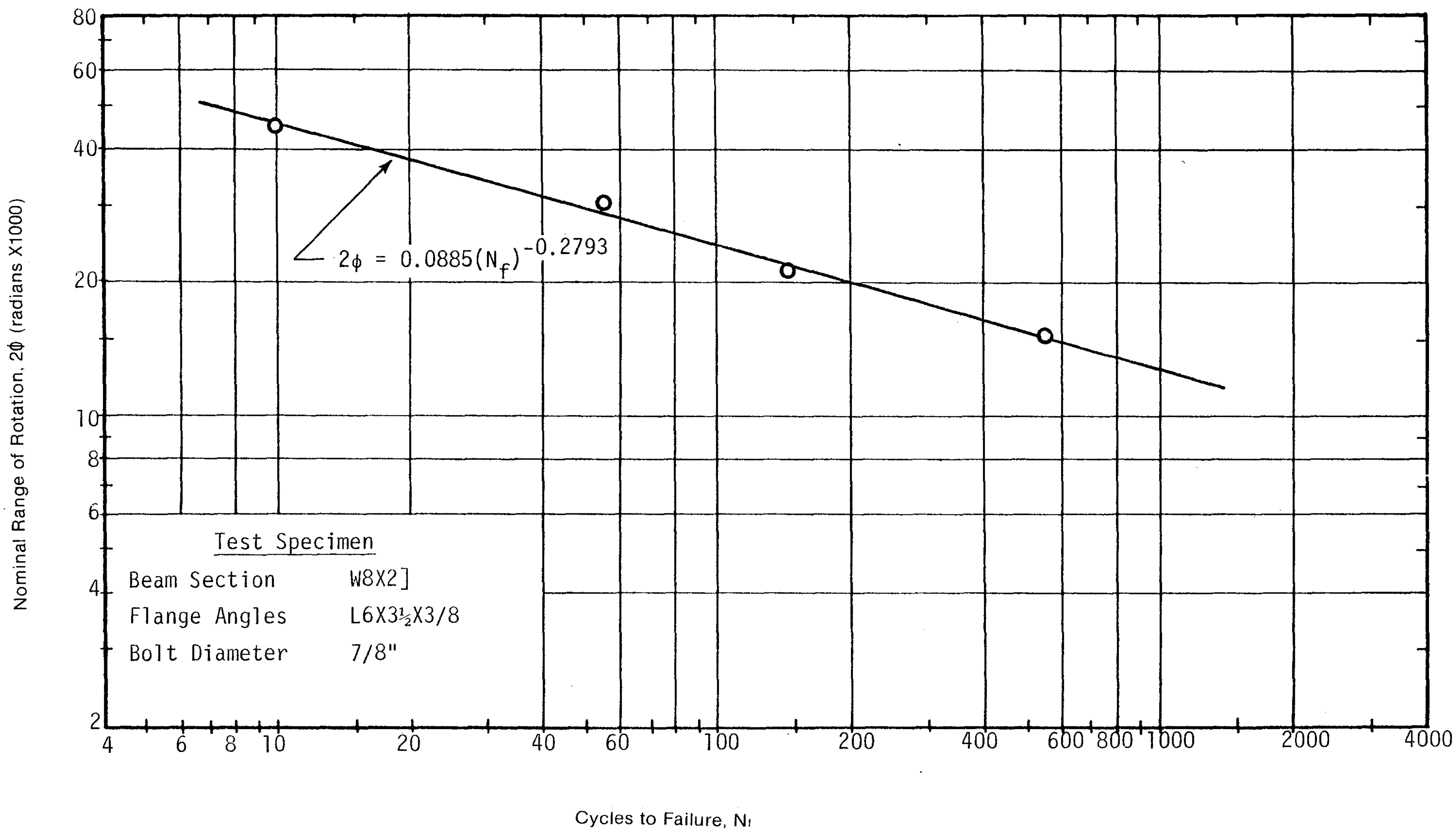


FIG. 3.49 CONSTANT AMPLITUDE CYCLIC TEST BEHAVIOR — W8X21 BEAM CONNECTIONS (FLANGE ANGLE THICKNESS = 3/8")

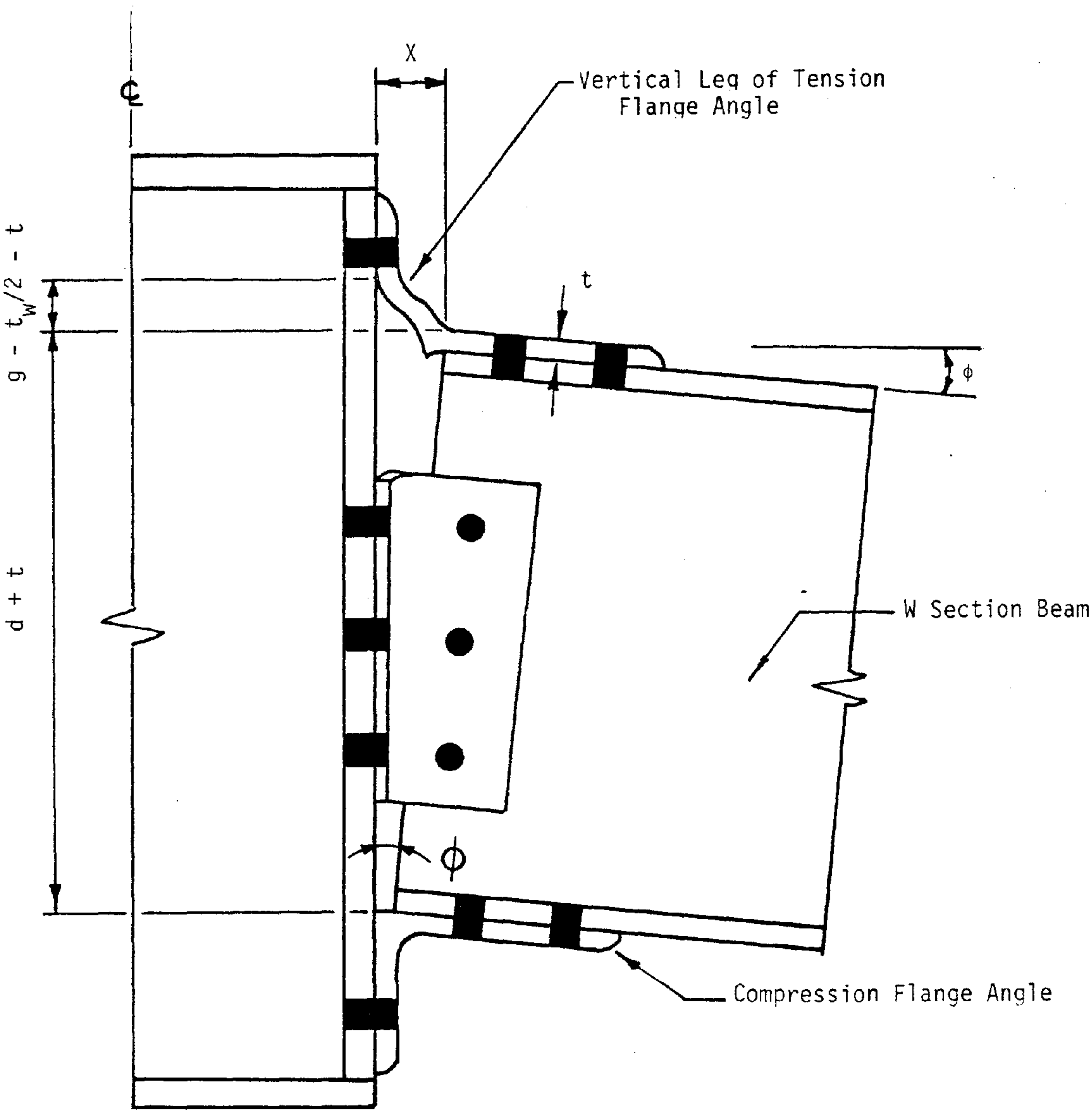


FIG. 4.1a DEFLECTED CONFIGURATION FOR FLANGE ANGLE MODEL

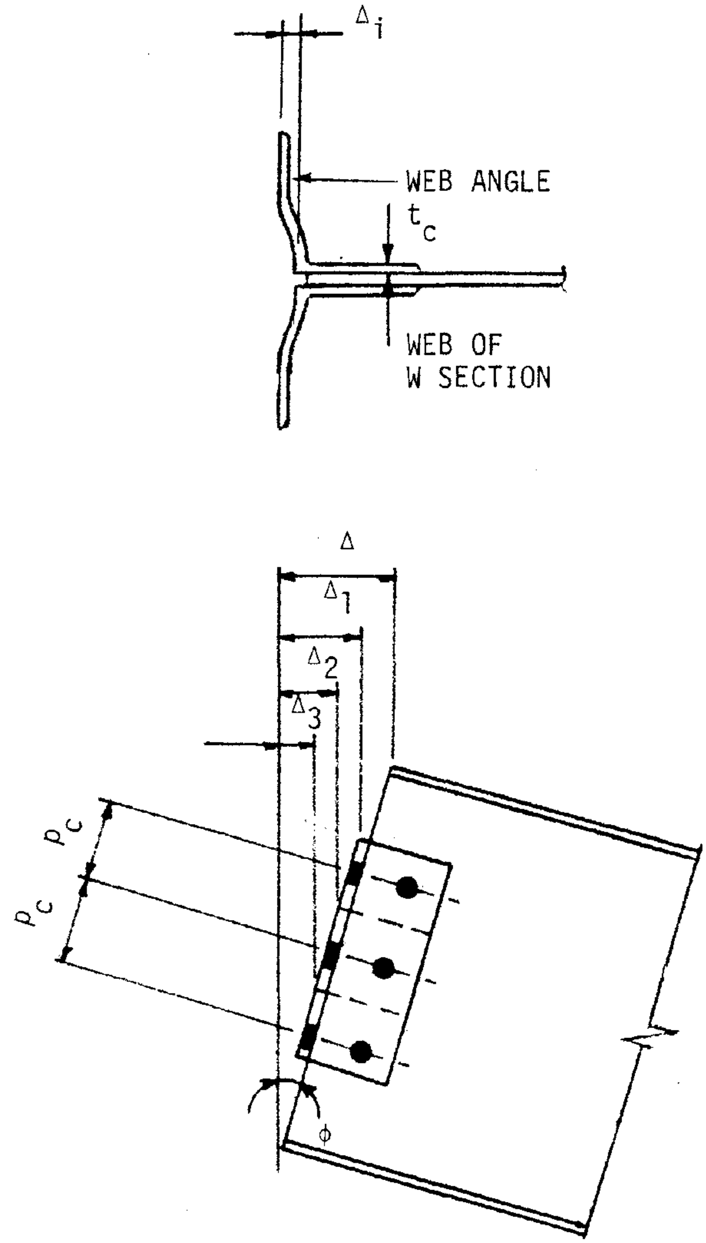


FIG. 4.1b DEFLECTED CONFIGURATION FOR WEB ANGLE MODEL

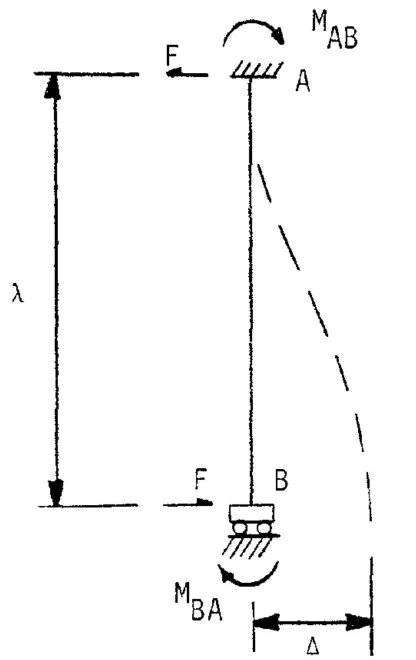


FIG. 4.2a TERMINOLOGY FOR IDEALIZED BEAM MODEL OF FLANGE ANGLE

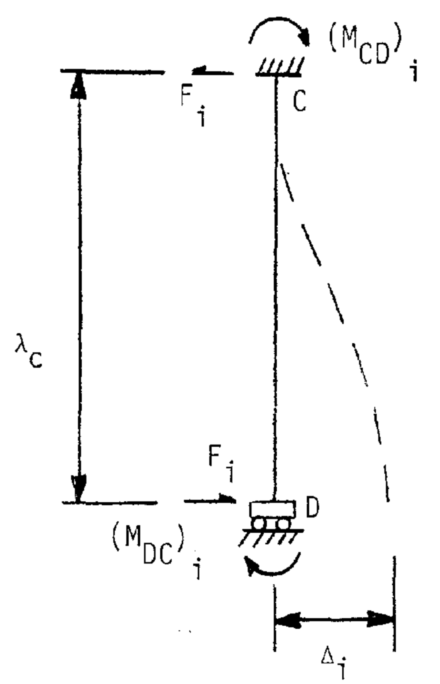


FIG. 4.2b TERMINOLOGY FOR IDEALIZED BEAM MODEL OF WEB ANGLE

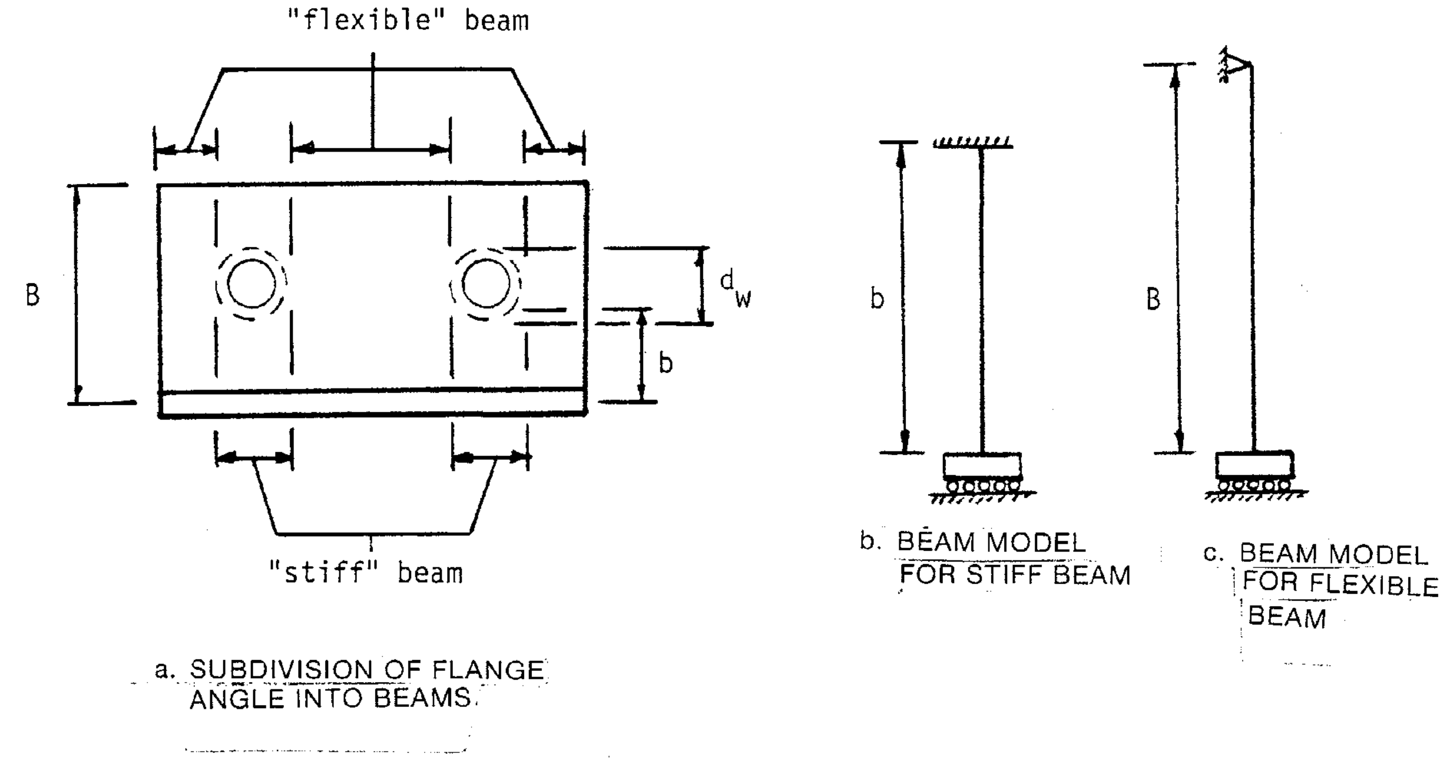


FIG. 4.3a SEGMENTAL BEAM MODEL FOR FLANGE ANGLE

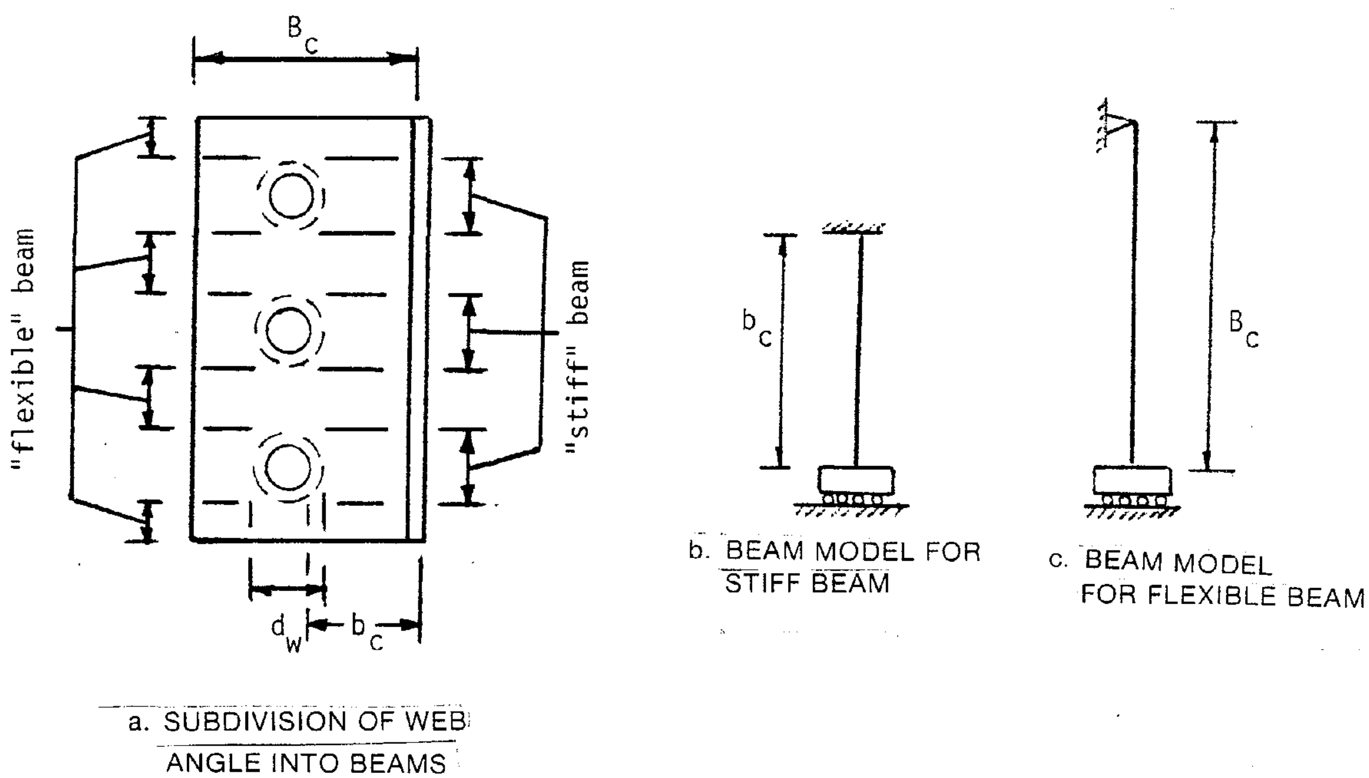


FIG. 4.3b SEGMENTAL BEAM MODEL FOR WEB ANGLE

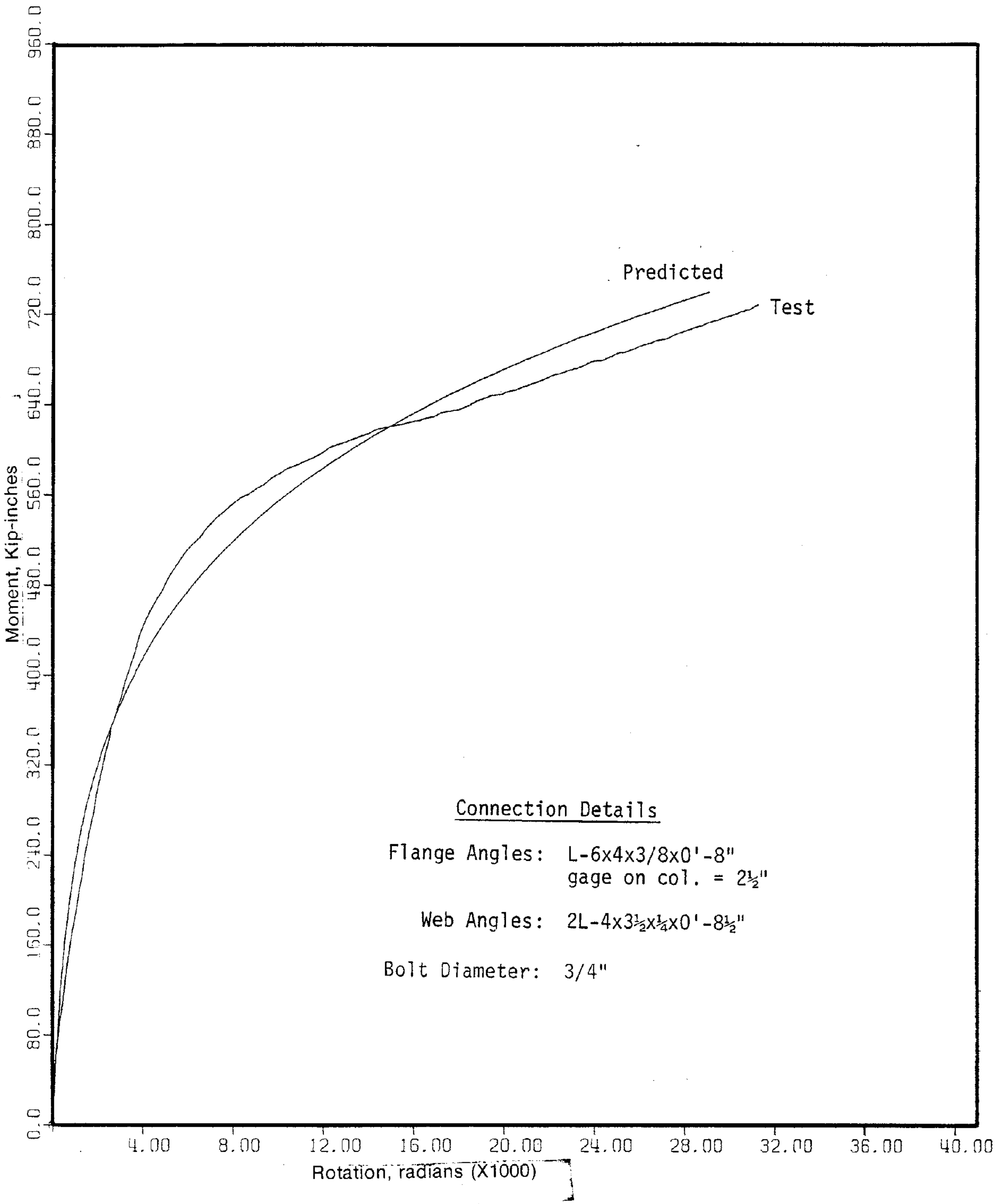


FIG. 4.4 COMPARISON OF PREDICTED MOMENT-ROTATION CURVE WITH TEST RESULTS FOR SPECIMEN 14S1

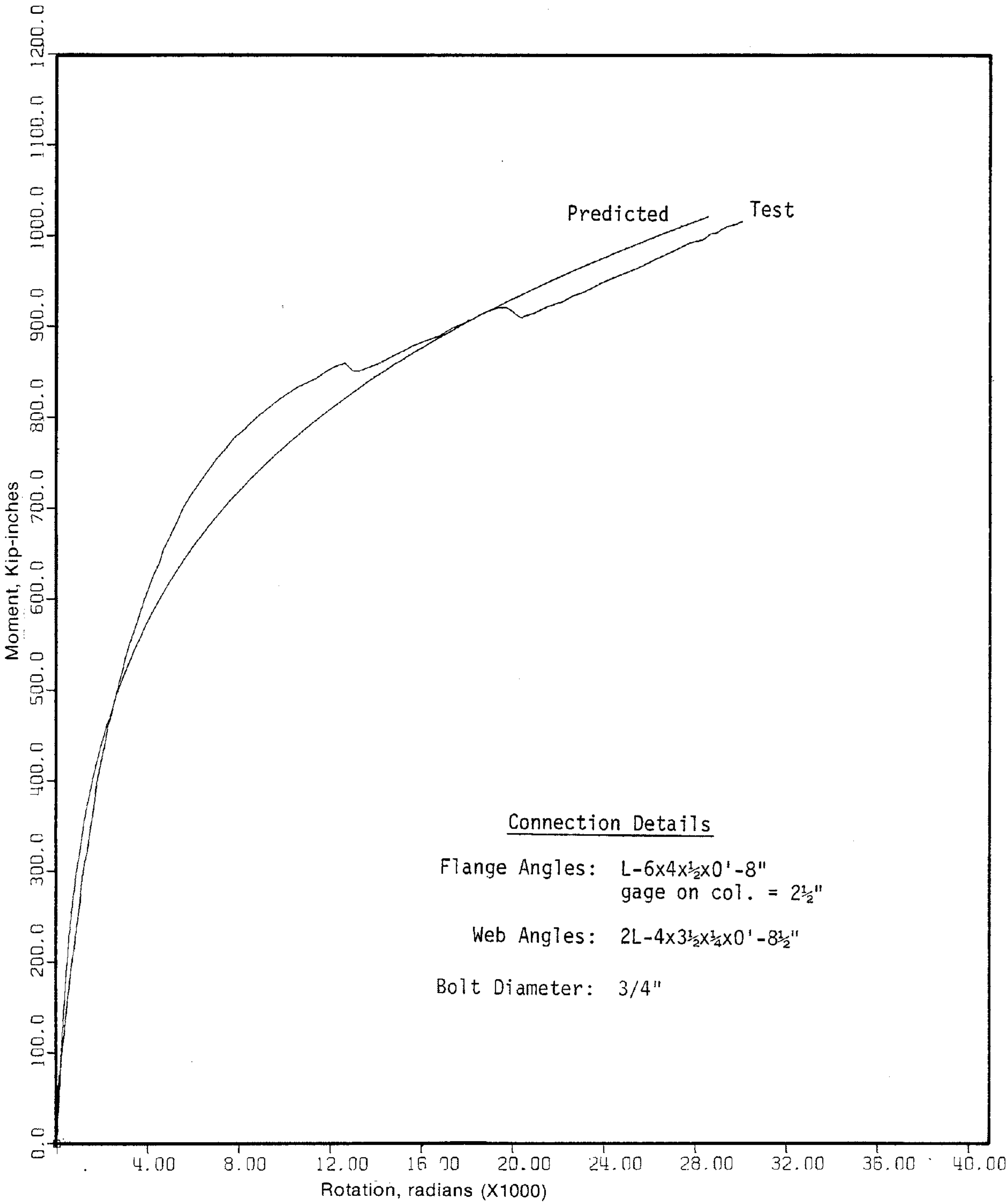


FIG. 4.5 COMPARISON OF PREDICTED MOMENT-ROTATION CURVE WITH TEST RESULTS FOR SPECIMEN 14S2

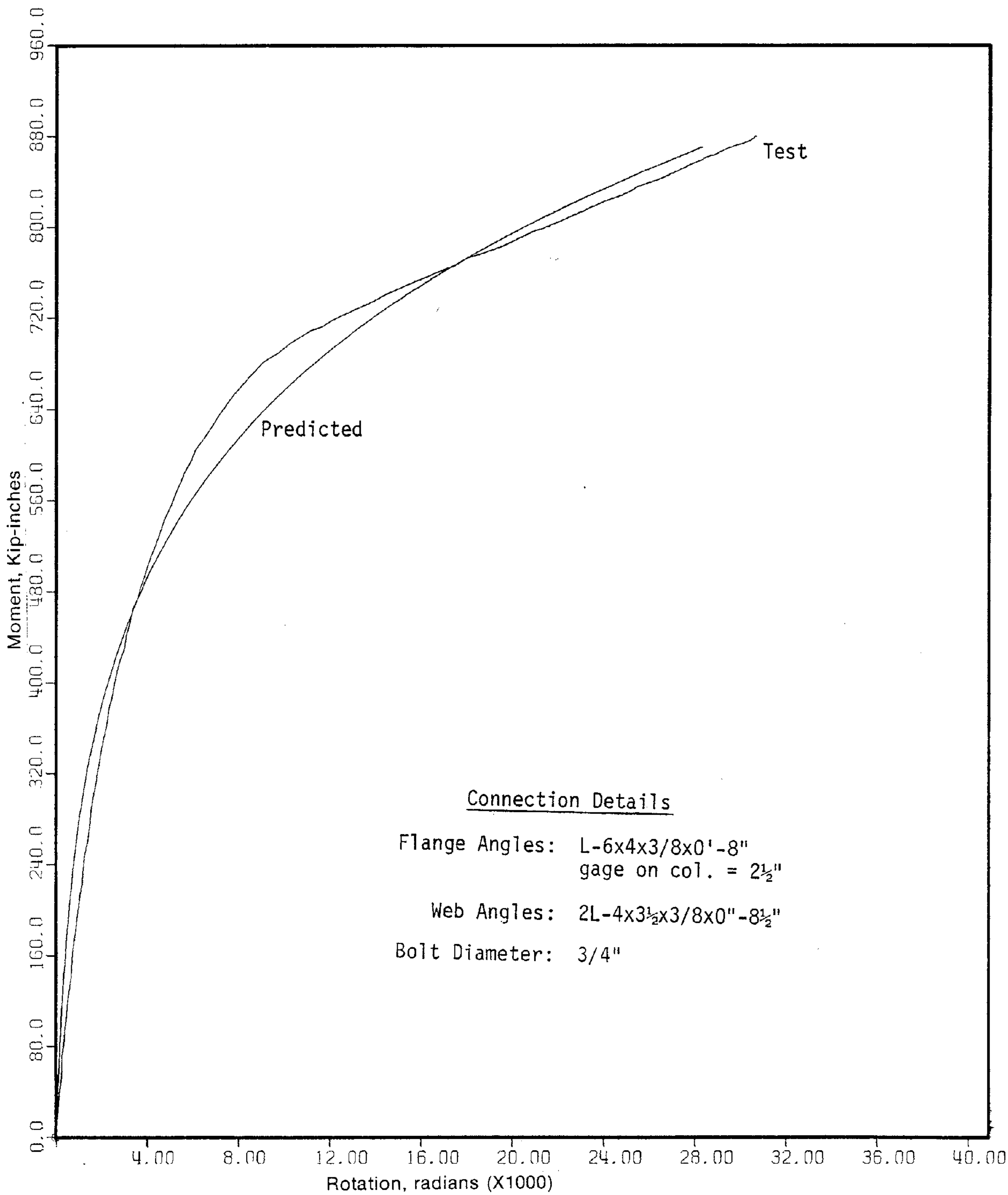


FIG. 4.6 COMPARISON OF PREDICTED MOMENT-ROTATION CURVE WITH TEST RESULTS FOR SPECIMEN 14S4

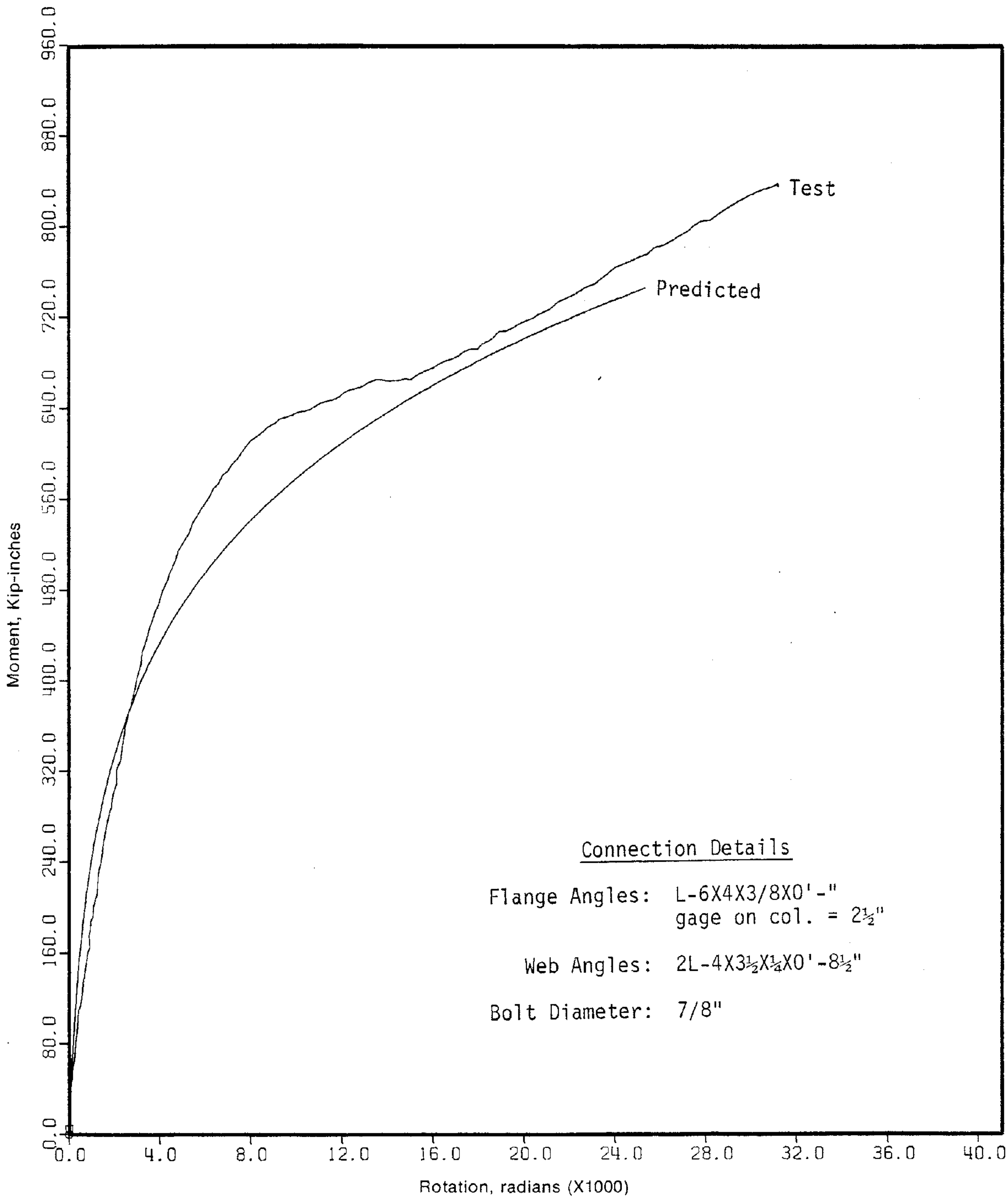


FIG. 4.7 COMPARISON OF PREDICTED MOMENT-ROTATION CURVE WITH TEST RESULTS FOR SPECIMEN 14S5

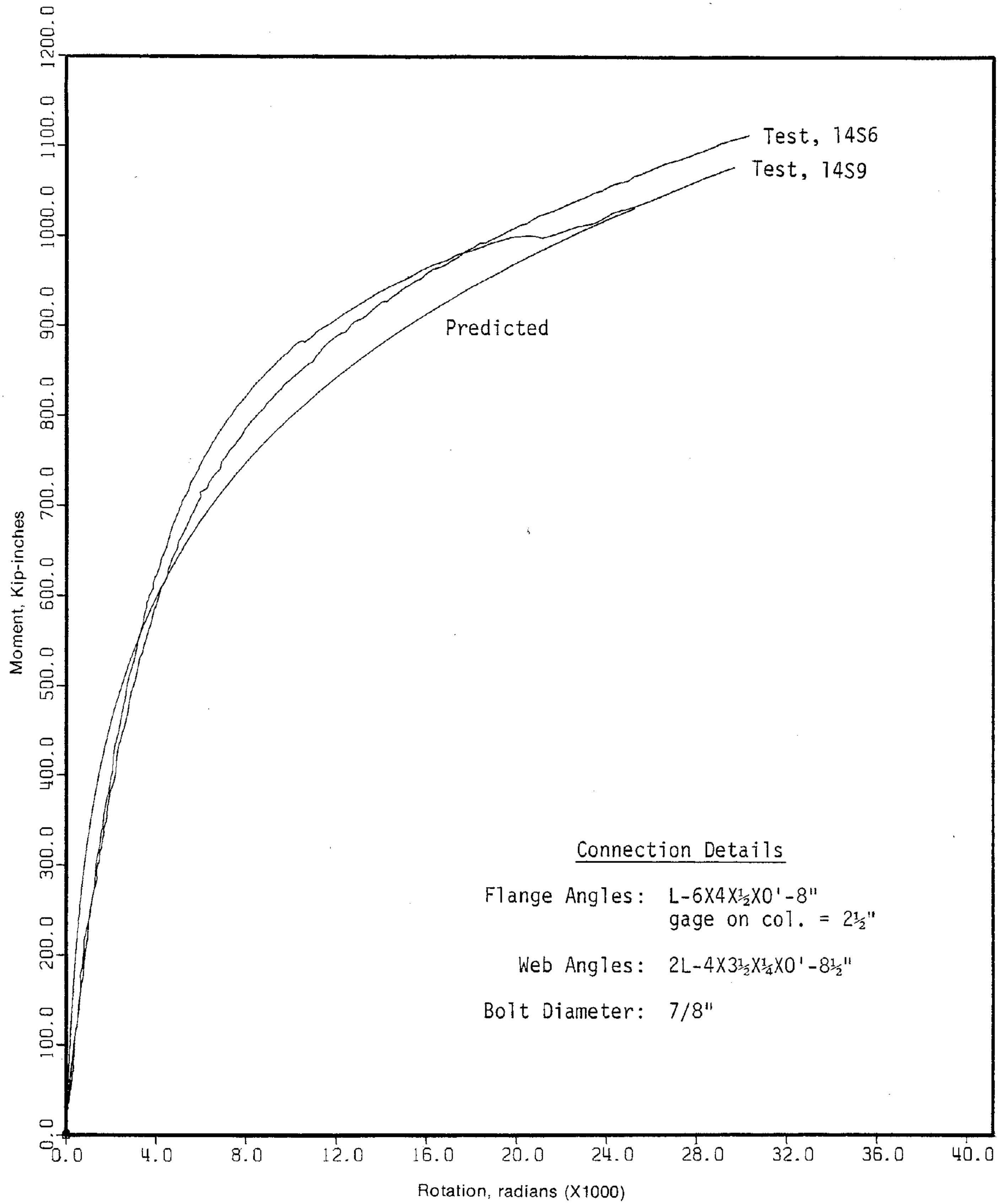


FIG. 4.8 COMPARISON OF PREDICTED MOMENT-ROTATION CURVE WITH TEST RESULTS FOR SPECIMENS 14S6 AND 14S9

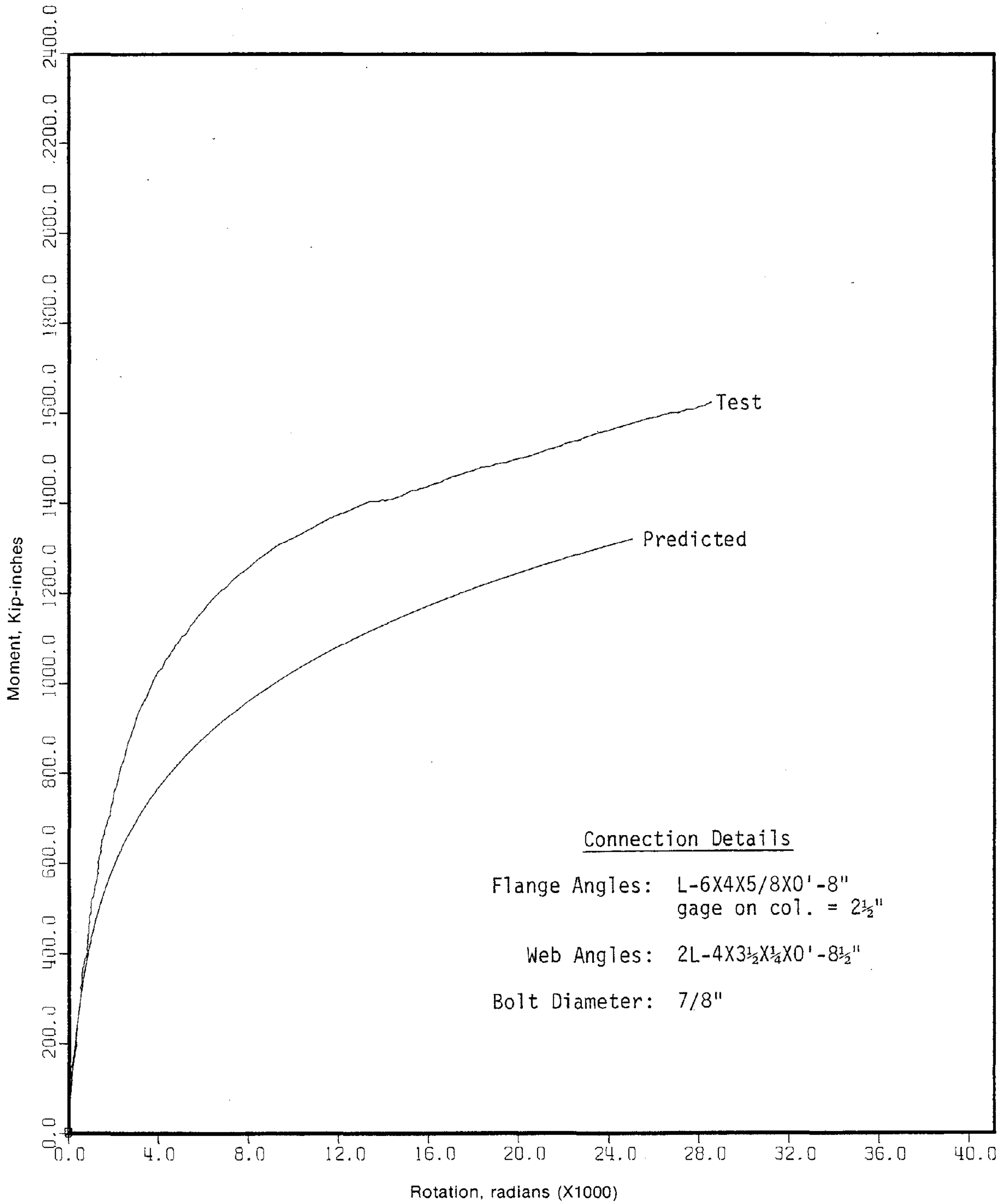


FIG. 4.9 COMPARISON OF PREDICTED MOMENT-ROTATION CURVE WITH TEST RESULTS FOR SPECIMEN 14S8

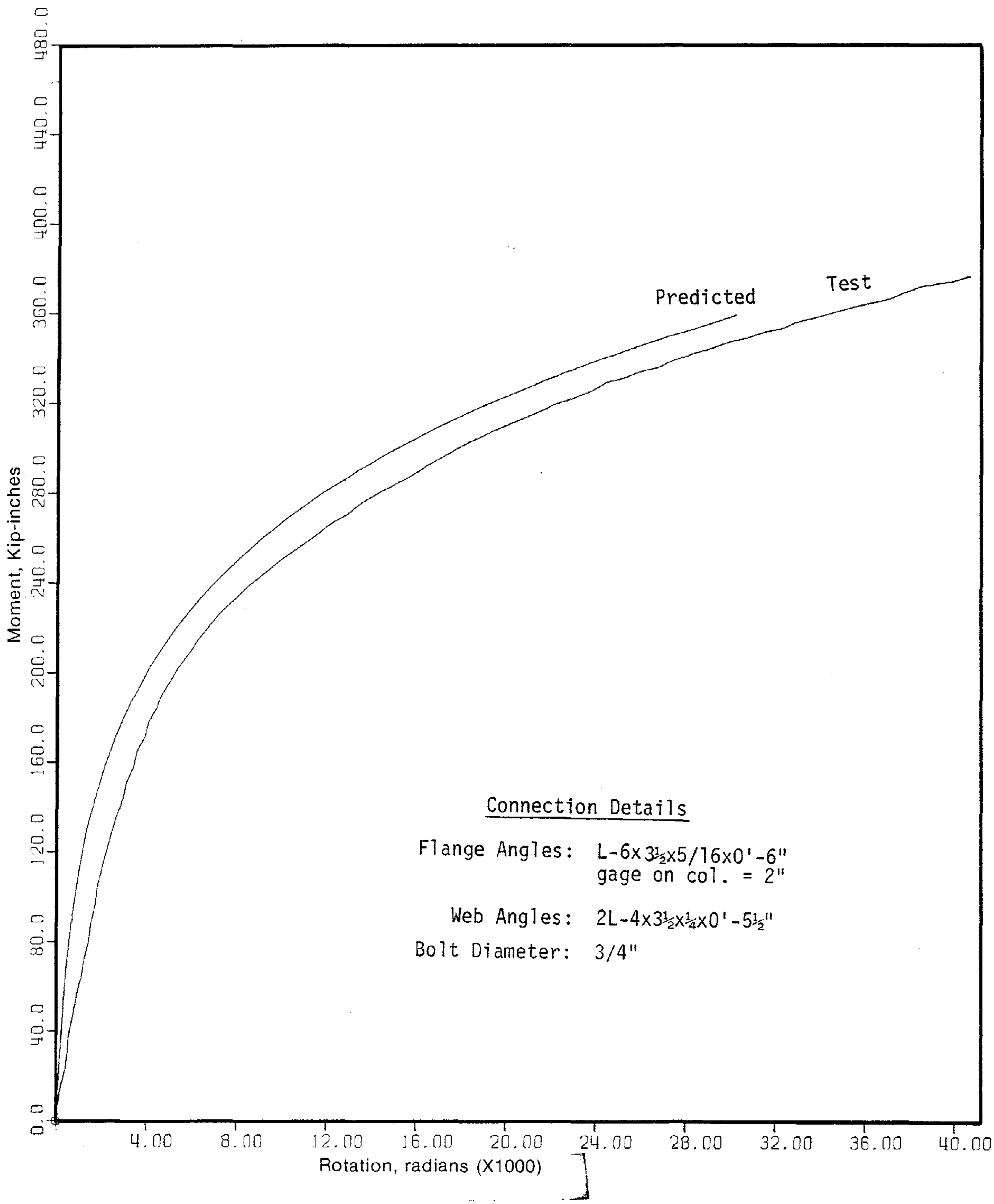


FIG. 4.10 COMPARISON OF PREDICTED MOMENT-ROTATION CURVE WITH TEST RESULTS FOR SPECIMEN 8S1

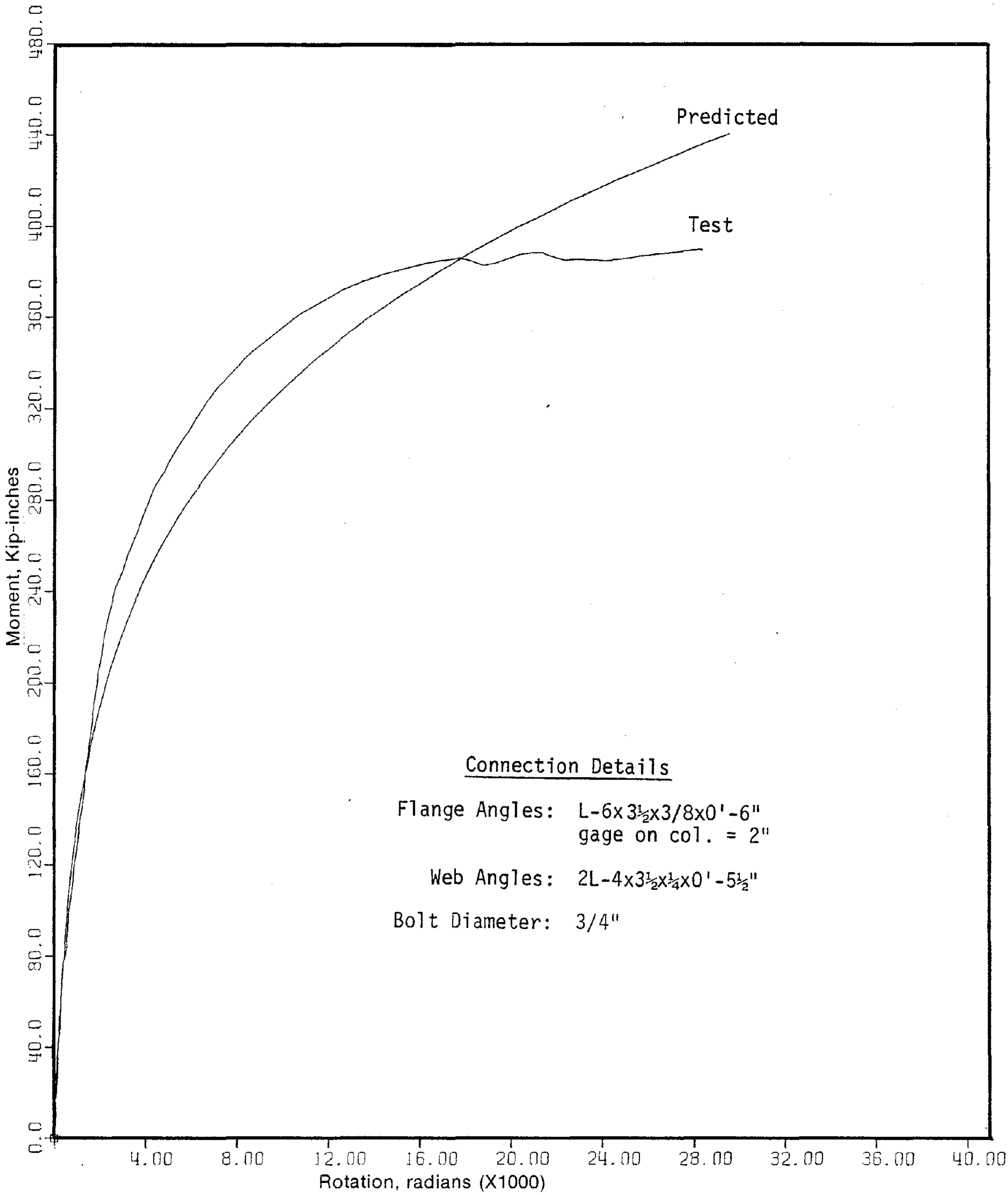


FIG. 4.11 COMPARISON OF PREDICTED MOMENT-ROTATION CURVE WITH TEST RESULTS FOR SPECIMEN 8S2

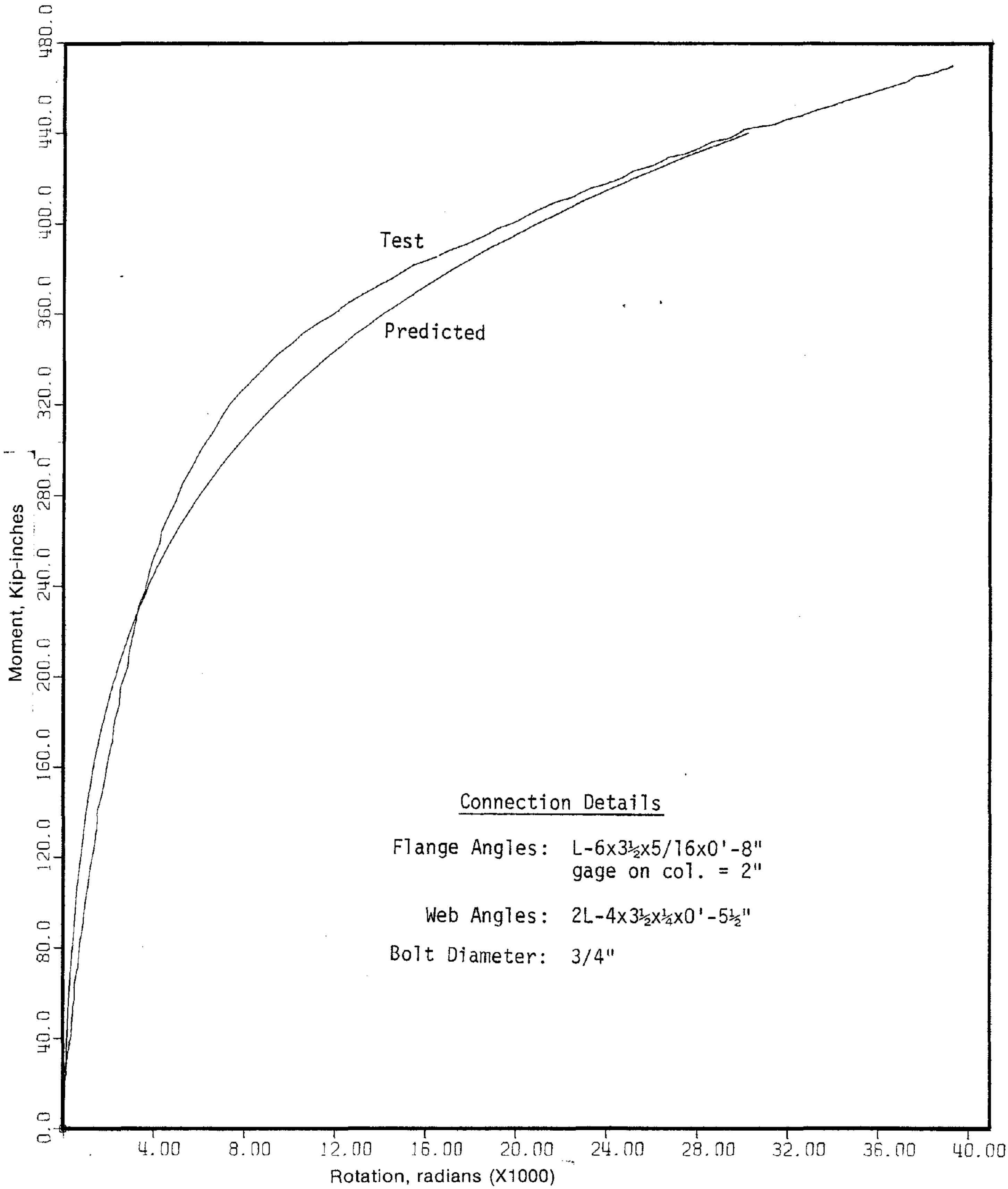


FIG. 4.12 COMPARISON OF PREDICTED MOMENT-ROTATION CURVE WITH TEST RESULTS FOR SPECIMEN 8S3

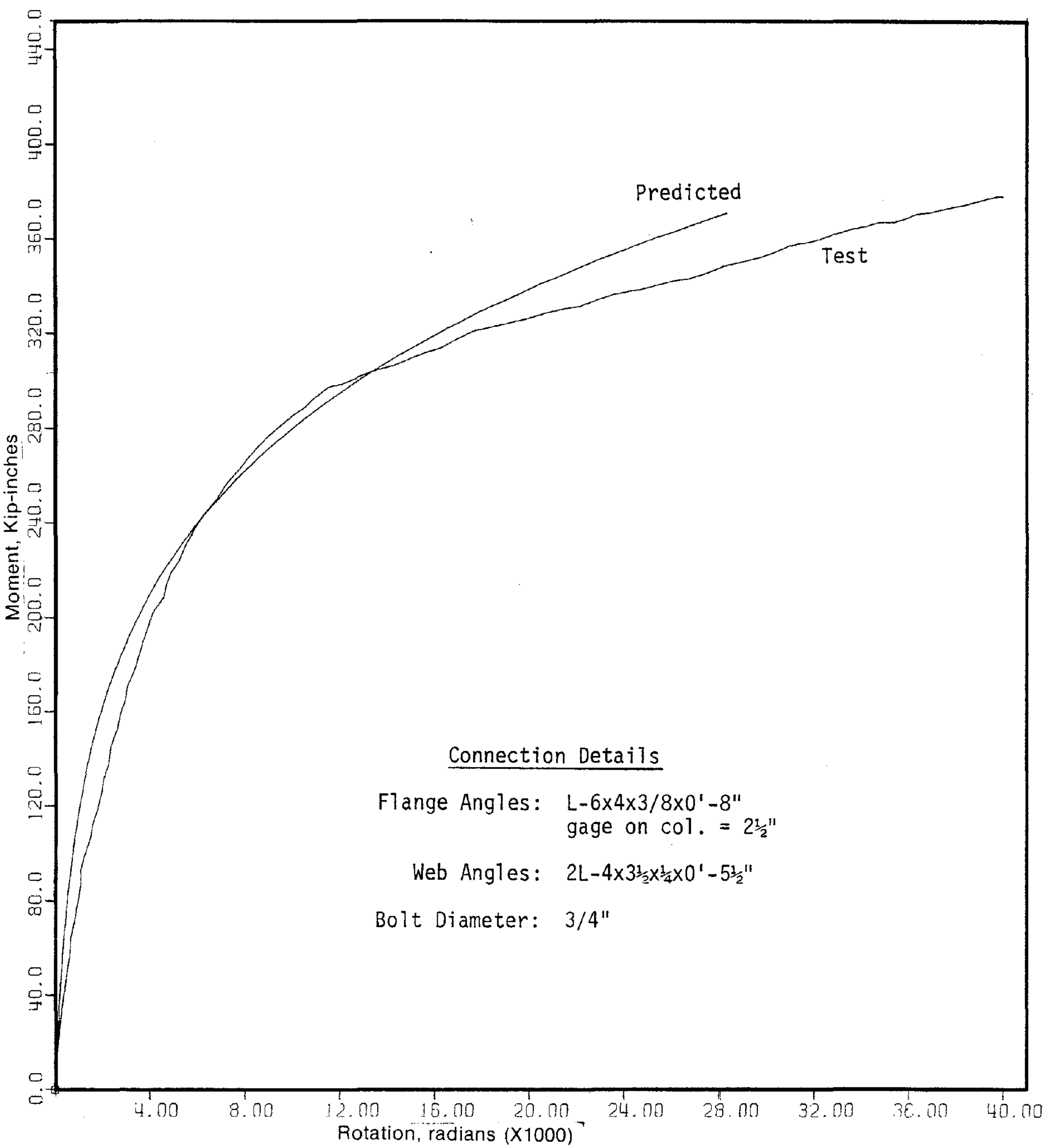


FIG. 4.13 COMPARISON OF PREDICTED MOMENT-ROTATION CURVE WITH TEST RESULTS FOR SPECIMEN 8S5

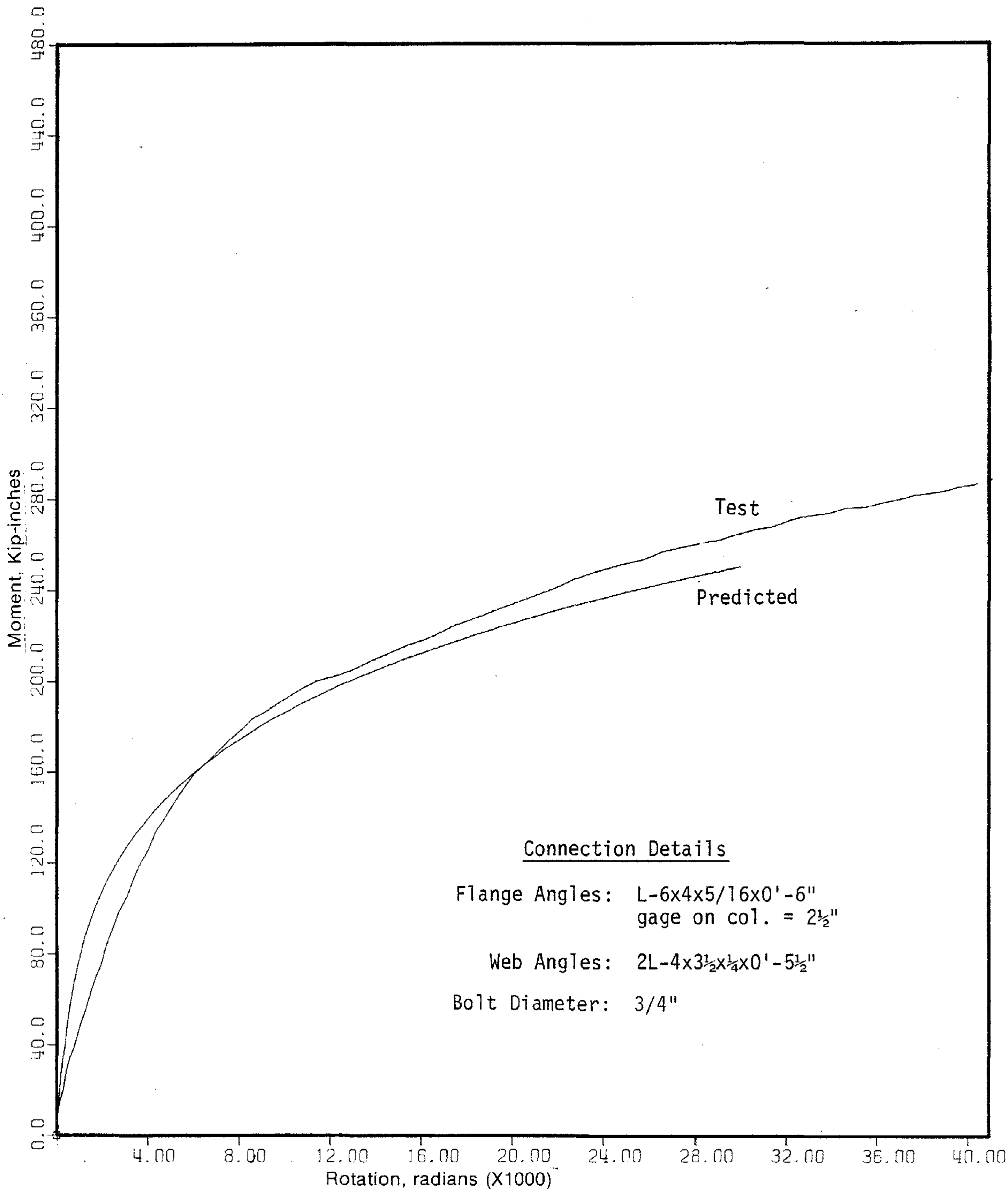


FIG. 4.14 COMPARISON OF PREDICTED MOMENT-ROTATION CURVE WITH TEST RESULTS FOR SPECIMEN 8S6

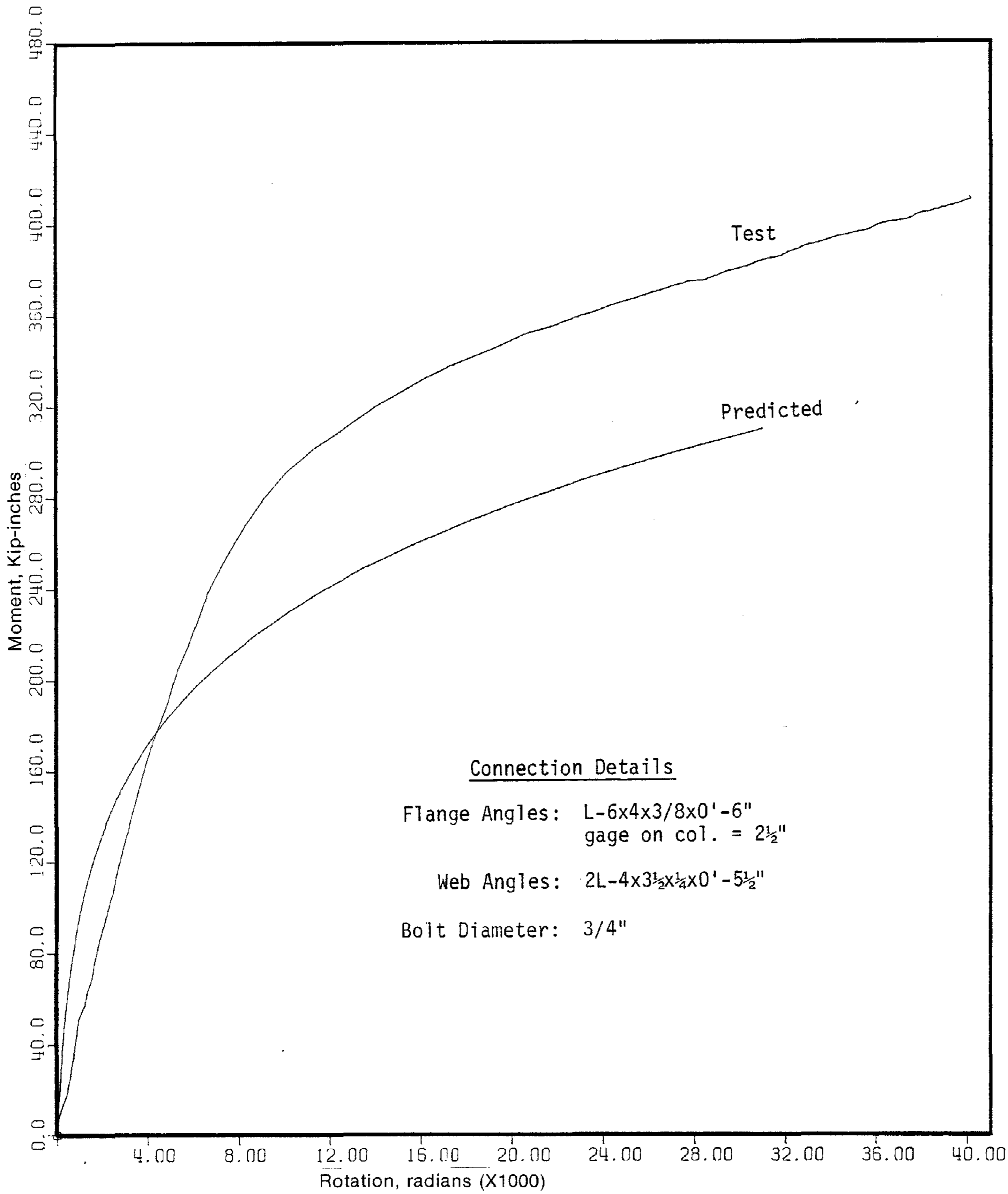


FIG. 4.15 COMPARISON OF PREDICTED MOMENT-ROTATION CURVE WITH TEST RESULTS FOR SPECIMEN 8S7

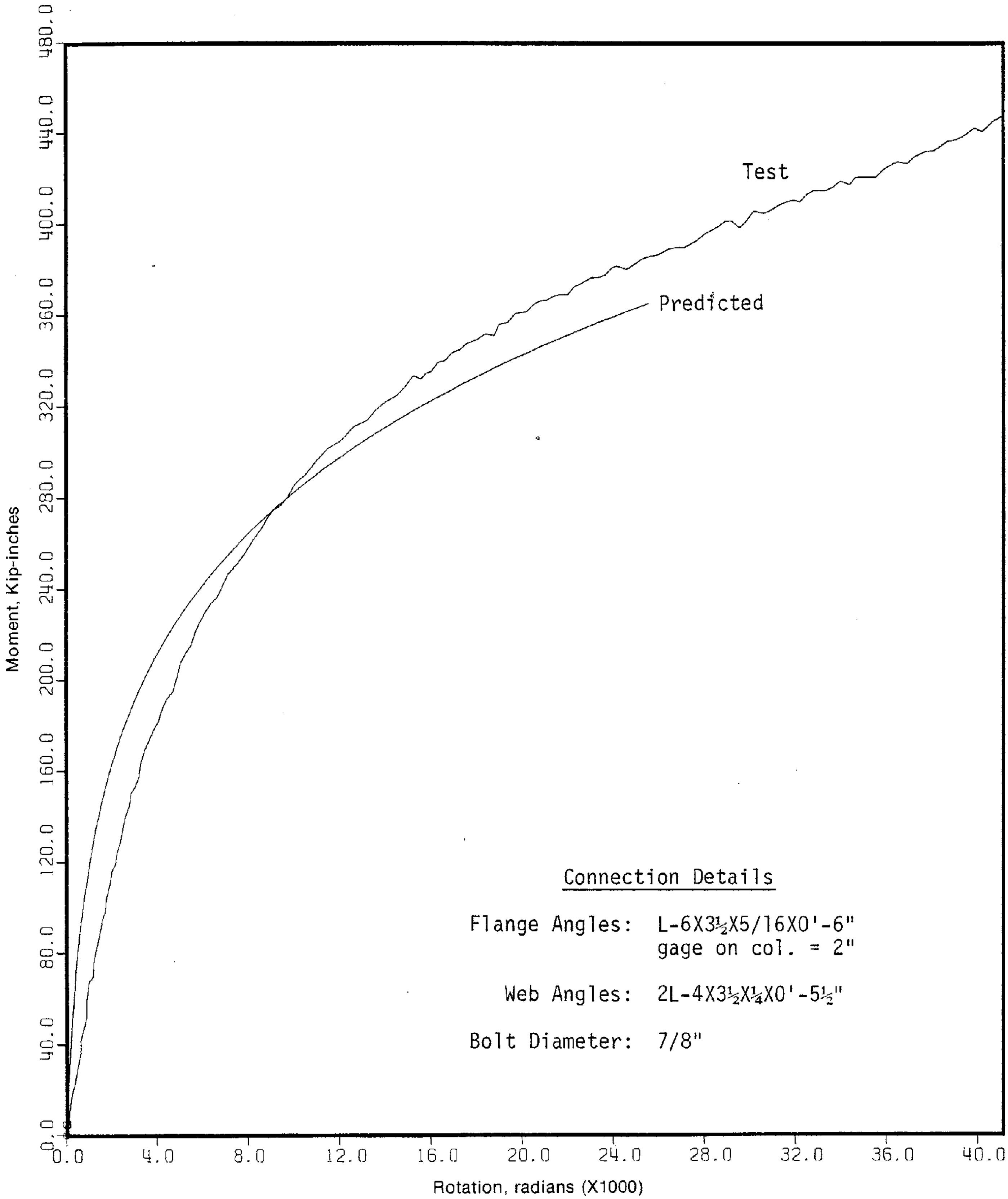


FIG. 4.16 COMPARISON OF PREDICTED MOMENT-ROTATION CURVE WITH TEST RESULTS FOR SPECIMEN 8S8

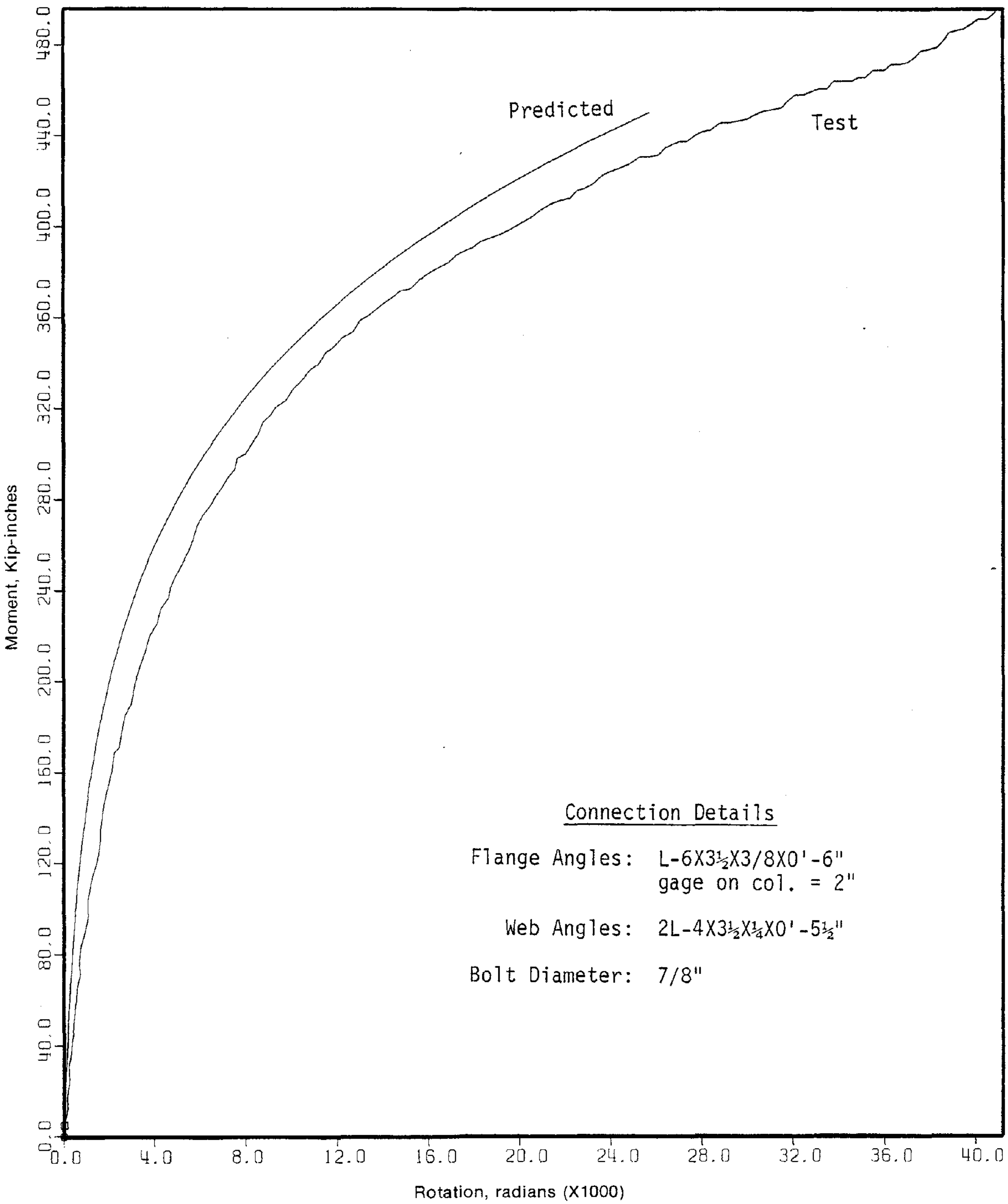


FIG. 4.17 COMPARISON OF PREDICTED MOMENT-ROTATION CURVE WITH TEST RESULTS FOR SPECIMEN 8S9

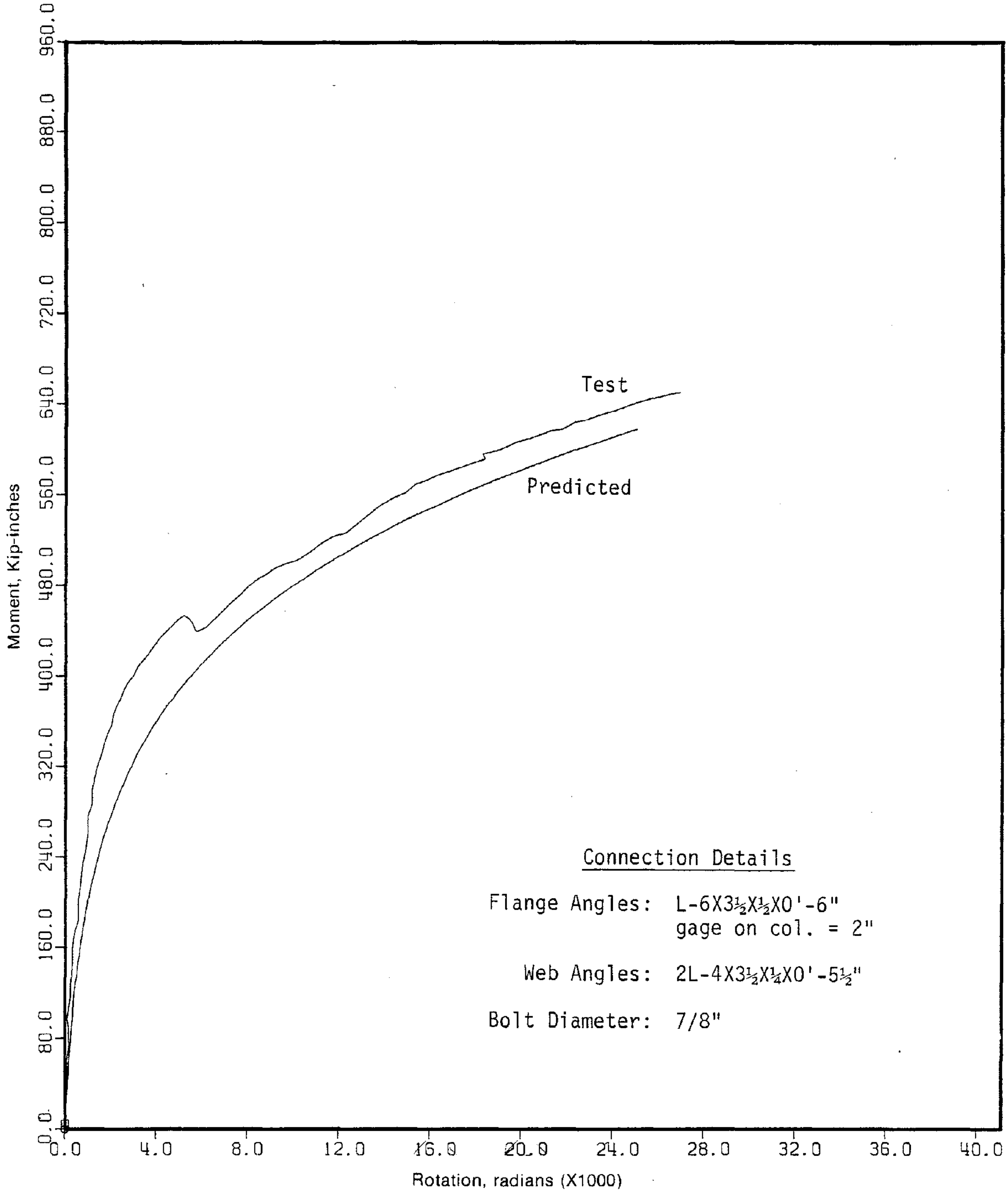


FIG. 4.18 COMPARISON OF PREDICTED MOMENT-ROTATION CURVE WITH TEST RESULTS FOR SPECIMEN 8S10

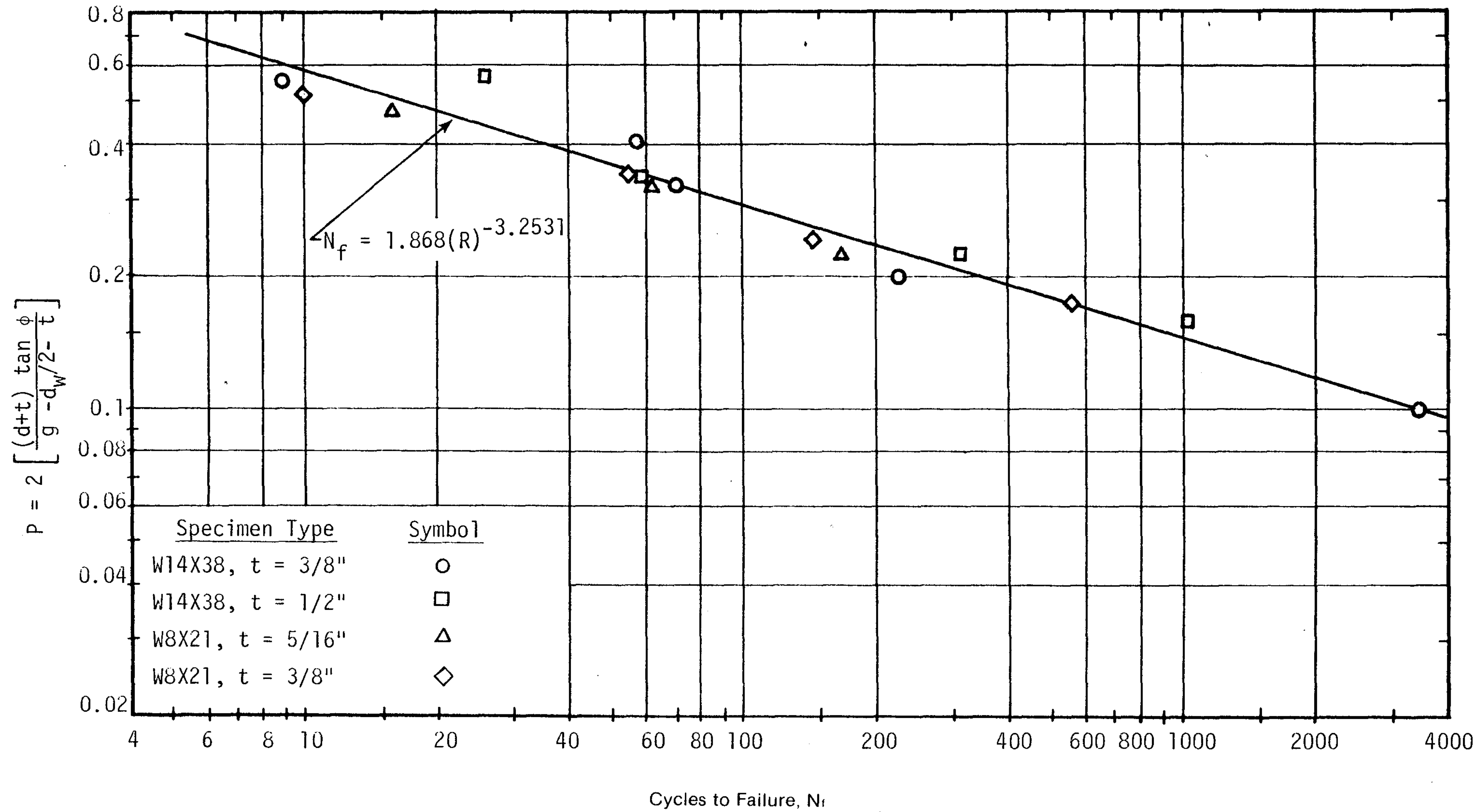


FIG. 4.19 COMPARISON OF TOTAL FATIGUE LIFE WITH NOMINAL FLANGE ANGLE CHORD ROTATION — ALL CONSTANT AMPLITUDE CYCLIC TESTS

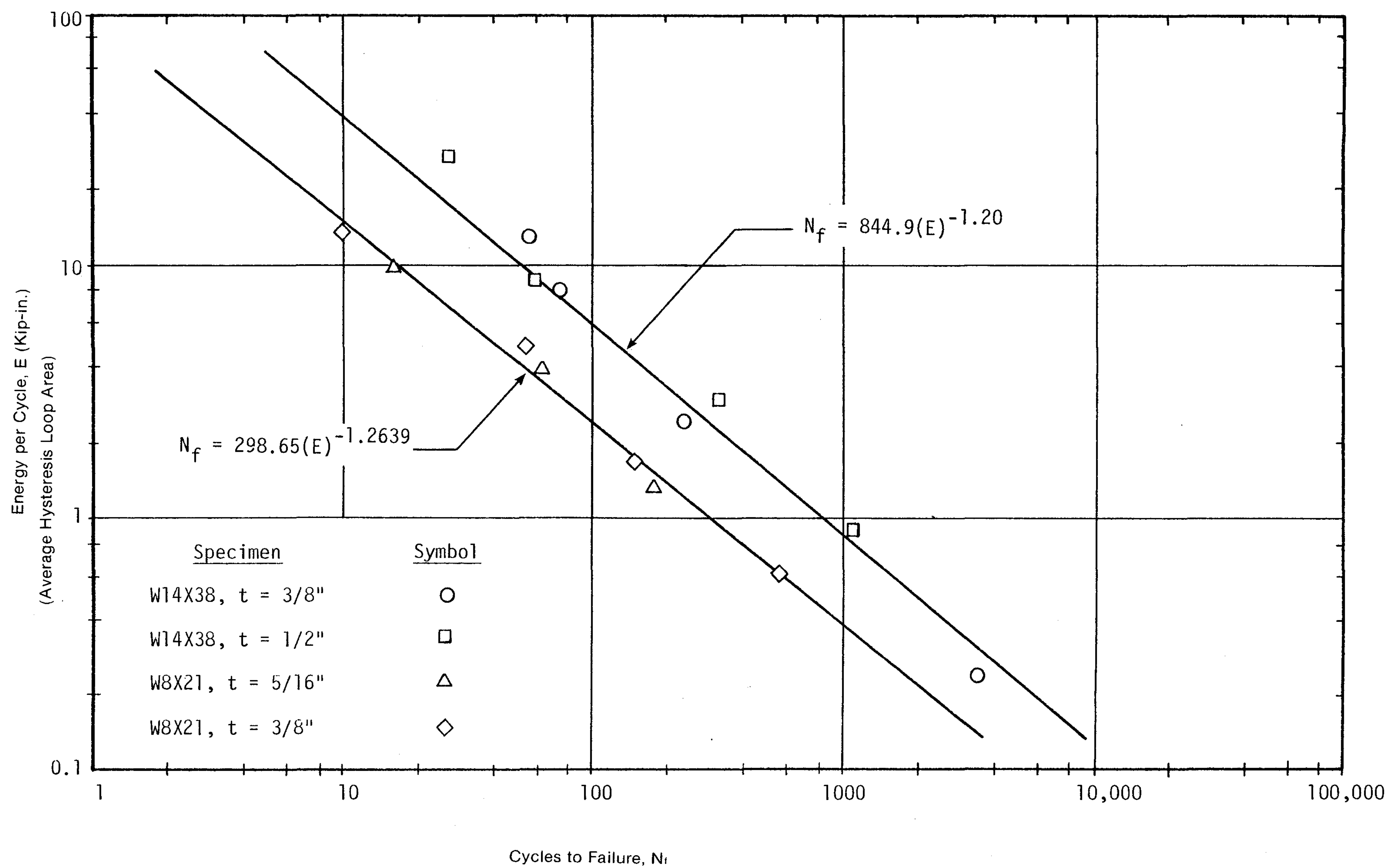


FIG. 4.20 COMPARISON OF TOTAL FATIGUE LIFE WITH AVERAGE AREA OF INDIVIDUAL HYSTERESIS LOOP — ALL CONSTANT AMPLITUDE CYCLE TESTS